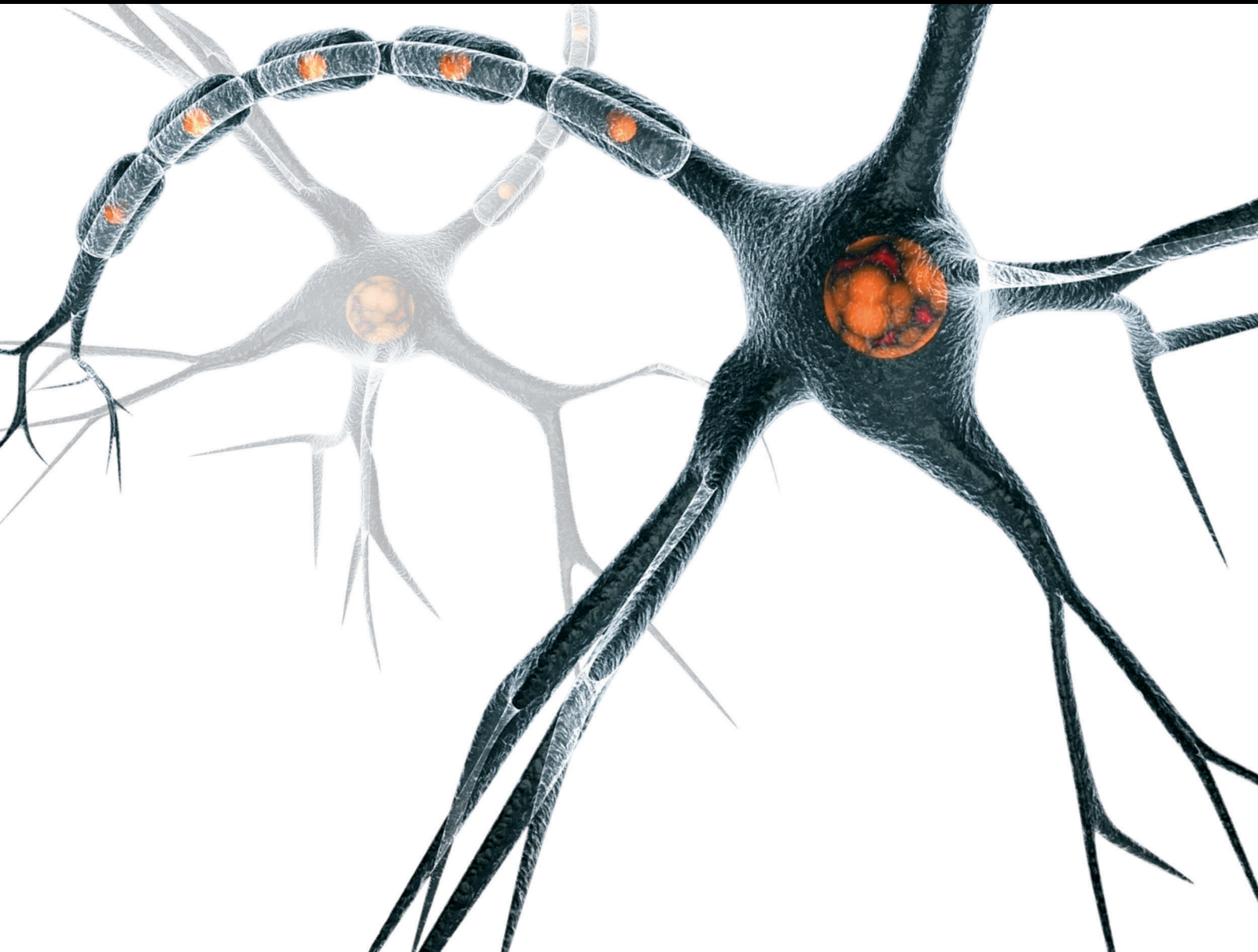# Cortical Circuitry and Synaptic Dysfunctions in Alzheimer's Disease and Other Dementias

Lead Guest Editor: Federico Ranieri
Guest Editors: Alberto Benussi, Mariagiovanna Cantone, Florinda Ferreri, and Javier Márquez-Ruiz

Cortical Circuitry and Synaptic Dysfunctions in Alzheimer's Disease and Other Dementias

Cortical Circuitry and Synaptic Dysfunctions in Alzheimer's Disease and Other Dementias

Lead Guest Editor: Federico Ranieri
Guest Editors: Alberto Benussi, Mariagiovanna Cantone, Florinda Ferreri, and Javier Márquez-Ruiz

Chief Editor

Michel Baudry, USA

Editorial Board

Contents

Relationship between Urinary Alzheimer-Associated Neuronal Thread Protein and Apolipoprotein Epsilon 4 Allele in the Cognitively Normal Population

Yuxia Li (ID), Meimei Kang (ID), Can Sheng (ID), Guanqun Chen (ID), Taoran Li (ID), Jun Wang (ID), Yanning Cai (ID), Rong Wang (ID), and Ying Han (ID)

Editorial

Cortical Circuitry and Synaptic Dysfunctions in Alzheimer's Disease and Other Dementias

Federico Ranieri [1], **Alberto Benussi** [2], **Mariagiovanna Cantone** [3], **Florinda Ferreri** [4], and **Javier Márquez-Ruiz** [5]

[1]*Unit of Neurology, Department of Neuroscience, Biomedicine and Movement Sciences, University of Verona, Verona, Italy*
[2]*Unit of Neurology, Department of Clinical and Experimental Sciences, University of Brescia, Italy*
[3]*Department of Neurology, Sant'Elia Hospital, ASP Caltanissetta, Caltanissetta, Italy*
[4]*Unit of Neurology and Neurophysiology, Department of Neuroscience, University of Padova, Padova, Italy*
[5]*Department of Physiology, Anatomy and Cell Biology, Pablo de Olavide University, Seville, Spain*

Correspondence should be addressed to Federico Ranieri; federico.ranieri@univr.it

A main challenge of current research on primary degenerative dementia is establishing a causal and temporal link between structural alterations, synaptic and circuit dysfunction, and cognitive decline. Experimental data support the view that the observable symptoms of dementia are only the tip of an iceberg, made up of neuropathological alterations which accumulate over time and lead to loss of synaptic connections and dysfunction of cortical circuitry [1].

In the clinical setting, current biomarkers are mainly based on the detection of amyloid deposition and neuronal injury. Increasing evidence also suggests a role for functional neuroimaging and electrophysiological parameters, derived from functional MRI (fMRI), electroencephalography (EEG), and transcranial magnetic stimulation, as biomarkers of dysfunction of neurotransmission and synaptic plasticity in specific types of primary dementia [2–6].

By considering the two major proteinopathies underlying Alzheimer's disease (AD), amyloid beta (Aβ) dysregulation, and Tau phosphorylation, the initial view of Aβ peptide accumulation acting as a key upstream event leading to neurodegeneration was put under revision since it has been acknowledged that these two neuropathological processes might be initiated independently [7, 8]. Indeed, while amyloid accumulation can progress over more than two decades [9], Aβ markers are not strongly related to cognitive decline as markers of neurodegeneration [1]. Significantly, in sporadic AD, impairment of long-term potentiation- (LTP-) like cortical plasticity was found to be associated with a higher cerebrospinal fluid total-Tau level and with a faster progression of cognitive decline [6].

In this effort to establish a link with functional impairment, in AD, attention has long been focused on the central cholinergic deficit and impairment of synaptic plasticity, but recent findings also point towards different neurotransmitter systems, prominently towards selective dopaminergic neuron degeneration leading to hippocampal LTP dysfunction as a possible upstream phenomenon [10]. A primary dysfunction of synaptic plasticity, possibly favored by genetic factors, has also been hypothesized as the leading cause of molecular and histopathological modifications [11].

A better understanding of such alterations is required for the development of drugs that target specific pathological mechanisms. Moreover, the early detection of pathological changes is crucial for the use of novel disease-modifying

treatments that need to be administered early in the disease course [12].

The present Special Issue collects nine articles that contribute to the investigation of cortical circuit and synaptic dysfunctions related to molecular alterations.

Within the debate on the relationship between $A\beta$ and Tau pathology, S. Mondragón-Rodríguez et al. review evidence supporting an alternative hypothesis on the role of Tau phosphorylation as a possible neuroprotective rather than neurodegenerative mechanism, acting by preventing synaptic overexcitation during the early stages of AD development. In this article, the authors propose that phosphorylation of Tau's microtubule domain is a fundamental part of the regulatory mechanisms controlling the activity of NMDA glutamate receptors and synaptic coupling. The presented hypothesis has important implications for current therapeutic approaches aimed at reducing Tau and phosphorylated Tau (pTau) levels. Further knowledge on the link between $A\beta$ and Tau/pTau at the synapse is needed to support the hypothetic non-pathological role of pTau.

M. A. Aguiar-Furucho and F. J. R. Peláez simulated the effects of brain aging, so as to reproduce early AD stages, on a computational model of cortical circuits (of somatosensory, visual, and auditory cortices) involved in the first level of processing of sensory afferent inputs. The model, which has learning capabilities, includes cholinergic excitatory projections to thalamo-cortical neurons and inhibitory GABAergic interneurons. Within this model, the authors show that, in the presence of impaired GABA-A signaling, which has been described in AD pathophysiology, the reduction of afferent inputs determines a dysregulation of neuronal excitability that may facilitate a state of hypermetabolism. While the above model is focused on function rather than on a specific biological substrate, it provides a hypothesis that sensory/cognitive stimulus reduction might not only facilitate dementia by weakening cognitive reserve but also represent a direct pathophysiological mechanism of neurodegeneration.

J. Li et al. provide an overview of the GABAergic circuitry, and they highlight the mechanisms through which hippocampal GABAergic impairment may cause cognitive deficits under an ischemic environment, particularly at chronic ischemic stages. They review evidence of ischemia-induced changes of the GABAergic system, which has a significant role in promoting neural development and formation of local neural circuits, including GABA interneurons, extracellular GABA neurotransmitters, and GABA receptors. Moreover, to bring new insights and strategies to solving this kind of emerging cognitive deficits, they also describe exogenous cell transplantation technology, which is effectively supposed to improve cognition by modulating the GABAergic system.

As far as the $A\beta$ is concerned, C. Gauthier-Umaña et al. investigated alterations of synaptic activity and plasticity in an animal model of early $A\beta$ pathology. Results show that soluble $A\beta$ microinjection in the commissural CA3-to-CA1 circuit increased synaptic variability, impaired long-term plasticity, increased gamma and high-frequency oscillations (121-250 Hz), and induced a significant γ amplitude-modulating θ phase shift in anaesthetized Wistar rats. Based on these results, the authors propose the observed abnor-mality in θ-to-γ phase-amplitude coupling as a putative biomarker of $A\beta$-induced synaptic dysfunction in the early stages of AD development.

L. Jorge et al. correlated $A\beta$ pathology and structural changes between the retinal and primary visual cortex thicknesses in a population of AD patients, by means of integrated imaging techniques. Combining optical coherence tomography, magnetic resonance, and positron emission tomography imaging, the authors measured retinal and primary visual cortex thicknesses, $A\beta$ retention, and neuroinflammation. They report that the primary visual cortex showed increased amyloid-binding potential, in the absence of neuroinflammation, with a positive association between the synapse-rich inner plexiform layers of the retina and the primary visual cortex. This retino-cortical interplay might thus reflect changes in synaptic function resulting from $A\beta$ deposition in AD, even when neuronal loss is still not evident.

Interestingly, to therapeutic prospects based on counteracting mechanisms of $A\beta$-related synaptic damage, C. Sheng et al. present a study aimed at clarifying the molecular basis of the effects of an empirically used traditional Chinese medicine compound. They characterized the composition of Bushen-Tiansui Formula (BTF), generated a chromatographic fingerprint profile, and evaluated the effects of BTF on cognition and memory functions in a rat model of AD. The oral administration of BTF reversed the cognitive defects by reversing the $A\beta_{1-42}$ fibril-induced reduction of synaptic marker expression and by promoting the expression of Brain-Derived Neurotrophic Factors and the activation of the TrkB/Akt/CREB signaling pathway. This approach points to the importance of accurately defining the potential biological targets of any newly proposed treatment strategy.

Relevant to the early diagnosis of AD, H. Liu et al. explore the possibility of improving the sensitivity of fMRI measures of cortical connectivity that can be used to predict progression from Mild Cognitive Impairment (MCI) to AD. They used the L1-norm linear regression model to test the small-world attributes of the brain networks of three groups of subjects composed, respectively, by 33 MCI, 24 AD, and 27 healthy controls. They found that the L1-norm was more sensitive to detect slight small-world network changes in the early stages of AD with respect to the traditional Pearson correlation analysis.

Y. Li et al. investigated the relationship between Urinary Alzheimer-Associated Neuronal Thread Protein (AD7c-NTP), a marker of neuronal degeneration, and Apolipoprotein Epsilon (ApoE) 4 allele in the cognitively normal population. AD7c-NTP has been shown to be increased in patients with MCI and AD, colocalizing with neurofibrillary tangles and dystrophic neurites. In this study, while no significant differences in urinary AD7c-NTP levels were observed between patients with subjective cognitive decline and healthy controls, AD7c-NTP levels were significantly higher in subjects with ApoE3/4 and 4/4, indicating that also in subjective cognitive decline ApoE4 may modify AD7c-NTP levels, which are related to Tau and $A\beta$ deposition. These findings are extremely relevant for the study of subjective cognitive decline, a stage in which patients report self-experienced persistent decline in cognitive capacity in

comparison with a previously normal status, potentially concealing a prodromal state of AD, and that will probably become a target of disease-modifying treatments.

Finally, the advancements in next-generation sequencing (NGS) techniques have allowed for rapid, efficient, and cost-time-effective genetic variant detection. In their article, G. Lanza et al. performed a neurogenetic study through an ad hoc NGS-based custom sequencing gene panel to screen 16 genes in different types of degenerative cognitive disorders. Notwithstanding the preliminary value of the study, some rare genetic variants with a probable disease association were detected, thus suggesting translational perspectives in the diagnosis and management of a wide range of neurodegenerative disorders.

Taken together, findings of the studies in this collection point to the importance of shedding light on the molecular bases and the pathophysiological mechanisms leading to dementia, as this might improve the early diagnostic and prognostic accuracy and therapeutic options.

Conflicts of Interest

F.R., A.B., M.C., F.F., and J.M.-R. declare that they have no conflicts of interest regarding the publication of this special issue.

Federico Ranieri
Alberto Benussi
Mariagiovanna Cantone
Florinda Ferreri
Javier Márquez-Ruiz

References

[1] C. R. Jack Jr., D. S. Knopman, W. J. Jagust et al., "Tracking pathophysiological processes in Alzheimer's disease: an updated hypothetical model of dynamic biomarkers," *Lancet Neurology*, vol. 12, no. 2, pp. 207–216, 2013.

[2] R. Sperling, "The potential of functional MRI as a biomarker in early Alzheimer's disease," *Neurobiology of Aging*, vol. 32, no. S1, pp. S37–S43, 2011.

[3] A. H. Meghdadi, M. Stevanović Karić, M. McConnell et al., "Resting state EEG biomarkers of cognitive decline associated with Alzheimer's disease and mild cognitive impairment," *PLoS One*, vol. 16, no. 2, article e0244180, 2021.

[4] A. Benussi, M. Grassi, F. Palluzzi et al., "Classification accuracy of transcranial magnetic stimulation for the diagnosis of neurodegenerative dementias," *Annals of Neurology*, vol. 87, no. 3, pp. 394–404, 2020.

[5] A. Benussi, M. Grassi, F. Palluzzi et al., "Classification accuracy of TMS for the diagnosis of mild cognitive impairment," *Brain Stimulation*, vol. 14, no. 2, pp. 241–249, 2021.

[6] C. Motta, F. Di Lorenzo, V. Ponzo et al., "Transcranial magnetic stimulation predicts cognitive decline in patients with Alzheimer's disease," *Journal of Neurology, Neurosurgery, and Psychiatry*, vol. 89, no. 12, pp. 1237–1242, 2018.

[7] S. A. Small and K. Duff, "Linking Aβ and Tau in late-onset Alzheimer's disease: a dual pathway hypothesis," *Neuron*, vol. 60, no. 4, pp. 534–542, 2008.

[8] S. W. Pimplikar, R. A. Nixon, N. K. Robakis, J. Shen, and L. H. Tsai, "Amyloid-independent mechanisms in Alzheimer's disease pathogenesis," *The Journal of Neuroscience*, vol. 30, no. 45, pp. 14946–14954, 2010.

[9] V. L. Villemagne, S. Burnham, P. Bourgeat et al., "Amyloid β deposition, neurodegeneration, and cognitive decline in sporadic Alzheimer's disease: a prospective cohort study," *Lancet Neurology*, vol. 12, no. 4, pp. 357–367, 2013.

[10] A. Nobili, E. C. Latagliata, M. T. Viscomi et al., "Dopamine neuronal loss contributes to memory and reward dysfunction in a model of Alzheimer's disease," *Nature Communications*, vol. 8, no. 1, article 14727, 2017.

[11] G. Barthet and C. Mulle, "Presynaptic failure in Alzheimer's disease," *Progress in Neurobiology*, vol. 194, p. 101801, 2020.

[12] F. Panza, M. Lozupone, G. Logroscino, and B. P. Imbimbo, "A critical appraisal of amyloid-β-targeting therapies for Alzheimer disease," *Nature Reviews. Neurology*, vol. 15, no. 2, pp. 73–88, 2019.

Research Article

Acute Effects of Two Different Species of Amyloid-β on Oscillatory Activity and Synaptic Plasticity in the Commissural CA3-CA1 Circuit of the Hippocampus

Cécile Gauthier-Umaña ⬤,[1] **Jonathan Muñoz-Cabrera ⬤,**[2] **Mario Valderrama ⬤,**[3] **Alejandro Múnera,**[2] **and Mauricio O. Nava-Mesa ⬤**[1]

[1]*Neuroscience Research Group (NEUROS), Escuela de Medicina y Ciencias de la Salud, Universidad del Rosario, Bogotá, Colombia*
[2]*Behavioral Neurophysiology Laboratory, Physiological Sciences Department, School of Medicine, Universidad Nacional de Colombia, Bogotá, Colombia*
[3]*Deparment of Biomedical Engineering, Universidad de los Andes, Bogotá, Colombia*

Correspondence should be addressed to Mauricio O. Nava-Mesa; monavam@usal.es

Recent evidence indicates that soluble amyloid-β (Aβ) species induce imbalances in excitatory and inhibitory transmission, resulting in neural network functional impairment and cognitive deficits during early stages of Alzheimer's disease (AD). To evaluate the *in vivo* effects of two soluble Aβ species (Aβ_{25-35} and Aβ_{1-40}) on commissural CA3-to-CA1 (cCA3-to-CA1) synaptic transmission and plasticity, and CA1 oscillatory activity, we used acute intrahippocampal microinjections in adult anaesthetized male Wistar rats. Soluble Aβ microinjection increased cCA3-to-CA1 synaptic variability without significant changes in synaptic efficiency. High-frequency CA3 stimulation was rendered inefficient by soluble Aβ intrahippocampal injection to induce long-term potentiation and to enhance synaptic variability in CA1, contrasting with what was observed in vehicle-injected subjects. Although soluble Aβ microinjection significantly increased the relative power of γ-band and ripple oscillations and significantly shifted the average vector of θ-to-γ phase-amplitude coupling (PAC) in CA1, it prevented θ-to-γ PAC shift induced by high-frequency CA3 stimulation, opposite to what was observed in vehicle-injected animals. These results provide further evidence that soluble Aβ species induce synaptic dysfunction causing abnormal synaptic variability, impaired long-term plasticity, and deviant oscillatory activity, leading to network activity derailment in the hippocampus.

1. Introduction

Alzheimer's disease (AD), the most common type of dementia and progressive neurodegenerative disorder worldwide, is characterized by selective neuronal loss, and two histopathological features in *postmortem* tissue are extracellular amyloid plaques composed of amyloid beta peptide (Aβ) and intracellular neurofibrillary tangles composed of hyperphosphorylated tau protein [1]. Recent evidence indicates that soluble forms of Aβ induce glutamatergic, cholinergic, and GABAergic imbalance, resulting in functional impairment of neural networks during early AD stages [2–5]. In fact, Aβ-induced synaptic dysfunction precedes selective neuronal degeneration and may explain memory impairment during early AD stages and mild cognitive impairment, a prodromal stage of AD [6, 7]. Although therapies based on modulation of GABAergic neurotransmission have been proposed for AD [8], current symptomatic therapies include cholinesterase inhibitors and NMDA antagonists only [9]. New Aβ-targeted immunotherapies have been tested in several clinical trials but without a clear clinical benefit [10]; therefore, no course-modifying treatment has been

developed to date because of a lack of understanding of the fundamental mechanisms underlying AD, as well as the physiological role of amyloid peptides.

Senile plaques in AD patients and animal models consist of $A\beta_{1-40}$ and $A\beta_{1-42}$ ($A\beta_{1-42}$ mainly in the core of early plaques and $A\beta_{1-40}$ in vascular amyloid deposits) [11, 12]. It has been suggested that short $A\beta$ fragments, such as $A\beta_{25-35}$, constitute the biologically active forms of $A\beta$ and are thus responsible for the neurotoxic properties of $A\beta_{1-40}$ and $A\beta_{1-42}$ [13]. $A\beta_{25-35}$ may be expressed in AD brains [14–16] possibly from enzymatic cleavage of $A\beta_{1-40}$ [15, 16]. Several studies indicate similar effects in the brain of either short or long forms of $A\beta$ [13–15]. However, $A\beta_{25-35}$ produces more acute toxic effects than $A\beta_{1-42}$ because of its higher solubility [17], and it also has different effects on synaptic plasticity and intracellular pathophysiological mechanisms compared with $A\beta_{1-40}$ and $A\beta_{1-42}$ [18–20].

The hippocampus and entorhinal cortex are peculiarly susceptible to deleterious $A\beta$ effects during early AD stages [21]. Hippocampal plasticity, necessary for learning and memory processes, is tuned by θ activity, which depends on acetylcholine release from the medial septum [2]. Moreover, the septum and hippocampus are reciprocally interconnected and functionally coupled through GABAergic and glutamatergic connections to form the septohippocampal system [2, 22]. Each of these neurotransmitters contributes to hippocampal rhythmicity [23]. Moreover, θ and γ activities are associated through inhibitory synapses between GABAergic parvalbumin interneurons and pyramidal neurons [24]. Such oscillatory activity, including phase-to-amplitude coupling of θ and γ activity, is necessary for adequately encoding and storing information in the cortex and hippocampus [25–27]. *In vivo* studies have shown the relevance of the CA3-CA1 synapse in associative learning and memory processing [28, 29] and its implications in AD through animal models [30]. In a very recent study, the electrophysiological activity of the CA3-CA1 region in humans was correlated with memory tasks (i.e., delayed match-to-sample) and it resembles synaptic hippocampal responses observed in rodents in the same areas [31]. Therefore, studies based on animal models may provide physiological information that could be applied in specific regions of clinical relevance in the human brain.

There are tight correlations among long-term potentiation (LTP) mechanisms, θ-γ oscillations, and hippocampal-dependent memories [32–34]. Event-locked oscillatory activity in hippocampal formation and hippocampus-related structures is necessary for learning and long-term memory processes, as well as for declarative and spatial memory functions, which are impaired in early stages of AD [3, 34, 35]. Accumulating evidence indicates that $A\beta$ affects θ, δ, and γ bands in different preclinical models of AD [3, 36]. Similarly, EEG recordings in AD patients show pathological changes of network oscillations in a wide range of frequencies (i.e., α/θ ratio, γ coherence, θ and δ synchronization) [37, 38]. Studies using an animal model of AD (transgenic CRND8 mice) indicate that alterations in θ-γ cross-frequency coupling might be used as an early biomarker of AD [39]. In another study, acute LTP impairment by $A\beta_{1-42}$ was related to alterations in oscillatory activity in θ-γ coupling at perforant

path-dentate gyrus synapses [40]. Various studies have reported that changes in the spectral power of brain oscillations are related to LTP induction and expression [32, 33, 41, 42] and have shown a relationship between changes in single-synapse and network oscillation activity. Therefore, $A\beta$-induced LTP impairment might be associated with oscillatory activity changes in brain structures affected during initial stages of AD.

Several aggregated $A\beta$ forms and configurations may explain variable effects during AD progression. Considering the huge differences between experimental models (*in vivo vs. in vitro*), time of exposure to $A\beta$ (acute *vs.* chronic), and differences in $A\beta$ aggregation states (monomeric, oligomeric, and fibrillary), the reported $A\beta$ effects on neuronal activity have been divergent in terms of excitability, active and passive membrane properties, network activity, and neural plasticity [22, 43–47]. Despite the large number of studies, little is known about the effects of diverse soluble $A\beta$ forms on oscillatory activity, excitability, or synaptic plasticity [47, 48]. The aim of the present study was, therefore, to evaluate $A\beta_{25-35}$ and $A\beta_{1-40}$ effects on hippocampal oscillations (power spectral density and phase-amplitude coupling) and basal transmission, variability, and long-term plasticity in cCA3-to-CA1 synapses. We found that LTP impairment induced by acute administration of soluble $A\beta$ ($A\beta_{1-40}$ and $A\beta_{25-35}$) is associated with abnormal synaptic variability and increased power of γ-band and ripple network oscillations and derailed θ-to-γ phase-to-amplitude coupling in CA1. Such $A\beta$-induced disruption in synaptic plasticity and network activity may underlie abnormalities in information processing and memory encoding.

2. Material and Methods

2.1. Ethical Statement. All procedures performed on living animals were performed in conformance with Animal Research: Reporting *In Vivo* Experiments (ARRIVE) guidelines [49], following the Guide for the Care and Use of Laboratory Animals (8th edition, National Institutes of Health) and fulfilling the Colombian regulation (Law 84/1989 and Resolution 8430/1993). In addition, every experimental design and all procedures were approved by the Universidad del Rosario Ethics Committee.

2.2. Animals. Seventeen 16-20-week-old male Wistar rats, weighing $300 \pm 30\,g$, were used as experimental subjects. Experimental animals were supplied by the Universidad Nacional de Colombia animal facilities. Animals were housed in a sound-attenuated room in polycarbonate cages, in groups of four, under controlled environmental conditions: $20 \pm 1°C$ temperature, $50 \pm 10\%$ relative humidity, and $12\,h$ light/dark cycle (lights on from 07:00 to 19:00). Animals had food and water available *ad libitum*. Experiments were performed in the morning. Special care was taken to minimize animal suffering and to reduce the number of animals used.

Sample size was calculated according to the following formula [50]: sample size $= 2SD^2(Z^{\propto/2} + Z^{\beta})^2/d^2$, where $SD = 6.85$, $Z^{\propto/2} = 1.96$ with $\propto = 0.05$, $Z^{\beta} = 0.84$ with $\beta = 0.2$.
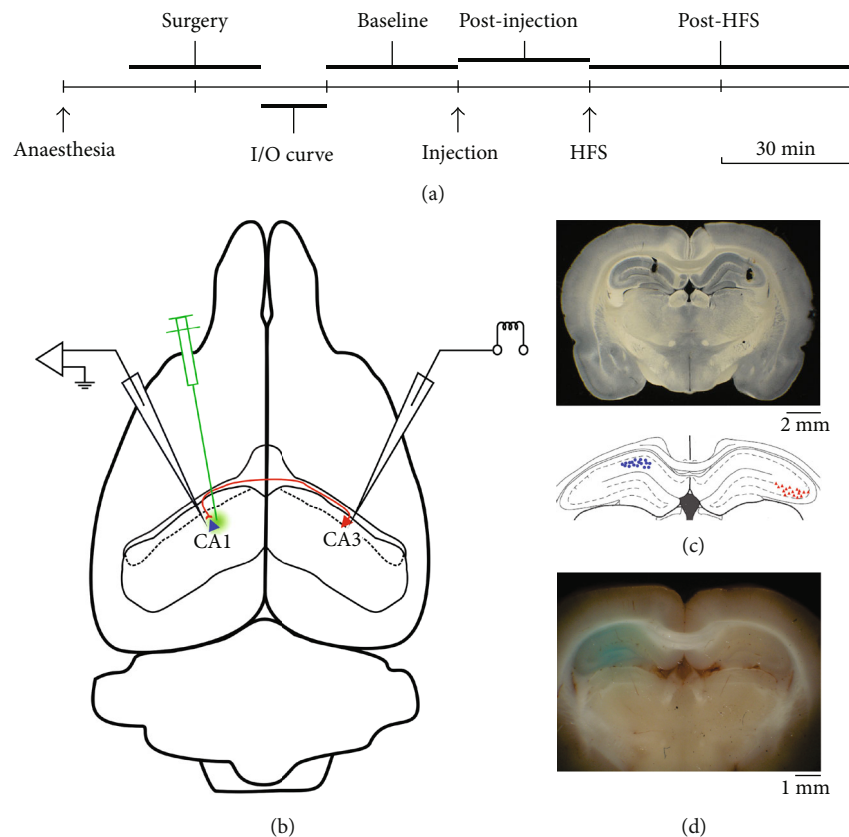
FIGURE 1: Experimental timeline and preparation. (a) Timeline indicating the experimental procedures during a recording session. (b) Diagram of a rat brain illustrating microelectrode cannula (for local field potential recording and microinjection in left CA1) and stimulating electrode (in right CA3) locations. (c) Panoramic photograph of an obliquely illuminated coronal brain slice containing representative electrolytic lesions made by passing current through recording (left) and stimulating (right) electrodes (upper panel), paired to a corresponding coronal diagram of the hippocampus (extracted and modified from the bregma: -3.6 mm diagram of Paxinos' rat brain atlas), summarizing recording (left, blue circles) and stimulating (right, red triangles) electrode placement in each experimental subject. (d) Panoramic photograph of a brain block containing methylene blue-coloured left hippocampus, attesting adequate diffusion of the injected solution.

Statistical power = 80%, and $d = 14$. The minimum sample number per group was 5.

2.3. Experimental Design and Timeline.

Animals were randomly assigned to any of three groups: (1) control group ($n = 6$), receiving vehicle microinjection; (2) $A\beta_{25-35}$ group ($n = 6$), receiving $A\beta_{25-35}$ peptide microinjection; and (3) $A\beta_{1-40}$ group ($n = 5$), receiving $A\beta_{1-40}$ peptide microinjection.

In brief, each experiment proceeded as follows: (1) under general anaesthesia, recording and stimulation electrodes were stereotactically inserted in CA1 and contralateral CA3; (2) once stable responses were obtained, the input/output relationship was established; (3) 30 min baseline recording was done to characterize basal synaptic efficiency; (4) the designed solution was microinjected in CA1; (5) the microinjected solution's effect on synaptic transmission was characterized by recording synaptic responses for 30 min after microinjection; (6) high-frequency tetanic stimulation was done to induce long-term plasticity; and (7) the effect of high-frequency stimulation (HFS) on synaptic efficiency was characterized by recording synaptic responses for 60 min after HFS (Figure 1(a)).

2.4. Surgery.

Under general anaesthesia induced with 1.5 g/kg of 25% urethane (Sigma-Aldrich, St. Louis, USA) and 10 mg/kg of xylazine (Rompun®, Bayer, Leverkusen, Germany) (intraperitoneal injection), the subject was placed in a rat stereotaxic frame (SR-6R, Narishige Inc., Tokyo, Japan). Nociceptive responses (tail prick and paw withdrawal reflex) were evaluated during the experiment. In case of slight motor response, an additional injection of urethane at 50% of the initial dose was administered. The respiratory and cardiac rates were monitored during the whole experiment, and a heating blanket was used to avoid hypothermia. Because we were interested in evaluating $A\beta$ effects on NMDA-dependent synaptic plasticity, we chose urethane as the anaesthetic agent, taking into account that it has been reported to have no significant effects on NMDA-type glutamate receptors when given in intermediate doses [51, 52]; however, anaesthetic doses of urethane depress or even abolish 7-12 Hz atropine-resistant theta activity [53], but left 4-7 Hz atropine-sensitive theta oscillations unaltered. Longitudinal fronto-occipital incision, followed by connective and muscle tissue dissection, was used to expose the skull. Two holes were drilled in parietal bones: one for inserting a

recording electrode aimed at left CA1 (stereotaxic coordinates from the bregma: $AP = -3.8$ mm, $L = 2.5$ mm, left) and one for inserting a stimulating electrode aimed at right CA3 (stereotaxic coordinates from the bregma: $AP = -3.8$ mm, $L = 3.7$ mm, right) [54]. In order to reduce variability between subjects, we always use the same electrode configuration. The dura mater was cut and removed through the holes in order to allow electrode insertion (Figure 1(b)).

2.5. In Vivo Extracellular Electrophysiology. A microelectrode cannula (a 5 MΩ impedance enamel-coated wire attached to a 25-G needle), for local field potential (LFP) recording and microinjection, was inserted 2.5 mm from the pial surface, through the skull hole for left CA1 (vide supra for stereotaxic coordinates), using a hydraulic micromanipulator (SM-25C, Narishige Inc., Tokyo, Japan). A stimulating concentric bipolar electrode was lowered 3.5 mm from the pial surface, through the skull hole for right CA3 (vide supra for stereotaxic coordinates), using a micromanipulator (SM-25A, Narishige Inc., Tokyo, Japan). A silver electrode was placed in neck musculature as a reference.

CA1 field activity was magnified (100x) using an AC-coupled preamplifier (NEX-1, Biomedical Engineering, New York, USA). The preamplified signal was then band-pass filtered (0.1 Hz and 10 kHz cut-off frequencies) and further amplified at 20x (yielding 2000x total gain). This conditioned signal was digitized using an analogue-to-digital converter (DigiData 1200, Molecular Devices, San José, USA) with 10 kHz sampling frequency and stored for offline analysis using commercial (Clampfit, Molecular Devices, San José, USA) and purpose-designed software.

CA3 was stimulated by applying 100 μs monophasic square pulses, delivered at 0.33 Hz frequency, using a stimulus isolation unit (Isolator-11, Molecular Devices, San José, USA), controlled by a pulse generator (9514 Plus, Quantum Composers, Bozeman, USA). Stimulus intensity (100-400 μA) was adjusted so as to obtain stable and reliable CA1 field excitatory postsynaptic potentials (fEPSP). The depth of the stimulating and recording electrodes from the pial surface was finely adjusted so as to obtain short latency fEPSP, with a waveform characteristic of CA1 stratum pyramidale.

Once a stable CA1 fEPSP was achieved, threshold stimulus intensity was established by decreasing the intensity to one-half the previous one until the fEPSP failure rate was equal to or higher than 50% (characteristically 50 to 200 μA). Stimulus intensity was then successively doubled until fEPSP response saturation was attained (characteristically 4 to 8 times the threshold intensity). Then, the stimulus intensity required to obtain ~50% of maximal response (I_{50}) was selected to evaluate short- and long-term plasticity from then on. Basal synaptic activity was characterized by recording CA3 stimulation-evoked fEPSP in CA1 (I_{50} intensity, 100 μs duration, and 0.1 Hz frequency) for 30 min. Intrahippocampal microinjection effect on basal synaptic activity was characterized by recording such fEPSP for 30 min after microinjection. Long-term potentiation at cCA3-to-CA1 synapses was induced by delivering six trains (1 s length, 100 Hz frequency) at 60 s intertrain intervals (HFS). HFS

effect on cCA3-to-CA1 synaptic efficiency was studied by recording left CA1 response to right CA3 stimulation (I_{50} intensity, 100 μs duration, and 0.1 Hz frequency) for 60 min. Deep anaesthetic level was maintained throughout the whole recording session using supplementary anaesthetic doses (about every 4 hours) to attain stable and reliable activity in CA1 [55].

Once the recording session ended, a terminal dose of anaesthesia (urethane 2 g/kg and xylazine 10 mg/kg, intraperitoneal) was given and the location of stimulating and recording electrode tips was marked by passing continuous current through them delivered by a precision current source (Midgard, Stoelting, Wood Dale, USA). The subject's brain was removed and submerged in 4% paraformaldehyde for 3 days; then, 100 μm thick coronal slices encompassing stimulating and recording sites were obtained using a vibratome (1000 Plus, Vibratome, Bannockburn, USA). The electrodes' position and diffusion trace of microinjection coloured solution were documented by examining the slices with a stereoscope (SZX16, Olympus, Tokyo, Japan) and taking digital photographs (Cybershot DSCW7, Sony, Tokyo, Japan) under oblique back-illumination (Figure 1(c)).

2.6. Preparation of Vehicle and Aβ Peptide Solutions. Among many soluble Aβ species, $A\beta_{25-35}$ and $A\beta_{1-40}$ (Sigma-Aldrich, St. Louis, USA) were chosen for the present work on the basis of their aggregation kinetics, neurotoxicity, and pathogenicity. On the one hand, postmortem examination of AD patients' brains yielded that $A\beta_{1-40}$ accounts for approximately 90% of total Aβ peptide in senile plaques [56]. On the other hand, $A\beta_{25-35}$ aggregates more rapidly and displays more neurotoxicity than $A\beta_{1-40}$ [13, 57]. $A\beta_{25-35}$ and $A\beta_{1-40}$ peptides were prepared as previously described [22, 43, 45]. Briefly, peptides were dissolved in 0.9% normal saline solution with 0.5% methylene blue to 1.5 mM concentration and stored at -20°C. Aliquots were defrosted and incubated at 37°C for 24 h before experiments [58, 59]. The vehicle solution was therefore 0.9% normal saline with 0.5% methylene blue. Methylene blue was used to attest adequate diffusion in the hippocampal CA1 region of either vehicle or Aβ peptides (Figure 1(d)).

2.7. Intrahippocampal Microinjection. Once a baseline recording was obtained, a Hamilton syringe connected through 12-G tubing was used to inject 2 μL of the designed solution (either vehicle, $A\beta_{25-35}$, or $A\beta_{1-40}$) at a 1 μL/min rate through the microelectrode cannula inserted in the left hippocampal CA1 region. $A\beta_{25-35}$ and $A\beta_{1-40}$ dose (3 nM) and total injection volume (2 μL) were chosen according to previous reports [60–63]. Stimulation and recording were restarted three minutes after microinjection in order to allow diffusion and prevent leakage of injected solution.

2.8. Data Analysis. Electrophysiological data analyses were planned to characterize the effects of both microinjected solutions on basal cCA3-to-CA1 synaptic responses, cCA3-to-CA1 long-term plasticity, and CA1 oscillatory activity. To do so, recordings were divided into 5 min windows around stimulation events and analysed in time, frequency,

(a)

(b)

(c)

(d)
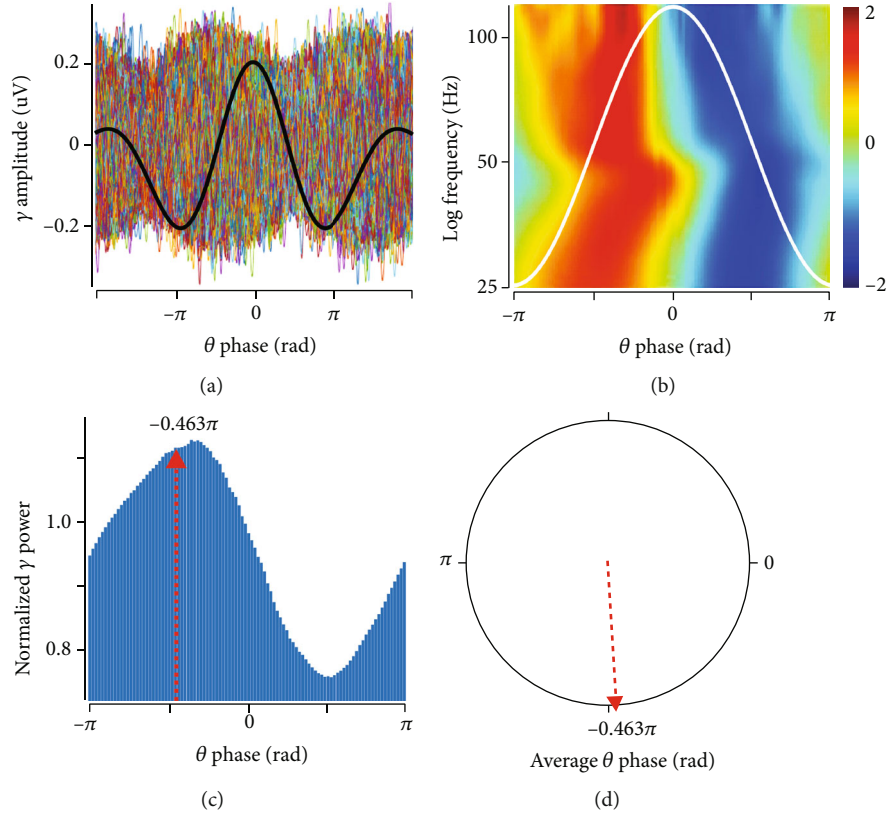
FIGURE 2: θ-to-γ phase-amplitude coupling (PAC) analysis process. (a) Filtered LFP in θ (black trace) and γ bands (coloured traces) are represented; θ trace is the average of n theta cycles, aligned around their maximum amplitude (downscaled to fit γ amplitude); each θ cycle-concurrent γ activity is presented in superposition using the abovementioned alignment. (b) Average normalized γ band scalogram (colour scale) relative to the θ phase (illustrated as a white trace). (c) Normalized γ band spectral power average as a function of the θ phase. (d) Average vector of (c) indicating dominant-phase θ-to-γ PAC.

and time-frequency domains. Time domain analysis was related to fEPSP first component slope measurement. Frequency domain analysis was focused on calculating relative power spectral density (rPSD) in δ (0.5-3.9 Hz), θ (4-7.9 Hz), α (8-11.9 Hz), β (12-24.9 Hz), γ (25-120 Hz), HFO_1 (121-250 Hz), and HFO_2 (250-500 Hz) bands, using Welch's method. Time-frequency domain analysis was done by building scalograms for each window, using the Morse wavelet decomposition [64, 65]; then, γ band scalogram averages were triggered by each θ cycle time window to determine phase-amplitude coupling (PAC) [66] (Figure 2). Detailed information about mathematical data processing, which was done using self-written scripts using MATLAB R2017a® (The MathWorks, Inc., Natick, Massachusetts, USA), can be found in Supplementary Materials (available here).

2.9. Statistics. According to data distribution normality, determined using the Shapiro-Wilk test, long-term plasticity and PSD data from experimental groups were compared using either one-way ANOVA or Kruskal-Wallis one-way analysis of variance by rank modules of SigmaPlot 12.0 (Systat Software, Inc., San José, California, USA). Variability of cCA3-to-CA1 synaptic responses from experimental groups was compared using Levene's test [67]. The resulting angle from the average PAC vector in the experimental

groups was compared using the MATLAB toolbox for circular statistics [68].

3. Results

3.1. Aβ Did Not Alter Synaptic Efficiency but Induced Changes in Synaptic Variability. No significant difference was found between the experimental groups during baseline recording before ($H_{(2)} = 0.153$, $p = 0.797$, $n = 16$) or after intrahippocampal injection ($F_{(2,13)} = 1.541$, $p = 0.251$, $n = 16$: Figure 3(a)). However, fEPSP slope variability significantly changed after intrahippocampal injection ($F_{(2,461)} = 64.898$, $p < 0.001$, $n = 16$); *post hoc* analysis showed that Aβ_{1-40} microinjection significantly increased cCA3-to-CA1 synaptic variability more than the other treatments (control *vs.* Aβ_{25-35}: $F_{(1,317)} = 0.004$, $p = 0.951$, $n = 11$; control *vs.* Aβ_{1-40}: $F_{(1,287)} = 71.932$, $p < 0.001$, $n = 10$; and Aβ_{1-40}*vs.* Aβ_{25-35}: $F_{(1,318)} = 86.351$, $p < 0.001$, $n = 11$). Variability progressively increased in control and Aβ_{25-35} groups after both injection (control: $F_{(1,606)} = 19.232$, $p < 0.001$, $n = 5$; Aβ_{25-35}: $F_{(1,636)} = 23.761$, $p < 0.0001$, $n = 6$) and HFS (control: $F_{(1,438)} = 63.522$, $p < 0.0001$, $n = 5$; Aβ_{25-35}: $F_{(1,438)} = 49.588$, $p < 0.0001$, $n = 6$). By contrast, even though variability in the Aβ_{1-40} group increased substantially after being injected

(a)

(b)
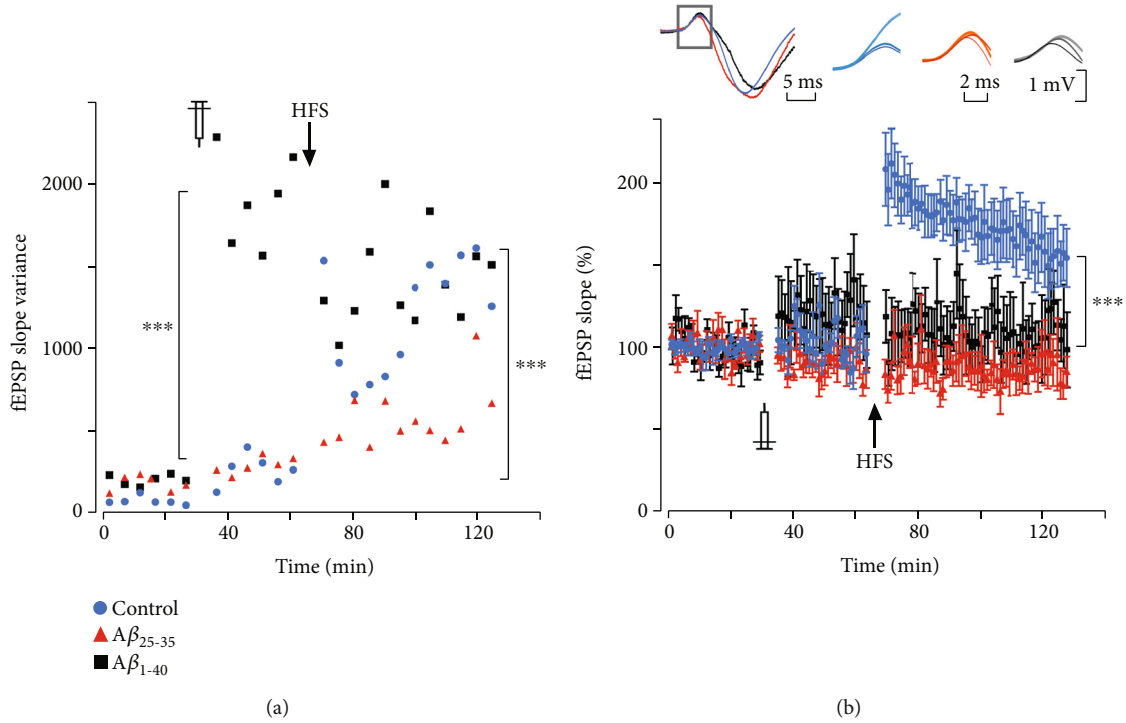
FIGURE 3: Intrahippocampal Aβ injections altered synaptic variability and impaired LTP in cCA3-to-CA1 synapse. Temporal evolution of slope variability (a) and magnitude (b) of cCA3 stimulation-evoked EPSP in CA1 recorded along three consecutive experimental stages, from left to right: (1) 30 min before peptide injection (baseline), (2) 30 min after intrahippocampal injection, and (3) after HFS (six 1 s, 100 Hz trains, delivered every 60 s). EPSP variability increased after intrahippocampal injection, being significantly higher in the Aβ_{1-40} group. HFS induced significant LTP in vehicle-injected subjects but not in Aβ-injected ones. In (a), each dot represents 5 min variance of slope; in (b), each dot illustrates 2 min mean ± standard error of the mean (SEM). Inset in (b): left—representative whole CA1 fEPSP average from each experimental group evoked by I_{50} stimuli delivered in contralateral CA3 (the region representing the monosynaptic component is outlined by a gray rectangular box); right—three sets of average traces (10 trials per average) of the monosynaptic component of cCA3 stimulation-evoked CA1 field potential obtained during baseline (thin line, dark colour), after intrahippocampal injection (intermediate line, intermediate colour), and after HFS (thick line, light colour) for each experimental group (control, blue; Aβ_{25-35}, red; and Aβ_{1-40}, black). ***Significant differences between groups ($p < 0.001$). Data from each experimental group were normalized respecting the average value obtained during the last 15 min of baseline.

($F_{(1,606)} = 299.08$, $p < 0.0001$, $n = 5$), it did not change after HFS ($F_{(1,438)} = 0.63$, $p = 0.428$, $n = 5$).

3.2. Aβ Impaired Long-Term Synaptic Plasticity. HFS induced significant fEPSP slope increase in vehicle-injected subjects (from $100 \pm 0.91\%$ to $198.8 \pm 14\%$, $H_{(2)} = 9.5$, $p = 0.009$, $n = 5$). By contrast, both Aβ_{25-35} and Aβ_{1-40} impaired such HFS-induced fEPSP slope increase (Aβ_{25-35}: from $100 \pm 1.29\%$ to $89.45 \pm 16\%$, $F_{(2,17)} = 0.504$, $p = 0.614$, $n = 6$; Aβ_{1-40}: from $100 \pm 1.84\%$ to $113.5 \pm 25\%$, $F_{(2,17)} = 0.938$, $p = 0.418$, $n = 5$; Figure 3(b)). Indeed, fEPSP slope change after HFS was significantly different between groups ($F_{(2,15)} = 17.741$, $p < 0.001$, $n = 16$); post hoc analysis (Tukey's test) showed that vehicle-injected subjects displayed fEPSP slope increase significantly greater than Aβ_{25-35}- and Aβ_{1-40}-injected ones (control vs. Aβ_{25-35}: $Q = 8.146$, $p < 0.001$, $n = 11$; control vs. Aβ_{1-40}: $Q = 6.083$, $p = 0.002$, $n = 10$), while these later groups were not significantly different to each other ($Q = 1.792$, $p = 0.437$, $n = 11$). These results show that soluble Aβ microinjection impairs cCA3-to-CA1 long-term synaptic plasticity.

3.3. Aβ_{25-35} Induced Increase in γ and HFO$_1$ Band Relative PSD. Intrahippocampal injection of Aβ_{25-35} induced significant increases in relative PSD (Figure 4) in γ (Figure 4(a), left column, $F_{(2,11)} = 8.237$, $p = 0.007$, $n = 17$) and HFO$_1$ (Figure 4(b), left column, $H_{(2)} = 6.408$, $p = 0.029$, $n = 17$) bands, but not in other bands. Neither Aβ_{1-40} nor vehicle injection induced significant changes in relative PSD in any band (Suppl. Table 1). In Aβ_{25-35}-injected subjects, HFS did not induce additional changes in γ (Figure 4(a), right column; 5 min: $F_{(2,11)} = 3.036$, $p = 0.089$; 30 min: $H_{(2)} = 1.96$, $p = 0.403$; and 60 min: $F_{(2,11)} = 1.502$, $p = 0.265$), HFO$_1$ (Figure 4(b), right column; 5 min: $F_{(2,11)} = 0.063$, $p = 0.940$; 30 min: $F_{(2,11)} = 0.224$, $p = 0.803$; and 60 min: $F_{(2,11)} = 0.341$, $p = 0.718$), or any other band. HFS did not induce significant changes in relative PSD in any band in vehicle- or Aβ_{1-40}-injected subjects (Suppl. Table 2). In summary, only Aβ_{25-35}, which is the more toxic soluble species of Aβ, induced increased energy contribution in gamma and HFO$_1$ bands, but HFS did not further modify such changes.
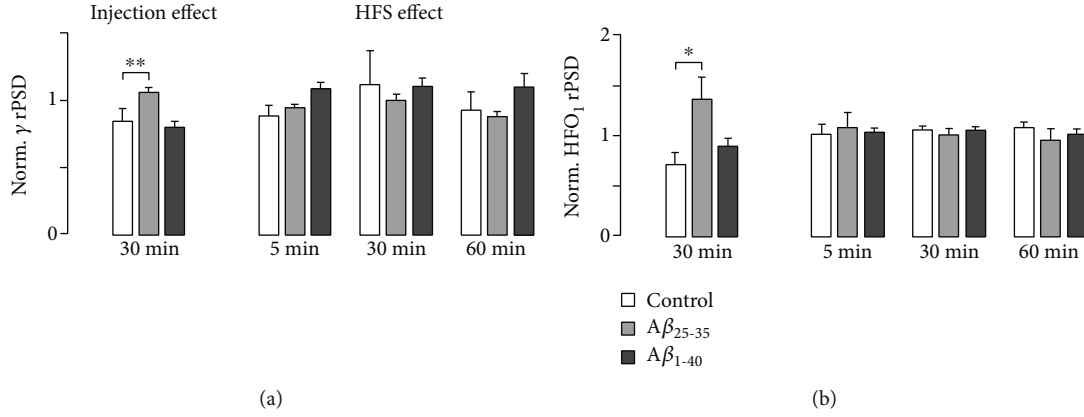
FIGURE 4: Peptide injection but not HFS increased rPSD in γ and HFO1 bands. Bar diagrams illustrating rPSD in γ (a) and HFO1 (b) bands. The left panel shows the effect of peptide or vehicle, 30 min after injection, normalized respecting baseline rPSD in the same bands. The right panel shows the effect of HFS normalized regarding rPSD calculated after injection in the same bands. Bars and whiskers represent each group's mean + SEM. *Significant difference respecting the control group during baseline ($p < 0.05$); **significant difference respecting each group after peptide injection ($p < 0.01$).
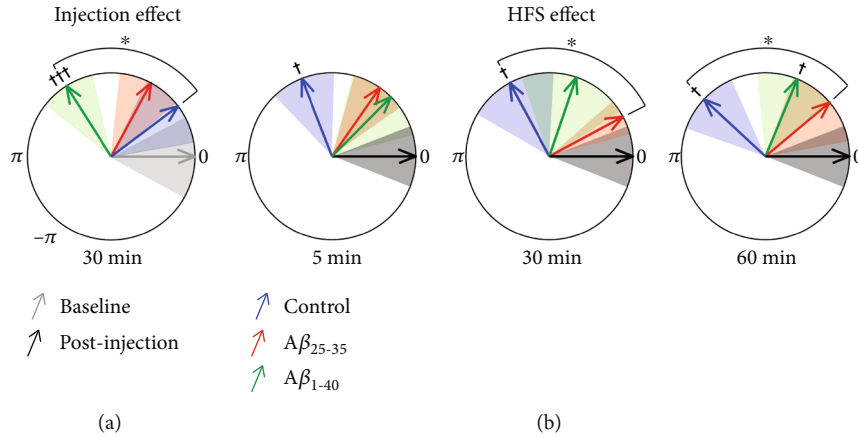
FIGURE 5: Peptide injection and HFS shifted the θ-to-γ PAC average phase vector. (a) Circular diagram illustrating the intrahippocampal microinjection-induced shift of the θ-to-γ PAC average phase vector for each group respecting the baseline vector. (b) Circular diagrams illustrating the time evolution (at 5, 30, and 60 min) of HFS-induced shift of the θ-to-γ PAC average phase vector for each group respecting the microinjection vector. Coloured arrows indicate average vector angles (control, blue; Aβ25-35, red; and Aβ1-40, green); correspondingly coloured shaded areas illustrate the standard error of angles for each group. Significant differences relative to the reference vector ($^\dagger p < 0.05$, $^{\dagger\dagger\dagger} p < 0.001$); significant differences between groups ($^* p < 0.05$).

3.4. Aβ Injection Shifted θ-γ Phase-Amplitude Coupling but Impaired HFS-Induced Shift.

To determine if the γ amplitude was linked to the θ phase at the hippocampus, different approaches can be used to calculate PAC. In this case, we calculated the average high-frequency γ power over the modulating low band in θ individual cycles. This method is especially useful when the modulating band is not constant over the length of the experiment. The power distribution was obtained by averaging the entire band, and this average gives a single value for the modulation between the pairs of frequency bands (γ-θ) (for details, see Figure 2 and Supplementary Materials).

Aβ_{1-40} injection induced a significant γ amplitude-modulating θ phase shift ($\sim 122°$; $F_{(1,8)} = 37.220$, $p < 0.001$); neither vehicle ($F_{(1,6)} = 1.59$, $p = 0.254$) nor Aβ_{25-35} ($F_{(1,9)} = 3.26$, $p = 0.104$) injection induced significant shifts in such modulating phase (Figure 5(a)). Planned intergroup comparisons showed that the Aβ_{1-40} injection-induced phase shift was significantly greater than vehicle injection-induced ($F_{(1,6)} = 7.71$, $p = 0.03$) and Aβ_{25-35} injection-induced ($F_{(1,9)} = 4.76$, $p = 0.05$) phase shifts; vehicle and Aβ_{25-35} injection-induced phase shifts were not significantly different to each other ($F_{(1,7)} = 0.43$, $p = 0.53$).

Taking each group injection-induced phase shift as a reference, it was found that HFS induced a significant phase shift (~ 112-$137°$) in vehicle-injected subjects (Figure 5(b), blue arrows; $F_{(3,16)} = 4.47$, $p = 0.002$); this phase shift persisted for up to 1 h after HFS (5 min: $F_{(1,4)} = 9.25$, $p = 0.038$; 30 min: $F_{(1,4)} = 7.07$, $p = 0.05$; and 60 min: $F_{(1,4)} = 13.11$, $p = 0.022$). In Aβ_{1-40}-injected subjects, HFS induced a smaller phase shift (~ 45-$70°$) that reached significance only 60 min

later ($F_{(3,16)} = 1.21$, $p = 0.338$; 5 min: $F_{(1,8)} = 0.72$, $p = 0.421$; 30 min: $F_{(1,8)} = 0.82$, $p = 0.392$; and 60 min: $F_{(1,8)} = 5.55$, $p = 0.046$). By contrast, HFS did not induce a significant phase shift in $A\beta_{25-35}$-injected animals ($F_{(3,16)} = 1.03$, $p = 0.4073$; 5 min: $F_{(1,8)} = 2.75$, $p = 0.136$; 30 min: $F_{(1,8)} = 0.92$, $p = 0.366$; and 60 min: $F_{(1,8)} = 0.25$, $p = 0.631$).

4. Discussion

This experiment's main findings were that, even though intrahippocampal microinjection of soluble species of $A\beta$ did not change basal transmission, it significantly affected several other properties of cCA3-to-CA1 synapses: (1) $A\beta_{1-40}$ enhanced basal synaptic variability significantly more than other treatments did but impaired HFS-induced variability increase; (2) $A\beta_{25-35}$ injection significantly increased gamma and HFO1 band relative PSD; (3) both soluble amyloid beta peptides ($A\beta_{25-35}$ and $A\beta_{1-40}$) impaired HFS-induced LTP; and (4) $A\beta_{1-40}$ injection induced a significant γ amplitude-modulating θ phase shift (~122°) but, as $A\beta_{25-35}$ did, impaired the occurrence of a HFS-induced phase shift.

$A\beta$ peptides have been repeatedly highlighted as crucial AD pathogenetic initiators. Although the underlying mechanism is not yet fully understood, some studies have indicated that $A\beta$ can impair synaptic transmission and plasticity, leading to changes in spine density and, eventually, synaptic pruning [69–71]. We have found that intrahippocampal microinjection of soluble $A\beta$ in anaesthetized rats affected cCA3-CA1 synapse variability and impaired long-term synaptic plasticity. Overall, such results concur with those of other studies, which have shown that high $A\beta$ oligomer concentration interferes with synaptic efficiency and plasticity [61, 62, 72]. There is a mild increase in fEPSP slope variability after intrahippocampal injection of the vehicle. A similar effect has been observed in other types of *in vivo* preparations [73, 74], possibly due to a mechanical and osmotic effect of the saline solution. Another possibility of that change may involve methylene blue; however, the toxic effects of this molecule *in vitro* have been reported at concentrations higher than 100 μM (around ten times our preparation) [75, 76]. Methylene blue might inhibit $A\beta$ oligomerization in a dose-dependent manner (ranging from 0.01 to 445 μM), but that effect is observed only after several days of incubation (4 to 8 days) [77]. We found that injection of $A\beta_{1-40}$, but not $A\beta_{25-35}$, induces significant increases in variability in cCA3-to-CA1 synaptic responses without significant changes in fEPSP slope. In agreement with our results, several *in vivo* studies found that the injection of different amyloid species did not affect hippocampal baseline synaptic potential amplitude or slope [60, 74, 78]. Synaptic variability is determined, among many factors, by presynaptic axonal noise, as well as release probability fluctuations [79]. On the one hand, $A\beta_{1-42}$ has been found to induce spike widening, which would increase synaptic release due to increased calcium influx into presynaptic boutons [80]; $A\beta_{25-35}$ has also been reported to produce spike broadening, but using doses one order of magnitude higher than the one used in our experiment [81]. On the other hand, $A\beta_{1-42}$ oligomers depress release probability

at CA3-CA1 synapses [82]; moreover, glutamatergic synaptic transmission could be either enhanced or reduced by $A\beta_{1-40}$, depending on its concentration and the specific pyramidal cell type affected [44]. Such opposing mechanisms could explain the observed $A\beta_{1-40}$-induced synaptic variability increase, without significant changes in average fEPSP slope. It is plausible that the $A\beta_{25-35}$ concentration we used was not enough to induce significant changes in synaptic variability (however, it did affect other synaptic and network properties).

Although neither $A\beta$-intrahippocampal injection nor HFS induced significant CA1 global power spectrum changes (Suppl. Tables 3 and 4), specific frequency band rPSD computation evidenced that injection with $A\beta_{25-35}$, but not $A\beta_{1-40}$ nor HFS, induced a significant γ and HFO1 relative power increase. Transient (about 100 s) increases in γ and θ spectral power have been recorded in freely behaving adult rats' hippocampus immediately after LTP induction [32]. In the present experiment, such early PSD changes in control subjects were not detected given the 5 min window in our PSD analysis algorithm, which was not designed to detect short-lived changes.

Both γ oscillations and ripples (140-200 Hz) in the CA1 hippocampal region depend critically on the fast-spiking activity of parvalbumin- (PV-) expressing basket cells [83]. $A\beta$ oligomers have been shown to directly interact with receptor tyrosine-protein kinase erbB-4, increasing its phosphorylation state [84]; erbB-4 activation increases PV interneuron-dependent oscillatory activity [85]. PV interneurons' increased activity, which has been described during early stages of AD models in association with subtle cognitive deficits [86, 87], seems to represent an initial adaptive response to $A\beta$ oligomer deposition, which is followed later by PV interneuron dysfunction and more severe cognitive deficits [7, 88]. It is plausible that $A\beta_{25-35}$ has more affinity than $A\beta_{1-40}$ for erbB-4.

It has been found that γ band (25-120 Hz) activity increases in close association with locomotor behaviour [89, 90], working memory [91], and memory replay [92]. Hippocampal oscillations at frequencies higher than 100 Hz, also known as ripples (140-200 Hz), have been described to have several implications in cognitive processes [93]. In fact, ripples have been associated with learning and memory consolidation in humans and animals [94–97]. The observed soluble $A\beta$ species-induced modifications in γ band and ripple oscillations in neural circuits are, therefore, associated with synaptic dysfunction and cognitive impairments [47, 98–100].

Both $A\beta$ species used in our experiment ($A\beta_{25-35}$ and $A\beta_{1-40}$) impaired HFS-induced LTP in cCA3-to-CA1 synapses. This deleterious effect has been extensively reported, and many possible underlying mechanisms have been identified; among them, those pointing towards excitatory/inhibitory imbalance are relevant to our findings. $A\beta$-induced calcium dyshomeostasis underlies distorted synaptic transmission, plasticity, and oscillatory activity in the brain. However, depending on exposure time, brain region, oligomer type, and receptor subunits involved, soluble amyloid has been reported not only to inhibit calcium

influx through NMDA receptors in cultured hippocampal [101] or cortical neurons [102] but also to increase NMDA-mediated calcium influx in mouse brains *in vivo* [103]. In addition, deleterious effects of $A\beta_{1-42}$ and $A\beta_{1-40}$ on NMDA function and LTP are reverted by a specific GLUN2B receptor antagonist [104]. Acute *in vivo* and *ex vivo* $A\beta_{1-42}$ administration deteriorates $GABA_B$-mediated inhibitory transmission in CA3-to-CA1 synapses and impairs HFS-induced LTP of excitatory [48] as well as inhibitory potentials [105], and such effects are reverted by pharmacological activation of G-protein-gated inwardly rectifying potassium (GirK) channels. $A\beta_{25-35}$ has been found to act *ex vivo* as a GirK channel antagonist in CA3 pyramidal neurons [22]. $A\beta$-induced malfunction of NMDA and GirK channel conductance in pyramidal neurons might contribute, along with PV interneuron dysfunction, to hippocampal network instability, manifested through LTP impairment and aberrant rhythm generation, which may underlie subtle cognitive derailments observed during early AD stages.

Intrahippocampal injection of $A\beta_{1-40}$ significantly shifted the resulting angle from the average θ-to-γ PAC vector. In vehicle-injected subjects, HFS induced a significant phase shift of the average θ-to-γ PAC vector persisting up to 60 min. Besides impairing HFS-induced LTP, both $A\beta_{25-35}$ and $A\beta_{1-40}$ blocked the phase shift of the average θ-to-γ PAC vector, with the $A\beta_{25-35}$ effect persisting longer. Increases in θ-to-γ coupling have been described in freely behaving rats after HFS-induced LTP; in that experiment, acute $A\beta_{1-42}$ treatment not only impaired LTP but also diminished θ-to-γ coupling [40]. θ-nested γ oscillations in CA1 depend on out-of-phase firing sequences of PV interneurons, pyramidal cells, somatostatin-positive (SST) neurons, and CA3-activated feedforward inhibitory interneurons during population θ oscillations, eventually opening windows for synaptic plasticity during specific θ phases [106]. Perisomatic inhibition by PV interneurons, associated with temporal silencing of feedforward inhibition acted by SST interneurons, allows calcium spike-associated plasticity; conversely, dendritic inhibition by feedforward interneurons prevents calcium spikes but facilitates pyramidal neuron output [106, 107]. Phase synchronization of firing in such a network depends on the relative contribution of PV (γ band) and SST (θ band) interneurons [108]; therefore, θ-to-γ coupling phase shift represents specific variations in such contributions. The observed $A\beta$ injection-induced phase shift, as well as the impairment of HFS-induced phase shifts, may be due to its effect on PV interneurons [84, 85, 106] and on SST interneurons [108]. There may also be pyramidal cell contribution to such network dysfunction; in fact, $A\beta_{25-35}$ reduces $GABA_B$-dependent GirK channel activity in pyramidal neurons [22]; this may enhance excitatory pyramidal cell influence on PV and SST interneurons, which would further destabilize the network. Interestingly, in a recent clinical study, restoration of temporal cortex θ-to-γ PAC was associated with working memory performance improvement in older adults [109].

5. Conclusions

The present study results indicate that changes in the functional relationships between θ, γ, and ripple oscillatory network activity in the hippocampus are highly correlated with amyloid-induced synaptic plasticity dysfunction in a model of early amyloid-β pathology (similar to what has been reported in early AD stages). Taken together, these results show that intrahippocampal microinjection of soluble forms of $A\beta$ affects synaptic variability and plasticity and modifies neural processing and network activity, changes that might underlie cognitive deficits observed in early AD models. $A\beta$-induced derailment of the tight functional relationship in hippocampal circuits between θ oscillation (controlled by SST interneurons as well as by medial septum and entorhinal cortex inputs) and γ activity (controlled by PV interneurons) implies a dysregulation of the crosstalk of cholinergic, glutamatergic, and GABAergic systems during early AD stages, leading to impaired information processing and encoding. Therefore, the abnormality in θ-to-γ PAC hereby described is worth evaluating as a putative early biomarker of $A\beta$-induced synaptic dysfunction in AD, long before neurodegeneration is established.

AD is a chronic and complex neurological disorder that involves several mechanisms (i.e., neuroinflammation and oxidative stress) additional to amyloid pathology. For that reason, it is important to start considering the role of θ-to-γ PAC in behavioural models of AD that involve tauopathy and selective chronic neurodegeneration, as well as to test it in further clinical trials through noninvasive electrophysiological methods in patients with mild cognitive impairment and major neurocognitive disorder.

Data Availability

Additional data set can be sent by request. Detailed information of methods and results are included in Supplementary Materials.

Disclosure

A preliminary version of this work was presented as a poster in the Joint Meeting of International Brain Research Organization & Federation of Asian-Oceanian Neuroscience Societies.

Conflicts of Interest

The authors declare that they have no conflicts of interest.

Authors' Contributions

Mauricio O. Nava-Mesa and Alejandro Múnera contributed equally to this work.

Acknowledgments

Supplementary Materials

This section includes supplementary methods and supplementary data (Supplementary Tables 1–4). (*Supplementary Materials*)

References

[1] M. Goedert and M. G. Spillantini, "A century of Alzheimer's disease," *Science*, vol. 314, no. 5800, pp. 777–781, 2006.

[2] L. V. Colom, "Septal networks: relevance to theta rhythm, epilepsy and Alzheimer's disease," *Journal of Neurochemistry*, vol. 96, no. 3, pp. 609–623, 2006.

[3] J. J. Palop and L. Mucke, "Network abnormalities and interneuron dysfunction in Alzheimer disease," *Nature Reviews Neuroscience*, vol. 17, no. 12, pp. 777–792, 2016.

[4] R. W. Van Hooren, J. M. Riphagen, H. I. Jacobs, and Alzheimer's Disease Neuroimaging Initiative, "Inter-network connectivity and amyloid-beta linked to cognitive decline in preclinical Alzheimer's disease: a longitudinal cohort study," *Alzheimer's Research & Therapy*, vol. 10, no. 1, p. 88, 2018.

[5] F. C. Quevenco, S. J. Schreiner, M. G. Preti et al., "GABA and glutamate moderate beta-amyloid related functional connectivity in cognitively unimpaired old-aged adults," *Neuro-Image: Clinical*, vol. 22, article 101776, 2019.

[6] D. J. Selkoe, "Alzheimer's disease is a synaptic failure," *Science*, vol. 298, no. 5594, pp. 789–791, 2002.

[7] L. Verret, E. O. Mann, G. B. Hang et al., "Inhibitory interneuron deficit links altered network activity and cognitive dysfunction in Alzheimer model," *Cell*, vol. 149, no. 3, pp. 708–721, 2012.

[8] M. O. Nava-Mesa, L. Jiménez-Díaz, J. Yajeya, and J. D. Navarro-Lopez, "GABAergic neurotransmission and new strategies of neuromodulation to compensate synaptic dysfunction in early stages of Alzheimer's disease," *Frontiers in Cellular Neuroscience*, vol. 8, p. 167, 2014.

[9] L.-B. Gao, X.-F. Yu, Q. Chen, and D. Zhou, "Alzheimer's disease therapeutics: current and future therapies," *Minerva Medica*, vol. 107, no. 2, pp. 108–113, 2016.

[10] R. J. Caselli, T. G. Beach, D. S. Knopman, and N. R. Graff-Radford, "Alzheimer disease: scientific breakthroughs and translational challenges," *Presented at the Mayo Clinic Proceedings*, vol. 92, no. 6, pp. 978–994, 2017.

[11] T. Iwatsubo, A. Odaka, N. Suzuki, H. Mizusawa, N. Nukina, and Y. Ihara, "Visualization of Aβ42 (43) and Aβ40 in senile plaques with end-specific Aβ monoclonals: evidence that an initially deposited species is Aβ42 (43)," *Neuron*, vol. 13, no. 1, pp. 45–53, 1994.

[12] A. Güntert, H. Döbeli, and B. Bohrmann, "High sensitivity analysis of amyloid-beta peptide composition in amyloid deposits from human and PS2APP mouse brain," *Neuroscience*, vol. 143, no. 2, pp. 461–475, 2006.

[13] L. Millucci, L. Ghezzi, G. Bernardini, and A. Santucci, "Conformations and biological activities of amyloid beta peptide 25-35," *Current Protein and Peptide Science*, vol. 11, no. 1, pp. 54–67, 2010.

[14] C. J. Pike, A. J. Walencewicz-Wasserman, J. Kosmoski, D. H. Cribbs, C. G. Glabe, and C. W. Cotman, "Structure-activity analyses of beta-amyloid peptides: contributions of the beta 25-35 region to aggregation and neurotoxicity," *Journal of Neurochemistry*, vol. 64, no. 1, pp. 253–265, 1995.

[15] I. Kaneko, K. Morimoto, and T. Kubo, "Drastic neuronal loss in vivo by β-amyloid racemized at Ser 26 residue: conversion of non-toxic [D-Ser 26] β-amyloid 1–40 to toxic and proteinase-resistant fragments," *Neuroscience*, vol. 104, no. 4, pp. 1003–1011, 2001.

[16] M. Gruden, T. Davudova, M. Mališauskas et al., "Autoimmune responses to amyloid structures of Aβ(25–35) peptide and human lysozyme in the serum of patients with progressive Alzheimer's disease," *Dementia and Geriatric Cognitive Disorders*, vol. 18, no. 2, pp. 165–171, 2004.

[17] S. Varadarajan, J. Kanski, M. Aksenova, C. Lauderback, and D. A. Butterfield, "Different mechanisms of oxidative stress and neurotoxicity for Alzheimer's Aβ (1– 42) and Aβ (25– 35)," *Journal of the American Chemical Society*, vol. 123, no. 24, pp. 5625–5631, 2001.

[18] A. R. Korotzer, E. R. Whittemore, and C. W. Cotman, "Differential regulation by β-amyloid peptides of intracellular free Ca2+ concentration in cultured rat microglia," *European Journal of Pharmacology: Molecular Pharmacology*, vol. 288, no. 2, pp. 125–130, 1995.

[19] H. Hiruma, T. Katakura, S. Takahashi, T. Ichikawa, and T. Kawakami, "Glutamate and amyloid β-protein rapidly inhibit fast axonal transport in cultured rat hippocampal neurons by different mechanisms," *Journal of Neuroscience*, vol. 23, no. 26, pp. 8967–8977, 2003.

[20] R. Rönicke, A. Klemm, J. Meinhardt, U. H. Schröder, M. Fändrich, and K. G. Reymann, "Aβ mediated diminution of MTT reduction—an artefact of single cell culture?," *PLoS One*, vol. 3, no. 9, article e3236, 2008.

[21] H. Moreno, W. E. Wu, T. Lee et al., "Imaging the Aβ-related neurotoxicity of Alzheimer disease," *Archives of Neurology*, vol. 64, no. 10, pp. 1467–1477, 2007.

[22] M. O. Nava-Mesa, L. Jiménez-Díaz, J. Yajeya, and J. D. Navarro-Lopez, "Amyloid-β induces synaptic dysfunction through G protein-gated inwardly rectifying potassium channels in the fimbria-CA3 hippocampal synapse," *Frontiers in Cellular Neuroscience*, vol. 7, p. 117, 2013.

[23] F. Sotty, M. Danik, F. Manseau, F. Laplante, R. Quirion, and S. Williams, "Distinct electrophysiological properties of glutamatergic, cholinergic and GABAergic rat septohippocampal neurons: novel implications for hippocampal rhythmicity," *The Journal of Physiology*, vol. 551, no. 3, pp. 927–943, 2009.

[24] E. C. Fuchs, A. R. Zivkovic, M. O. Cunningham et al., "Recruitment of parvalbumin-positive interneurons determines hippocampal function and associated behavior," *Neuron*, vol. 53, no. 4, pp. 591–604, 2007.

[25] G. Buzsáki and A. Draguhn, "Neuronal oscillations in cortical networks," *Science*, vol. 304, no. 5679, pp. 1926–1929, 2004.

[26] O. Jensen and L. L. Colgin, "Cross-frequency coupling between neuronal oscillations," *Trends in Cognitive Sciences*, vol. 11, no. 7, pp. 267–269, 2007.

[27] F. P. Battaglia, K. Benchenane, A. Sirota, C. M. Pennartz, and S. I. Wiener, "The hippocampus: hub of brain network communication for memory," *Trends in Cognitive Sciences*, vol. 15, no. 7, pp. 310–318, 2011.

[28] A. Gruart, M. D. Muñoz, and J. M. Delgado-García, "Involvement of the CA3–CA1 synapse in the acquisition of associative learning in behaving mice," *Journal of Neuroscience*, vol. 26, no. 4, pp. 1077–1087, 2006.

[29] A. Gruart and J. M. Delgado-García, "Activity-dependent changes of the hippocampal CA3–CA1 synapse during the acquisition of associative learning in conscious mice," *Genes, Brain and Behavior*, vol. 6, no. s1, pp. 24–31, 2007.

[30] J. M. Muñoz-Cabrera, A. G. Sandoval-Hernández, A. Niño et al., "Bexarotene therapy ameliorates behavioral deficits and induces functional and molecular changes in very-old triple transgenic mice model of Alzheimer´s disease," *PLoS One*, vol. 14, no. 10, article e0223578, 2019.

[31] R. T. Wicks, M. R. Witcher, D. E. Couture et al., "Hippocampal CA1 and CA3 neural recording in the human brain: validation of depth electrode placement through high-resolution imaging and electrophysiology," *Neurosurgical Focus*, vol. 49, no. 1, article E5, 2020.

[32] A. Bikbaev and D. Manahan-Vaughan, "Relationship of hippocampal theta and gamma oscillations to potentiation of synaptic transmission," *Frontiers in Neuroscience*, vol. 2, no. 1, pp. 56–63, 2008.

[33] A. Bikbaev and D. Manahan-Vaughan, "Metabotropic glutamate receptor, mGlu5, regulates hippocampal synaptic plasticity and is required for tetanisation-triggered changes in theta and gamma oscillations," *Neuropharmacology*, vol. 115, pp. 20–29, 2017.

[34] D. Habib, C. K. Tsui, L. G. Rosen, and H. C. Dringenberg, "Occlusion of low-frequency-induced, heterosynaptic long-term potentiation in the rat hippocampus in vivo following spatial training," *Cerebral Cortex*, vol. 24, no. 11, pp. 3090–3096, 2014.

[35] M. J. Jutras, P. Fries, and E. A. Buffalo, "Oscillatory activity in the monkey hippocampus during visual exploration and memory formation," *Proceedings of the National Academy of Sciences of the United States of America*, vol. 110, no. 32, pp. 13144–13149, 2013.

[36] F. Peña-Ortega, "Amyloid beta-protein and neural network dysfunction," *Journal of Neurodegenerative Diseases*, vol. 2013, Article ID 657470, 8 pages, 2013.

[37] V. Nimmrich, A. Draguhn, and N. Axmacher, "Neuronal network oscillations in neurodegenerative diseases," *Neuromolecular Medicine*, vol. 17, no. 3, pp. 270–284, 2015.

[38] J. Wang, Y. Fang, X. Wang, H. Yang, X. Yu, and H. Wang, "Enhanced gamma activity and cross-frequency interaction of resting-state electroencephalographic oscillations in patients with Alzheimer's disease," *Frontiers in Aging Neuroscience*, vol. 9, p. 243, 2017.

[39] R. Goutagny, N. Gu, C. Cavanagh et al., "Alterations in hippocampal network oscillations and theta–gamma coupling arise before Aβ overproduction in a mouse model of Alzheimer's disease," *European Journal of Neuroscience*, vol. 37, no. 12, pp. 1896–1902, 2013.

[40] A. N. Kalweit, H. Yang, J. Colitti-Klausnitzer et al., "Acute intracerebral treatment with amyloid-beta (1–42) alters the profile of neuronal oscillations that accompany LTP induction and results in impaired LTP in freely behaving rats," *Frontiers in Behavioral Neuroscience*, vol. 9, p. 103, 2015.

[41] I. Sánchez-Rodríguez, S. Temprano-Carazo, A. Nájera et al., "Activation of G-protein-gated inwardly rectifying potassium (Kir 3/Gir K) channels rescues hippocampal functions in a mouse model of early amyloid-β pathology," *Scientific Reports*, vol. 7, no. 1, pp. 1–13, 2017.

[42] A. N. Kalweit, B. Amanpour-Gharaei, J. Colitti-Klausnitzer, and D. Manahan-Vaughan, "Changes in neuronal oscillations accompany the loss of hippocampal LTP that occurs in an animal model of psychosis," *Frontiers in Behavioral Neuroscience*, vol. 11, p. 36, 2017.

[43] J. Santos-Torres, A. Fuente, J. M. Criado, A. S. Riolobos, M. Heredia, and J. Yajeya, "Glutamatergic synaptic depression by synthetic amyloid β-peptide in the medial septum," *Journal of Neuroscience Research*, vol. 85, no. 3, pp. 634–648, 2007.

[44] Y. Wang, T. H. Zhou, Z. Zhi, A. Barakat, L. Hlatky, and H. Querfurth, "Multiple effects of β-amyloid on single excitatory synaptic connections in the PFC," *Frontiers in Cellular Neuroscience*, vol. 7, p. 129, 2013.

[45] S. Ashenafi, A. Fuente, J. Criado, A. Riolobos, M. Heredia, and J. Yajeya, "β-Amyloid peptide 25–35 depresses excitatory synaptic transmission in the rat basolateral amygdala 'in vitro'," *Neurobiology of Aging*, vol. 26, no. 4, pp. 419–428, 2005.

[46] J. J. Palop and L. Mucke, "Amyloid-β–induced neuronal dysfunction in Alzheimer's disease: from synapses toward neural networks," *Nature Neuroscience*, vol. 13, no. 7, pp. 812–818, 2010.

[47] A. I. Gutiérrez-Lerma, B. Ordaz, and F. Peña-Ortega, "Amyloid beta peptides differentially affect hippocampal theta rhythms in vitro," *International Journal of Peptides*, vol. 2013, Article ID 328140, 11 pages, 2013.

[48] I. Sánchez-Rodríguez, S. Djebari, S. Temprano-Carazo et al., "Hippocampal long-term synaptic depression and memory deficits induced in early amyloidopathy are prevented by enhancing G-protein-gated inwardly-rectifying potassium channel activity," *Journal of Neurochemistry*, vol. 153, no. 3, pp. 362–376, 2020.

[49] C. Kilkenny, W. Browne, I. C. Cuthill, M. Emerson, and D. G. Altman, "Animal research: reporting in vivo experiments: the ARRIVE guidelines," *British Journal of Pharmacology*, vol. 160, no. 7, pp. 1577–1579, 2010.

[50] J. Charan and N. Kantharia, "How to calculate sample size in animal studies?," *Journal of Pharmacology & Pharmacotherapeutics*, vol. 4, no. 4, pp. 303–306, 2013.

[51] K. Hara and R. A. Harris, "The anesthetic mechanism of urethane: the effects on neurotransmitter-gated ion channels," *Anesthesia & Analgesia*, vol. 94, no. 2, pp. 313–318, 2002.

[52] M. P. Sceniak and M. B. Mac Iver, "Cellular actions of urethane on rat visual cortical neurons in vitro," *Journal of Neurophysiology*, vol. 95, no. 6, pp. 3865–3874, 2006.

[53] R. Kramis, C. H. Vanderwolf, and B. H. Bland, "Two types of hippocampal rhythmical slow activity in both the rabbit and the rat: relations to behavior and effects of atropine, diethyl ether, urethane, and pentobarbital," *Experimental Neurology*, vol. 49, no. 1, pp. 58–85, 1975.

[54] G. Paxinos and C. Watson, *A Stereotaxic Atlas of the Rat Brain*, Academic, New York, NY, USA, 1998.

[55] S. Zandieh, R. Hopf, H. Redl, and M. G. Schlag, "The effect of ketamine/xylazine anesthesia on sensory and motor evoked potentials in the rat," *Spinal Cord*, vol. 41, no. 1, pp. 16–22, 2003.

[56] C. Morgan, M. Colombres, M. T. Nuñez, and N. C. Inestrosa, "Structure and function of amyloid in Alzheimer's disease," *Progress in Neurobiology*, vol. 74, no. 6, pp. 323–349, 2004.

[57] L. Millucci, R. Raggiaschi, D. Franceschini, G. Terstappen, and A. Santucci, "Rapid aggregation and assembly in aqueous solution of Aβ (25–35) peptide," *Journal of Biosciences*, vol. 34, no. 2, pp. 293–303, 2009.

[58] F. Peña, B. Ordaz, H. Balleza-Tapia et al., "Beta-amyloid protein (25–35) disrupts hippocampal network activity: role of Fyn-kinase," *Hippocampus*, vol. 20, no. 1, pp. 78–96, 2010.

[59] R. N. Leão, L. V. Colom, L. Borgius, O. Kiehn, and A. Fisahn, "Medial septal dysfunction by Aβ-induced KCNQ channel-block in glutamatergic neurons," *Neurobiology of Aging*, vol. 33, no. 9, pp. 2046–2061, 2012.

[60] A. W. Schmid, M. A. Lynch, and C. E. Herron, "The effects of IL-1 receptor antagonist on beta amyloid mediated depression of LTP in the rat CA1 in vivo," *Hippocampus*, vol. 19, no. 7, pp. 670–676, 2009.

[61] A. V. Goryacheva, S. V. Kruglov, M. G. Pshennikova et al., "Adaptation to intermittent hypoxia restricts nitric oxide overproduction and prevents beta-amyloid toxicity in rat brain," *Nitric Oxide*, vol. 23, no. 4, pp. 289–299, 2010.

[62] S. Hajipour, A. Sarkaki, Y. Farbood, A. Eidi, P. Mortazavi, and Z. Valizadeh, "Effect of gallic acid on dementia type of Alzheimer disease in rats: electrophysiological and histological studies," *Basic and Clinical Neuroscience*, vol. 7, no. 2, pp. 97–106, 2016.

[63] M. Y. Stepanichev, A. Ivanov, N. Lazareva, and N. Gulyaeva, "Neurodegenerative changes induced by injection of ß-amyloid peptide fragment (25-35) in hippocampus are associated with NGF-signalling activation," *Bulletin of Russian State Medical University*, vol. 1, no. 1, 2016.

[64] M. Le Van Quyen and A. Bragin, "Analysis of dynamic brain oscillations: methodological advances," *Trends in Neurosciences*, vol. 30, no. 7, pp. 365–373, 2007.

[65] J. M. Lilly and S. C. Olhede, "Generalized Morse wavelets as a superfamily of analytic wavelets," *IEEE Transactions on Signal Processing*, vol. 60, no. 11, pp. 6036–6041, 2012.

[66] A. B. Tort, R. Komorowski, H. Eichenbaum, and N. Kopell, "Measuring phase-amplitude coupling between neuronal oscillations of different frequencies," *Journal of Neurophysiology*, vol. 104, no. 2, pp. 1195–1210, 2010.

[67] A. Trujillo-Ortiz and R. Hernandez-Walls, *Levene test: Levene's test for homogeneity of variances*, 2003, https://www.mathworks.com/matlabcentral/fileexchange/3375-levenetest MATLAB Central File Exchange.

[68] P. Berens, "Circ Stat: a MATLAB toolbox for circular statistics," *Journal of Statistical Software*, vol. 31, no. 10, pp. 1–21, 2009.

[69] H. Hsieh, J. Boehm, C. Sato et al., "AMPAR removal underlies Aβ-induced synaptic depression and dendritic spine loss," *Neuron*, vol. 52, no. 5, pp. 831–843, 2006.

[70] G. M. Shankar, B. L. Bloodgood, M. Townsend, D. M. Walsh, D. J. Selkoe, and B. L. Sabatini, "Natural oligomers of the Alzheimer amyloid-protein induce reversible synapse loss by modulating an NMDA-type glutamate receptor-dependent signaling pathway," *Journal of Neuroscience*, vol. 27, no. 11, pp. 2866–2875, 2007.

[71] W. Wei, L. N. Nguyen, H. W. Kessels, H. Hagiwara, S. Sisodia, and R. Malinow, "Amyloid beta from axons and dendrites reduces local spine number and plasticity," *Nature Neuroscience*, vol. 13, no. 2, pp. 190–196, 2010.

[72] J. J. Palop and L. Mucke, "Synaptic depression and aberrant excitatory network activity in Alzheimer's disease: two faces of the same coin?," *Neuromolecular Medicine*, vol. 12, no. 1, pp. 48–55, 2010.

[73] K. J. Thompson, M. L. Mata, J. E. Orfila, E. J. Barea-Rodriguez, and J. L. Martinez Jr., "Metabotropic glutamate receptor antagonist AIDA blocks induction of mossy fiber-CA3 LTP in vivo," *Journal of Neurophysiology*, vol. 93, no. 5, pp. 2668–2673, 2005.

[74] A. W. Schmid, D. B. Freir, and C. E. Herron, "Inhibition of LTP in vivo by beta-amyloid peptide in different conformational states," *Brain Research*, vol. 1197, pp. 135–142, 2008.

[75] L. Vutskits, A. Briner, P. Klauser et al., "Adverse effects of methylene blue on the central nervous system," *Anesthesiology*, vol. 108, no. 4, pp. 684–692, 2008.

[76] M. Oz, D. E. Lorke, M. Hasan, and G. A. Petroianu, "Cellular and molecular actions of methylene blue in the nervous system," *Medicinal Research Reviews*, vol. 31, no. 1, pp. 93–117, 2011.

[77] M. Necula, L. Breydo, S. Milton et al., "Methylene blue inhibits amyloid Aβ oligomerization by promoting fibrillization," *Biochemistry*, vol. 46, no. 30, pp. 8850–8860, 2007.

[78] D. B. Freir, D. A. Costello, and C. E. Herron, "Aβ25–35-induced depression of long-term potentiation in area CA1 in vivo and in vitro is attenuated by verapamil," *Journal of Neurophysiology*, vol. 89, no. 6, pp. 3061–3069, 2003.

[79] A. Neishabouri and A. A. Faisal, "Axonal noise as a source of synaptic variability," *PLoS Computational Biology*, vol. 10, no. 5, p. e1003615, 2014.

[80] F. Scala, S. Fusco, C. Ripoli et al., "Intraneuronal Aβ accumulation induces hippocampal neuron hyperexcitability through A-type K+ current inhibition mediated by activation of caspases and GSK-3," *Neurobiology of Aging*, vol. 36, no. 2, pp. 886–900, 2015.

[81] H. Yin, H. Wang, H. Zhang, N. Gao, T. Zhang, and Z. Yang, "Resveratrol attenuates Aβ-induced early hippocampal neuron excitability impairment via recovery of function of potassium channels," *Neurotoxicity Research*, vol. 32, no. 3, pp. 311–324, 2017.

[82] Y. He, M. Wei, Y. Wu et al., "Amyloid β oligomers suppress excitatory transmitter release via presynaptic depletion of phosphatidylinositol-4, 5-bisphosphate," *Nature Communications*, vol. 10, no. 1, pp. 1–18, 2019.

[83] D. Schlingloff, S. Káli, T. F. Freund, N. Hájos, and A. I. Gulyás, "Mechanisms of sharp wave initiation and ripple generation," *Journal of Neuroscience*, vol. 34, no. 34, pp. 11385–11398, 2014.

[84] H. Zhang, L. Zhang, D. Zhou et al., "Ablating ErbB4 in PV neurons attenuates synaptic and cognitive deficits in an animal model of Alzheimer's disease," *Neurobiology of Disease*, vol. 106, pp. 171–180, 2017.

[85] R. H. Andersson, A. Johnston, P. A. Herman et al., "Neuregulin and dopamine modulation of hippocampal gamma oscillations is dependent on dopamine D4 receptors," *Proceedings of the National Academy of Sciences of the United States of America*, vol. 109, no. 32, pp. 13118–13123, 2012.

[86] S. Hijazi, T. S. Heistek, P. Scheltens et al., "Early restoration of parvalbumin interneuron activity prevents memory loss and network hyperexcitability in a mouse model of Alzheimer's disease," *Molecular Psychiatry*, vol. 25, no. 12, pp. 3380–3398, 2020.

[87] J.-O. Hollnagel, S. Elzoheiry, K. Gorgas et al., "Early alterations in hippocampal perisomatic GABAergic synapses

and network oscillations in a mouse model of Alzheimer's disease amyloidosis," *PLoS One*, vol. 14, no. 1, article e0209228, 2019.

[88] E. Verdaguer, S. Brox, D. Petrov et al., "Vulnerability of calbindin, calretinin and parvalbumin in a transgenic/knock-in APPswe/PS1dE9 mouse model of Alzheimer disease together with disruption of hippocampal neurogenesis," *Experimental Gerontology*, vol. 69, pp. 176–188, 2015.

[89] G. Buzsáki and C. H. Vanderwolf, "Cellular bases of hippocampal EEG in the behaving rat," *Brain Research Reviews*, vol. 6, no. 2, pp. 139–171, 1983.

[90] C. Kemere, M. F. Carr, M. P. Karlsson, and L. M. Frank, "Rapid and continuous modulation of hippocampal network state during exploration of new places," *PLoS One*, vol. 8, no. 9, article e73114, 2013.

[91] J. Yamamoto, J. Suh, D. Takeuchi, and S. Tonegawa, "Successful execution of working memory linked to synchronized high-frequency gamma oscillations," *Cell*, vol. 157, no. 4, pp. 845–857, 2014.

[92] M. F. Carr, M. P. Karlsson, and L. M. Frank, "Transient slow gamma synchrony underlies hippocampal memory replay," *Neuron*, vol. 75, no. 4, pp. 700–713, 2012.

[93] M. T. Kucewicz, J. Cimbalnik, J. Y. Matsumoto et al., "High frequency oscillations are associated with cognitive processing in human recognition memory," *Brain*, vol. 137, no. 8, pp. 2231–2244, 2014.

[94] N. Axmacher, C. E. Elger, and J. Fell, "Ripples in the medial temporal lobe are relevant for human memory consolidation," *Brain*, vol. 131, no. 7, pp. 1806–1817, 2008.

[95] G. Girardeau, K. Benchenane, S. I. Wiener, G. Buzsáki, and M. B. Zugaro, "Selective suppression of hippocampal ripples impairs spatial memory," *Nature Neuroscience*, vol. 12, no. 10, pp. 1222-1223, 2009.

[96] W. Ramadan, O. Eschenko, and S. J. Sara, "Hippocampal sharp wave/ripples during sleep for consolidation of associative memory," *PLoS One*, vol. 4, no. 8, article e6697, 2009.

[97] G. Girardeau and M. Zugaro, "Hippocampal ripples and memory consolidation," *Current Opinion in Neurobiology*, vol. 21, no. 3, pp. 452–459, 2011.

[98] J. E. Driver, C. Racca, M. O. Cunningham et al., "Impairment of hippocampal gamma (γ)-frequency oscillations in vitro in mice overexpressing human amyloid precursor protein (APP)," *European Journal of Neuroscience*, vol. 26, no. 5, pp. 1280–1288, 2007.

[99] V. Villette, F. Poindessous-Jazat, A. Simon et al., "Decreased rhythmic GABAergic septal activity and memory-associated oscillations after hippocampal amyloid-pathology in the rat," *Journal of Neuroscience*, vol. 30, no. 33, pp. 10991–11003, 2010.

[100] F. Peña-Ortega and R. Bernal-Pedraza, "Amyloid beta peptide slows down sensory-induced hippocampal oscillations," *International Journal of Peptides*, vol. 2012, Article ID 236289, 8 pages, 2012.

[101] D. Gavello, C. Calorio, C. Franchino et al., "Early alterations of hippocampal neuronal firing induced by Abeta 42," *Cerebral Cortex*, vol. 28, no. 2, pp. 433–446, 2018.

[102] I. Ferreira, L. Bajouco, S. Mota, Y. Auberson, C. Oliveira, and A. Rego, "Amyloid beta peptide 1–42 disturbs intracellular calcium homeostasis through activation of GluN2B-containing N-methyl-d-aspartate receptors in cortical cultures," *Cell Calcium*, vol. 51, no. 2, pp. 95–106, 2012.

[103] M. Arbel-Ornath, E. Hudry, J. R. Boivin et al., "Soluble oligomeric amyloid-β induces calcium dyshomeostasis that precedes synapse loss in the living mouse brain," *Molecular Neurodegeneration*, vol. 12, no. 1, pp. 1–14, 2017.

[104] G. Rammes, F. Seeser, K. Mattusch et al., "The NMDA receptor antagonist radiprodil reverses the synaptotoxic effects of different amyloid-beta (Aβ) species on long-term potentiation (LTP)," *Neuropharmacology*, vol. 140, pp. 184–192, 2018.

[105] I. Sánchez-Rodríguez, A. Gruart, J. M. Delgado-García, L. Jiménez-Díaz, and J. D. Navarro-López, "Role of GirK channels in long-term potentiation of synaptic inhibition in an in vivo mouse model of early amyloid-β pathology," *International Journal of Molecular Sciences*, vol. 20, no. 5, article 1168, 2019.

[106] K. Park, J. Lee, H. J. Jang, B. A. Richards, M. M. Kohl, and J. Kwag, "Optogenetic activation of parvalbumin and somatostatin interneurons selectively restores theta-nested gamma oscillations and oscillation-induced spike timing-dependent long-term potentiation impaired by amyloid β oligomers," *BMC Biology*, vol. 18, no. 1, p. 7, 2020.

[107] B. P. Graham and E. Spera, "On phasic inhibition during hippocampal theta," *Network: Computation in Neural Systems*, vol. 25, no. 1–2, pp. 3–19, 2014.

[108] H. Chung, K. Park, H. J. Jang, M. M. Kohl, and J. Kwag, "Dissociation of somatostatin and parvalbumin interneurons circuit dysfunctions underlying hippocampal theta and gamma oscillations impaired by amyloid β oligomers in vivo," *Brain Structure and Function*, vol. 225, no. 3, pp. 935–954, 2020.

[109] R. M. Reinhart and J. A. Nguyen, "Working memory revived in older adults by synchronizing rhythmic brain circuits," *Nature Neuroscience*, vol. 22, no. 5, pp. 820–827, 2019.

Research Article

Alzheimer's Disease as a Result of Stimulus Reduction in a GABA-A-Deficient Brain: A Neurocomputational Model

Mariana Antonia Aguiar-Furucho [1,2] **and Francisco Javier Ropero Peláez** [2,3]

[1]*Engineering, Neuroscience and Bio-Inspired Systems Study Group (GENeSis), Department of Electrotechnics (DAELT), Universidade Tecnológica Federal do Paraná (UTFPR), Paraná 80230-901, Brazil*
[2]*Center for Neuroscience and Behavior, Institute of Psychology, University of São Paulo, São Paulo, Brazil*
[3]*Center of Mathematics, Computation and Cognition (CMCC), Universidade Federal do ABC, Brazil*

Correspondence should be addressed to Mariana Antonia Aguiar-Furucho; marianafurucho@utfpr.edu.br
and Francisco Javier Ropero Peláez; francisco.pelaez@ufabc.edu.br

Several research studies point to the fact that sensory and cognitive reductions like cataracts, deafness, macular degeneration, or even lack of activity after job retirement, precede the onset of Alzheimer's disease. To simulate Alzheimer's disease earlier stages, which manifest in sensory cortices, we used a computational model of the koniocortex that is the first cortical stage processing sensory information. The architecture and physiology of the modeled koniocortex resemble those of its cerebral counterpart being capable of continuous learning. This model allows one to analyze the initial phases of Alzheimer's disease by "aging" the artificial koniocortex through synaptic pruning, by the modification of acetylcholine and GABA-A signaling, and by reducing sensory stimuli, among other processes. The computational model shows that during aging, a GABA-A deficit followed by a reduction in sensory stimuli leads to a dysregulation of neural excitability, which in the biological brain is associated with hypermetabolism, one of the earliest symptoms of Alzheimer's disease.

1. Introduction

Since Alzheimer's disease (AD) is a complex, multifaceted illness (see Subsection 1.1), it is difficult to evaluate the relationship between the many factors involved (genetic, cognitive, social, sensory, neural, and molecular). This relationship should be sought at the level of the neural circuits that process information, either from the senses or from other areas of the brain. Neurons in these circuits are so tightly packed [1] that inserting electrodes in predetermined neurons to assess their operation is very costly. Even with the advent of optogenetics, which allows neurons to be activated by light [2], the task of studying circuit-level interactions of neurons, by changing their parameters and connectivity, is still a significant challenge that is easily tackled with neurocomputing models [3]. Neurocomputational modeling has

strong theoretical support from the area of artificial neural networks (ANNs), in which different arrangements of neuron-like units contribute to the development of artificial intelligence (AI) systems. Although neural networks (NNs) models are far from being biological, they can be used to understand biological NNs. Concepts like neural competition, synaptic weight adjustment, activation-function shifting, vector separation, and pattern normalization contribute to understanding not only artificial but also biological NNs.

One of the most exciting applications of NNs models is the creation of brain disease models. Such a model can be developed by "lesioning" an ANN that in "healthy" conditions performs functions like learning, pattern completion, abstraction, generalization, and categorization.

According to the seminal book *Neural Modeling of Brain and Cognitive Disorders*, "recently, a new direction has

emerged, that of using "lesioned" neural models to study several brain and cognitive disorders from a computational point of view" ([4], p.3).

In 1996, when this book was published, there were well-developed models of memory, generalization, and categorization implemented in artificial NNs. However, there was still a lack of knowledge about how these operations take place in real neural circuits. For this reason, earlier computer models of neurological disorders made use of conventional artificial NNs models rather than biologically plausible neural circuits. Even with the lack of biological realism, these first computer models attempted to model amnesia [5], dyslexia [6, 7], stroke [8], phantom limbs [9], Parkinson's and Huntington's diseases [10], schizophrenia [11], and even AD [12, 13]. Over time, with an increasing understanding of biological neural circuits, realistic neural models of AD appeared [14]. While some of these models tried to emulate the hippocampal function [15, 16], others like Stefanovski et al. model [17] performed whole-brain simulations for inferring candidate mechanisms of AD.

Realistic neurocomputational models endowed with operations at molecular levels can be very costly in computational terms. On the other hand, the so-called phenomenological models (see Section 1.2 in [18]) are simplified models that try to capture the minimum characteristics capable of simulating the basic operations of the modeled phenomenon. In phenomenological models, the focus is the function, not the details of the substrate in which the activity takes place. For example, in the case of biological neurons, they are modeled by mimicking their input-output operations without regard to molecular complexities. We adopted this latter type of model for our simulations.

Initially, instead of simulating brain impairment, our priority was to develop operational models of brain structures like the thalamus [19, 20], the amygdala [21], and the koniocortex [22, 23]. When their initial operation was satisfactory, the way of further evaluating them was by modeling brain disorders. For example, in a previous paper [24], incomplete sensory patterns when entering the artificial model of the thalamus yielded a reconstructed copy reminiscent of hallucinations in actual schizophrenic patients. This result led to propose a correlation between the genetic lack of thalamic afferents from prefrontal and temporal areas [25] and the so-called positive symptoms of schizophrenia. A similar strategy allowed the assessment of the circuit linking the thalamus and the amygdala, which led to an effective therapy for treating specific phobias [21]. We also modeled the koniocortex, the first cortical layer receiving inputs from the sensory thalamus [23, 26]. Once modeled, learning emerges competitively with spiny stellate (SS) neurons behaving in a "winner-take-all" (WTA) manner (In a pool of neurons, "winner-take-all" means that the most activated neuron starts firing while the others keep silent.). The artificial koniocortex performs stimuli (input patterns) classifications the same way competitive NNs do (i.e., by firing a single neuron for each category of stimuli presented to the network).

As will be shown in Subsection 1.2, there is a strong positive correlation between the onset of AD and stimulus

reduction in the nervous system. This stimulus reduction can be of two types:

(a) A sensory reduction like in macular degeneration, deafness, or cataracts

(b) Cognitive task reduction, like in retirement, loss of employment, or loss of or separation from relatives

Since the koniocortex model performs memorizing tasks, simultaneously dealing with input patterns, it seems the right candidate for testing the hypothesis correlating to the AD onset and the reduction of sensory stimuli. Furthermore, cortical sensory areas like the koniocortex are also the first ones to be affected by AD [27]. This fact was not so evident at the beginning of AD research, due to the difficulty in identifying amyloid plaques in these areas because they appear in their mildest diffuse or amorphous forms. Beach and McGeer were able to highlight these diffuse plaques by using the Bielschowsky stain technique [28]. Recently, advanced technologies like Spatial Proteomics Analysis have not only shown AD-related protein alterations at sensory cortices but also demonstrated that the evolution of AD begins in sensory and motor cortices where the disease appears in its mildest forms [29]. Other studies give further support to these findings and show that SS neurons in the koniocortex undergo significant density decrements and dendritic loss during aging [30] and AD [31].

As mentioned previously, biologically plausible computational models can be tested by "lesioning" them in ways similar to the lesions experienced in their biological counterparts. For assessing whether the koniocortex model mimics Alzheimer's symptoms, we simulate its "aging" by altering its parameters. Although this "aging" operation seems somewhat unspecific, the main factors of nervous system aging are not unknown to scientists (see Subsection 1.3). They might be reproduced in a modeled neural circuit, as will be explained.

One property of neurons in the koniocortex model that is essential for learning processes is called intrinsic plasticity (IP) [32, 33]. IP dynamically adjusts neurons' firing threshold performing a dual-type operation (see the appendix):

(a) In the case of very active neurons, IP makes the neuron's firing threshold more positive for lowering its firing rate in the future. Neurons do this by eliminating intrinsic channels (like L-type Ca^{2+} channels, Na^+ channels, and delayed rectifier K^+ channels) from the neuron's membrane ([33], Section 4)

(b) Conversely, in the case of low neuronal activity, IP makes the firing threshold less positive, which increases the firing rate in the future. Neurons do this by placing intrinsic channels in the cell membrane. Porter et al. [34] associates the excessive expression of calcium channels in the neuron's membrane to neurotoxicity and AD

In NNs models, the position of the firing threshold roughly coincides with the rightwards shift of the neuron's activation function (see Figure 1) that in many cases is "s"-shaped (or sigmoidal) like the one used by Desai ([33], Fig.
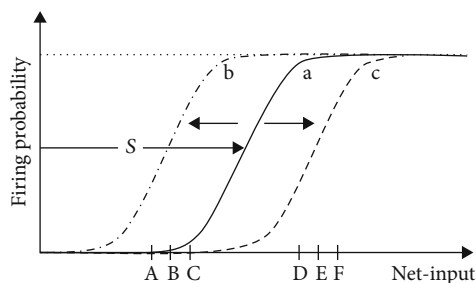
FIGURE 1: Intrinsic plasticity. (a) The continuous line at the center represents the activation function at a hypothetical initial state. (b) When the net-input values are diminished as in A, B, and C, the sigmoidal activation function shifts leftwards. (c) When the net-input values grow like in the case of D, E, and F, the sigmoidal activation function shifts rightwards.

3.a) to explain IP. In neurocomputational models, the terms "shift" and "firing threshold" are interchangeable. The value of the shift is between zero and one: zero corresponding to the minimum firing threshold and 1 to the maximum firing threshold.

IP is a homeostatic process in which the shift/threshold tends to follow the average neural activity (ANA). Depending on the velocity in which this ANA moves, the average shift will quickly reach the ANA, or it will dynamically oscillate around it until eventually catching it up.

This latter process might be related to the putative link (see Section 1.2) between the onset of AD and stimuli reduction, as may occur during job retirement or separation from relatives. When neurons suddenly diminish their activity due to stimuli reduction, IP initially operates by making the neuron's firing threshold less positive so that the neuron becomes more easily fired. Ideally, this process makes the neuron more active until it gradually stabilizes. However, in nonideal conditions, an oscillatory process around the ANA occurs. In this process, hyperactivation and hypoactivation alternate until the ANA and the shift match. Along this process, the neuron's IP adjusts the shifts by either creating or eliminating intrinsic channels. The continuous production/elimination of intrinsic channels makes use of significant metabolic resources leading to hypermetabolism (see Subsection 1.4.4). Hypermetabolism [35] appears in Magnetic Resonance Imaging (MRI) and Positron Emission Tomography (PET) scans of AD patients and is simultaneous with the stage of Mild Cognitive Impairment (MCI), in which patients experience difficulties in recalling recent memories. It also precedes the stage of beta-amyloid plaque proliferation (a review of all the stages of AD is presented in Subsection 1.4).

Since the koniocortex network is able to continuously learn new patterns during its regular operation, one can evaluate its learning performance over time. We initially use an integral (nondamaged) network and subsequently apply several types of damage associated with aging (see Subsection 1.3 and Table 1). Finally, we reduce the intensity (module) of the input patterns. We will see that when this reduction takes place in a network with impaired GABA-A inhibition, a persistent oscillatory dynamic takes place. Although oscillations are an integral part of learning, persistent oscillations can dis-

rupt learning. Continuous oscillations also lead to hypermetabolism. Since phenomenological models do not usually deal with molecular properties, our koniocortex model cannot directly assess hypermetabolism. Instead of this, to know whether the koniocortex model is reaching the stage of hypermetabolism, we continuously evaluate both the average output and the average shift of neurons. When these two markers engage in a persistent oscillatory dynamic, this fact determines the onset of the hypermetabolic stage.

Next, we provide more detailed explanations of some of the concepts presented in Introduction.

1.1. General Description. Characterized as a chronic, degenerative, and fatal disease, AD accounts for 60%-70% of dementia diagnoses worldwide [36] and is estimated to affect 106.2 million persons or 1 in 85 persons by the year 2050 [37]. The disease is partly hereditary, due to pathogenic genetic mutations, as well as external factors like dietary habits, and usually affects people over 65 years of age ([38], p.3).

Dietary patterns are a risk criterion as well as a factor of protection against the incidence of AD. Among the nutritional habits considered beneficial for reducing the risk of AD are those that stimulate the consumption of antioxidants, vitamins, polyphenols, fruits, vegetables, polyunsaturated fatty acids, fish, and tea, such as the Japanese and Mediterranean diets [39]. On the other hand, a large intake of red meat, butter, and high-fat dairy increases the risk of developing AD [40].

One of the first symptoms reported by patients and caregivers is difficulty in remembering facts, events, and names of people close to them. However, an AD diagnosis requires the presence of other concurrent problems like mental confusion, impaired executive functions, apathy, and communication difficulties [41]. According to Masters et al. ([38], p.9), the average clinical duration of AD is between eight and ten years, preceded by preclinical and prodromal phases, and a maximum span of 20 years.

Histopathologically, a key feature is a proliferation of senile plaques, aggregations of the insoluble form of the β-amyloid peptide (Aβ), not only in the entorhinal cortex, hippocampus, and associative cortices [42] but also, in a milder way, in sensory and motor cortices where AD starts according to Spatial Proteomics Analysis techniques [29]. Neurofibrillary tangles formed by the tau protein are also characteristic of the disease. They appear in cortical neurons, mainly in the entorhinal cortex, hippocampus, frontal cortex, and temporal and parietal lobes [42].

1.2. Principal Causes of Stimulus Reduction due to Age. Decreased sensory stimulation usually takes place due to the loss of sensory receptors or due to age-related health problems, such as macular degeneration, deafness, or cataracts. Retirement, a sedentary lifestyle, or the loss of relatives and friends could be external factors that contribute to decreasing the intellectual and cognitive stimuli experienced by older persons. Let us study these phenomena by classifying them into the following two types.

1.2.1. Sensory Reduction. Macular degeneration, cataracts, or deafness are different ways in which sensory reduction

TABLE 1: Description of the performed tests and their corresponding parameters. Abbreviations: (a) GABA-A: this column shows the percentage of epochs in which GABA-A deficit initiates. (b) ACh: this column exhibits the percentage of epochs in which ACh deficit begins. (c) Pruning: the values indicate the percentage of epochs in which pruning initiates. (d) S_R: the values below this title indicate the percentage of epochs in which stimulus reduction starts. (e) STM: the values below this title indicate the percentage of epochs in which the experiment of short-term memory initiates. (f) Mem: when memantine treatment (i.e., an NMDA blocker simulation) is applied, the numeric value shows the percentage of epochs in which memantine treatment initiates.

Test	Experiment	Parameters					
		GABA-A	ACh	Pruning	S_R	STM	Mem
Normal aging	a.1 Test of short-term memory	Ok	Ok	75%	No	70%	No
	a.2 Reduction of sensory stimuli and short-term memory test	Ok	Ok	75%	60%	70%	No
Aging with impaired GABA-A receptors	b.1 No sensory reduction	50%	Ok	75%	No	No	No
	b.2 Reduction of sensory stimuli	50%	Ok	75%	60%	No	No
	b.3 Reduction of sensory stimuli and short-term memory test	50%	Ok	75%	60%	70%	No
	b.4 Reduction of sensory stimuli, short-term memory test and administration of an NMDA receptor blocker (memantine)	50%	Ok	75%	60%	70%	55%
Aging with ACh deficiency	c.1 No sensory reduction	Ok	50%	75%	No	No	No
	c.2 Reduction of sensory stimuli	Ok	50%	75%	60%	No	No
	c.3 Reduction of sensory stimuli and short-term memory test	Ok	50%	75%	60%	70%	No
	c.4 Reduction of sensory stimuli, short-term memory test and administration of memantine	Ok	50%	75%	60%	70%	55%
Aging with GABA-A impairment at 50% of epochs. Recovery at 75% of epochs	d.1 Sensory stimulus reduction, short-term memory stimulus, and recovery of GABA-A receptor functionality. Pruning is present as in previous experiments modeling healthy brain aging	50%-75%	Ok	75%	60%	85%	No

appears in elders. Age-related macular degeneration (AMD) is a neurodegenerative disease that affects the macula (the central region of the retina), causing progressive loss of vision. AMD affects 15% of people between 65 and 74, 25% of people between 75 and 84, and 30% of people older than 85; it also shares many characteristics with AD, including oxidative stress and inflammation [43]. According to Kaarniranta et al. [43], studies on AMD are "interesting opportunities to understand the early signs of AMD that might be associated with AD pathology as well." According to Javaid et al. [44], eye examinations allow an earlier diagnosis of AD because $A\beta$ plaque deposition and hyperphosphorylated tau protein first appear in the retina. These authors point out that AD patients display an increased prevalence of cataracts affecting visual acuity.

Regarding deafness (which affects 30% of adults over 60), Lin et al. [45] show that early treatment for deafness postpones the onset of AD symptoms.

1.2.2. Cognitive Task Reduction: Retirement, Loss of Employment, etc. Using data from the Survey of Health, Aging and Retirement (SHARE) in Europe, Adam et al. [46] examined whether the cognitive decline in aging could be affected by occupation or more specifically by inactivity after retirement and the relationship of these variables to participants' physical and mental health. The research revealed that retirees or individuals who never had a professional activity had lower performance on cognitive and occupational tests compared with professionally active participants ([46], p.385). Furthermore, retired people who engaged in cognitively stimulating activities or had social or religious involvement performed better than those who did not [46].

Lupton et al. [47] showed that late retirement acts as a protective factor against AD by postponing its age of onset, while the education level or type of occupation had no effect. In line with those results, Grotz et al. ([48], p.9) showed a strong positive correlation between the appearance of the first symptoms of AD and early retirement, indicating that postponing retirement by one year delays AD by 0.3 years.

Bonsang et al. [49] and Finkel et al. [50] confirmed that promoting the participation of older workers in the labor

force delays cognitive decline and thus the occurrence of associated impairments.

1.3. Typical Nervous System Alterations due to Age. During normal aging, some neurophysiological changes impair long-term mnemonic systems and working memory: (a) the synaptic pruning of cortical neurons [51], (b) a reduction in the synthesis and release of acetylcholine (ACh) [52], and (c) the attenuation of inhibitory signaling of GABAergic interneurons in the hippocampus and prefrontal cortex (PFC) [53]. Next, we explain these processes in more detail.

1.3.1. Synaptic Pruning. Although synaptic pruning (also known as synaptic connection harvesting) is associated with AD, it also occurs at every stage of a healthy brain's development and maturation. Synaptic pruning obeys Lamarck's law: "use it or lose it" by keeping only the reinforced connections during learning. According to Gopnik et al. [54], there is a decay from 15,000 synaptic connections to approximately 7,500 synaptic connections per neuron in older individuals. In an expressive graph ([55], Fig. 3), Huttenlocher depicts the evolution of synaptic density (in synapses per cubic milimeter) in the middle frontal gyrus as a function of age. It shows that this density increases from birth to around five years of age. From that point, synaptic density decreases until it stabilizes at around the age of 40 and starts falling again (about 75 years), linearly, until death.

Using mutant APP (beta-amyloid precursor protein) mice, Bezprozvanny and Mattson [56] showed a correlation between AD and synaptic pruning: the appearance of toxic forms of β-amyloid peptides (present in AD) is correlated with the loss of synaptic spines.

An article published by Nikolaev et al. [57] discusses the relationship between Aβ protein, "death receptor 6" (DR6 or TNFRSF21), synaptic pruning, and neuronal cell death. The DR6 receptor triggers cell death in response to low cell growth factor levels at specific periods of brain tissue development or when this tissue is damaged. The authors also present a loss/gain function model in which a fragment of the Aβ protein would bind to the DR6 receptor. This binding triggers neuronal degeneration and the self-destruction observed in AD. According to Nikolaev et al. [57], this mechanism occurs due to genetic causes or to the decrease in cell growth factors found in aging brain tissue.

A study by DeKosky and Scheff [58] supports the findings of Nikolaev et al. [57] by showing that the postmortem brain tissue from the right frontal lobe of patients with a mild form of AD exhibits decreased synaptic counts with an increase in the remaining contact area, compared with a control group. This fact suggests, according to the authors, that there is a "law of compensation," aimed at maintaining the total contact area of the synapses per unit volume at a stable level. However, this ability is lost throughout the progression of the disease. In its final stages, both the number of synapses and the total area of synaptic contact suffer a significant loss that negatively affects patients' cognitive capacity.

Horn et al. ([12], p.737) cite DeKosky and Scheff [58] in the development of their computational model of memory decay due to the gradual and progressive deterioration of synaptic connections during AD evolution, presenting a "framework for examining the interplay of synaptic deletion and compensation" [12].

1.3.2. Acetylcholine Deficit. Acetylcholine (ACh), one of the most abundant neurotransmitters present in the human brain, is directly involved with neural excitability, hippocampal-dependent learning [59], and memory processes [60]. Martinello et al. [59] demonstrate the importance of ACh for synaptic communication and, consequently, for memory formation.

The excessive neuronal loss characteristic of AD occurs mainly in cholinergic neurons of the basal forebrain (BFCN), which are also susceptible to axonal alterations, accumulation of phosphorylated tau protein, and formation of neurofibrillary tangles [61]. This set of factors led to the cholinergic hypothesis of AD. Francis et al. [62] proposed that an individual with AD presents degeneration of cholinergic neurons, a decrease in the activity of choline acetyltransferase (ChAT) and acetylcholinesterase (AChE), and reduction of ACh levels and cholinergic transmission mechanisms. According to them, these factors cause the cognitive impairment characteristic of the disease [63].

One of the treatments used in the earliest stages of AD includes drugs that act on cholinergic centers [62, 64], particularly on cholinesterase inhibitors. Although they contribute to improving the cognitive and behavioral aspects of AD, these medications do not prevent disease progression [64].

Although at first an ACh deficit seems to be one of the leading causes that disrupt the normal functioning of neuronal activity in AD, studies indicate that GABA-A may also play a critical role in the development of the disease [65].

1.3.3. GABA-A Deficit. GABAergic inhibitory interneurons (GABA: gamma-aminobutyric acid) play a crucial role in the regulation of neural dynamics. According to McQuail et al. [53], imbalances in this system might result in psychiatric damage and neurodegenerative diseases such as AD.

Although researchers initially asserted that GABAergic neurons are relatively preserved during aging, and in neurodegenerative pathologies, recent research shows that the GABA-A type undergoes significant changes due to age and may play a primary role in AD [65]. According to Limon et al. [66], there is a profound loss of GABA-A receptors in AD.

GABA-A receptors are ionotropic, contain intrinsic channels permeable to chlorine (Cl$^-$), and participate in most of the inhibitory connections of the brain through shunting inhibition [53]. Shunting inhibition is characterized by "an increase in conductance, leading to a reversal potential near the chlorine resting potential" ([67], p. 136). Shunting inhibition involves the entry of negatively charged Cl$^-$ into the neurons, which hampers action potential firing, thereby resulting in a mathematically divisive effect on cell depolarization [68] (this effect will be explained when presenting shunting basket neurons in Section 2 and also in Equation (A.3)).

Nowadays, there is an increasing interest in looking for nutrients that contribute to the synthesis of GABA-A receptors. According to Currais et al. [69], fisetin (present in fruits

and vegetables like strawberries, tomatoes, oranges, and cucumber) enhances mnemonic systems in healthy individuals. It mitigates the cognitive decline characteristic of neurodegenerative diseases such as AD. In line with this, Raygude et al. [70] showed that administering fisetin increases GABA-A levels in the brain. Another promising set of substances that contribute to the expression of GABA-A receptors in GABAergic synapses are terpenoids [71]. Terpenoids are found in vegetables and spices like salvia, peppermint, ginger, Curcuma longa, cinnamon, cloves, and mustard. Used in traditional medicine [72, 73] for improving cognitive functions, several authors cite terpenoids as promising therapeutic substances against AD [74, 75].

1.4. Stages of Alzheimer's Disease

1.4.1. Preclinical. The preclinical phase occurs approximately 12 years before the onset of symptoms. In this stage, the patient does not usually exhibit signs of dementia. Masters et al. [38] consider this phase a window for disease prevention because it is rather lengthy and exempt from severe cognitive impairments.

According to Masters et al. ([38], p.9), at this stage, there is an increase in levels of the main AD biomarkers, such as β-amyloid binder protein (Aβ deposition) and isoform 42 of the β-amyloid protein (CSF Aβ42). This latter biomarker can be identified in the cerebrospinal fluid (CSF) 20 years before the onset of the first symptoms.

At this stage, approximately 15 years before the onset of disease symptoms, there is also an increase in the level of tau protein in the cerebrospinal fluid (CSF tau) exceeding normal thresholds.

Reduced hippocampal volume, Clinical Dementia Rating-Sum of Boxes (CDR-SB) scores, and glucose metabolism levels (hypermetabolism at the preclinical stage and hypometabolism in the transition phase between the prodromal and clinical stages) are also considered important biomarkers of AD.

1.4.2. Prodromal. The prodromal phase begins with the sudden manifestation of cognitive symptoms related to dementia and memory loss at a level below that associated with AD ([38], p.9). High levels of disease biomarkers begin during this phase and extend towards the mild-to-moderate stage.

1.4.3. Mild Cognitive Impairment Stage. The Mild Cognitive Impairment (MCI) stage of AD occurs after the prodromal phase. The MCI stage is considered a preclinical phase because the changes observed in memory and cognitive functions differ from those considered normal during the aging process [76].

There are two types of MCI: (a) Simple Domain Amnestic MCI, which affects only memory, and (b) Multiple Domain Amnestic MCI, which affects memory and one or more cognitive functions like language, attention, perception, or executive functions. Busse et al. [77] reported that Multiple Domain Amnestic MCI can be considered a preclinical stage of AD.

Recently, the National Institute on Aging and the Alzheimer's Association have revised the criteria for the diagnosis of MCI as a preclinical indication of AD [78] and have recommended additional procedures for brain assessment, including testing biomarkers for Aβ and brain imaging.

1.4.4. From Hypermetabolism to Beta-Amyloid Plaque Creation. Hypermetabolism (increased glucose metabolism observed with fMRI and PET scans) occurs in subjects with MCI before the development of beta-amyloid plaques [35]. This fact is supported by Dickerson et al. findings [79], who reported increased hippocampal activation in MCI subjects. Busche et al. [80] studied individual cortical neurons in a mouse model of AD and reported increased neuronal activity in the direct vicinity of Aβ plaques. These authors suggest that this increased activity may also contribute to the calcium overload recently observed in neurites surrounding Aβ plaques. Regarding hypermetabolism and beta-amyloid plaque creation, Kim et al. [81] noticed that metabolism (measured by the uptake of FDG [18F] fluoro-2-deoxyglucose in the basal forebrain region) was higher in patients in the early stages of the disease and in MCI patients than those already diagnosed with AD and healthy subjects. According to those authors, this metabolic increase may be responsible for β-amyloid plaque formation leading to dementia ([81], p.935).

These metabolic changes, as well as perturbed calcium homeostasis, support the idea that Alzheimer's disease is related to mitochondrial dysfunction [82].

Finally, one of the latest manifestations of AD is hypoactivity, which is due, according to Bass and colleagues [83], to a combination of homeostatic alterations and Aβ plaque proliferation. As mentioned in Introduction, our computational model is not able to simulate the Aβ plaques proliferation, being only able to predict events until reaching the initial hypermetabolic stage that is associated with persistent neural oscillations.

2. Materials and Methods

As mentioned in Introduction, this research study is based on a computational model of the cerebral koniocortex that we developed in previous work [23, 26].

The term koniocortex, also known as granular cortex, means a cortex with a grainy texture (Konia "dust" in Greek) due to the high density of spiny stellate (SS) neurons. It refers to the different cortical regions with a distinctive inner granular layer (layer IV). The koniocortex includes Brodmann areas 1-3 (somatic sensory cortex), 17 (visual cortex), and 41 (auditory cortex). All these areas are like topographic maps that undergo plastic changes in their boundaries and receptive fields according to sensory experience. These changes are mainly due to NMDA receptors in koniocortex spiny stellate (SS) cells [84].

The cytoarchitecture of the koniocortex is depicted in Figure 2. SS neurons receive excitatory and inhibitory afferents, each of which has two types.

(1) Excitatory afferents:

    (a) Autapses [85]

    (b) Afferents from thalamocortical neurons (TC) in the thalamus that process sensory information
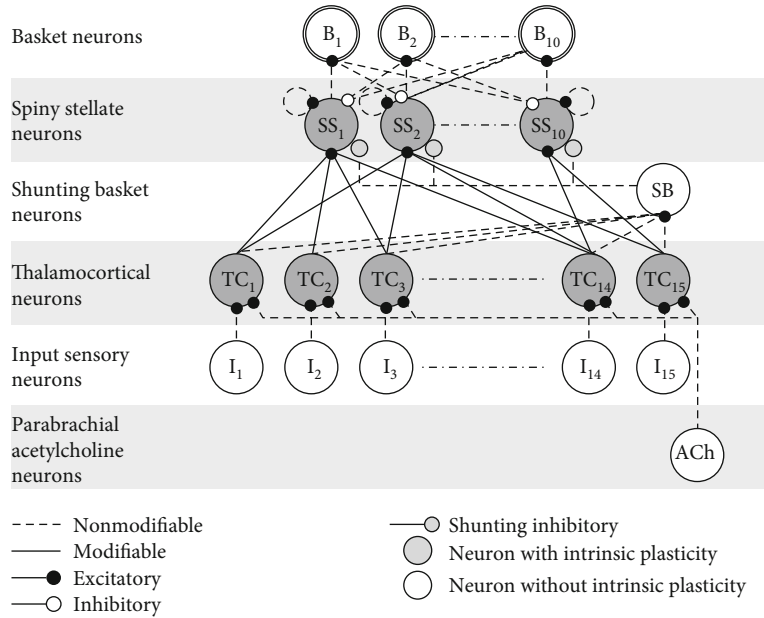
FIGURE 2: Cytoarchitecture of the koniocortex network in which acetylcholinergic neurons from the parabrachial nucleus project to thalamocortical neurons. The neurons that specifically belong to the koniocortex are the spiny stellate (SS) neurons, the inhibitory basket neurons (B), and the shunting basket (SB) neurons.

(2) Inhibitory afferents:

   (a) Basket neurons (B) that are stimulated by nearby excitatory SS neurons and exhibit the steepest activation-function slope among all neurons in the koniocortex ([86], Figure 3)

   (b) Shunting basket neurons (SB), which, according to Angulo et al. [87], accomplish linear summation of their thalamocortical afferents. In mathematical terms, this operation is called l1-norm (see Equation (A.2) in the appendix). These neurons use this result to produce a type of shunting/divisive inhibition ([88], p.1225) over SS neurons. This divisive inhibition is due to the GABA-A receptor used in shunting basket neurons' axon terminals. The concatenation of these two operations (the l1-norm and the division) means that shunting basket neurons perform a sort of normalization in their targets, the SS neurons (see Equation (A.3) in the appendix)

As previously mentioned, we developed a phenomenological model of the koniocortex in which we took into account the main functionalities of each of the neurons. Each neuron communicates with the following one by transmitting its output, a value between 0 and 1 that in spiking models corresponds to the neuron's firing rate. This value, when multiplied by a synaptic weight, is the synaptic contribution to the next neuron (see the appendix explaining the mathematical background).

The koniocortex model can learn how to classify input patterns like a conventional competitive NN. Although the artificial koniocortex deals with input patterns of any size,

we used patterns represented in a 5×3 grid (Figure 3), a total of 11 alphanumerical patterns. Ten patterns were numbers (0 to 9), and one was a letter (X). These patterns were forcedly placed at the output of the $5 \times 3 = 15$ sensory input neurons (I) of the koniocortex model (see cytoarchitecture depicted in Figure 2).

The learning processes take place in our simulations along 2,000 epochs, that is to say, 2,000 repetitions of the complete set of patterns that represent the life span of our model. Within these 2,000 epochs, we will model several natural processes taking place in the human brain from birth to death. Before 50% of repetitions, ten SS neurons of the koniocortex compete to recognize each one of the numerical patterns, so that, in the end, a single neuron fires for each one of the presented numbers. This type of specificity occurs because the synaptic weights of each neuron evolve to reflect the distinctive characteristics of each numerical pattern. In the end, when the synaptic weights of each neuron match the unique features of each number, the firing of a specific neuron takes place.

Although the synaptic weights of each SS neuron evolve to match the differential characteristics of each input pattern (not the complete input pattern), we still would like to recover the entire numerical pattern that fires each neuron for assessing the correctness of the pattern classification. For this purpose, it was necessary to create a recurrent ancillary network consisting of a set of virtual feedback connections ([26], Figure 6(b)) from spiny neurons to sensory neurons. At the end of the training, the collection of virtual weights exiting each SS neuron recreates the whole pattern that produces the firing of each spiny neuron. We will use this strategy for recalling the numerical pattern associated with each spiny neuron throughout training and test whether the modeled AD affects stored memories. In Results, we will see that when
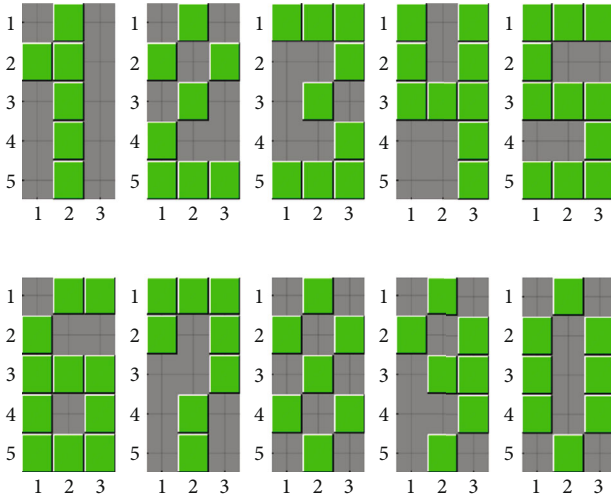
FIGURE 3: Alphanumeric input patterns presented as inputs to the koniocortex model.

simulating AD, the numerical patterns (recalled through these virtual connections) degenerate, and neurons lose their specificity, firing in front of more than one number.

When inputting each numerical pattern (by making numbers appear at the output of the sensory neuron's layer), this input information should spread until reaching the SS neurons. From the SS neuron's layer, the information propagates towards both the basket neurons' layer and the input neurons' layer (to the latter through the recurrent connections of the ancillary network). For allowing sensory information propagates across all layers, thereby producing a competitive interaction between spiny neurons, each numerical pattern should remain at the input during eight iterations. In each iteration, the program calculates the neuron's outputs, weights, and shifts, according to Equations (A.4) to (A.7) in the appendix. It is important to emphasize that the koniocortex network and the recurrent ancillary network update simultaneously (all their weights and shifts update at the same iteration). It is as if both networks constituted a single associative network of the type shown in ([26], Figure 9).

In the present simulations, patterns were input to the network sequentially, although they could also appear randomly. We found that when patterns are sequential, autapses are not necessary for a correct learning process. However, for the emergence of competitive learning in the case of random patterns, autapses are required (see the last paragraph of Section 3.3 in [26]).

In this simulation, the learning factor ξ (Equation (A.4)) was set to 0.0019, and the shifting velocity v (Equation (A.7)) to 0.0199. We obtained these optimal values by using a genetic algorithm for optimizing WTA processes in the SS neuron's layer. Nonmodifiable weights were set to W_{SS-SB} = 0.98, W_{I-TC} = 1.0, W_{SB-SS} = 0.5, and W_{SS-SS}= 0.85 in the autapses. Modifiable weights from TC to SS neurons and from SS to I neurons of the ancillary network start with negligible random values. The steepness factor k in the sigmoid of all neurons except for basket neurons was set to k = 40. The activation function of basket neurons (that have the stee-

pest activation) is linear. All the sigmoidal function shifts were set initially to 0.061.

In Results, we will analyze the computational processes taking place in the koniocortex model that, when disrupted, might lead the model to behave like the brain of patients in the initial stages of AD (see Table 2). We will do this by using the point of view of an ANN designer. Although most ANNs are biologically implausible, some theoretical aspects of ANNs are valid for any NN, either artificial or biological. For example, we will study two crucial computational processes mentioned in seminal treatises [89, 90]. The two computational processes necessary for achieving successful learning in competitive NNs are

(a) input pattern separation

(b) input pattern normalization

Regarding the first, when the angular separation between input patterns is small, a winning neuron can win again for many other input patterns, thereby precluding other competitive neurons from winning. One way of separating input patterns and preserving their distinctive features is to subtract their mean (also called moving average), as shown in Figure 4.

In the case of the koniocortex model, this process occurs at the level of thalamocortical neurons. This is related to IP, explained in the appendix. According to Peláez et al. [26], "Intrinsic plasticity is also highly important at the thalamocortical neuron level (second layer). In this layer, intrinsic plasticity contributes to subtracting the average neuron's activity level from current activity. The previous assertion means that the average pattern is subtracted from each incoming pattern, thus contributing to highlighting the differences between input patterns."

According to Martinello et al. [59], ACh from the parabrachial nucleus induces IP in thalamocortical neurons, thereby boosting the pattern separation process described above. An age-related cholinergic impairment might hinder this separation process so that, in the end, input pattern separation no longer occurs.

The second computational process (see "computational process" column in Table 2) for achieving successful learning in the koniocortex is normalization. As mentioned in Subsection 1.3.3, shunting basket neurons (SB in Figure 2) produce shunting/divisive inhibition of SS neurons through their GABA-A synapses [88]. As explained in [87], prior to this process, SB neurons perform a linear summation of their thalamocortical afferents. These two operations, division, and summation participate in a normalization process that consists of dividing the weighted sum of thalamocortical outputs by their l1-norm (the sum of thalamocortical outputs), according to Equation (A.3) in the appendix. This normalization of neuronal input patterns is necessary for a fair competition between spiny neurons. Shunting basket neurons are, therefore, responsible for the process of normalization in the koniocortex model (see the "computational process" column in Table 2).

This normalization process, when damaged (see "age-dependent damage" and "computational failure due to age" in Table 2), can impair competitive learning in the koniocortex model.

TABLE 2: Here, we list the computational processes performed by each type of neuron in each layer of the koniocortex model. The consequences of several lesions (due to age) in these different layers are also mentioned. When these lesions coincide with a reduction of sensory stimulation, we expect a further degree of deterioration that resembles AD. In the last column, we enumerate some pharmacological treatments to counteract the failures listed in previous columns.

Type of neurons in each layer	Computational process	Age-dependent damage	Computational failure due to aging	Expected failure due to sensory loss & aging	Pharmacological treatment
Basket neurons	Neural competition	Neural loss, GABA reduction	Discrimination deficits	Discrimination deficits	
Spiny stellate neurons	Patterns learning in synaptic weights	Pruning of synaptic connections	Problems in novel pattern learning	Hypermetabolism, forgetting, learning problems	NMDA blockers avoid forgetting but preclude new learning
Shunting basket neurons	Normalization	GABA-A synthesis reduction	Lack of normalization	Hypermetabolism, difficulty in novel pattern learning	
Thalamocortical neurons	Input patterns' separation	ACh deficit affects intrinsic plasticity	Failure in pattern separation processes	Slow or inefficient learning	DSE inhibitors increase acetylcholine
Input sensory neurons	Input detection	Damage of sensory receptors	Sensory deficit + GABA deficit ⟶ AD	Sensory stimuli contrast deficits	
Parabrachial acetylcholine neurons	Boost of intrinsic plasticity and patterns' separation in TC neurons	Cholinergic neuron degeneration	Problems in patterns' separation	Problems in patterns' separation	Acetylcholinesterase inhibitors increase acetylcholine

(a) (b)
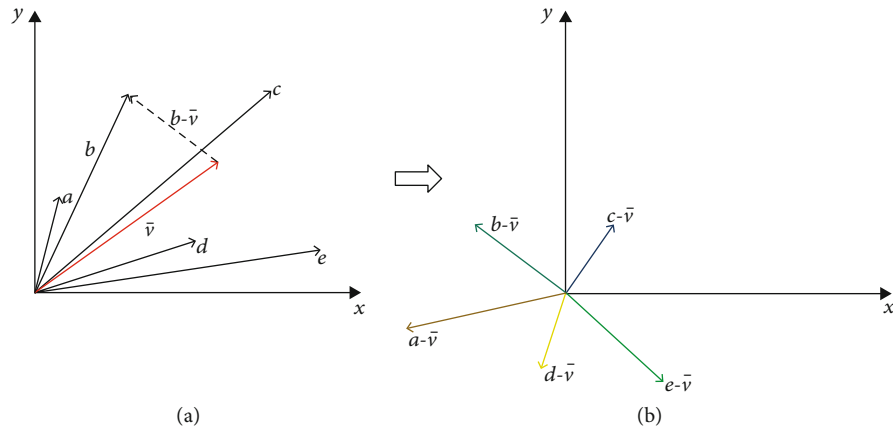
FIGURE 4: (a) One way of emphasizing the distinctive features of a set of vectors a, b, c, d consists in subtracting their average vector (as in the case of vector b). (b) In this way, vectors become more separated (in terms of the angle between them).

Another computational process that is important for allowing learning processes in the koniocortex model is the competition between SS neurons due to lateral inhibition (see Figure 2). Basket neurons (whose activation function was modeled as a linear function without IP) are involved in this process by performing a conventional subtractive type of inhibition.

Regarding learning, it is not possible without functional NMDA channels in stellate neurons' spines. For keeping memories intact in NMDA synapses, even at the risk of pre-

cluding newer learning processes, NMDA synapses can be "frozen" with NMDA blockers such as memantine, as mentioned in the last column.

The other computational process impaired due to age is the input vector separation process occurring in thalamocortical neurons (recall comments to Figure 4). If, according to Martinello et al. [59], ACh boosts IP, the reduction of ACh would negatively affect IP by slowing down sigmoid shifting. When the sigmoid is unable to follow the ANA (recall introduction), this lack of synchronicity adversely affects pattern
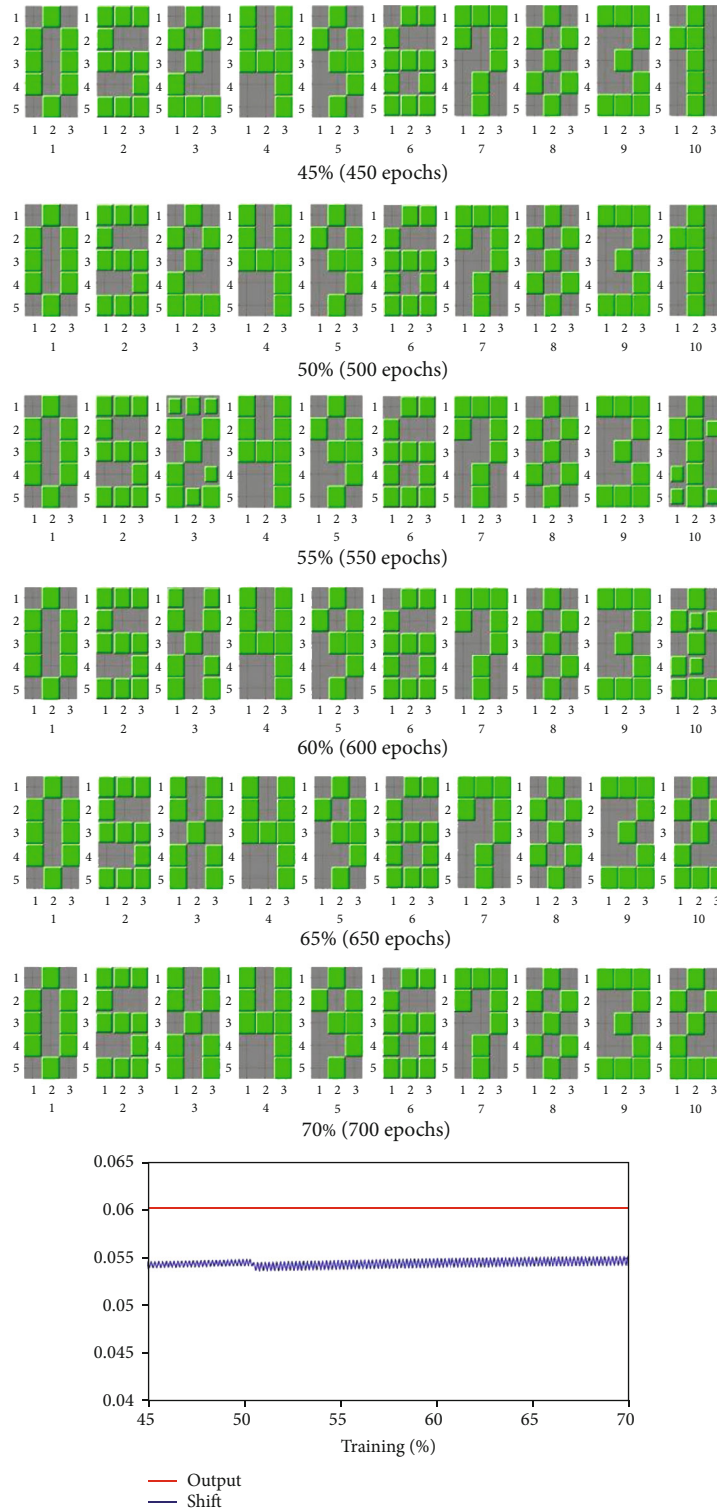
FIGURE 5: Example of koniocortex continuous learning under physiological (not defective) conditions. Each of the six rows represents the learning status at a selected epoch (iteration), being 1,000 the total number of epochs. In each of the six rows, ten synaptic weight matrices are corresponding to each one of the ten spiny neurons in the simulation, being each spiny neuron identified by a number below each matrix. The relative size of the fifteen green tiles in each matrix corresponds to the relative value of the weights of the recurrent virtual connections from spiny to input neurons. When, at epoch 500, one of the training patterns, pattern one, was substituted by a new pattern, pattern X, there is a process of weight reorganization for deciding which spiny neuron will fire in front of pattern X. At the end (see rows corresponding to epochs 650 and 700), spiny neuron three fires in front of pattern X and spiny neuron ten fires when pattern two is presented to the koniocortex model. In the bottom graph, we depict two curves: the red curve is the average output and the blue curve the average shift along with iterations. Both curves exhibit stable and regular behaviors.
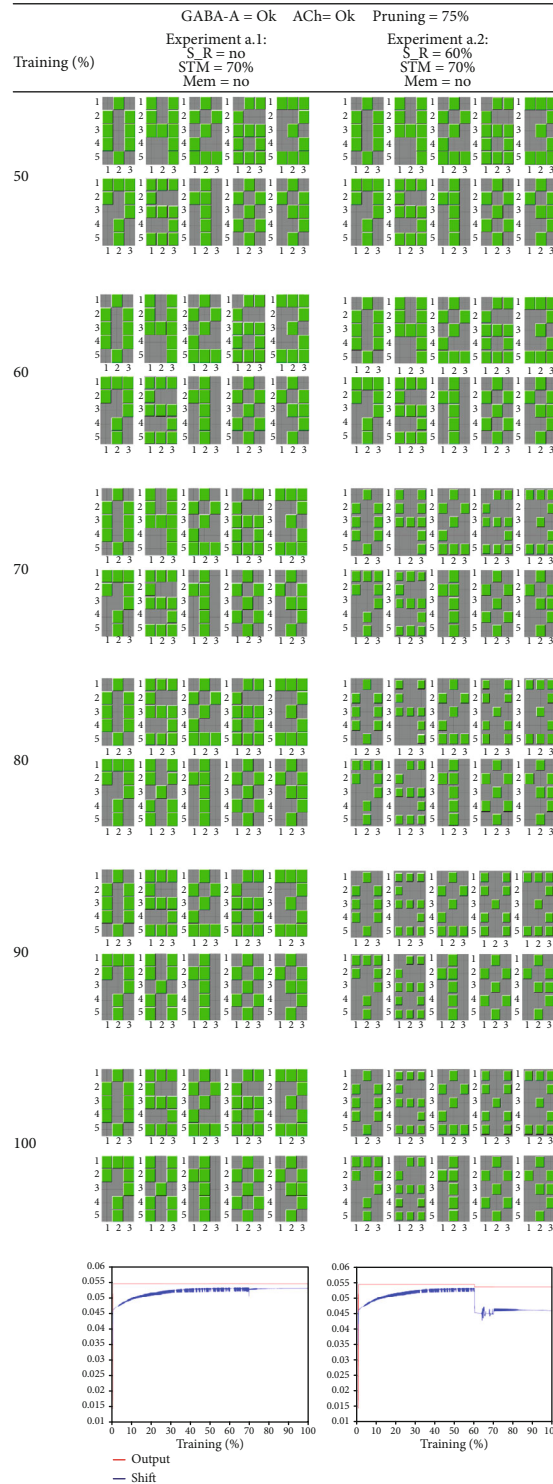
FIGURE 6: Normal aging. The two columns of this table show the koniocortex model behavior while performing a short-term memory (STM) task consisting of substituting one of the numerical patterns by pattern X. This substitution starts at 70% of epochs. In both experiments, the levels of GABA-A and ACh levels are normal, and pruning is also normal (starting at 75% of epochs). "Mem = no" means that in these experiments, we did not simulate the introduction of an NMDA blocker (memantine). At the bottom of each column, we show the evolution of the average output (in red) and average shift (in blue) of all neurons. Experiment a.1: the label "S_R = no" at the header of the first column means that there is no reduction of stimuli in this experiment. As seen in the block corresponding to 80% of training, the network successfully learns pattern X. Experiment a.2: the label "S_R = 60%" at the header of the second column indicates that there was a reduction of stimuli at 60% of repetitions. From this point, the average output and average shift experiment a sudden fall but stabilize rapidly. The presentation of a new pattern X at 70% of epochs does not alter the ongoing network dynamics in any significant way. Labels: S_R = sensory reduction; STM = short-term memory; Mem = memantine application; ACh = acetylcholine reduction in thalamocortical neurons.

FIGURE 7: This table shows two cases without GABA-A signaling: the column on the left without sensory reduction and the column on the right with sensory reduction. At the bottom of each column, we show the evolution of the average output (in red) and average shift (in blue) of all neurons. Labels: S_R = sensory reduction; STM = short-term memory; Mem = memantine; ACh = acetylcholine reduction in thalamocortical neurons. In experiment b.1 (left column), there is no reduction of stimuli, and we see that, although an episodic period of acute output oscillations occurred, homeostatic mechanisms are capable of driving the network to equilibrium again. By examining the blocks, we see that pattern recall was permanently impaired. However, acute oscillations related to hypermetabolism and disease progression were extinguished. In experiment b.2, the withdrawal of GABA-A at 50% of epochs was the precondition for the production of intense oscillations when the sensory reduction took place at 60% of epochs. At the same time, at 60% of epochs, neurons lost their pattern specificity so that several neurons processed the same pattern (number 1). Sustained oscillations are associated with hypermetabolism and the progression of AD.
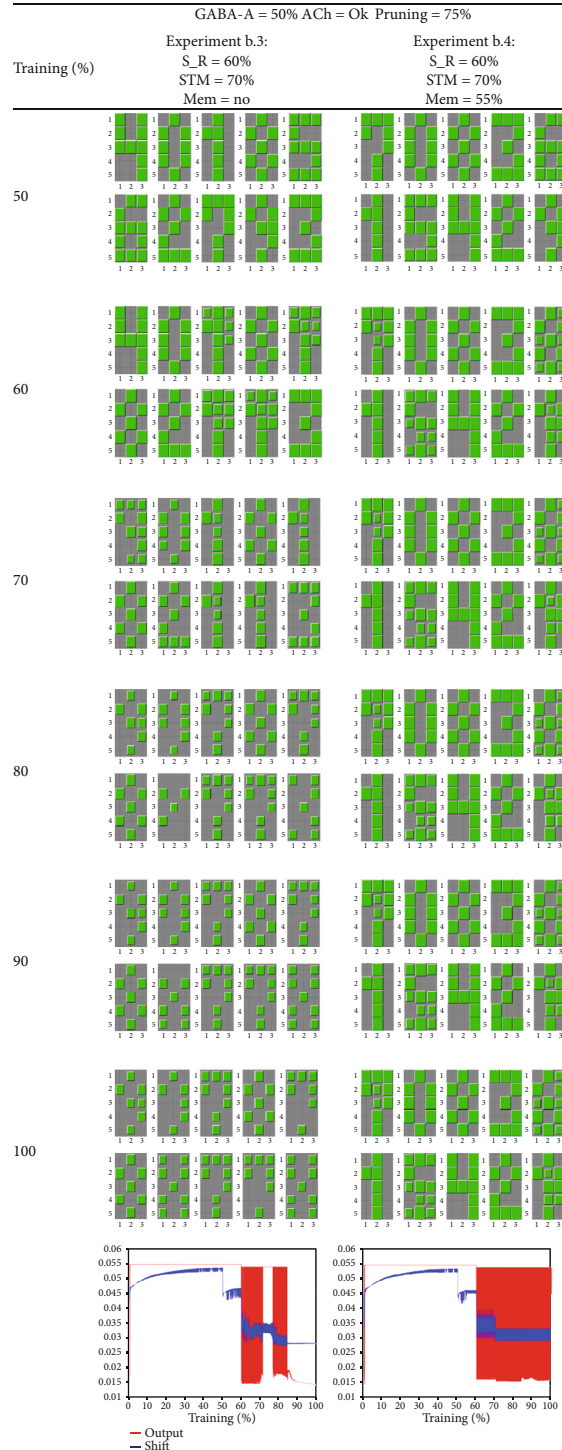
FIGURE 8: This table shows the koniocortex model behavior when the reduction of sensory stimuli takes place after a reduction in GABA-A. A short-term memory (STM) learning task is shown in the first and second columns, consisting of learning an "X" pattern in substitution of one of the numerical patterns that constitute the learning set. In the second column, we evaluate the usage of NMDA blockers like memantine. At the bottom of each column, we show the evolution of all neurons' average output (in red) and average shift (in blue). Experiment b.3: the pattern "X" presented at 70% of repetitions is successfully learned. Despite this apparent success, the univocal correspondence between patterns and neurons that were compromised at 60% of epochs did not return to normal. Notice that episodes of oscillation and stabilization are intermingled and that learning a new pattern stabilizes the network, although this stable situation is usually transitory. In experiment b.4, the administration of an NMDA blocker like memantine took place at 55% of epochs. Numerical pattern memories are kept intact, but, when introducing pattern "X" at 70% of repetitions, the network was incapable of learning it. Stimulus reduction at 60% in a GABA-A-depleted network contributed to the initiation of persistent oscillations. Labels: S_R = sensory reduction; STM = short-term memory; Mem = memantine; ACh = acetylcholine reduction in thalamocortical neurons.
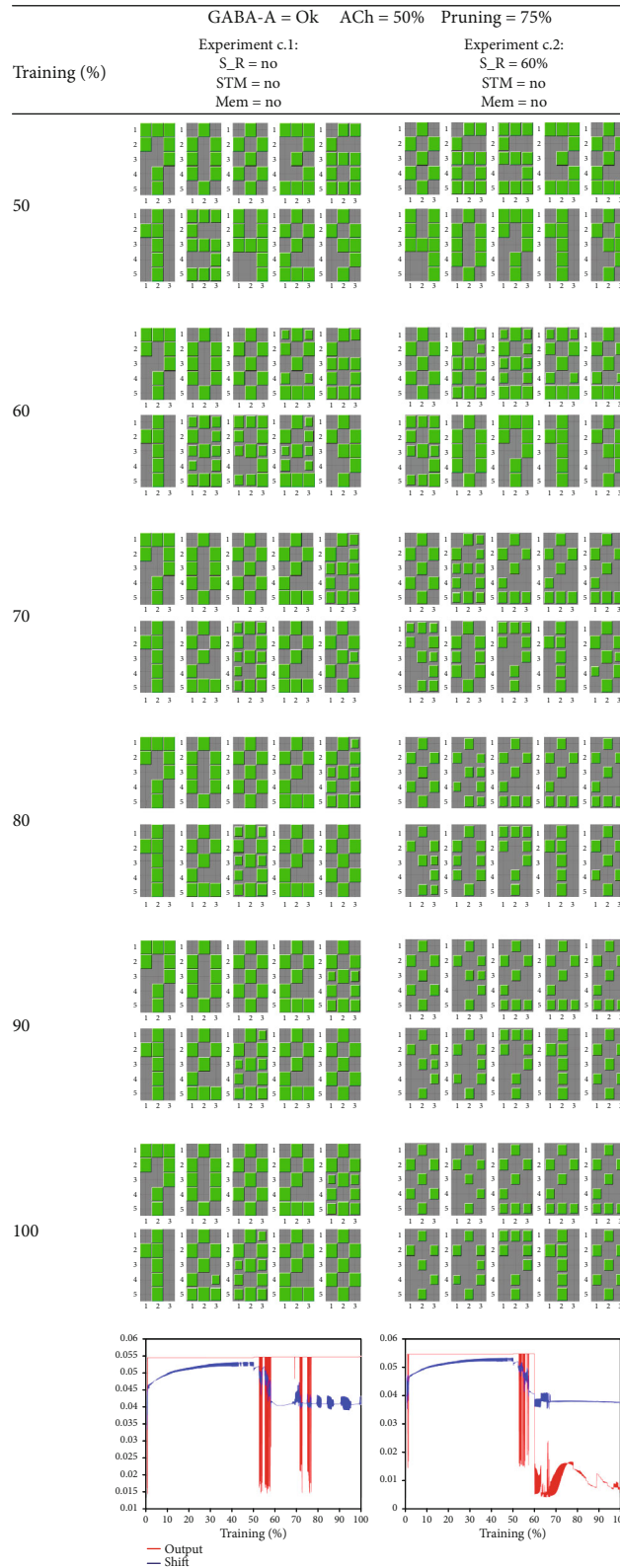
FIGURE 9: In these experiments, we reduce the effect of ACh at 50% of epochs. Experiment c.1, in which no other modification is involved, represents a control test for comparison with subsequent experiments. In this case, the bottom graph exhibits sparse oscillations of the average output. Experiment c.2, in which stimulus reduction takes place at 60% of epochs, produced smaller but sustained oscillations that are harmful to learning patterns. Labels: S_R = sensory reduction; STM = short-term memory; Mem = memantine; ACh = acetylcholine reduction in thalamocortical neurons.

separation and competitive learning. However, many competitive networks do not use this preliminary process of pattern separation and still do their job. Consequently, we do not expect that slowing down sigmoid shifting (by reducing or zeroing factor v in Equation (A.7)) will significantly impair learning.

The following is our eight-stage protocol:

(1) Initially, the network's goal is to learn ten different numerical patterns (Figure 3). Learning takes place when each SS neuron fires only in front of one specific numerical character. Simultaneously, each SS neuron produces a copy of each current pattern, as explained in this section. If the copy is identical, learning is Ok. The more different the copy, the more unsuccessful is the learning process

(2) At half the number of repetitions, we "age" the network by either simulating GABA-A impairment or a lack of ACh. GABA-A impairment is modeled by eliminating the normalization operation performed by shunting basket neurons. The lack of ACh that precludes the sigmoid shift is simulated, as previously explained, by setting parameter v to zero in thalamocortical neurons

(3) At 60% of the total amount of repetitions, we apply stimulus reduction by dividing each component of the numerical patterns by two ("pixel value"/2).

(4) At 70% of the repetitions, we evaluate network performance using a short-term memory task. In this case, one of the numerical patterns (randomly selected) is replaced by the letter "X." The network's performance during the task of learning this new pattern can be evaluated by the reader by conferring the numerical learned by each neuron (as explained in stage 1)

(5) In some simulations (at 55% of the repetitions), we test the situation of applying an NMDA blocker (like memantine). We perform this test by preventing synaptic weight modifications

(6) To assess hypermetabolism, we calculate the average output of all modeled neurons (not counting sensory neurons) over time. Hypermetabolism takes place when the average output is persistently oscillatory

(7) We also assess the temporal evolution of the average neurons' firing threshold, that is to say, the average shift (not counting sensory neurons). Hypermetabolism is associated with average shift changes because these changes involve intrinsic channel creation and elimination

(8) When the number of iterations is higher than 75%, synaptic pruning (see Section 1.3.1) starts running in the network. According to Huttenlocher [55], at the age of 74 (after a long period during which synaptic density stabilizes around 11.05×10^8 synapses/mm^3) synaptic density begins a steady decay at a rate of 18.63×10^6 synapses/mm^3 per year. Trans-

lating these values to our artificial model, at 74% of the iterations, we start a pruning process in which 1.7% of the synapses (those with the smallest synaptic weights) are pruned at each iteration

3. Results

The koniocortex model used here for testing the AD has fifteen neurons in its input layer, fifteen neurons in its thalamocortical neurons' layer, ten neurons in the spiny stellate neurons' layer, and ten neurons in the upper basket neurons' layer (Figure 2). The learning process of the koniocortex model allows the recognition of a set of 10 numerical patterns. A 5×3 grid displays these numbers. All these numeric patterns are presented sequentially to the network in each epoch. Once each number is input to the network, its activation is "propagated" until all layers are activated. One thousand epochs were enough for the NN to learn that when a specific SS neuron strongly fires in front of one particular numerical pattern, the remaining neurons should remain inactive. This WTA process occurs naturally as an emergent consequence of the individual computation of each neuron without the need to monitor the network externally. Lateral inhibition and IP are the main driving forces for the emergence of this WTA process.

To computationally test AD, we added one thousand additional epochs. These repetitions were intended to simulate the reduction of sensory stimuli and the GABA-A and ACh deficiencies that are customary in an aged brain. We will also evaluate how the network behaves in a continuous learning task, after substituting one of the patterns by a completely new one, an "X" pattern in the middle of typical training. We intend to do this experiment under defective conditions of the network so that we could evaluate how the capacity of continuous learning of the network is affected by the different types of impairment. For comparison purposes, we first present to the reader the same experiment under physiological conditions (without any kind of impairment). Each row of Figure 5 represents the results of training the koniocortex model along with a certain number of iterations (epochs). It shows that each one of the ten spiny neurons becomes specialized in recognizing a specific numerical pattern. This fact means that, when we present a numerical pattern to the network, one single spiny neuron "fires" (i.e., is active) while the other neurons remain muted. For example, only neuron "one" fires when pattern zero is presented at epoch 450 (see the first case in the first row). When spiny neuron "one" fires, it "evokes" number zero in the form of a green pixels' matrix, each pixel corresponding to the weight of a recurrent connection from itself (spiny neuron 1) to the input neurons. This process occurs at the recurrent ancillary network mentioned in Section 2. In the case the matrix was ambiguous or defective, it would mean that either a change of pattern or a memory problem is occurring in that neuron.

In this physiological example, when we reach 50% of the total number of epochs (500 epochs), we remove a numerical pattern, in this case, pattern 1, from the training set, and put the letter X in place. At epoch 550, we see that spiny neuron three and spiny neuron ten are "evoking" unclear, ambiguous

patterns. This fact means that neurons are readjusting their weights for recognizing the new pattern X and forgetting the older pattern one. At epoch 600, the weights of spiny neuron 3 (that formerly "evoked" pattern two) evolve to represent pattern X. At epoch 600, the weights of spiny neuron 10 are still under transformation. This transformation is complete at epoch 650 when the recurrent weights from spiny neuron 10 evolve to represent pattern two. In this way, neuron ten that previously fired in front of pattern one now fires when pattern two is input to the network. At the same time, neuron three that fired when pattern two was input to the network, now fires in front of pattern X. At epochs 650, and epoch 700, the property of continuous learning of the koniocortex allowed the network to forget pattern 1 and learn pattern X. The bottom graph exhibits two curves, one curve in red and the other in blue representing the evolution of the average output and the average shift, respectively (without including sensory neurons). Both curves are stable and regular, although the blue curve exhibits small continuous oscillations.

As previously announced, this same short-term memory (STM) test will be performed in some of the simulations when training reaches 70% of epochs under nonphysiological (defective) conditions.

Figures 6–11, will show the different tests performed in the koniocortex model. Each column header will indicate the type of alteration performed in the network and the percentage of epochs when the alteration took place. The meanings of the abbreviations inside the headers are as follows:

(a) Pruning = 75% means that the elimination of weak connections occurs from 75% of iterations

(b) GABA − A = 50% means that, at 50% of training epochs, the normalization resulting from GABA-A activity is eliminated

(c) ACh = 50% means that a reduction of ACh occurs at 50% of repetitions. In computational terms, this means that the sigmoid function stops shifting when parameter v becomes zero

(d) S_R = 60% means that there is a reduction of sensory stimuli (S_R) at 60% of all repetitions

(e) STM = 70% means that a short-term memory test (STM) is performed by replacing a randomly selected pattern with the "X" pattern at 70% of the repetitions

(f) Mem = 55% means that synaptic weight modification is prevented due to the use of memantine (Mem) at 55% of the repetitions

As synaptic pruning is present in every aging person (>75 years of age), all experiments run with pruning. The description of the performed tests and their corresponding parameters are summarized in Table 1.

We repeated each of the experiments 20 times. Since the initial weights and neuron firing thresholds are random, different results are produced until the network stabilizes. This type of variation mainly occurs during the first 100 epochs. After this number of epochs, the experiments evolve similarly and become consistent across repetitions. For this reason, we

randomly selected one of the repetitions as a representative of each experiment (see Figures 6–11).

Under each one of the headers, there is a column of blocks. Inside each block, there are ten different numerical patterns. From left to right and from top to bottom, each of the ten numbers represents the patterns that are recalled by the ancillary network when each one of the ten stellate spiny neurons fires. For example, the block that appears in a row labeled 70 represents the ten patterns that are recalled by the ten SS neurons at 70% of repetitions. In this block, for example, the third numerical pattern in the upper row is the pattern recalled by the third SS neuron.

Finally, the bottom curves represent the evolution of the average output and shift of neurons, in terms of the percentage of epochs. These graphs help in the identification of hypermetabolism, which is the preliminary manifestation of AD. Hypermetabolism appears when there are intense and persistent oscillations both in the average output and average shift. Persistent oscillations are associated with a continuous process of allocation and elimination of intrinsic channels in the neuron's membrane.

Now, we proceed to explain the behavior in each column of the tables.

Let us start with Figure 6, which shows the experiments modeling healthy aging. In experiment a.1, we simulate the case of a healthy normal koniocortex in which we blocked neither GABA-A, ACh, nor NMDA. Pruning follows the normal statistical tendency described in the last paragraph of Materials and Methods, thereby starting at 75% of the total epochs. The task of learning a new pattern at 70% of repetitions is successful, as can be seen in the block at 80% in which we substitute a random numerical pattern (in this case number 4) by pattern "X."

The evolution of the average output (in red) and average shift (in blue) of all modeled neurons appears at the bottom of each column. In the case of healthy aging, the oscillations observed in the output when substituting the pattern are negligible.

In experiment a.2 (also corresponding to healthy aging), stimuli diminish at 60% of the epochs (S_R = 60%). As previously explained, we do this by dividing each component of the numerical patterns by two (pixel value/2). Starting at the block corresponding to 70% of epochs, we see that the patterns recalled by each one of the neurons become fainter. Immediately after stimulus reduction, there is a temporary shift stabilization that quickly leads to a regime of discrete oscillations of the average shift. Although there are a few oscillations during the initial iterations, which is the normal expected behavior, the average output in (red) remains stable in all subsequent iterations.

Let us continue with Figure 7 and Figure 8 showing the experiments that model aging associated with impaired GABA-A receptors. In experiment b.1, we withdrew normalization (due to GABA-A shunting neurons) at 50% of repetitions. In this experiment, there is neither stimulus reduction nor an STM task. This experiment was performed to demonstrate the impact of GABA-A reduction alone, without the presence of other concomitant factors. In this case, the first column in Figure 7 shows an episodic pattern recall impairment from around 60% of epochs. At the same time, the
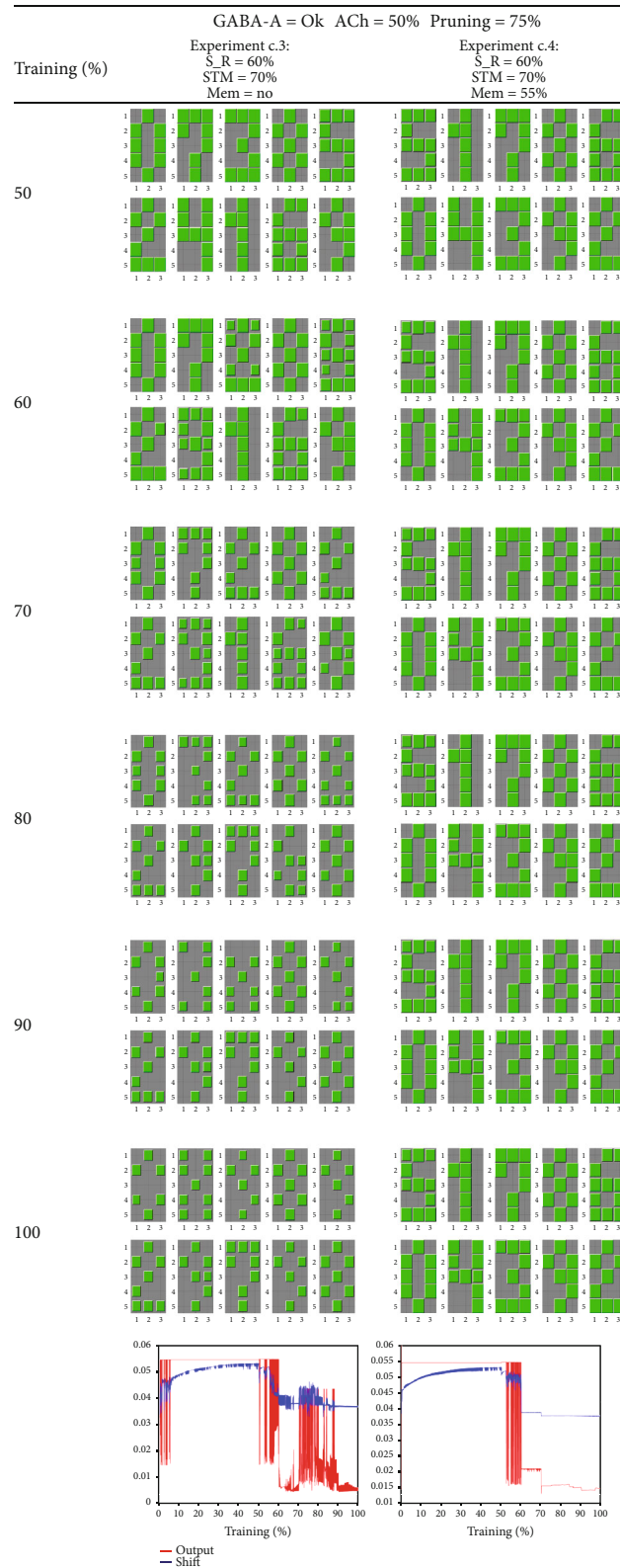
FIGURE 10: This table shows the koniocortex model response when GABA-A levels are normal, and we reduce ACh at 50% of repetitions. Sensory reduction also takes place at 60% of total repetitions, and a memory test is performed at 70%. Experiment c.3: an NMDA blocker (like memantine) is not used. Oscillations are present initially when ACh is reduced and, especially afterward, during the process of learning the new pattern X. Experiment c.4: an NMDA blocker (like memantine) is applied at 55% of epochs. In this case, plasticity is eliminated; the network remains at its former stability level (without oscillatory activity) although it is not able to learn the testing pattern X. Labels: S_R = sensory reduction; STM = short-term memory; Mem = memantine; ACh = acetylcholine reduction in thalamocortical neurons.
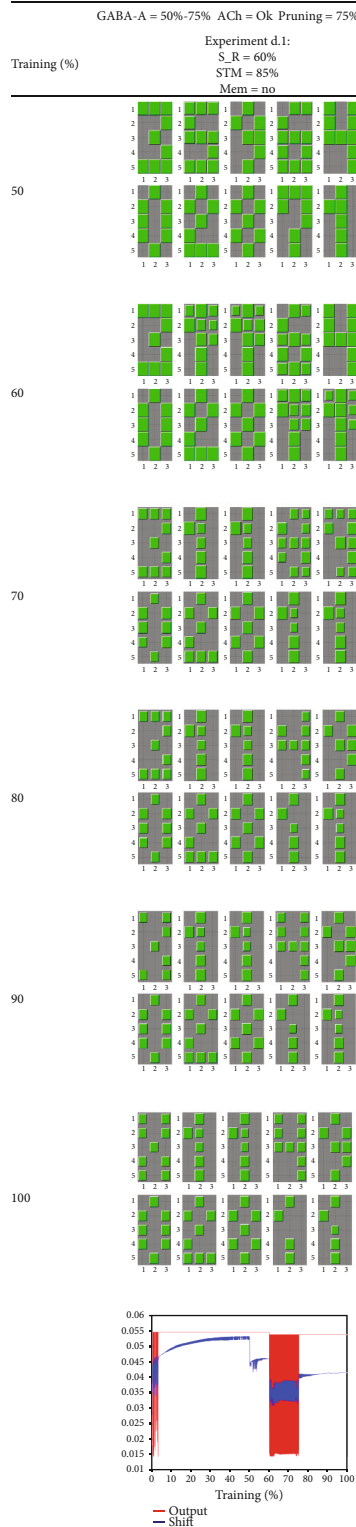
FIGURE 11: This table presents a case in which GABA-A normalization is recovered despite the usual process of network aging. After the elimination of GABA-A normalization that occurred at 50% of epochs, pattern learning was impaired; that is to say, patterns were poorly recovered, and neurons lost their pattern specificity. With the reduction of sensory stimuli at 60% of epochs, the average shift and output started an intense oscillatory dynamic that suddenly disappeared when GABA-A normalization was reinstalled at 75% of repetitions. After this recovery, the network was capable of learning pattern X, while the recovery of the remaining numerical patterns was damaged. At this later stage, in which many of the connections were pruned, learning is a difficult process requiring much more repetitions than in an intact network. Labels: S_R = sensory reduction; STM = short-term memory; Mem = memantine; ACh = acetylcholine reduction in thalamocortical neurons.

average output (see bottom graph) exhibited a transitory abrupt oscillation that quickly ended due to compensatory factors (intrinsic and synaptic plasticity). Although oscillations ceased, the impairment in patterns' recalling was permanent. This case means that although GABA-A deficit alone does not have catastrophic consequences in terms of hypermetabolism (because oscillations cease), there could be some sequels in terms of memory deficits.

In experiment b.2, besides normalization due to GABA-A withdrawal at 50% of repetitions, stimulus reduction occurred at 60% of epochs. When running the program, we see that at 50% of training, each neuron still processes a different numerical pattern, as expected. From this moment in which GABA-A normalization stopped, patterns' recalling was impaired. Patterns' memorization worsens, and neurons lost their specificity for patterns; that is to say, several neurons fire in front of the same pattern.

Experiment b.3 is shown in the first column of Figure 8 and is similar to the previous one (b.2): each neuron had learned to identify a specific numerical pattern, and, at 50% of epochs, we eliminate the normalization performed by GABA-A. Like in the previous case, the lack of normalization impaired learning so that the univocal correspondence between neurons and patterns was lost. As before, with stimulus reduction at 60% of epochs, abrupt oscillations appeared in the shifts and outputs. Despite this, at 70% of epochs, we applied the task of substituting one of the patterns by pattern X. The network learned pattern X, but the univocal correspondence between patterns and neurons continues impaired. It seems that learning a new pattern contributes to stabilization because the oscillations dampen during pattern X presentation.

Experiment b.4 is like the previous one but with the introduction of an NMDA blocker at 55% of repetitions. Although the network did not forget the numerical patterns, it was not able to learn the new pattern "X" when introduced at 70% of epochs. Differently from the previous case, the presentation of pattern X does not dampen the oscillations.

In summary, an NMDA blocker contributes to preserve older memories but is not capable of preventing the oscillatory dynamics due to stimulus reduction.

The experiments of Figure 9 (c.1 and c.2) and Figure 10 (c.3. and c.4) are designed for testing whether ACh deficit alone is able to produce AD symptoms. Let us recall that the ACh deficit (due to an impairment of the parabrachial nucleus) weakens the preliminary process of input vector separation that takes place in thalamocortical neurons. Experiment c.1 represents a control test for comparison with the next ones. The graph at the bottom of the table shows sparse bursts of oscillations in the outputs and shifts. When we analyzed learning, epoch by epoch, we noticed that during these bursts, the association between neurons and learned patterns is impaired.

In experiment c.2, stimulus reduction is applied at 60% of epochs. In this case, stimulus reduction, instead of increasing the oscillations, seems to dampen them. These sustained oscillations are responsible for the learning impairments seen in the following blocks along training epochs.

In experiments c.3 and c.4, we use the combination of features of experiment c.2 with a short-term memory experiment (STM) for evaluating the use of an NMDA blocker (i.e., memantine). As in previous cases, the STM test consists of substituting a randomly selected pattern by pattern X at 70% of epochs. When this test is done in experiment c.3 without an NMDA blocker application, the NN learned pattern X, but the process was slower and generated intense oscillations. In the experiment c.4, oscillations are abolished when using an NMDA blocker at the expense of not being able to learn pattern X.

Experiments c.1 to c.4 shows that when GABA-A inhibition is normal, ACh deficit produces oscillations that are sparser and weaker than in the case of the association of GABA-A and stimulus reduction. In the cases of ACh deficit, many strategies contribute to abolishing the oscillations, like the NMDA blocker application. Even the reduction of stimuli (that was catastrophic in the case of GABA-A deficit) can help to dampen the oscillations. In contrast (as shown in experiment c.3), STM stimulation can be counterproductive, especially in the absence of memantine. It seems that the cognitive stimulation (STM test) can be either beneficial or harming depending on whether there is either a GABA-A deficit or an ACh deficit, respectively.

The purpose of Figure 11 is to simulate a possible recovery from hypermetabolism when GABA-A signaling returns to normal levels. In this experiment, there was no ACh deficit. Hypermetabolism was manifested by the persistent oscillations of the average shifts and outputs. These oscillations were the consequence of GABA-A deficit followed by stimulus reduction, as shown in examples b.2, b.3, and b.4. At 75% of epochs, GABA-A levels were restored. From this moment, there was a moderate recovery of the patterns recalling capacity, and when an STM test was introduced with pattern X at 85% of epochs, the test was successful. Despite this, the process of synaptic pruning that started at 75% altered the usual course of learning, which, in this case, took longer than in a normal situation and did not end until reaching 100% of epochs. This experiment shows that when GABA-A levels return to normal, there is a real possibility of recovery (although this would depend on the severity of further damage due to beta-amyloid plaque accumulation).

It would be possible to create new alternative computer experiments for testing different therapies like combining NMDA blockers, cognitive stimulation, cholinesterase inhibitors, etc. In these alternative experiments, the correct scheduling of each treatment would be of great importance. Testing these therapies first in the computer and, afterward, with real subjects will be extremely useful and will contribute to the development of an optimal therapeutic strategy.

4. Discussion

The experiments presented here show that it is possible to evaluate the evolution of AD with a computational model of a brain structure with learning capabilities under different scenarios. We created these scenarios by combining the effects of neuromodulators, pharmacological drugs, and sensory patterns. In this study, we chose the koniocortex because, as mentioned in Introduction, AD begins in sensory cortices [27–29] (although appearing in its mildest form).

Besides, this structure is directly associated with sensory stimuli, which we were interested in assessing. Another advantage of the modeled koniocortex is that it exhibits successful emergent learning so that we can test the effects of AD along with a learning task.

As seen in Results, we decided to exhibit neurons' average output and their firing thresholds (shifts) over 2,000 training epochs (as mentioned, the presentation of the whole set of numbers constitutes one epoch).

We also presented the appearance of the memorized patterns over epochs. In this way, we displayed three crucial variables related to AD: first, the red curves allow us to study neurons' average firing probability and identify hypermetabolism. Secondly, the blue curves enable us to see the shifting of the firing threshold and infer the amount of intrinsic channel allocations in neurons' membranes (the smaller the shift, the higher the number of intrinsic channels). Thirdly, the appearance of memorized patterns over the epochs allows us to monitor long and short-term memory in the network. We assessed these variables by altering the input stimuli or simulating a treatment. Our interest in monitoring the possible oscillatory activity in the average firing and shift related to hypermetabolism is because hypermetabolism is the prelude to the more harmful consequences of AD: β-amyloid plaque creation and memory impairments. Hypermetabolism would be the consequence of continually placing and deleting intrinsic channels when the neuron's firing threshold (activation function's shift) tries unsuccessfully to reach an equilibrium point. Although hypermetabolism and neuronal activity are related concepts, hypermetabolism can be easily monitored in human patients using PET and MRI scans.

The main result derived from our model is that, although stimulus reduction is innocuous in a young, healthy brain, it ignites hypermetabolism in a brain with GABA-A signaling deficits. ACh impairments are also able to produce hypermetabolism more moderately. This is because we discovered that GABA-A and ACh are involved in computational processes that facilitate pattern normalization and pattern separation, respectively, during the learning processes performed in the brain [26]. In this way, disruption of the algorithms involved in learning processes in the brain seems to be at the origin of the destructive processes of AD. Regarding learning, brain structures like the koniocortex adjust their synaptic weights so that they acquire stable values through homeostatic processes in which IP compensates for weight variations [22]. In a previous article, we suggested that impairments in IP are a crucial factor for the onset of AD [91]. The importance of IP in learning and AD has been corroborated by Dunn and Kaczorowski [92]. Calcium homeostasis processes underlying AD are also discussed in Popugaeva et al. [93].

The explanation behind the oscillatory behavior triggered when stimulus reduction takes place in a GABA-A-deficient brain is that GABA-A shunting basket neurons produce a sort of pattern normalization (see Section 1.3 and explanation of Equation (A.3) in the appendix) over incoming sensory patterns. When these basket neurons correctly perform their normalizing function, the resulting computation is as if all sensory patterns were always similar in size. In this

case, GABA-A represents a protective factor that acts even in the case of reduced stimuli (which, due to GABA-A, are resized, i.e., normalized). When the protective factor of GABA-A is not present, reduction of stimuli (like in macular degeneration, deafness, and retirement) triggers a process in which neurons lower their firing threshold through IP to adequately respond to weaker stimuli (recall explanations of Equations (A.6) and (A.7) in the appendix). For this process, extra intrinsic channels are allocated in the cellular membrane, having this process a high metabolic cost. Although in an ideal situation, neurons would adjust their firing thresholds until they gradually reach a new lower threshold, in our simulations, these adjustments take place in an oscillatory manner. In this case, firing threshold adjustments take place along a continuous recurrent process of allocation and elimination of intrinsic channels. Repeating these processes, thousands of times would produce a much higher cost in metabolic terms than when intrinsic channels are simply gradually allocated.

During intrinsic channel allocation processes, the intense firing of neurons is another process that contributes to enhancing hypermetabolism. Besides impaired neural homeostatic processes, intense firing has been considered another cause of β-amyloid plaque deposition [94, 95]. Thus, the preemptive usage of low doses of antiepileptic drugs like diazepam [96] and levetiracetam [97] has been shown to have a neuroprotective effect in AD.

When instead of a GABA-A deficit, there is ACh depletion, the preliminary process of input vector separation is affected, as explained in Figure 4. Without this vector's separation process, the subsequent WTA operation requires more epochs to be accomplished. This is manifested in the short-term memory test performed in experiment c.3, in which the modest oscillations associated with ACh deficits grew significantly. It seems that in this case, cognitive stimulation is counterproductive and could contribute to exacerbating hypermetabolism. In experiment c.4, we see that by using an NMDA blocker, oscillations completely disappear at the expense of not being capable of learning the new pattern X. This fact could justify the success of treatments combining NMDA blockers (memantine) and acetylcholinesterase inhibitors (donepezil) [98] in a background of milder oscillations related to an ACh deficit [99].

In the case of GABA-A deficit, the oscillations that appear after stimulus reduction are much higher in frequency (see curves in experiments b.2, b.3, b.4, and d.1) than those related to ACh impairment (experiments c.2 and c.3). The existence of a relationship between GABA interneuron malfunction and intense neural oscillatory activity was pointed out by Verret et al. [100] when working in AD animal models. Regarding a possible AD treatment, experiment d.1 is designed to test whether the complete recovery of GABA-A functionality at 75% of epochs can stop the oscillations. We see that not only the intense oscillatory activity completely disappears but also the learning capability of the network is wholly recovered so that it was possible for the network to learn a new pattern (pattern X) that was presented at 85% of computer iterations (in Figure 11, the tiles in green show that this pattern was learned entirely at 100% of epochs by number one stellate neuron).

These computational results support recent pharmacological studies focusing on GABA-A neurons' protecting drugs [101–103]. Experiment a.2 shows that when GABA-A functionality is preserved, no oscillations take place even in the case of stimulus reduction. As mentioned in Section 1.3.3, the ingestion of nutrients like fisetin (strawberries, tomatoes, oranges, and cucumber) and terpenoids (salvia, peppermint, ginger, Curcuma longa, cinnamon, cloves, and mustard) collaborates in the synthesis and expression of GABA-A receptors.

Although the results of the present experiment are encouraging, we should acknowledge, however, that we assessed AD by modeling a particular brain structure and that other brain structures related to learning also deserve evaluation. It is possible that the same computational process that seems impaired in the koniocortex, i.e., pattern separation and pattern normalization, might also be defective in other parts of the brain, thereby generating an abnormal oscillatory dynamic. These prospective assessments performed in more comprehensive models might contribute to support our hypothesis that AD is a consequence of stimulus reduction in a brain with GABA-A deficit. Although, as mentioned in Introduction, we prefer to perform such tests on models whose functionality is clear to us, we do not underestimate the potential of existing realistic models of the entire brain [14, 17]. We believe that the most significant drawback presented by these comprehensive models is that most of them surprisingly fails to use the property of IP. We believe that by incorporating IP into these models, new functionalities would emerge from them, such as learning and pattern completion capabilities, in such a way that they could also be used to model the cognitive impairments of AD.

5. Conclusions

As mentioned in Introduction, AD is a multifaceted illness in which the factors involved are usually separately analyzed. In this work, we combine many of these factors, interacting dynamically inside a computational model of the cerebral koniocortex, the first cortical relay station to process sensory information, and also one of the early nervous system structures that are affected by AD.

We tested this hypothesis with the koniocortex model engaged in the task of learning ten numerical patterns. The model underwent a short-term memory test by substituting one random pattern by pattern X in the middle of learning. Another situation performed with the koniocortex simulation was to stop the synaptic weight adjustment as when using an NMDA blocker. During these scenarios, we assessed whether the network exhibits hypermetabolism, which is a common feature during the initial stages of AD. Due to the possibility of an increment in computational complexity, instead of metabolism, we evaluated a related measurement: the average output of all koniocortex neurons.

The computation shows that the onset of AD is related to a reduction of sensory/cognitive stimuli (like in deafness, macular degeneration, or retirement) when there is a preexistent deficit in GABA-A. In computational terms, the lack of pattern normalization due to the divisive inhibition of basket neurons leads to an oscillatory behavior of the neurons' outputs and their firing thresholds. In real neurons, the continuous adjustment of the neuronal firing threshold by allocating and eliminating intrinsic ion channels exhausts neurons' metabolic resources, driving them to the phase of beta-amyloid plaque deposition that is beyond the scope of our study.

Although our hypothesis should be tested in animal models and, afterward, with real patients, we suggest that in the meantime, for preserving elders' health, their caregivers should be on alert in front of scenarios that contribute to the reduction of the sources of stimuli. A confinement situation for epidemic contention could be a nowadays example of these scenarios. In this type of situation, it would be desirable to look for alternative sources of cognitive and sensory stimuli for this group of people.

Appendix

Mathematical Foundations of Koniocortex Network

In this section, we describe the equations used in the koniocortex model in which the neurons' output yields a probability value ranging from 0 to 1. For simplicity, we do not model neurons' axon cable phenomena.

The koniocortex is a competitive model in which the neuron's net-input is calculated by a vector projection. For this calculation, we compute the inner product of weight vectors and the normalized input patterns (lowercase notation meaning vector normalization):

$$\vec{i} = \frac{\vec{I}}{\left\| \vec{I} \right\|}. \tag{A.1}$$

The type of normalization used here is the l1-norm:

$$\left\| \vec{I} \right\| = \sum_{i=1}^{n} |I_i|. \tag{A.2}$$

One way of interpreting neurons' weights is as if they were the components of a vector prototype $\vec{T}^j$ so that $\vec{T}^j = \vec{W}^j = [W_{j1}, W_{j2}, \cdots, W_{jn}]$. In this way, the net-input of neurons can be calculated as $net_j = \| \vec{W}^j \cdot \vec{i} \| = \| \vec{T}^j \cdot \vec{i} \| = \| \vec{T}^j_{\vec{I}} \|$ which is the projection of prototype $\vec{T}^j$ over the ongoing input pattern. Although in NNs models the net-input value is dimensionless, it is conceptually equivalent to the postsynaptic activation that in electrophysiology is measured in volts.

In the case of spiny neurons (which undergo competition), we calculate this same result another way:

$$net_j = \frac{\left\| \vec{W}^j \cdot \vec{I} \right\|}{\left\| \vec{I} \right\|}, \tag{A.3}$$
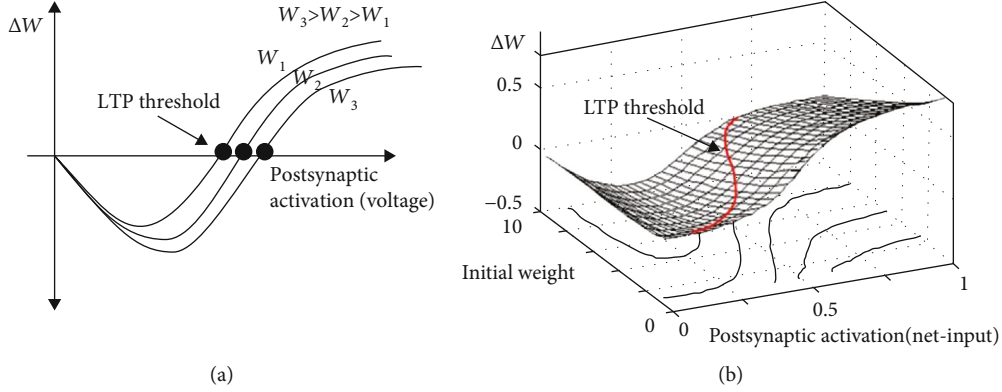
FIGURE 12: (a) Shape of curves obtained with real neurons for different initial synaptic weights w_i. In this case, the experiment consisted of injecting current in the presynaptic neuron and measuring the postsynaptic voltage. The point where curves cross the horizontal axis is called the long-term potentiation threshold. (b) Family of curves obtained in the computer model through the presynaptic rule (adapted from Figure 2 in [105]). Both graphs exhibit metaplasticity: the rightward elongation of the curves along the horizontal axis for higher values of initial synaptic weights. For a more detailed explanation of how the curves were obtained, we suggest the reader to study References ([105] (Section 2), ([22] (Section 3.2)).

where the numerator is the weighted input from excitatory thalamocortical neurons. The denominator corresponds to the operation produced by a shunting basket neuron when performing a sequence of two operations (a) the calculation of an l1-norm, $\|\vec{I}\|$, by summing the thalamocortical inputs and (b) placing this result in the denominator according to the shunting/divisive type of inhibition of GABA-A neurons.

The incremental version of the presynaptic rule was used in the koniocortex model for altering synaptic weights:

$$\Delta W = \xi I(O - W), \tag{A.4}$$

where O and I are postsynaptic and presynaptic action potential probabilities and ξ is a small positive constant, the so-called "learning factor." This learning factor value was set to 0.0019. Synaptic plasticity freezing due to an NMDA blocker was simulated by setting this value to 0.

The plasticity curves yielding the variation of synaptic weight in terms of postsynaptic voltage that were empirically obtained by Artola et al. [104] (see Figure 12(a)) are very similar to the curves depicted in Figure 12(b) obtained by using the presynaptic rule equation [22, 105]. The presynaptic rule also models metaplasticity [106, 107], a property of biological synapses that elongates the plasticity curves rightwards for higher initial synaptic weights, as shown in both graphs of Figure 12.

The function that relates the neuron's output in terms of its postsynaptic activation can be modeled in different ways (like a linear, sigmoidal, and Gaussian function). In the case of the koniocortex, inhibitory neuron activation functions were modeled as linear functions. For modeling sensory, thalamocortical, and spiny neurons, we used the following equation yielding the output of the neuron, O_j, in terms of its net-input (postsynaptic activation):

$$O_j = \frac{1}{1 + e^{-k\left(\text{net}_j - s_j\right)}}, \tag{A.5}$$

where s_j is the shift of the activation function ranging from 0 to 1 and k is a steepness factor whose value depends on the type of neurons.

Biological neurons exhibit a property called intrinsic plasticity (IP) [32]. According to this property, the sigmoidal activation function gradually shifts rightwards or leftwards, leveling the activation of highly or scarcely activated neurons, respectively (see Figure 1). The so-called shift parameter s_j, ranging from zero to one, is used to model the sigmoidal curve rightward shift. The shift value corresponds to the steepest point of the sigmoid curve and is equivalent to the classical concept of "firing threshold." We can formulate the activation function as

$$O_j = f\left(\left\|\vec{T}_I^{\,j}\right\|, s_j\right). \tag{A.6}$$

According to Desai ([33], p.398), the activation function relates a neuron's output (its firing rate) to its input (the synaptic current it receives). If the input is too low, the cell will hardly ever fire, because of the spike threshold [The firing threshold.]; if it is too high, the firing rate will saturate, because there is some physical limit on how fast a neuron can fire. Between the two is a sensitive region, where the neuron's output is a function of its inputs. One strategy for dealing with fluctuations in input – caused, for example, by synapse formation or Hebbian potentiation – is to shift the position or slope of the f–I curve so that the sensitive region always corresponds well with average input.

We proposed the following equation [22] for calculating the shift of the activation function, s, at time t in terms of the shift and output probability of the neuron at time t-1:

$$s_t = \frac{v \cdot O_{t-1} + s_{t-1}}{v + 1}, \tag{A.7}$$

where v is a small factor that adjusts the shifting speed of the
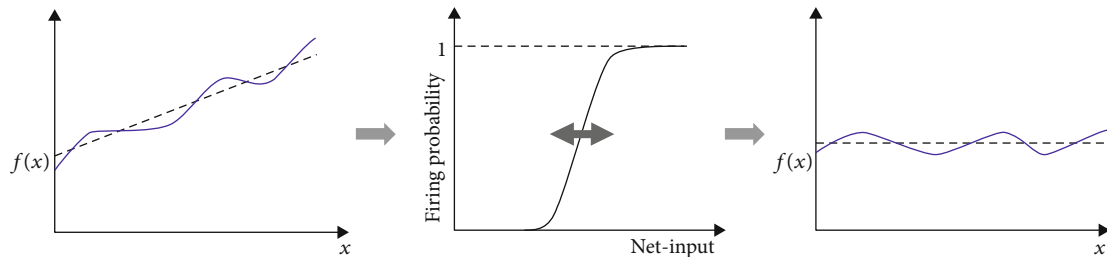
Figure 13: When a time series $f(x)$ is placed at the single input of a neuron with intrinsic plasticity property, the output of the neuron is the same time series $f(x)$ but with its moving average removed.

activation function. Its value is 0.0199 in the koniocortex simulation. The initial shift, s, was 0.061 in all neurons. When neurons are highly activated, the tendency of the shift factor, s, is to increase, thereby shifting the activation function rightwards. When neurons are less activated, the tendency of the shift factor, s, is to decrease, so that the activation function is shifted leftwards (see Figure 1).

One compelling case that occurs in thalamocortical neurons refers to a single input neuron, where IP contributes to removing the moving average of a series of input values ([26], section 2), making the neuron behave like a high-pass filter (see Figure 13).

When, instead of a single neuron, there is a matrix of neurons receiving patterns (like the case of thalamocortical neurons), subsequent patterns undergo the subtraction of their moving average (which is also a pattern), thereby making patterns more separated from each other, like in Figure 4. This input vector separation effect stops when we eliminate the movement of the sigmoid by zeroing factor v. In the real koniocortex, this happens when ACh neurons are blocked or die, thereby losing their boosting effect over intrinsic thalamocortical plasticity.

Data Availability

The computational codes used in this manuscript are available at https://osf.io/hkx9w. This material included the MATLAB code used to support the findings of this study.

Conflicts of Interest

The authors declare no conflicts of interest.

Authors' Contributions

Mariana Antonia Aguiar-Furucho and Francisco Javier Ropero Peláez contributed equally to this work. All authors have approved the submitted version.

Acknowledgments

References

[1] A. Schüz and G. Palm, "Density of neurons and synapses in the cerebral cortex of the mouse," *Journal of Comparative Neurology*, vol. 286, no. 4, pp. 442–455, 1989.

[2] G. P. Dugué, W. Akemann, and T. Knöpfel, "A comprehensive concept of optogenetics," *Progress in Brain Research*, vol. 196, pp. 1–28, 2012.

[3] P. S. Churchland and T. J. Sejnowski, *The Computational Brain*, The MIT Press/Bradford Books, Cambridge, MA, 1992.

[4] J. A. Reggia, E. Ruppin, and R. S. Berndt, "Modeling brain and cognitive disorders," in *Neural Modeling of Brain and Cognitive Disorders*, J. A. Reggia, E. Ruppin, and R. S. Berndt, Eds., vol. 6 of Progress in Neural Processing, pp. 3–39, World Scientific, USA, 1996.

[5] J. L. McClelland, D. E. Rumelhart, and PDP Research Group, "Chapter 25: Amnesia and distributed memory," in *Parallel Distributed Processing: Explorations in the Microstructure of Cognition: Psychological and Biological Models*, vol. 2, pp. 503–527, MIT Press, Cambridge, MA, USA, 1986.

[6] J. A. Reggia, P. M. Marsland, and R. S. Berndt, "Competitive dynamics in a dual-route connectionist model of print-to-sound transformation," *Complex Systems*, vol. 2, no. 5, pp. 509–547, 1988.

[7] K. E. Patterson, M. S. Seidenberg, and J. L. McClelland, "Connections and disconnections: acquired dyslexia in a computational model of reading processes," in *Parallel distributed processing: Implications for psychology and neurobiology*, R. G. M. Morris, Ed., pp. 131–181, Oxford University Press, UK, 1989.

[8] J. A. Reggia, S. Goodall, Y. Chen, E. Ruppin, and C. Whitney, "Modeling post-stroke cortical map reorganization," in *Neural Modeling of Brain and Cognitive Disorders*, J. A. Reggia, E. Ruppin, and R. S. Berndt, Eds., vol. 6 of Progress in Neural Processing, pp. 283–302, World Scientific, USA, 1996.

[9] M. Spitzer, "Phantom limbs, self-organizing feature maps, and noise-driven neuroplasticity," in *Neural Modeling of Brain and Cognitive Disorders*, J. A. Reggia, E. Ruppin, and R. S. Berndt, Eds., vol. 6 of Progress in Neural Processing, pp. 273–282, World Scientific, USA, 1996.

[10] J. L. Contreras-Vidal, H. L. Teulings, and G. E. Stelmach, "A Neural Network Model of Movement Production In Parkinson's Disease And Huntington's Disease," in *Neural Modeling of Brain and Cognitive Disorders*, J. A. Reggia, E. Ruppin, and R. S. Berndt, Eds., vol. 6 of Progress in Neural Processing, pp. 377–392, World Scientific, USA, 1996.

[11] R. E. Hoffman, "Neural networks, cortical connectivity and schizophrenic psychosis," in *Neural Modeling of Brain and Cognitive Disorders*, pp. 441–456, 1996.

[12] D. Horn, E. Ruppin, M. Usher, and M. Herrmann, "Neural network modeling of memory deterioration in Alzheimer's disease," *Neural Computation*, vol. 5, no. 5, pp. 736–749, 1993.

[13] M. E. Hasselmo, "Runaway synaptic modification in models of cortex: implications for Alzheimer's disease," *Neural Networks*, vol. 7, no. 1, pp. 13–40, 1994.

[14] V. Cutsuridis and A. A. Moustafa, "Computational models of Alzheimer's disease," *Scholarpedia*, vol. 12, no. 1, p. 32144, 2017.

[15] E. D. Menschik and L. H. Finkel, "Neuromodulatory control of hippocampal function: towards a model of Alzheimer's disease," *Artificial Intelligence in Medicine*, vol. 13, no. 1-2, pp. 99–121, 1998.

[16] M. A. Gluck, C. E. Myers, M. M. Nicolle, and S. Johnson, "Computational models of the hippocampal region: implications for prediction of risk for Alzheimers disease in nondemented elderly," *Current Alzheimer Research*, vol. 3, no. 3, pp. 247–257, 2006.

[17] L. Stefanovski, P. Triebkorn, A. Spiegler et al., "Linking molecular pathways and large-scale computational modeling to assess candidate disease mechanisms and pharmacodynamics in Alzheimer's disease," *Frontiers in Computational Neuroscience*, vol. 13, 2019.

[18] T. Trappenberg, *Fundamentals of Computational Neuroscience*, Oxford University Press, Oxford, UK, 2009.

[19] F. J. R. Peláez, "A formal representation of thalamus and cortex computation," in *Brain processes, theories, and models: an international conference in honor of WS McCulloch 25 years after his death*, vol. 1996, pp. 154–163, MIT Press, Las Palmas de Gran Canaria, Cambridge, MA, USA, 1996.

[20] J. R. Pelaez, "Plato's theory of ideas revisited," *Neural Networks*, vol. 10, no. 7, pp. 1269–1288, 1997.

[21] L. C. Granado, R. Ranvaud, and J. R. Peláez, "A spiderless arachnophobia therapy: comparison between placebo and treatment groups and six-month follow-up study," *Neural Plasticity*, vol. 2007, 11 pages, 2007.

[22] F. J. R. Peláez and D. Andina, "Do biological synapses perform probabilistic computations?," *Neurocomputing*, vol. 114, pp. 24–31, 2013.

[23] F. J. R. Peláez and A. C. Godoi, "From forced to natural competition in a biologically plausible neural network," in *Advances in Self-Organizing Maps*, P. A. Estévez, J. C. Príncipe, and P. Zegers, Eds., vol. 198, pp. 95–104, Springer, 2013.

[24] F. J. R. Peláez, "Towards a neural network based therapy for hallucinatory disorders," *Neural Networks*, vol. 13, no. 8-9, pp. 1047–1061, 2000.

[25] J. R. Pelaez, "Schizophrenia positive symptoms interpreted as cognitive hallucinations," *Lecture Notes in Computer Science*, vol. 2774, pp. 1156–1163, 2003.

[26] F. J. R. Peláez, M. A. Aguiar-Furucho, and D. Andina, "Intrinsic plasticity for natural competition in koniocortex-like neural networks," *International Journal of Neural Systems*, vol. 26, no. 5, p. 1650040, 2016.

[27] R. R. Romito-DiGiacomo, H. Menegay, S. A. Cicero, and K. Herrup, "Effects of Alzheimer's disease on different cortical layers: the role of intrinsic differences in A susceptibility," *The Journal of Neuroscience*, vol. 27, no. 32, pp. 8496–8504, 2007.

[28] T. G. Beach and E. G. McGeer, "Senile plaques, amyloid ?-protein, and acetylcholinesterase fibres: laminar distributions in Alzheimer's disease striate cortex," *Acta Neuropathologica*, vol. 83, no. 3, pp. 292–299, 1992.

[29] J. Xu, S. Patassini, N. Rustogi et al., "Regional protein expression in human Alzheimer's brain correlates with disease severity," *Communications Biology*, vol. 2, no. 1, pp. 1–15, 2019.

[30] I. Mavroudis, F. Petrides, M. Manani et al., "Original article Dendritic and spinal alterations of the spiny stellate cells of the human visual cortex during normal aging," *Folia Neuropathologica*, vol. 3, no. 3, pp. 261–269, 2012.

[31] I. A. Mavroudis, D. F. Fotiou, M. G. Manani et al., "Dendritic pathology and spinal loss in the visual cortex in Alzheimer's disease: a Golgi study in pathology," *International Journal of Neuroscience*, vol. 121, no. 7, pp. 347–354, 2011.

[32] N. S. Desai, L. C. Rutherford, and G. G. Turrigiano, "Plasticity in the intrinsic excitability of cortical pyramidal neurons," *Nature Neuroscience*, vol. 2, no. 6, pp. 515–520, 1999.

[33] N. S. Desai, "Homeostatic plasticity in the CNS: synaptic and intrinsic forms," *Journal of Physiology-Paris*, vol. 97, no. 4-6, pp. 391–402, 2003.

[34] N. M. Porter, O. Thibault, V. Thibault, K. C. Chen, and P. W. Landfield, "Calcium channel density and hippocampal cell death with age in long-term culture," *Journal of Neuroscience*, vol. 17, no. 14, pp. 5629–5639, 1997.

[35] A. Ashraf, Z. Fan, D. J. Brooks, and P. Edison, "Cortical hypermetabolism in MCI subjects: a compensatory mechanism?," *European Journal of Nuclear Medicine and Molecular Imaging*, vol. 42, no. 3, pp. 447–458, 2015.

[36] World Health Organization, *Dementia: A Public Health Priority*, World Health Organization, 2012.

[37] R. Brookmeyer, E. Johnson, K. Ziegler-Graham, and H. M. Arrighi, "Forecasting the global burden of Alzheimer's disease," *Alzheimer's & Dementia*, vol. 3, no. 3, pp. 186–191, 2007.

[38] C. L. Masters, R. Bateman, K. Blennow, C. C. Rowe, R. A. Sperling, and J. L. Cummings, "Alzheimer's disease," *Nature Reviews, Disease Primers*, vol. 1, no. 1, 2015.

[39] N. Hu, J. T. Yu, L. Tan, Y. L. Wang, L. Sun, and L. Tan, "Nutrition and the Risk of Alzheimer's Disease," *BioMed research international*, vol. 2013, Article ID 524820, 12 pages, 2013.

[40] Y. Gu, J. W. Nieves, Y. Stern, J. A. Luchsinger, and N. Scarmeas, "Food combination and Alzheimer disease risk," *Archives of Neurology*, vol. 67, no. 6, pp. 699–706, 2010.

[41] Alzheimer's Association, "2017 Alzheimer's disease facts and figures," *Alzheimer's & Dementia*, vol. 13, no. 4, pp. 325–373, 2017.

[42] T. Revett, G. B. Baker, J. Jhamandas, and S. Kar, "Glutamate system, amyloid β peptides and tau protein: functional interrelationships and relevance to Alzheimer disease pathology," *Journal of Psychiatry and Neuroscience*, vol. 38, no. 1, pp. 6–23, 2013.

[43] K. Kaarniranta, A. Salminen, A. Haapasalo, H. Soininen, and M. Hiltunen, "Age-related macular degeneration (AMD): Alzheimer's disease in the eye?," *Journal of Alzheimer's Disease*, vol. 24, no. 4, pp. 615–631, 2011.

[44] F. Z. Javaid, J. Brenton, L. Guo, and M. F. Cordeiro, "Visual and ocular manifestations of Alzheimer's disease and their use as biomarkers for diagnosis and progression," *Frontiers in neurology*, vol. 7, 2016.

[45] F. R. Lin, E. J. Metter, R. J. O'Brien, S. M. Resnick, A. B. Zonderman, and L. Ferrucci, "Hearing loss and incident dementia," *Archives of Neurology*, vol. 68, no. 2, pp. 214–220, 2011.

[46] S. Adam, Bonsang Eric, C. Grotz Catherine, and Perelman Sergio, "Occupational activity and cognitive reserve: implications in terms of prevention of cognitive aging and Alzheimer’s disease," *Clinical Interventions in Aging*, vol. 8, pp. 377–390, 2013.

[47] M. K. Lupton, D. Stahl, N. Archer et al., "Education, occupation and retirement age effects on the age of onset of Alzheimer's disease," *International Journal of Geriatric Psychiatry*, vol. 25, no. 1, pp. 30–36, 2009.

[48] C. Grotz, L. Letenneur, E. Bonsang et al., "Retirement age and the age of onset of Alzheimer's disease: results from the ICTUS study," *PLOS ONE*, vol. 10, no. 2, p. e0115056, 2015.

[49] E. Bonsang, S. Adam, and S. Perelman, "Does retirement affect cognitive functioning?," *Journal of Health Economics*, vol. 31, no. 3, pp. 490–501, 2012.

[50] D. Finkel, R. Andel, M. Gatz, and N. L. Pedersen, "The role of occupational complexity in trajectories of cognitive aging before and after retirement," *Psychology and Aging*, vol. 24, no. 3, pp. 563–573, 2009.

[51] M. L. Feldman and C. Dowd, "Loss of dendritic spines in aging cerebral cortex," *Anatomy and Embryology*, vol. 148, no. 3, pp. 279–301, 1975.

[52] G. E. Gibson and C. Peterson, "Aging decreases oxidative metabolism and the release and synthesis of acetylcholine," *Journal of Neurochemistry*, vol. 37, no. 4, pp. 978–984, 1981.

[53] J. A. McQuail, C. J. Frazier, and J. L. Bizon, "Molecular aspects of age-related cognitive decline: the role of GABA signaling," *Trends in Molecular Medicine*, vol. 21, no. 7, pp. 450–460, 2015.

[54] A. Gopnik, A. N. Meltzoff, and P. K. Kuhl, *The Scientist in the Crib: What Early Learning Tells us about the Mind*, William Morrow Paperbacks, 2000.

[55] P. R. Huttenlocher, "Synaptic density in human frontal cortex - developmental changes and effects of aging," *Brain Research*, vol. 163, no. 2, pp. 195–205, 1979.

[56] I. Bezprozvanny and M. P. Mattson, "Neuronal calcium mishandling and the pathogenesis of Alzheimer's disease," *Trends in Neurosciences*, vol. 31, no. 9, pp. 454–463, 2008.

[57] A. Nikolaev, T. McLaughlin, D. O'Leary, and M. Tessier-Lavigne, "APP binds DR6 to trigger axon pruning and neuron death via distinct caspases," *Nature*, vol. 457, no. 7232, pp. 981–989, 2009.

[58] S. T. DeKosky and S. W. Scheff, "Synapse loss in frontal cortex biopsies in Alzheimer's disease: correlation with cognitive severity," *Annals of Neurology*, vol. 27, no. 5, pp. 457–464, 1990.

[59] K. Martinello, Z. Huang, R. Lujan et al., "Cholinergic afferent stimulation induces axonal function plasticity in adult hippocampal granule cells," *Neuron*, vol. 85, no. 2, pp. 346–363, 2015.

[60] A. Blokland, "Acetylcholine: a neurotransmitter for learning and memory?," *Brain Research Reviews*, vol. 21, no. 3, pp. 285–300, 1995.

[61] C. Geula, N. Nagykery, A. Nicholas, and C. K. Wu, "Cholinergic neuronal and axonal abnormalities are present early in aging and in Alzheimer disease," *Journal of Neuropathology & Experimental Neurology*, vol. 67, no. 4, pp. 309–318, 2008.

[62] P. T. Francis, A. M. Palmer, M. Snape, and G. K. Wilcock, "The cholinergic hypothesis of Alzheimer's disease: a review of progress," *Journal of Neurology, Neurosurgery, and Psychiatry*, vol. 66, no. 2, pp. 137–147, 1999.

[63] A. Sereniki and M. A. B. F. Vital, "A doença de Alzheimer: aspectos fisiopatológicos e farmacológicos," *Revista de Psiquiatria do Rio Grande do Sul*, vol. 30, no. 1, 2008supplement 0, 2008.

[64] E. Engelhardt, S. M. Brucki, J. L. S. Cavalcanti et al., "Tratamento da Doença de Alzheimer: recomendações e sugestões do Departamento Científico de Neurologia Cognitiva e do Envelhecimento da Academia Brasileira de Neurologia," *Arquivos de Neuro-Psiquiatria*, vol. 63, no. 4, pp. 1104–1112, 2005.

[65] Y. Li, H. Sun, Z. Chen, H. Xu, G. Bu, and H. Zheng, "Implications of GABAergic neurotransmission in Alzheimer's disease," *Frontiers in aging neuroscience*, vol. 8, 2016.

[66] A. Limon, J. M. Reyes-Ruiz, and R. Miledi, "Loss of functional GABAA receptors in the Alzheimer diseased brain," *Proceedings of the National Academy of Sciences of the United States of America*, vol. 109, no. 25, pp. 10071–10076, 2012.

[67] M. F. Bear, B. W. Connors, and M. A. Paradiso, *Neuroscience: Exploring the Brain*, Jones & Bartlett Learning, LLC, 2016.

[68] G. R. Holt and C. Koch, "Shunting inhibition does not have a divisive effect on firing rates," *Neural Computation*, vol. 9, no. 5, pp. 1001–1013, 1997.

[69] A. Currais, C. Farrokhi, R. Dargusch et al., "Fisetin reduces the impact of aging on behavior and physiology in the rapidly aging SAMP8 mouse," *The Journals of Gerontology: Series A*, vol. 73, no. 3, pp. 299–307, 2018.

[70] K. S. Raygude, A. D. Kandhare, P. Ghosh, and S. L. Bodhankar, "Anticonvulsant effect of fisetin by modulation of endogenous biomarkers," *Biomedicine & Preventive Nutrition*, vol. 2, no. 3, pp. 215–222, 2012.

[71] A. Kessler, H. Sahin-Nadeem, S. C. R. Lummis et al., "GABAA receptor modulation by terpenoids from Sideritis extracts," *Molecular Nutrition & Food Research*, vol. 58, no. 4, pp. 851–862, 2014.

[72] G. P. Eckert, "Traditional used plants against cognitive decline and Alzheimer disease," *Frontiers in Pharmacology*, vol. 1, 2010.

[73] Y. Jiang, H. Gao, and G. Turdu, "Traditional Chinese medicinal herbs as potential AChE inhibitors for anti-Alzheimer's disease: a review," *Bioorganic Chemistry*, vol. 75, pp. 50–61, 2017.

[74] K. Y. Yoo and S. Y. Park, "Terpenoids as potential anti-Alzheimer's disease therapeutics," *Molecules*, vol. 17, no. 3, pp. 3524–3538, 2012.

[75] K. A. Wojtunik-Kulesza, K. Targowska-Duda, K. Klimek et al., "Volatile terpenoids as potential drug leads in Alzheimer's disease," *Open Chemistry*, vol. 15, no. 1, pp. 332–343, 2017.

[76] B. Dubois and M. L. Albert, "Amnestic MCI or prodromal Alzheimer's disease?," *The Lancet Neurology*, vol. 3, no. 4, pp. 246–248, 2004.

[77] A. Busse, A. Hensel, U. Gühne, M. C. Angermeyer, and S. G. Riedel-Heller, "Mild cognitive impairment: long-term course of four clinical subtypes," *Neurology*, vol. 67, no. 12, pp. 2176–2185, 2006.

[78] J. C. Morris, "Revised criteria for mild cognitive impairment may compromise the diagnosis of Alzheimer disease dementia," *Archives of Neurology*, vol. 69, no. 6, pp. 700–708, 2012.

[79] B. C. Dickerson, D. H. Salat, D. N. Greve et al., "Increased hippocampal activation in mild cognitive impairment compared to normal aging and AD," *Neurology*, vol. 65, no. 3, pp. 404–411, 2005.

[80] M. A. Busche, G. Eichhoff, H. Adelsberger et al., "Clusters of hyperactive neurons near amyloid plaques in a mouse model of Alzheimer's disease," *Science*, vol. 321, no. 5896, pp. 1686–1689, 2008.

[81] M. J. Kim, K. M. Lee, Y. D. Son, H. Jeon, Y. B. Kim, and Z. H. Cho, "Increased basal forebrain metabolism in mild cognitive impairment: an evidence for brain reserve in incipient dementia," *Journal of Alzheimer's Disease*, vol. 32, no. 4, pp. 927–938, 2012.

[82] M. P. Mattson, M. Gleichmann, and A. Cheng, "Mitochondria in neuroplasticity and neurological disorders," *Neuron*, vol. 60, no. 5, pp. 748–766, 2008.

[83] B. Bass, S. Upson, K. Roy, E. L. Montgomery, T. O. Jalonen, and I. V. Murray, "Glycogen and amyloid-beta: key players in the shift from neuronal hyperactivity to hypoactivity observed in Alzheimer's disease?," *Neural Regeneration Research*, vol. 10, no. 7, pp. 1023–1025, 2015.

[84] I. A. Fleidervish, A. M. Binshtok, and M. J. Gutnick, "Functionally distinct NMDA receptors mediate horizontal connectivity within layer 4 of mouse barrel cortex," *Neuron*, vol. 21, no. 5, pp. 1055–1065, 1998.

[85] V. E. Okhotin, "Cytophysiology of spiny stellate cells in the striate cortex and their role in the excitatory mechanisms of intracortical synaptic circulation," *Neuroscience and Behavioral Physiology*, vol. 36, no. 8, pp. 825–836, 2006.

[86] L. G. Nowak, R. Azouz, M. V. Sanchez-Vives, C. M. Gray, and D. A. McCormick, "Electrophysiological classes of cat primary visual cortical neurons in vivo as revealed by quantitative analyses," *Journal of Neurophysiology*, vol. 89, no. 3, pp. 1541–1566, 2003.

[87] M. C. Angulo, J. Rossier, and E. Audinat, "Postsynaptic glutamate receptors and integrative properties of fast-spiking interneurons in the rat neocortex," *Journal of Neurophysiology*, vol. 82, no. 3, pp. 1295–1302, 1999.

[88] Q. Q. Sun, J. R. Huguenard, and D. A. Prince, "Barrel cortex microcircuits: thalamocortical feedforward inhibition in spiny stellate cells is mediated by a small number of fast-spiking interneurons," *Journal of Neuroscience*, vol. 26, no. 4, pp. 1219–1230, 2006.

[89] J. L. McClelland and D. E. Rumelhart, *Explorations in Parallel Distributed Processing: A Handbook of Models, Programs, and Exercises*, MIT Press, Cambridge, MA, USA, 1988.

[90] D. E. Rumelhart, J. L. McClelland, and AU, *Parallel Distributed Processing: Explorations in the Microstructure of Cognition: Foundations*, vol. 1, The MIT Press, Cambridge, MA, USA, 1986.

[91] M. A. Aguiar, R. A. Furucho, A. Negrão, and F. J. R. Peláez, "A computational model of memories disruption in Alzheimer disease," in *AD/PD 2013, The11th International Conference on Alzheimer's and Parkinson's Diseases*, pp. 6–10, Florence, Italy, 2013.

[92] A. R. Dunn and C. C. Kaczorowski, "Regulation of intrinsic excitability: roles for learning and memory, aging and Alzheimer's disease, and genetic diversity," *Neurobiology of Learning and Memory*, vol. 164, p. 107069, 2019.

[93] E. Popugaeva, O. L. Vlasova, and I. Bezprozvanny, "Restoring calcium homeostasis to treat Alzheimer's disease: a future perspective," *Neurodegenerative Disease Management*, vol. 5, no. 5, pp. 395–398, 2015.

[94] M. A. Busche and A. Konnerth, "Neuronal hyperactivity - a key defect in Alzheimer's disease?," *BioEssays*, vol. 37, no. 6, pp. 624–632, 2015.

[95] A. Stargardt, D. F. Swaab, and K. Bossers, "The storm before the quiet: neuronal hyperactivity and Aβ in the presymptomatic stages of Alzheimer's disease," *Neurobiology of Aging*, vol. 36, no. 1, pp. 1–11, 2015.

[96] V. Pilipenko, K. Narbute, J. Pupure, J. Rumaks, B. Jansone, and V. Klusa, "Neuroprotective action of diazepam at very low and moderate doses in Alzheimer's disease model rats," *Neuropharmacology*, vol. 144, pp. 319–326, 2019.

[97] A. Bakker, G. Krauss, M. Albert, C. Stark, S. Bassett, and M. Gallagher, "P4-349: Clinical efficacy of low dose levetiracetam for hippocampal hyperactivity in amnestic mild cognitive impairment," *Alzheimer's & Dementia*, vol. 7, no. 4S, Part 24, p. e34, 2011.

[98] R. Chen, P. T. Chan, H. Chu et al., "Treatment effects between monotherapy of donepezil versus combination with memantine for Alzheimer disease: a meta-analysis," *PLOS ONE*, vol. 12, no. 8, p. e0183586, 2017.

[99] E. R. Peskind, S. G. Potkin, N. Pomara et al., "Memantine treatment in mild to moderate Alzheimer disease: a 24-week randomized, controlled trial," *The American Journal of Geriatric Psychiatry*, vol. 14, no. 8, pp. 704–715, 2006.

[100] L. Verret, E. O. Mann, G. B. Hang et al., "Inhibitory interneuron deficit links altered network activity and cognitive dysfunction in Alzheimer model," *Cell*, vol. 149, no. 3, pp. 708–721, 2012.

[101] M. Solas, E. Puerta, and M. J. Ramirez, "Treatment options in Alzheimer´s disease: the GABA story," *Current Pharmaceutical Design*, vol. 21, no. 34, pp. 4960–4971, 2015.

[102] R. Anand, K. D. Gill, and A. A. Mahdi, "Therapeutics of Alzheimer's disease: past, present and future," *Neuropharmacology*, vol. 76, Part A,, pp. 27–50, 2014.

[103] M. Marcade, J. Bourdin, N. Loiseau et al., "Etazolate, a neuroprotective drug linking GABAAreceptor pharmacology to amyloid precursor protein processing," *Journal of Neurochemistry*, vol. 106, no. 1, pp. 392–404, 2008.

[104] A. Artola, S. Brocher, and W. Singer, "Different voltage-dependent thresholds for inducing long-term depression and long-term potentiation in slices of rat visual cortex," *Nature*, vol. 347, no. 6288, pp. 69–72, 1990.

[105] F. J. R. Peláez and M. G. Simões, "A computational model of synaptic metaplasticity," in *IJCNN'99. International Joint Conference on Neural Networks. Proceedings (Cat. No.99CH36339)*, vol. 1, pp. 6–11, Washington, DC, USA, USA, 1999.

[106] W. C. Abraham and M. F. Bear, "Metaplasticity: the plasticity of synaptic plasticity," *Trends in Neurosciences*, vol. 19, no. 4, pp. 126–130, 1996.

[107] W. C. Abraham and W. P. Tate, "Metaplasticity: a new vista across the field of synaptic plasticity," *Progress in Neurobiology*, vol. 52, no. 4, pp. 303–323, 1997.

Review Article

The Effects of GABAergic System under Cerebral Ischemia: Spotlight on Cognitive Function

Juan Li,[1] Luting Chen,[2] Feng Guo,[1] and Xiaohua Han [1]

[1]*Department of Rehabilitation Medicine, Tongji Hospital, Tongji Medical College, Huazhong University of Science and Technology, Wuhan, Hubei, China*
[2]*Department of Rehabilitation Medicine, General Hospital of the Yangtze River Shipping, Wuhan, Hubei, China*

Correspondence should be addressed to Xiaohua Han; hanxiao1470@hust.edu.cn

In this review, we present evidence about the changes of the GABAergic system on the hippocampus under the ischemic environment, which may be an underlying mechanism to the ischemia-induced cognitive deficit. GABAergic system, in contrast to the glutamatergic system, is considered to play an inhibitory effect on the central nervous system over the past several decades. It has received widespread attention in the area of schizophrenia and epilepsy. The GABAergic system has a significant effect in promoting neural development and formation of local neural circuits of the brain, which is the structural basis of cognitive function. There have been a number of reviews describing changes in the GABAergic system in cerebral ischemia in recent years. However, no study has investigated the changes in the system in the hippocampus during cerebral ischemic injury, which results in cognitive impairment, particularly at the chronic ischemic stage and the late phase of ischemia. We present a review of the changes of the GABAergic system in the hippocampus under ischemia, including GABA interneurons, extracellular GABA neurotransmitter, and GABA receptors. Several studies are also listed correlating amelioration of cognitive impairment by regulating the GABAergic system in the hippocampus damaged under ischemia. Furthermore, exogenous cell transplantation, which improves cognition by modulating the GABAergic system, will also be described in this review to bring new insight and strategy on solving cognitive deficits caused by cerebral ischemia.

1. Introduction

Cerebral ischemia is hypoperfusion of the blood through brain tissue caused by a pathologic constriction or obstruction of its blood vessels or an absence of blood circulation. Both transient and chronic cerebral ischemia or chronic cerebral hypoperfusion can lead to damage or death of brain cells and other pathophysiological changes. Meanwhile, cerebral hypoperfusion is considered a major cause of vascular dementia (VD) [1] and an underlying pathological mechanism of Alzheimer's disease (AD) [2]. Thus, one of the main threats of cerebral ischemia is the impairment of cognitive function. The GABAergic system of the mammalian brain consists of GABA-releasing cells and receptors that bind GABA [3]. A growing body of research in recent decades has shown that the GABAergic system is strongly associated with cognitive function, which plays an important role in

neurological diseases, such as VD [4], AD [5], depression [6], and schizophrenia [7]. However, ischemia can cause damage to the GABAergic system in brain regions that are related to cognitive function, such as the hippocampus, amygdala, and prefrontal cortex [8–10]. Therefore, the impairment of the GABAergic system is considered one of the mechanisms affecting cognition. Over the past few years, with extensive studies about the relationship between the hippocampus and cognitive function, the hippocampus has been observed to play a central role in the cognitive map. This means that the brain builds a unified representation of the spatial environment to support memory and guide future action [11]. Thus, this review focuses on the effect of cerebral ischemia on cognitive disorder induced by the deficit of the GABAergic system. We describe the changes of the GABAergic system on the hippocampus under the condition of ischemia and summarize some of the evidence that can improve

cognitive function by regulating the GABAergic system of the hippocampus. Furthermore, as cell transplantation has played a significant role in almost every medical field in recent years, we introduce some studies about cell transplantation to improve cognition via the contribution of the GABAergic system.

2. The Overview of the GABAergic System

GABAergic system involves GABA-releasing cells, the biosynthesis and metabolic degradation of GABA, its release, and interaction with receptors. In the hippocampus, GABAergic interneurons are in the minority and account for about 10–15% of the total number of neurons. They make a vast difference in all aspects of cortical circuit function and regulation because of its remarkable diversity, extensive distribution, and intimate contact with pyramidal cells [12]. On the basis of the expression of specific molecular markers, according to the molecular classification, the GABAergic interneurons can be divided into five main groups: parvalbumin (PV), somatostatin (SOM/SS), neuropeptide Y (NPY), vasoactive intestinal peptide (VIP), and cholecystokinin (CCK) interneuron [13]. Gamma-aminobutyric acid (GABA), as a chief inhibitory neurotransmitter in the developmentally mature mammalian central nervous system, is synthesized from glutamic acid by glutamic acid decarboxylase (GAD), which has two GAD subtypes, GAD65 and GAD67. GABA is stored in synaptic vesicles, released in synaptic cleft triggered by the nerve impulse, and then interacts with its receptors. There are three different classes of GABA receptors, namely, ionotropic GABAA and GABAC receptors and metabotropic GABAB receptors in the central nervous system [14, 15]. Of these, GABAA and GABAB receptors have received the greatest amount of attention in cerebral ischemia [16, 17]. The GABAA receptors are ligand-gated pentameric chloride channels and composed from a variety of subunits that include α (subtypes 1–6), β (1–4), γ (1–3), δ, ε, π, and ρ which have different sensitivities to GABA and modulatory drugs [18]. Furthermore, the GABAA receptors have two main modes of operation, phasic and tonic. The phasic effects of GABA are seen in GABAergic synapses, whereas the tonic inhibition is through extrasynaptic receptors that report GABA as a volume transmitter and set an excitability threshold for cortical neurons [3]. The GABAA receptors found extrasynaptically are comprised of relatively rare subunits, particularly $\alpha4$, $\alpha6$, and δ. Generally, δ-subunit containing the GABAA receptors are extrasynaptic, but vice-versa is not true [19]. $\alpha5\beta1\gamma2$ is located postsynaptically, but $\alpha5\beta2\gamma2$ and $\alpha5\beta3\gamma2$ isoforms are extrasynaptic [20]. As a kind of metabolic receptor, GABAB receptor localizes in both the presynaptic and postsynaptic terminals, which has two subunits, GABAB1 and GABAB2 [21]. GABA transporters (GAT1–4) remove GABA from the synaptic cleft. This is followed by its catabolization by GABA transaminase (GABA-T), an enzyme that converts brain GABA into succinate semialdehyde, which can be converted to succinic acid and enters the citric acid cycle.

3. Effects of Cerebral Ischemia on the GABAergic System: Hippocampus

After cerebral ischemia, numerous studies have shown that a number of changes happened on the GABAergic system at the hippocampal area using in vivo models and in vitro oxygen-glucose deprivation (OGD) experiment. From the survival and function of GABA interneurons and intracellular and extracellular levels of the GABA neurotransmitter, to GABA signal transmissions, cerebral ischemia can induce the process of pathological variations on the GABAergic system as discussed below.

3.1. GABA Interneurons. Although some reports showed that the GABA interneurons were insensitive to ischemia, compared with principal neurons [22], several others have shown that the interneurons in the hippocampus are vulnerable to ischemia. For example, in addition to excitatory cells, SS- and NPY-expressing interneurons were lost from the dentate hilus in the days following ischemic injury. Simultaneously in CA1, the number of neurons containing only NPY decreased, while the number of neurons expressing both NPY and SS increased as the interneurons changed their patterns of peptide expression [23]. The PV immunoreactivity was unchanged up to two days after ischemia. However, at five and 14 days after ischemia, a conspicuous reduction of PV immunoreactivity was observed in interneurons of the hippocampal CA1 sector. Furthermore, a significant decrease in PV immunoreactivity was found in the interneurons of the hippocampal CA3 sector [24]. In another study, following transient cerebral ischemia (bilateral carotid occlusion for 2 min) in the gerbil, the GABAergic interneurons (labeled the GABAA receptor a1-subunit) developed severely beaded dendrites after 3–4 days throughout all layers of area CA1, and the varicose and fragmented appearance of a1-subunit-positive dendrites up to five weeks after ischemia was observed. However, there were no ischemia-induced changes in dendrites immunolabeled with the a1-subunit within area CA3 or the dentate gyrus [25]. On the contrary, a larger population of spiny interneurons disappeared from the hilus (feedback inhibitory interneurons) and stratum lucidum of CA3 (feedforward inhibitory interneurons) in a complete forebrain ischemia model induced by four-vessel occlusion after 12–14 months [26]. Since there are different ideas about whether the hippocampal GABA interneurons are resistant to ischemia, there are several possible explanations for this discrepancy. These include (1) a remarkable diversity of the GABA interneurons contributing to their functional versatility in shaping the spatiotemporal dynamics of neural circuit operations underlying cognition, which, in turn, demonstrate different sensitivities to ischemia within the hippocampus. Perhaps, the detection markers that represent the GABA interneurons are distinct. They are GABA, GAD67/65, GABA receptors, PV, SST, and so on. Some markers cannot replace all of the GABA interneurons [27]. Furthermore, the expression of these markers is regulated under the pathological process of cerebral ischemic injury. For example, one study showed neurons coexpressing SS and NPY before ischemia added to the number of neurons containing SS

alone after ischemia [23]. However, the different reaction to ischemia brings a distinct outcome. During the hypoxic condition, the interneurons that expressed HIF-1α are more tolerant to a severe environment [28]. Another study showed that resistance of the interneurons to ischemic damage could be related to a lower expression level of pH-sensitive leakage potassium channels (TASK) currents compared to pyramidal cells [29]. (2) GABA interneurons have a different metabolic system from principal neurons. For instance, the GABA shunt is another energy metabolic pathway in addition to the Krebs cycle, which plays a critical role in cerebral hypoperfusion to produce ATP to help the interneurons survive (we will discuss this below). (3) GABA interneurons in different regions of the hippocampus have different sensitivity to ischemia. With changes in peptide expression patterns, the interneurons in the CA1 subfield seem more likely to survive compared to the dentate gyrus and CA3 subfield [26]. (4) Different durations of ischemia lead to a diverse hostile environment. As described above, there are different ischemic models, such as transient ischemia and chronic hypoperfusion, and a distinct duration of vascular occlusion. However, due to different experimental purposes, the detection time of the GABA interneurons after ischemia was different, which means that the interneurons may experience pathological states, from injury to loss. Even though GABA interneurons in the hippocampus have a certain tolerance to ischemia compared with the principal cells, however, long-term and chronic ischemia can affect its substructure and function. For example, Zhan et al. showed that the excitability of interneurons in CA1 declined due to impaired Na+ channel activation in the transient cerebral ischemia model, and this may be one of the reasons for excitotoxicity that contributes to pyramidal cell death [30].

3.2. GABA Neurotransmitter. GABA, as the opposite of excitatory neurotransmitter-glutamate, is crucial for normal neurologic function [31]. At the initial stage of ischemia, the toxicity of enhanced excitatory amino acid function was thought to be one of the causes of cell death, and enhancing extracellular GABA levels had neuroprotective effects at an early time [32]. However, extracellular GABA levels varied significantly in different periods of cerebral ischemia. One study showed an increase of GABA after the ligation of the bilateral carotid artery for 5 min and reperfusion for 60 min in the gerbil hippocampus [33]. Huang et al. showed that in the permanent middle cerebral artery occlusion (pMCAO) model and the transient cerebral focal ischemia (tMCAO) model, the levels of GABA decrease after seven days [34]. Another research showed that GABA in the hippocampal CA1 subfield was decreased significantly after one month in permanent bilateral occlusion of the common carotid arteries (two-vessel occlusion, 2VO) procedures [35]. GAD, GAT, and GABA-T, as synthesis, transport, and decomposition tools of GABA, respectively, can affect the level of GABA when they have a change during cerebral ischemic injury. However, just like the temporal alteration of GABA, some of them got significantly altered in the CA1 region after ischemia. The immunoreactivities of the GAD isoforms were markedly elevated in the CA1 region at 30 min postischemia,

then recovered to baseline at 3 h, but the intensity of GAD67, and not GAD65, markedly increased at 24 h postischemia. GAT-1 expressions were elevated in the CA1 region at 12 h postischemia, which were involved in the reverse transport of GABA, not reuptake, to enhance the level of extracellular GABA, as an inhibitory neurotransmitter. Meanwhile, the GABA-T immunoreactivity in the CA1 area decreased simultaneously. In contrast, at 24 h postischemia, both GAT-1 (involved in reuptake of GABA) and GABA-T expressions in the CA1 area was enhanced, which was considered to be a degradation of GABA as a neurotransmitter, but enhancement as a metabolite [36]. Thus, these changes may explain why extracellular GABA levels increase during early ischemia and decrease at the chronic phase (we will discuss below). Importantly, all of those abnormal changes would have a great influence not only on the hippocampus and its local circle but also on other brain regions. For example, GAD67 deficiency in parvalbumin interneurons produces deficits in inhibitory transmission and network disinhibition in the mouse prefrontal cortex [37]. For the changes of extracellular GABA levels at different times of ischemia, Rochelle et al. summarized several mechanisms for an early increase in extracellular GABA during ischemia [38]. About the late decrease, several explanations can be proposed, includingthe following: (1) the dysfunction of GABA interneurons, which release GABA as their neurotransmitter. The GABA interneurons show their insensitivity to the early hypoperfusion (just like we discuss above), but their substructure and function would be damaged with the extension of ischemic time. (2) The decline of release and reuptake of GABA [39]. Volgyi et al. showed that GABAergic synaptic transmission-related proteins, sodium- and chloride dependent GABA transporter 1 (SLC6A1), and GABA type B receptor subunit 2 (GABABR2), decreased during chronic cerebral hypoperfusion [40]. (3) The GABA shunt: in addition to being a neurotransmitter, GABA is also a metabolic substance. The GABA shunt is a conserved energy metabolic pathway, which generates succinate from amino acids and thus is an anaplerotic pathway to the Krebs cycle to produce ATP [41]. The GABA shunt consists of three enzymatic reactions catalyzed by glutamate decarboxylase (GAD), GABA transaminase (GABA-T), and succinic semialdehyde dehydrogenase (SSADH), which can be activated in cerebral hypoperfusion [34, 36, 40, 42]. During the chronic phase, to adapt the state of glucose deficiency and hypoxia, the GABA interneurons change their energy metabolic pathway to acquire ATP. So, this may be one of the reasons the GABA interneurons survive, but also the reason for the lower level of GABA at a later phase. In general, the change of GABA levels is to accommodate the pathological process of ischemia in the brain.

3.3. GABA Receptors. It is well known that both GABAA and GABAB receptors play a big role in cognition. After hypoperfusion, in addition to the normal level of GABA neurotransmitters, GABA signal transmissions also play an important role. However, a number of studies have shown that the expression of both GABAA and GABAB receptors was generally decreased in the acute and chronic phases [10, 25]. For example, in one study, animals treated with 2VO

procedures showed that the expression of GABAB receptor 1 (GABABR1) in the hippocampal CA1 subfield was decreased significantly after one month [35]. Similarly, in another study, there was a marked decrease in both mRNA and protein expression of GABA subtypes (GABAA and GABAB) in different brain regions of rats at 30 days after 2VO, especially in the hippocampus [43]. In an OGD study to investigate the alteration of the protein levels of the GABAB1 and GABAB2 receptor subunits in rat organotypic hippocampal slice cultures by ischemia-like challenges, the result showed a marked decrease in the total levels of GABAB2 (~75%), while there was no significant change in the levels of GABAB1 after 24 h [44]. Furthermore, there was a difference in the expression of subunits and the location of receptors. In in vitro experiment, exposure of hippocampal slices to OGD for 90 min shows downregulation of all the synaptic GABAAR subunits of ~40% for α1 subunits, ~20% for α2 subunits, and~35% for β3 and γ2 subunits, but no effect was found for the δ subunit [45]. Liu et al. show that five weeks after induction of hypoperfusion, the surface expression of GABAA receptor α1 subunit was significantly decreased, but an intracellular expression of GABAA receptor α1 subunit was significantly increased [46]. Thus, the change of GABA receptors after ischemia is not only an expression of decline but also involves selective expression of subunits and stability of localization. Mele et al. showed that the internalization of GABAAR was dependent on glutamate receptor activation and mediated by dephosphorylation of the β3 subunit at serine 408/409, and the expression of phosphomimetic mutant GABAAR β3 subunits prevented receptor internalization and protected hippocampal neurons from ischemic cell death [45]. Therefore, this is one of the reasons why GABA receptors decrease in the early stage of ischemia and phosphorylation of Ser408/409 in the GABAAβ3 subunit, and Ser892 in the GABAB 2 subunit will increase the induction rate and magnitude of LTP at the hippocampus in 2VO rats [43].

In conclusion, the GABA interneurons may keep relatively intact cellular morphology after cerebral ischemia, but the substructural integrity of GABA interneurons, the normal level of extracellular GABA, and the natural function of GABA receptors would be required for regular functioning of a network such as the hippocampus.

4. Improvement of Cognitive Function by Regulating GABAergic System after Cerebral Ischemia

Just like we summarized above, cerebral ischemia has a huge effect on the GABAergic system, especially in the hippocampus, including loss or dysfunction of the GABA interneurons, abnormal levels of GABA neurotransmitter, selective patterns of expression, and decreased activity on GABA receptors. Numerous studies have shown that the GABAergic system has a strong relationship with cognitive function. Therefore, regulating the GABAergic system in the hippocampus after cerebral ischemia is another way to improve cognition. Meanwhile, neuroprotection during ischemia in

the hippocampus, which can be modulated via the GABAergic system, contributes a lot to cognitive function [32]. For this reason, it will be discussed in this section.

4.1. Neuroprotection on the Hippocampus by Regulating GABAergic System. As already established, the hippocampus presents a critical role in cognitive function. Neurons of the hippocampus, as the basic structure or constitution, serve its local circuitry and process information. Since the loss of hippocampal neurons would induce the cognitive deficits [47], specifically, neuron loss in the hippocampus is one of the primary pathological processes of AD [48], which is the most common type of dementia. Thus, protecting the hippocampal neurons from damage caused by ischemia is an important strategy to reduce cognitive damage. Muscimol and baclofen, as GABA A receptor and GABA B receptor agonist, respectively, are often used in in vivo and in vitro experimental studies. In an in vivo study, muscimol and baclofen were coapplied on a brain ischemia model induced by the four-vessel occlusion (4-VO). The result showed that this intervention markedly decreased the neuronal loss in the hippocampal CA1 region. Interestingly, another discovery in this experiment was that the protection of baclofen was much weaker than muscimol [49]. This neuroprotective effect on the hippocampus by working on receptors can be found in a variety of ischemia models, including middle cerebral artery occlusion (MCAO) [50], transient brain hypoperfusion [51], chronic cerebral hypoperfusion [46], and OGD [52]. There are several mechanisms to explain the neuroprotective effects by regulating the GABAergic system: (1) the inhibition of apoptosis: a study showed that coactivation of the GABA A receptor and GABA B receptor triggered the additive neuroprotection to the hippocampal CA1 neurons by activation of the PI-3K/Akt pathway and inhibiting the ASK1-c-Jun N-terminal protein kinase cascade [49]. As direct Akt substrates, glycogen synthase kinase 3 (GSK-3) would be enhanced after cerebral hypoperfusion [53]. This process was involved in the pathological process of apoptosis and led to cognitive problems [54]. However, GSK-3 would be suppressed upon phosphorylation by Akt. (2) The recovery of ATP: diazepam, another agonist of GABA A receptor, was applied to hippocampal slices of adult rats exposed to OGD, showing that diazepam could completely restore ATP and prevented releasing of cytochrome c from the mitochondria [55]. Because this could promote caspase-3 activation, which led to apoptosis of neurons, this could be another way to inhibit apoptosis. (3) The inhibition of autophagy: baclofen was applied in a chronic cerebral hypoperfusion model, and the results showed that activation of GABAB receptors suppressed not only cytodestructive autophagic activity through Akt/ERK-Bcl2-Beclin1 signaling pathway but also upregulated protective autophagy through the activation of the GABAA receptor-CX43/CX36 signaling pathway [46]. (4) Resistance to excitatory toxicity: coactivation of the GABA A receptor and GABA B receptor by muscimol and baclofen in rat 4-VO ischemic model showed that the intervention protected neurons from neuronal death through downregulating the function of NMDA receptors via attenuating the tyrosine phosphorylation of NR2A

subunit [56]. In another OGD study, activating the GABAA receptor by JM-1232(-) (JM) reduced the elevation of intracellular Ca2+ concentration during OGD [57]. In summary, neuroprotection on the hippocampus is extremely crucial because the structure of the hippocampus is the foundation of its function. Thus, applying GABAergic drugs to resist various death pathways should be the treatment of choice.

4.2. Improvement of Cognitive Function by Regulating GABAergic System. As we discussed above, cerebral ischemia leads to loss or dysfunction of the GABA interneurons, abnormal levels of GABA neurotransmitter, selective patterns of expression, and decreased activity on GABA receptors. Considering the difficulty of restoring the lost interneurons and promote the release of GABA neurotransmitter, modulating the activity of GABA receptors is more feasible. Because GABAA receptors have two main modes of operation, phasic and tonic, these two receptors mediate different physiological processes in normal circumstances. However, in the pathological process of ischemia, the two receptor-mediated effects are quite different. For example, although activating the GABAA receptor has a neuroprotective effect, however, the application of S44819, a kind of selective extrasynaptic α5-GABAA receptor inhibitor, can improve cognitive performance in preclinical models of vascular cognitive impairment (VCI) induced by permanent occlusion of the right common carotid artery (rUCO) [58]. However, dampening tonic inhibition too early after stroke may produce an opposite effect, that is, increased cell death [58, 59]. Collectively, drugs that selectively target the GABAA receptors subtype to interfere with GABAergic neurotransmission appear to be a promising strategy to facilitate poststroke recovery and/or to prevent cognitive deficits. The GABAB receptor is another potential site to play the role of cognitive enhancement. Baclofen, a GABAB receptor agonist, markedly improved the memory impairment and alleviated neuronal damage induced by 2VO after five weeks. The mechanism was that baclofen attenuated the decrease of surface expression of GABAB R1 and GABAB R2 and restored the balanced surface expression of HCN1/HCN2, which coregulated neuronal excitability with GABA receptors in the rat hippocampal CA1 area [4]. In another research, baclofen ameliorated cognitive deficits 2VO in rats by improving BDNF signaling and reverse Kir3 channel surface expressions in the hippocampal CA1 [60]. It has been proved that activation of GABA(B) receptors triggers the secretion of BDNF and promotes the maturation of GABAergic synapses in the newborn mouse hippocampus [61]. Furthermore, BDNF signaling plays an important role in the hippocampal long-term potentiation (LTP) and synaptic plasticity [62]. At 180 days posttransient cerebral ischemia, endogenous neural progenitor cells were found to differentiate into new GABAergic neurons, labeled glutamic decarboxylase 67 (GAD67), via the BDNF-TrkB pathway. Simultaneously, the new GABAergic neurons partially mediated the recovery of cognitive impairments [63]. Interestingly, clonidine, an α2-adrenergic receptor agonist, could ameliorate cognitive deficits and neuronal impairment induced by chronic cerebral hypoperfusion via the upregulation of GABABR1 and GAD67 in the hippocampal CA1. This may be related to the simultaneous release of GABA by stimulating adrenal receptors [64].

5. The Effect of Exogenous Neural Stem Cells on the GABAergic System

In recent years, cell transplantation technology is growing more promising. Interestingly, despite being difficult to operate, this technology brings new revelations. The neural stem cell transplantation can replace cells that have been lost or have lost their function, due to its inherent ability to differentiate into various cell phenotypes. Further, the transplanted cells can secrete combinations of trophic factors that modulate the molecular composition of the environment to evoke responses from resident cells [65, 66]. Because the GABAergic system suffers damage under cerebral ischemia, resulting in its dysfunction, regulating the GABAergic system and recovering its normal function become another method to protect neurons and improve cognition, as summarized above. However, those drugs work on receptors, which cannot repair damaged neurons. To compensate for the loss of the GABA interneurons, cell transplantation technology is conspicuous. In a study, phencyclidine (PCP), a noncompetitive NMDA receptor antagonist, was used to cause dysfunction of the GABAergic inhibitory interneurons in the prefrontal cortex (PFC) and cognitive deficits. Tanaka et al. showed that transplanting embryonic medial ganglionic eminence (MGE) cells, which would differentiate into a specific class of the GABAergic interneurons into prefrontal cortex (PFC), could prevent the induction of cognitive and sensory motor gating deficits by PCP. Specifically, the preventive effects were not reproduced by either transplantation of cortical projection neuron precursors into the mPFC or transplantation of MGE cells into the occipital cortex. So, the specific cell type damage in this area led to cognitive deficits and needed the specified cell type to repair in the right place [67]. Recent literature shows that causing the GABAergic interneuron impairments and aberrant neuronal activity in the hippocampal by apolipoprotein (apo) E4 and amyloid-β (Aβ) peptides might be another pathological process in AD-related mouse models and humans which could cause learning and memory deficits [68]. Tong et al. transplanted embryonic interneuron progenitors into the hippocampal hilus of aged apoE4 knockin mice with or without Aβ accumulation. The result was that transplantation of inhibitory interneurons developed into mature interneurons, functionally integrated into the hippocampal circuitry, and restored normal cognitive function in two widely used AD-related mouse models [69]. Furthermore, to ensure therapeutic benefits of transplanting exogenous neural stem cells and better adapt to the new environment, Martinez-Losa et al. made a genetic modification—Nav1.1-overexpressing on transplanted cells derived from the embryonic medial ganglionic eminence (MGE), many of which differentiated into the GABAergic interneurons in situ. The result showed that the Nav1.1-overexpressing group enhanced behavior-dependent gamma oscillatory activity, reduced network hypersynchrony, and improved cognitive

functions in human amyloid precursor protein- (hAPP-) transgenic mice, which simulated key aspects of AD, compared to the wild group [70]. Importantly, in addition to the function of replacement, exogenous neural stem cells also showed their paracrine actions, which released a wide array of trophic factors that drove the endogenous cell repair. Transplantation of BMSCs was capable of improving cognitive impairment via upregulating the hippocampal GABAergic system in a rat model of chronic cerebral hypoperfusion (via upregulating hippocampal GABA, GAD67, and GABABR1 expression in a rat model of chronic cerebral hypoperfusion) [35, 71]. In a traumatic brain injury treatment (TBI) model, transplantation of neural stem cells (NSCs) could effectively alleviate the formation of the glial scar, improve the survival rate of the hippocampal neurons, and improve the cognitive dysfunction in rats after TBI. The underlying mechanism may be related to NSCs' effects on inhibiting the release of Glu and maintaining the content of GABA [72]. The transplantation of exogenous neural stem cells could repair the GABAergic system in the damaged area and alleviate cognitive dysfunction. Since the GABAergic system is impaired by cerebral ischemia, transplantation of neural stem cells will be another new and feasible therapeutic method to improve the cognitive function after cerebral ischemia.

6. Conclusion

In this review, we summarized the changes of the GABAergic system on the hippocampus under ischemia, mainly including the substructural damage and some permanent loss of the GABA interneurons, time varyingly extracellular GABA neurotransmitter, and dysfunctional GABA receptors. We also outlined the evidence that GABAergic function decreased following ischemia to cause cognitive impairment, but it can be ameliorated by regulating the GABAergic system in numerous animal experiments. In this section, underlying mechanisms involve the protection of neurons in the hippocampus and the regulation of abnormal GABA signaling pathways, such as activating synaptic GABAA receptors and inhibiting the extrasynaptic receptors. But only a few clinical studies have demonstrated that cognitive impairment caused by ischemia is alleviated by the use of GABAergic drugs. The side effects of GABAergic drugs might limit their use in improving cognition [73]. Also, the exogenous cell transplantation may improve cognition by modulating the GABAergic system in many animal models. However, the animal research involved in transplantation of neural stem cells to rescue the cognitive deficits caused by cerebral ischemia is insufficient. However, it brings us new insight and strategy to solve this tremendous obstacle of the cognitive deficits caused by cerebral ischemic injury.

Data Availability

No data were used to support this study.

Conflicts of Interest

The authors declare that there is no conflict of interests regarding the publication of the paper.

References

[1] F. J. Wolters, H. I. Zonneveld, A. Hofman et al., "Cerebral perfusion and the risk of Dementia," *Circulation*, vol. 136, no. 8, pp. 719–728, 2017.

[2] J. H. Park, J. H. Hong, S. W. Lee et al., "The effect of chronic cerebral hypoperfusion on the pathology of Alzheimer's disease: a positron emission tomography study in rats," *Scientific Reports*, vol. 9, no. 1, article 14102, 2019.

[3] S. G. Brickley and I. Mody, "Extrasynaptic GABAA receptors: their function in the CNS and implications for disease," *Neuron*, vol. 73, no. 1, pp. 23–34, 2012.

[4] C. J. Li, Y. Lu, M. Zhou et al., "Activation of GABAB receptors ameliorates cognitive impairment via restoring the balance of HCN1/HCN2 surface expression in the hippocampal CA1 area in rats with chronic cerebral hypoperfusion," *Molecular Neurobiology*, vol. 50, no. 2, pp. 704–720, 2014.

[5] J. Zheng, H.-L. Li, N. Tian et al., "Interneuron accumulation of phosphorylated tau impairs adult hippocampal neurogenesis by suppressing GABAergic transmission," *Cell Stem Cell*, vol. 26, no. 3, pp. 462–466, 2020.

[6] C. Fee, M. Banasr, and E. Sibille, "Somatostatin-positive gamma-aminobutyric acid interneuron deficits in depression: cortical microcircuit and therapeutic perspectives," *Biological Psychiatry*, vol. 82, no. 8, pp. 549–559, 2017.

[7] M. Y. Xu and A. H. C. Wong, "GABAergic inhibitory neurons as therapeutic targets for cognitive impairment in schizophrenia," *Acta Pharmacologica Sinica*, vol. 39, no. 5, pp. 733–753, 2018.

[8] T. Teramoto, J. Qiu, J.-C. Plumier, and M. A. Moskowitz, "EGF amplifies the replacement of parvalbumin-expressing striatal interneurons after ischemia," *Journal of Clinical Investigation*, vol. 111, no. 8, pp. 1125–1132, 2003.

[9] B. Liu, Q. Dong, S. Zhang et al., "mGluR1,5 activation protects cortical astrocytes and GABAergic neurons from ischemia-induced impairment," *Neuroscience Research*, vol. 75, no. 2, pp. 160–166, 2013.

[10] H. Li, R. E. Siegel, and R. D. Schwartz, "Rapid decline of GABAA receptor subunit mRNA expression in hippocampus following transient cerebral ischemia in the gerbil," *Hippocampus*, vol. 3, no. 4, pp. 527–537, 1993.

[11] R. A. Epstein, E. Z. Patai, J. B. Julian, and H. J. Spiers, "The cognitive map in humans: spatial navigation and beyond," *Nature Neuroscience*, vol. 20, no. 11, pp. 1504–1513, 2017.

[12] K. A. Pelkey, R. Chittajallu, M. T. Craig, L. Tricoire, J. C. Wester, and C. J. McBain, "Hippocampal GABAergic inhibitory interneurons," *Physiological Reviews*, vol. 97, no. 4, pp. 1619–1747, 2017.

[13] J. DeFelipe, P. L. López-Cruz, R. Benavides-Piccione et al., "New insights into the classification and nomenclature of

cortical GABAergic interneurons," *Nature Reviews Neuroscience*, vol. 14, no. 3, pp. 202–216, 2013.

[14] N. G. Bowery, A. L. Hudson, and G. W. Price, "GABAA and GABAB receptor site distribution in the rat central nervous system," *Neuroscience*, vol. 20, no. 2, pp. 365–383, 1987.

[15] J. Bormann and A. Feigenspan, "GABAC receptors," *Trends in Neurosciences*, vol. 18, no. 12, pp. 515–519, 1995.

[16] P. R. Schofield, "The GABAA receptor: molecular biology reveals a complex picture," *Trends in Pharmacological Sciences*, vol. 10, no. 12, pp. 476–478, 1989.

[17] C. Chen, X. Zhou, J. He, Z. Xie, S. Xia, and G. Lu, "The roles of GABA in ischemia-reperfusion injury in the central nervous system and peripheral organs," *Oxidative Medicine and Cellular Longevity*, vol. 2019, Article ID 4028394, 19 pages, 2019.

[18] J. G. Best, C. J. Stagg, and A. Dennis, "Other significant metabolites: yyo-inositol, GABA, glutamine, and lactate," in *Magnetic Resonance Spectroscopy: Tools for Neuroscience Research and Emerging Clinical Applications*, C. Stagg and D. Rothman, Eds., pp. 122–138, Elsevier Inc, 2014.

[19] D. Belelli, N. L. Harrison, J. Maguire, R. L. Macdonald, M. C. Walker, and D. W. Cope, "Extrasynaptic GABAA receptors: form, pharmacology, and function," *The Journal of Neuroscience*, vol. 29, no. 41, pp. 12757–12763, 2009.

[20] X. Chen, A. Keramidas, and J. W. Lynch, "Physiological and pharmacological properties of inhibitory postsynaptic currents mediated by $\alpha 5\beta 1\gamma 2$, $\alpha 5\beta 2\gamma 2$ and $\alpha 5\beta 3\gamma 2$ GABA A receptors," *Neuropharmacology*, vol. 125, pp. 243–253, 2017.

[21] C. Xu, W. Zhang, P. Rondard, J. P. Pin, and J. Liu, "Complex GABAB receptor complexes: how to generate multiple functionally distinct units from a single receptor," *Frontiers in Pharmacology*, vol. 5, p. 12, 2014.

[22] L. P. Voytenko, I. V. Lushnikova, A. V. Savotchenko et al., "Hippocampal GABAergic interneurons coexpressing alpha7-nicotinic receptors and connexin-36 are able to improve neuronal viability under oxygen-glucose deprivation," *Brain Research*, vol. 1616, pp. 134–145, 2015.

[23] R. Bering, A. Draguhn, N. H. Diemer, and F. F. Johansen, "Ischemia changes the coexpression of somatostatin and neuropeptide Y in hippocampal interneurons," *Experimental Brain Research*, vol. 115, no. 3, pp. 423–429, 1997.

[24] T. Himeda, N. Hayakawa, H. Tounai, M. Sakuma, H. Kato, and T. Araki, "Alterations of interneurons of the gerbil hippocampus after transient cerebral ischemia: effect of pitavastatin," *Neuropsychopharmacology*, vol. 30, no. 11, pp. 2014–2025, 2005.

[25] J. R. Inglefield, C. A. Wilson, and R. D. Schwartz-Bloom, "Effect of transient cerebral ischemia on gamma-aminobutyric acidA receptor alpha 1-subunit-immunoreactive interneurons in the gerbil CA1 hippocampus," *Hippocampus*, vol. 7, no. 5, pp. 511–523, 1997.

[26] D. Arabadzisz and T. F. Freund, "Changes in excitatory and inhibitory circuits of the rat hippocampus 12-14 months after complete forebrain ischemia," *Neuroscience*, vol. 92, no. 1, pp. 27–45, 1999.

[27] X. Wang, F. Gao, J. Zhu et al., "Immunofluorescently labeling glutamic acid decarboxylase 65 coupled with confocal imaging for identifying GABAergic somata in the rat dentate gyrus-a comparison with labeling glutamic acid decarboxylase 67," *Journal of Chemical Neuroanatomy*, vol. 61-62, pp. 51–63, 2014.

[28] P. Ramamoorthy and H. Shi, "Ischemia induces different levels of hypoxia inducible factor-1α protein expression in interneurons and pyramidal neurons," *Acta Neuropathologica Communications*, vol. 2, no. 1, p. 51, 2014.

[29] S. Taverna, T. Tkatch, A. E. Metz, and M. Martina, "Differential expression of TASK channels between horizontal interneurons and pyramidal cells of rat hippocampus," *The Journal of Neuroscience*, vol. 25, no. 40, pp. 9162–9170, 2005.

[30] R. Z. Zhan, J. V. Nadler, and R. D. Schwartz-Bloom, "Impaired firing and sodium channel function in CA1 hippocampal interneurons after transient cerebral ischemia," *Journal of Cerebral Blood Flow and Metabolism*, vol. 27, no. 8, pp. 1444–1452, 2007.

[31] O. A. C. Petroff, "GABA and glutamate in the human brain," *The Neuroscientist*, vol. 8, no. 6, pp. 562–573, 2016.

[32] W. Chen Xu, Y. Yi, L. Qiu, and A. Shuaib, "Neuroprotective activity of tiagabine in a focal embolic model of cerebral ischemia," *Brain Research*, vol. 874, no. 1, pp. 75–77, 2000.

[33] X. C. Tang, M. R. Rao, G. Hu, and H. Wang, "Alterations of amino acid levels from striatum, hippocampus, and cerebral cortex induced by global cerebral ischemia in gerbil," *Acta Pharmacologica Sinica*, vol. 21, no. 9, pp. 819–823, 2000.

[34] Q. Huang, C. Li, N. Xia et al., "Neurochemical changes in unilateral cerebral hemisphere during the subacute stage of focal cerebral ischemia-reperfusion in rats: an ex vivo 1H magnetic resonance spectroscopy study," *Brain Research*, vol. 1684, pp. 67–74, 2018.

[35] Q. Long, Y. Hei, Q. Luo et al., "BMSCs transplantation improves cognitive impairment via up-regulation of hippocampal GABAergic system in a rat model of chronic cerebral hypoperfusion," *Neuroscience*, vol. 311, pp. 464–473, 2015.

[36] T.-C. Kang, S.-K. Park, I.-K. Hwang et al., "Spatial and temporal alterations in the GABA shunt in the gerbil hippocampus following transient ischemia," *Brain Research*, vol. 944, no. 1-2, pp. 10–18, 2002.

[37] M. S. Lazarus, K. Krishnan, and Z. J. Huang, "GAD67 deficiency in parvalbumin interneurons produces deficits in inhibitory transmission and network disinhibition in mouse prefrontal cortex," *Cerebral Cortex*, vol. 25, no. 5, pp. 1290–1296, 2015.

[38] R. D. Schwartz-Bloom and R. Sah, "γ-Aminobutyric acidA neurotransmission and cerebral ischemia," *Journal of Neurochemistry*, vol. 77, no. 2, pp. 353–371, 2001.

[39] C. Frahm, C. Haupt, F. Weinandy, G. Siegel, C. Bruehl, and O. W. Witte, "Regulation of GABA transporter mRNA and protein after photothrombotic infarct in rat brain," *The Journal of Comparative Neurology*, vol. 478, no. 2, pp. 176–188, 2004.

[40] K. Völgyi, P. Gulyássy, M. I. Todorov et al., "Chronic cerebral hypoperfusion induced synaptic proteome changes in the rat cerebral cortex," *Molecular Neurobiology*, vol. 55, no. 5, pp. 4253–4266, 2017.

[41] A. Salminen, P. Jouhten, T. Sarajarvi, A. Haapasalo, and M. Hiltunen, "Hypoxia and GABA shunt activation in the pathogenesis of Alzheimer's disease," *Neurochemistry International*, vol. 92, pp. 13–24, 2016.

[42] J. Y. Seo, C. H. Lee, J. H. Cho et al., "Neuroprotection of ebselen against ischemia/reperfusion injury involves GABA shunt enzymes," *Journal of the Neurological Sciences*, vol. 285, no. 1-2, pp. 88–94, 2009.

[43] L. Huang, L. B. Zhao, Z. Y. Yu et al., "Long-term inhibition of Rho-kinase restores the LTP impaired in chronic forebrain ischemia rats by regulating GABAA and GABAB receptors," *Neuroscience*, vol. 277, pp. 383–391, 2014.

[44] H. Cimarosti, S. Kantamneni, and J. M. Henley, "Ischaemia differentially regulates GABA(B) receptor subunits in organotypic hippocampal slice cultures," *Neuropharmacology*, vol. 56, no. 8, pp. 1088–1096, 2009.

[45] M. Mele, L. Ribeiro, A. R. Inacio, T. Wieloch, and C. B. Duarte, "GABA(A) receptor dephosphorylation followed by internalization is coupled to neuronal death in in vitro ischemia," *Neurobiology of Disease*, vol. 65, pp. 220–232, 2014.

[46] L. Liu, C. J. Li, Y. Lu et al., "Baclofen mediates neuroprotection on hippocampal CA1 pyramidal cells through the regulation of autophagy under chronic cerebral hypoperfusion," *Scientific Reports*, vol. 5, no. 1, article 14474, 2015.

[47] G. Li, H. Cheng, X. Zhang et al., "Hippocampal neuron loss is correlated with cognitive deficits in SAMP8 mice," *Neurological Sciences*, vol. 34, no. 6, pp. 963–969, 2013.

[48] M. J. West, P. D. Coleman, D. G. Flood, and J. C. Troncoso, "Differences in the pattern of hippocampal neuronal loss in normal ageing and Alzheimer's disease," *Lancet*, vol. 344, no. 8925, pp. 769–772, 1994.

[49] J. Xu, C. Li, X. H. Yin, and G. Y. Zhang, "Additive neuroprotection of GABA A and GABA B receptor agonists in cerebral ischemic injury via PI-3K/Akt pathway inhibiting the ASK1-JNK cascade," *Neuropharmacology*, vol. 54, no. 7, pp. 1029–1040, 2008.

[50] C. Jackson-Friedman, P. D. Lyden, S. Nunez, A. Jin, and R. Zweifler, "High dose baclofen is neuroprotective but also causes intracerebral hemorrhage: a quantal bioassay study using the intraluminal suture occlusion method," *Experimental Neurology*, vol. 147, no. 2, pp. 346–352, 1997.

[51] A. Sarnowska, M. Beresewicz, B. Zablocka, and K. Domanska-Janik, "Diazepam neuroprotection in excitotoxic and oxidative stress involves a mitochondrial mechanism additional to the GABAAR and hypothermic effects," *Neurochemistry International*, vol. 55, no. 1-3, pp. 164–173, 2009.

[52] P. E. Bickler, D. S. Warner, G. Stratmann, and J. A. Schuyler, "Gamma-aminobutyric acid-A receptors contribute to isoflurane neuroprotection in organotypic hippocampal cultures," *Anesthesia and Analgesia*, vol. 97, no. 2, pp. 564–571, 2003.

[53] A. ElAli, P. Theriault, P. Prefontaine, and S. Rivest, "Mild chronic cerebral hypoperfusion induces neurovascular dysfunction, triggering peripheral beta-amyloid brain entry and aggregation," *Acta Neuropathologica Communications*, vol. 1, no. 1, p. 75, 2013.

[54] S. A. Monaco, A. J. Matamoros, and W. J. Gao, "Conditional GSK3β deletion in parvalbumin-expressing interneurons potentiates excitatory synaptic function and learning in adult mice," *Progress in Neuro-Psychopharmacology & Biological Psychiatry*, vol. 100, article 109901, 2020.

[55] F. Galeffi, S. Sinnar, and R. D. Schwartz-Bloom, "Diazepam promotes ATP recovery and prevents cytochrome c release in hippocampal slices after in vitro ischemia," *Journal of Neurochemistry*, vol. 75, no. 3, pp. 1242–1249, 2000.

[56] F. Zhang, C. Li, R. Wang et al., "Activation of GABA receptors attenuates neuronal apoptosis through inhibiting the tyrosine phosphorylation of NR2A by Src after cerebral ischemia and reperfusion," *Neuroscience*, vol. 150, no. 4, pp. 938–949, 2007.

[57] T. Ogura, T. Hamada, T. Matsui et al., "Neuroprotection by JM-1232(-) against oxygen-glucose deprivation-induced injury in rat hippocampal slice culture," *Brain Research*, vol. 1594, pp. 52–60, 2015.

[58] I. Gacsalyi, K. Moricz, G. Gigler, K. Megyeri, P. Machado, and F. A. Antoni, "Persistent therapeutic effect of a novel α5-GABAA receptor antagonist in rodent preclinical models of vascular cognitive impairment," *European Journal of Pharmacology*, vol. 834, pp. 118–125, 2018.

[59] A. N. Clarkson, B. S. Huang, S. E. Macisaac, I. Mody, and S. T. Carmichael, "Reducing excessive GABA-mediated tonic inhibition promotes functional recovery after stroke," *Nature*, vol. 468, no. 7321, pp. 305–309, 2010.

[60] Y. Lu, C. J. Li, C. Chen et al., "Activation of GABAB2 subunits alleviates chronic cerebral hypoperfusion-induced anxiety-like behaviours: a role for BDNF signalling and Kir3 channels," *Neuropharmacology*, vol. 110, Part A, pp. 308–321, 2016.

[61] H. Fiorentino, N. Kuczewski, D. Diabira et al., "GABA(B) receptor activation triggers BDNF release and promotes the maturation of GABAergic synapses," *The Journal of Neuroscience*, vol. 29, no. 37, pp. 11650–11661, 2009.

[62] B. Lu, G. Nagappan, and Y. Lu, "BDNF and synaptic plasticity, cognitive function, and dysfunction," *Handbook of Experimental Pharmacology*, vol. 220, pp. 223–250, 2014.

[63] J. C. Lee, J. H. Park, J. H. Ahn et al., "New GABAergic neurogenesis in the hippocampal CA1 region of a gerbil model of long-term survival after transient cerebral ischemic injury," *Brain Pathology*, vol. 26, no. 5, pp. 581–592, 2016.

[64] Y. Lu, C. Li, M. Zhou et al., "Clonidine ameliorates cognitive impairment induced by chronic cerebral hypoperfusion via up-regulation of the GABABR1 and GAD67 in hippocampal CA1 in rats," *Pharmacology, Biochemistry, and Behavior*, vol. 132, pp. 96–102, 2015.

[65] P. R. Baraniak and T. C. McDevitt, "Stem cell paracrine actions and tissue regeneration," *Regenerative Medicine*, vol. 5, no. 1, pp. 121–143, 2010.

[66] C. M. Willis, A. M. Nicaise, L. Peruzzotti-Jametti, and S. Pluchino, "The neural stem cell secretome and its role in brain repair," *Brain Research*, vol. 1729, article 146615, 2020.

[67] D. H. Tanaka, K. Toriumi, K. Kubo, T. Nabeshima, and K. Nakajima, "GABAergic precursor transplantation into the prefrontal cortex prevents phencyclidine-induced cognitive deficits," *The Journal of Neuroscience*, vol. 31, no. 40, pp. 14116–14125, 2011.

[68] L. Verret, E. O. Mann, G. B. Hang et al., "Inhibitory interneuron deficit links altered network activity and cognitive dysfunction in Alzheimer model," *Cell*, vol. 149, no. 3, pp. 708–721, 2012.

[69] L. M. Tong, B. Djukic, C. Arnold et al., "Inhibitory interneuron progenitor transplantation restores normal learning and memory in ApoE4 knock-in mice without or with Aβ accumulation," *The Journal of Neuroscience*, vol. 34, no. 29, pp. 9506–9515, 2014.

[70] M. Martinez-Losa, T. E. Tracy, K. Ma et al., "Nav1.1-overexpressing interneuron transplants restore brain rhythms and cognition in a mouse model of Alzheimer's disease," *Neuron*, vol. 98, no. 1, pp. 75–89.e5, 2018.

[71] E. Sammali, C. Alia, G. Vegliante et al., "Intravenous infusion of human bone marrow mesenchymal stromal cells promotes functional recovery and neuroplasticity after ischemic stroke in mice," *Scientific Reports*, vol. 7, no. 1, p. 6962, 2017.

[72] M.-L. Luo, L. Pan, L. Wang et al., "Transplantation of NSCs promotes the recovery of cognitive functions by regulating neurotransmitters in rats with traumatic brain injury," *Neurochemical Research*, vol. 44, no. 12, pp. 2765–2775, 2019.

[73] A. J.-P. Schwitzguébel, C. Benaïm, S. Carda, A. M. Torea Filgueira, R. Frischknecht, and P. A. Rapin, "GABAergic drug use and global, cognitive, and motor functional outcomes after stroke," *Annals of Physical and Rehabilitation Medicine*, vol. 59, no. 5-6, pp. 320–325, 2016.

Research Article

Bushen-Tiansui Formula Improves Cognitive Functions in an $A\beta_{1-42}$ Fibril-Infused Rat Model of Alzheimer's Disease

Chenxia Sheng,[1] Panpan Xu,[1] Xinyi Liu,[2] Weijun Peng,[1] Daxiong Xiang,[2,3] and Shilin Luo [2,3]

[1]*Department of Integrated Traditional Chinese and Western Medicine, The Second Xiangya Hospital, Central South University, Changsha 410011, China*
[2]*Department of Pharmacy, The Second Xiangya Hospital, Central South University, Changsha 410011, China*
[3]*Hunan Provincial Engineering Research Center of Translational Medicine and Innovative Drug, Changsha 410011, China*

Correspondence should be addressed to Shilin Luo; shilin_luo@csu.edu.cn

Bushen-Tiansui Formula (BTF) was empirically updated from a classical prescription named Kong-Sheng-Zhen-Zhong pill. It is based on the traditional Chinese medicine theory of the mutual relationship between the brain and the kidney and is intended to treat neurodegenerative diseases. This formulation has been used for several years to treat patients with Alzheimer's disease- (AD-) like symptoms in our clinical department. However, the medicinal ingredients and the mechanisms by which BTF improves cognition and memory functions have not been characterized. In this study, we used UPLC-MS to generate a chromatographic fingerprinting of BTF and identified five possible active ingredients, including stilbene glycoside; epimedin A1, B, and C; and icariin. We also showed that oral administration of BTF reversed the cognitive defects in an $A\beta_{1-42}$ fibril-infused rat model of AD, protected synaptic ultrastructure in the CA1 region, and restored the expression of BDNF, synaptotagmin (Syt), and PSD95. These effects likely occurred through the BDNF-activated receptor tyrosine kinase B (TrkB)/Akt/CREB signaling pathway. Furthermore, BTF exhibited no short-term or chronic toxicity in rats. Together, these results provided a scientific support for the clinical use of BTF to improve learning and memory in patients with AD.

1. Introduction

Alzheimer's disease (AD) is the leading cause of dementia worldwide, but the etiology and pathogenesis of this disease have not been characterized. Accumulation of β-amyloid peptide ($A\beta$) in the brain and hyperphosphorylation and cleavage of the microtubule-associated protein Tau are hallmarks of AD [1]. However, over the last decade, a series of new drugs designed to clear neurofibrillary tangles have failed to improve or reverse AD, which indicated that neurofibrillary tangles correlated weakly with the degree of dementia in patients with AD [2]. In contrast, synaptic loss has been strongly correlated with cognitive impairment, and it may be the pathological basis of cognitive changes in AD [3].

Neurotrophins are growth factors that regulate neuronal development, differentiation, and survival. Brain-derived neu-rotrophic factor (BDNF) is an important neurotrophin that is distributed extensively throughout the central nervous system. BDNF binds to receptor tyrosine kinase B (TrkB) and triggers activation of the downstream TrkB/Akt and TrkB/CREB signaling pathways, resulting in the synthesis of synaptotagmin (Syt) and PSD95 in synapses. Synaptotagmin and PSD95 confer protection by regulating the repair of synapses and the reconstruction of neural circuits to improve learning and memory in animals with dementia [4–6]. Studies have shown that the expression of BDNF was reduced in the brains of patients with AD with synaptic loss [7]. A strategy of using BDNF as a therapeutic agent for neurologic disorders was carried out based on this preclinical evidence. Unfortunately, the outcomes of several clinical trials involved the intrathecal infusion of recombinant BDNF to treat patients with amyotrophic lateral sclerosis have been disappointing due to the short

in vivo half-life and poor delivery of BDNF [8, 9]. Thus, novel strategies to directly stimulate production and expression of BDNF by exploring drugs may result in better therapeutic outcomes.

Facing the treatment complexity of AD, a growing body of reports have suggested that traditional Chinese medical formulas (TCMFs) with multitarget effects may result in improved cognitive function [10–12]. Bushen-Tiansui Formula (BTF) is derived from a classic prescription, Kong-Sheng-Zhen-Zhong pill (Qianjin Formulas), and was empirically modified from this classic prescription by adjusting the composition and proportion of herbs. Its formula is intended to meet neurodegenerative diseases and embodies the Chinese medicine theory of the mutual relationships between the brain and the kidney, in which the core statements are that the deficiency of kidney function leads to the encephalon loss, and the kidney gives birth to the encephalon and the brain stores marrow [13]. BTF has been utilized for several years to treat patients with AD-like symptoms in our clinical department. Nonetheless, the pharmacological ingredients in BTF, and the mechanisms by which they improve cognitive and memory functions, have not been characterized. Our previous study reported that icariin, a major active component from *Herba Epimedium brevicornum* (Yin-Yang-Kuo) that belongs one of the herbs in BTF, improved synaptic plasticity in an $A\beta_{1-42}$ rat model of AD [14]. As a single compound, however, it will be a long-term task to develop it into an innovative promising drug for clinical use.

In this present study, we characterized the formula composition of BTF and generated a chromatographic fingerprint profile. We also evaluated the effects of BTF on cognition and memory functions in a rat model of AD and evaluated BFT-induced expression of BDNF and the activation of the TrkB/Akt/CREB cascaded signaling pathways. Our study provided scientific support for the clinical use of BTF to improve learning and memory in patients with AD.

2. Materials and Methods

2.1. Preparation of BTF Extract. BTF is comprised of six herbs mixed in the proportions summarized in Figure 1(a). All the mentioned botanical names can be checked following the database of http://www.theplantlist.org. The herbal names and Chinese names were retrieved from the 2015 edition of the Chinese pharmacopeia. All herbs in BTF were purchased from the TCM pharmacy of the Second Xiangya Hospital, Central South University (CSU), Changsha, Hunan Province. Voucher specimens (201605301-6) were well deposited at the department of integrated traditional Chinese and Western medicine at the Second Xiangya Hospital, CSU. The herbs were soaked in a 10 times volume of ddH$_2$O (w/v) for 1 h and then boiled twice for 1 h each. The two boiled solutions were combined and concentrated under vacuum and then freeze-dried to yield a lyophilized powder (output rate of 14.3% (w/w)). The lyophilized powder of BTF was stored at -20°C until used.

2.2. Chromatographic Fingerprint Analysis of BTF Extract. Ultrahigh-performance liquid chromatography-tandem mass spectrometer (UPLC-MS) was utilized to analyze the principal components in BTF. Standard compounds including stilbene glycoside (BWB50367), epimedin A1 (BWB50192), epimedin B (ASB-5159-010), epimedin C (ASB-5160-010), and icariin (GBW09541) were purchased from the National Standard Center. A CNW Athena C$_{18}$-WP column (4.6 mm × 150 mm , 5 μm) was used as a solid phase and maintained at 35°C while the spectrum analysis was performed. The mixture of water (A) and CH$_3$CN (B) was acted as a mobile phase with a gradient elution ratio as follows: 0-10 min 20%-30% B, 10-22 min 30% B, 22-25 min 30-33% B, and 25-30 min 33-80% B. The monitoring wavelength was 270 nm with a flow rate of 0.5 mL/min. Electrospray ionization (ESI) mode was used for mass spectrometry with a capillary voltage of 3500 V.

2.3. $A\beta_{1-42}$ Preformed Fibril Preparation. $A\beta_{1-42}$ (Sigma, USA) was dissolved at 1 mg/mL in hexafluoroisopropanol (HFIP) at room temperature and then sonicated in a bath sonicator for 5 min. The HFIP was evaporated using a gentle stream of nitrogen gas, and then nine volumes of ice-cold distilled water were added while vortexed occasionally. Keeping the solution on ice for 30 min, one volume of 10x fibril-forming buffer (0.2 M NaPi, 1.5 M NaCl, 0.2% NaN$_3$, pH 7.5) was added and vortexed repetitively. We sealed the solution tube and stored at 37°C for one week and vortexed daily. Fibril formation was verified using a Thioflavin T binding assay according to a previous report [15]. The $A\beta$ fibrils were stored at -80°C.

2.4. $A\beta_{1-42}$ Fibril-Infused Rat Model and BTF Treatment. The $A\beta_{1-42}$ fibril-infused rat model was established as described in our previous study [14]. In brief, adult male Sprague-Dawley (SD) rats (weight: 200–220 g) were anesthetized with isoflurane and then fixed in a stereotactic apparatus. The $A\beta_{1-42}$ fibrils (3 μL) were delivered bilaterally into the lateral ventricles at a rate of 0.5 μL/min (from bregma, anteroposterior (AP) −1.0 mm, 1.5 mm lateral to the sagittal suture, and 4.6 mm beneath the dura). An equivalent volume of sterile saline was injected as a sham group ($n = 8$). Following infusion for 3 days, rats that received the $A\beta_{1-42}$ infusion were randomly distributed to two groups ($n = 8$ for each group). According to clinical use dose, the test group was orally administered 27 g/kg BTF, and another group was orally administered an equivalent volume of sterile saline. The animals were dosed once per day for 28 days. The rats were assigned to gender- and age-matched treatment groups using a randomized block design. The total experimental period is summarized in Figure 2(a), and the experimental procedures were approved by the Review Committee of Central South University (Changsha, China).

2.5. Morris Water Maze Test. The Morris water maze test was carried out from 28 days after the beginning of BTF intervention. Rats in three groups were trained in a round, diluted ink water-filled tub (160 cm diameter × 90 cm height) in an environment rich with extra maze cues. An invisible escape platform (12 cm diameter × 25 cm height) was located in a fixed spatial location 1 cm below the water surface independent to utilize extra maze cues to determine the location of the platform. At the beginning of each trial, the rats were

placed in the water maze with their paws touching the wall from one of four different starting positions (N, S, E, and W). Each rat was subjected to four trials per day for five consecutive days with a 15-minute intertrial interval. The maximum trial length was 60 s, and the rats were manually guided to if they did not reach the platform in the allotted time. Upon reaching the invisible escape platform, the rats were left on it for an additional 10 s to allow for a survey of spatial cues in the environment to guide future navigation to the platform. The temperature of the water was monitored every hour and maintained between 22 and 25°C. Following the 5 days of task acquisition period, a probe trial was presented when the platform was removed, and the number of platform crossings and the percentage of time spent in the quadrant that previously contained the escape platform during task acquisition was recorded over 90 s. The whole trial process and the analysis of behavioral parameters were recorded through the ANY-maze video tracking system (Stoelting Co., USA).

2.6. *Electron Microscopy*. Synaptic ultrastructure detection was determined by electron microscopy as described previously [16]. Briefly, after deep anesthesia, rats were perfused transcardially with 4% paraformaldehyde in PBS. Hippocampal slices were postfixed in cold 2.5% glutaraldehyde, then dehydrated, soaked, and embedded through a graded acetone series. The embedded sections were dual-stained with uranyl acetate and lead citrate and visualized at 100 kV in a transmission electron microscope (Hitachi Ltd., Tokyo, Japan). Synapses were evaluated by the presence of synaptic vesicles and postsynaptic density, including the number of synapses, the width of each synaptic cleft, the thickness of the postsynaptic density, and the length of the synaptic active zone.

2.7. *Western Blotting*. Western blotting was performed using a standard protocol. Rat hippocampus tissue was sonicated and lysed with RIPA lysis buffer, and insoluble pellets were removed by centrifugation at $15,000 \times g$ for 15 min at 4°C. Protein concentration was measured using the BCA method, and the lysates were stored at -80°C until analysis. Equal amounts of protein (30-40 μg) were loaded for blotting with anti-p-TrkB/TrkB (1 : 1000, #sc-8058/#sc-7268, Santa Cruz Biotechnology, CA, USA), anti-p-Akt/Akt (1 : 1000, #4060/#9272), anti-p-CREB/CREB (1 : 500, #9189/#9197), anti-Syt (1 : 1000, #14558), and anti-PSD-95 (1 : 1000, #2507) (Cell Signaling Technology, Denver, MA, USA), and anti-BDNF (1 : 500, #108319, Abcam, Cambridge, UK).

2.8. *Immunohistochemistry*. Immunohistochemistry (IHC) was performed to visualize BDNF and p-Akt according to the manufacturer's instructions (Invitrogen). Briefly, free-floating 25 μm thick serial hippocampus sections were treated with 0.3% hydrogen peroxide for 10 min, and then, sections were rinsed three times with PBS and blocked in Reagent 1A for 10 min followed by incubation with BDNF (1 : 300) or p-Akt (1 : 500) antibody at 4°C overnight. After PBS washing, sections incubated with a biotinylated second antibody Reagent 1b followed by the conjugate enzyme Reagent 2 for each 10 min. Finally, a chromogen AEC single solution was utilized to develop the signals and captured in a

microscope (BX51TF, Olympus, Tokyo, Japan) with cellSens standard V3 detection system.

2.9. *Hematoxylin and Eosin Staining*. Multiple organs were collected and were immediately fixed in 4% formaldehyde. After immersion, organs were dehydrated by gradual soaking in alcohol and xylene, embedded in paraffin, and then sliced into 5 μm thick sections, which were stained with standard hematoxylin and eosin (H&E) staining protocol [17]. Sections were visualized under a digital optical microscope (Olympus, Tokyo, Japan).

2.10. *Statistical Analysis*. Statistical analysis was performed with Prism 7.0 (GraphPad software). All data were expressed as means ± SEM. from three or more independent experiments. Histological data were analyzed by one-way ANOVA. The threshold for significance for all experiments was set at $^*p < 0.05$, and smaller p values were represented as $^{**}p < 0.01$ and $^{\#}p < 0.001$.

3. Results

3.1. *Chromatographic Fingerprinting Analysis of BTF*. The pharmacological effect of traditional Chinese medicine formulas (TCMFs) is derived from combinations of active compounds. To investigate the possible major medicinal compounds in BTF, a qualitative assessment of ingredients was tentatively characterized the by UPLC-MS system and the chromatographic fingerprint was established as illustrated in Figure 1(b). Approximately 14 chromatographic peaks can be defined in the characteristic profile of BTF. According to the m/z ratio in the MS detection, five of these peaks (peak 1-5) were identified as stilbene glycoside (peak 1, m/z 405.1216 [M-H]$^-$), epimedin A1 (peak 2, m/z 837.5901 [M-H]$^-$), epimedin B (peak 3, m/z 807.2715 [M-H]$^-$), epimedin C (peak 4, m/z 821.2855 [M-H]$^-$), and icariin (peak 5, m/z 677.2433 [M+H]$^+$) (Figure 1(b)). These compounds were chemical components of *Radix Polygoni Multiflori* Preparata and *Herba Epimedii Brevicornus* based on the previous phytochemistry studies [18, 19]. Further, standard substances for these five compounds were purchased and their mixed solution was subjected to UPLC-MS analysis with the same elution conditions. The comparison of chromatograms showed similar UV absorption spectra and retention times for each peak. Therefore, these data suggested that stilbene glycoside; epimedin A1, B, and C; and icariin were characteristic components in BTF.

3.2. *Oral Administration of BTF Rescues Cognitive Deficits in* $A\beta_{1-42}$ *Fibril-Infused Rats*. To evaluate the effects of BTF on cognitive function in the AD model, hippocampus-dependent spatial memory in $A\beta_{1-42}$ fibril-infused rats was assessed using the Morris water maze test. The average escape latency to the hidden platform for each of the five acquisition days was calculated and plotted (Figures 2(b) and 2(c)). Two-way mixed ANOVA (group × training day) for latency revealed a main effect of the training day ($p < 0.05$) and of the group ($p < 0.05$), but there was no interaction (Figure 2(b)). The AUC of the escape latency was significantly greater in the saline-treated $A\beta_{1-42}$ fibril-infused rats
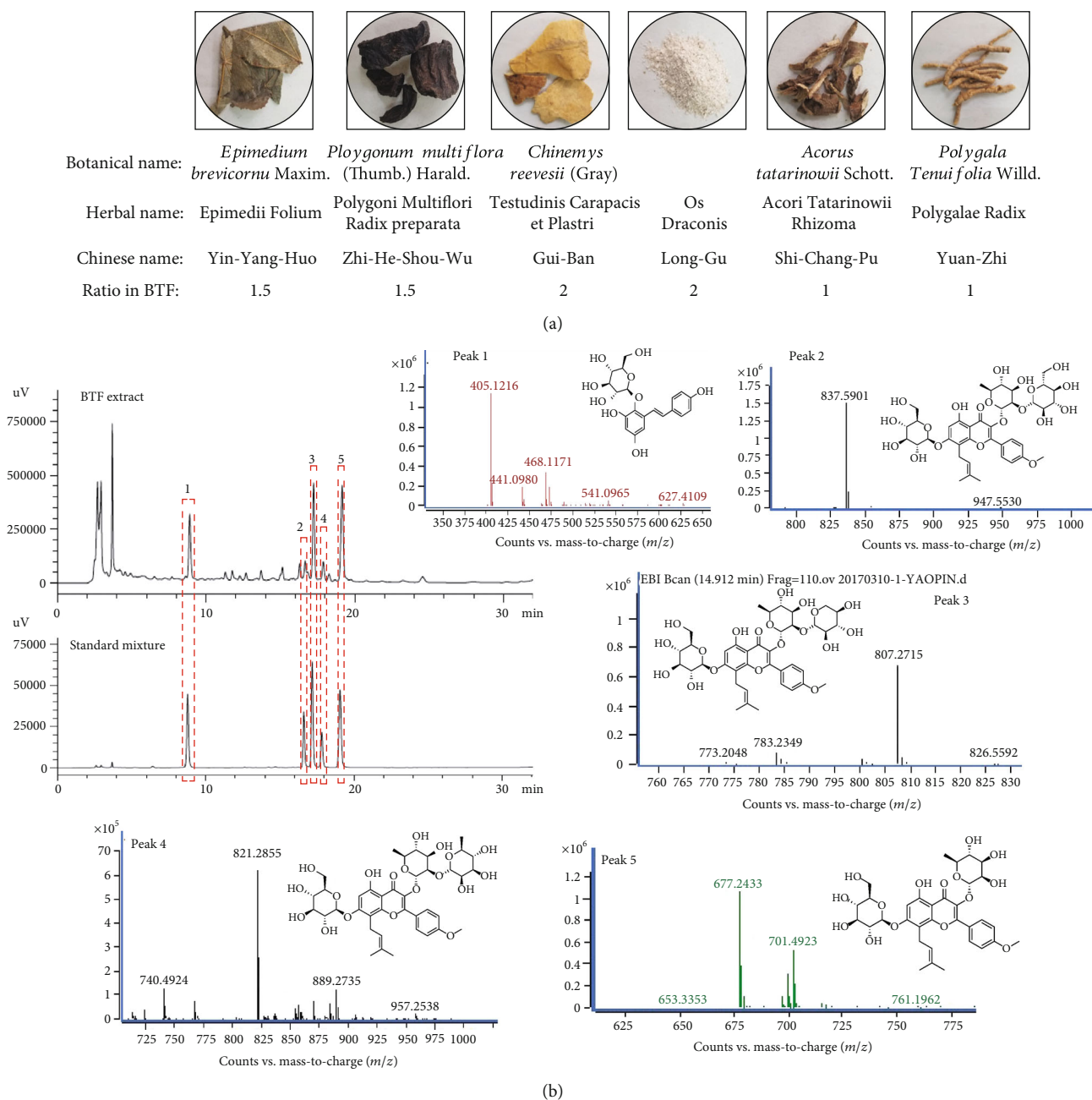
FIGURE 1: Herb information and chromatographic fingerprinting of the Bushen-Tiansui Formula (BTF). (a) Representative figures, herbal names, and Chinese names and the ratio of the corresponding herbs in BTF. (b) Chromatograms of BTF and a standard mixture, as well as m/z ratio and structure information of peaks 1-5 in the BTF chromatogram. Peak 1: stilbene glycoside; peak 2: epimedin A1; peak 3: epimedin B; peak 4: epimedin C; peak 5: icariin.

compared with that in the sham group, which indicated impaired acquisition of the spatial learning following intracerebroventricular injection of $A\beta_{1-42}$ fibrils. Memory recall for the platform location was assessed in the probe trial by removing the platform and allowing the rats to search for 90 s. Compared with the sham group, saline-treated $A\beta_{1-42}$ fibril-infused rats spent a significantly lower percentage of their time and fewer platform site crossing in the quadrant that formerly contained the hidden platform, which was indicative of severe deficits in spatial memory recall. Compared with the sham group rats, the $A\beta_{1-42}$ fibril-infused rats treated

with BTF spent a significantly greater percentage of time in the target quadrant and crossed the target quadrant more frequently (Figures 2(d)–2(f)), which demonstrated the rescue of spatial memory.

3.3. Oral Administration of BTF Prevents Synaptic Loss in $A\beta_{1-42}$ Fibril-Infused Rats.
Synaptic loss and decreased hippocampal synaptic plasticity are believed to be the basis of cognitive impairment in the early phases of AD [20]. We directly quantified the synaptic density and evaluated-synaptic ultrastructure parameters in the CA1 region of the
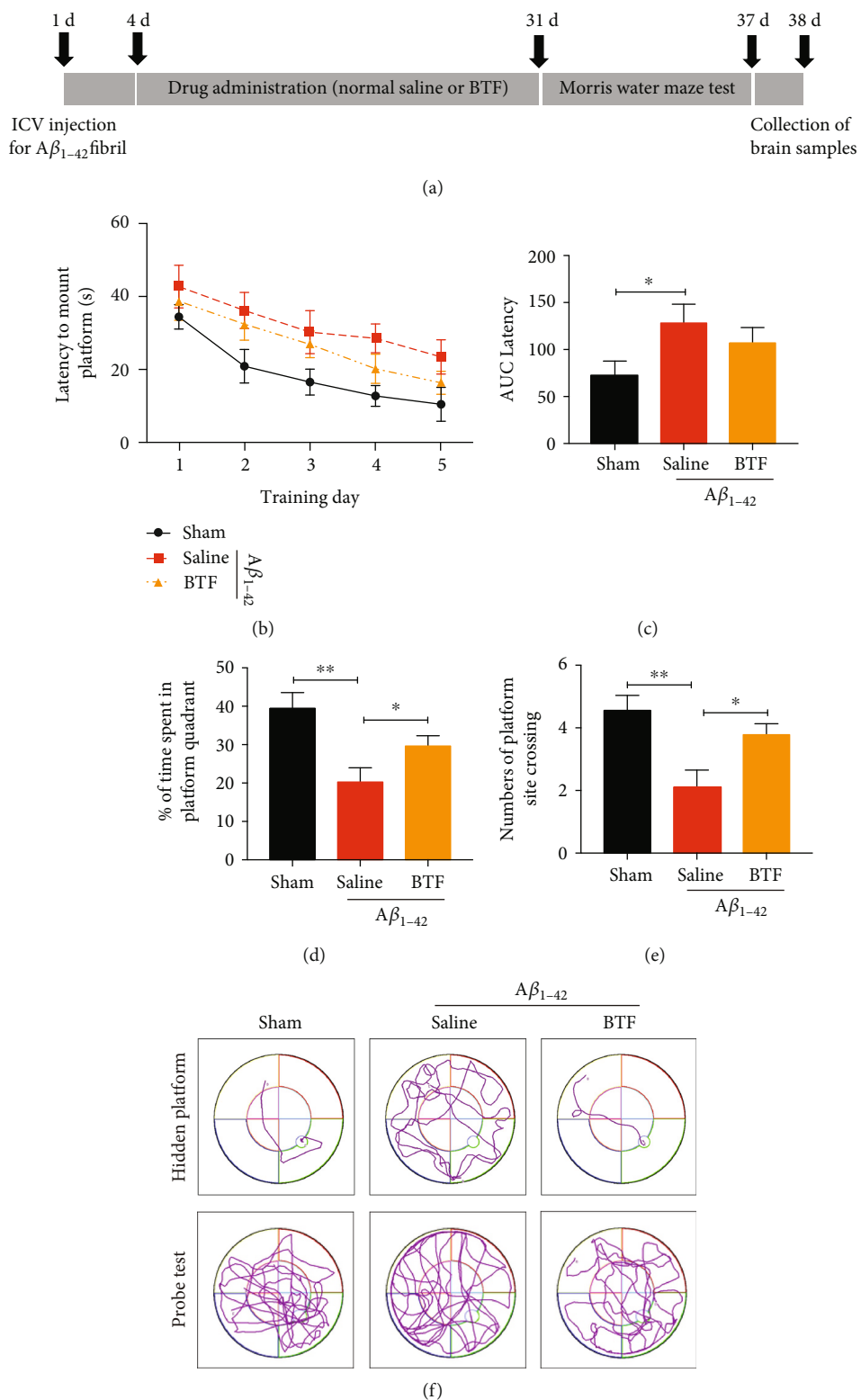
FIGURE 2: Oral administration of BTF rescues cognitive deficits in $A\beta_{1-42}$ fibril-infused rats. (a) The schedule of the treatment schedule and behavioral evaluation. (B-E) BTF improved cognitive functions in $A\beta_{1-42}$ fibril-infused rats. Rats ($n = 8$ or 9 per group) orally administered saline or BTF were trained in the water maze for 5 d. Data are presented as means ± SEM of latency to mount the escape platform (b), the AUC of latency (c), the percentage of time spent (d) ($F(2, 20) = 5.493$, $p = 0.0126$) and the number of crosses in the target quadrant (e) ($F(2, 20) = 7.216$, $p = 0.0044$). (f) Representative images of the swim paths of different rat groups in the hidden platform and probe tests. *$p < 0.05$, **$p < 0.01$ by one-way ANOVA with Tukey's multicomparison test compared with saline-treated $A\beta_{1-42}$ fibril-infused rats.

hippocampus using electron microscopy (EM). Saline-treated $A\beta_{1-42}$ fibril-infused rats showed significantly reduced synaptic density, perforated synapses, synaptic active zones length, and postsynaptic density thickness and increased synaptic cleft width. The oral administration of BTF significantly reversed these ultrastructure changes but did not alter the curvature of the synaptic interface (Figures 3(c)–3(g)). To confirm these findings, we performed immunoblotting for the presynaptic marker synaptotagmin and the postsynaptic marker PSD95. Saline-treated $A\beta_{1-42}$ fibril-infused rats displayed the considerably decreased expression of synaptotagmin and PSD95, which was indicative of synaptic degeneration in this AD model. Treatment with BTF reversed $A\beta_{1-42}$ fibril-induced reduction of synaptic marker expression (Figure 3(h)). These results indicated that oral administration of BTF inhibited synaptic loss and improved synaptic plasticity in $A\beta_{1-42}$ fibril-infused rats.

3.4. BTF Promotes BDNF Expression and Activates Downstream Signaling Pathways in the Rat Brain.
To explore the possible mechanisms by which BTF improved cognitive function in $A\beta_{1-42}$ fibril-infused rats, we investigated BDNF and its downstream signaling pathways. Following behavioral testing, we monitored BDNF expression in rat brains by immunoblotting analysis using an anti-BDNF antibody. Surprisingly, quantitative analysis revealed that BDNF was regained to normal levels in BTF-treated $A\beta_{1-42}$ fibril-infused rats. Furthermore, the expression of phosphorylated TrkB, but not total TrkB, was notably elevated following BTF treatment (Figure 4(a), 1-3$^{\text{th}}$ panels). As expected, the main proteins on TrkB signaling pathway were more prominently phosphorylated in $A\beta_{1-42}$ fibril-infused rats treated with BTF than in those treated with saline, as were the downstream activation of Akt/CREB signaling cascades (Figure 4(a)), which resulted in the synthesis of PSD95 in synapses. These results were confirmed by immunohistochemistry (IHC) staining of rat hippocampi using anti-BDNF (Figure 4(b)) and p-Akt S473 (Figure 4(c)). Therefore, these data indicated that the promotion of BDNF expression by BTF treatment led to the activation of its downstream TrkB-Akt/CREB signaling cascades might be responsible for the cognitive function improvement in AD rats.

3.5. Oral Administration of BTF Presents No Toxicity for Rats.
Drug safety is an important consideration in clinical investigations. As a compulsory experiment, we performed a 12-week chronic BTF toxicity study in Sprague-Dawley (SD) rats (200–220 g) with a daily dose of 54 g/kg. Continuous weekly weight records and the H&E staining of tissue sections from multiple organs (the heart, liver, spleen, lung, kidney, testis, and ovary) showed that there were no significant differences between rats administered with BTF and those administered with saline (Figures 5(a) and 5(b)). Besides, blood levels of RBC, HB, WBC, and ESR were within the normal ranges in rats that received BTF (data not shown). Thus, this study supports that the oral administration of BTF is safe and trustworthy for treating AD.

4. Discussion

Traditional Chinese medical formulas (TCMFs), developed based on the theory of the holistic body in traditional Chinese medicine (TCM), have been historically proven to be effective drugs in treating human diseases. Kidney-brain communication and reciprocity is one of the most important theories in TCM. This theory states that the kidney is a producer of the encephalon, and the cerebral marrow will be sufficient if the spirit in the kidney is exuberant [13]. Modern medical epidemiological data has shown that individuals at all stages of chronic kidney disease (CKD) are at higher risk of developing cognitive disorders and dementia [21]. Studies have proven that vascular injury, endothelial dysfunction, and direct neuronal toxicity may be potential factors in the pathophysiologic link of the kidney-brain axis [22–24]. "Kong-Sheng-Zhen-Zhong" pill was detailed in the classical medical book "Qianjin Formulas" written by Sun Simiao, a famous ancient Chinese medical expert. This formula is comprised of many nourishing herbs to achieve the treatment objectives that replenish vital essence, tonify kidney yin, and nourish the bone marrow [25]. Bushen-Tiansui Formula is an empirically improved version of the Kong-Sheng-Zhen-Zhon pill developed in our department by adjusting the composition and proportion of herbs, and the development of the application of BTF in neurological disorders was based on the theory of the kidney-brain axis. It has been shown to effectively treat neurodegenerative diseases, including AD. Specifically, BTF has been proven efficient in practice in our clinical department for improving cognitive and memory functions in patients with AD. Our discoveries about the development of a chromatographic fingerprint for BTF through the modern analytical techniques, and characterization of the mechanisms by which BTF improved cognition provided a scientific basis for expanded use of this formula.

UPLC-MS combines the efficient separation capabilities of UPLC and the great power in the structural characterization of MS and provides a new powerful approach to identify the constituents in TCMFs rapidly and accurately [26]. In addition, diode array detection (DAD) is a commonly used detection technique for HPLC analysis. The combined use of DAD and MS can provide excellent specificity by providing orthogonal information for each peak. Fragmentation can be used to identify compounds using databases, and novel compounds can be identified using data deconvolution software sand spectral matching. In our current study, five components were identified that were associated with two herbs in BTF (Figure 1(b)). According to phytochemistry studies [27, 28], the main components of Gui-Ban and Long-Gu were amino acids with no conjugated bonds and minerals, respectively, which do not typically contain chromophores and cannot be detected by UV analysis. Moreover, the monitoring wavelength of 270 nm may not have captured the absorbance of asarone and saponins present in Shi-Chang-Pu and Yuan-Zhi, respectively. Therefore, UV detection may not be sufficient to characterize BTF [29, 30]. Furthermore, the lack of commercial standards for analysis and characterization may also be a limiting factor. In terms of the brain availability of the molecules we identified by

(a)

(b)

(c)

(d)

(e)

(f)

(g)

(h)
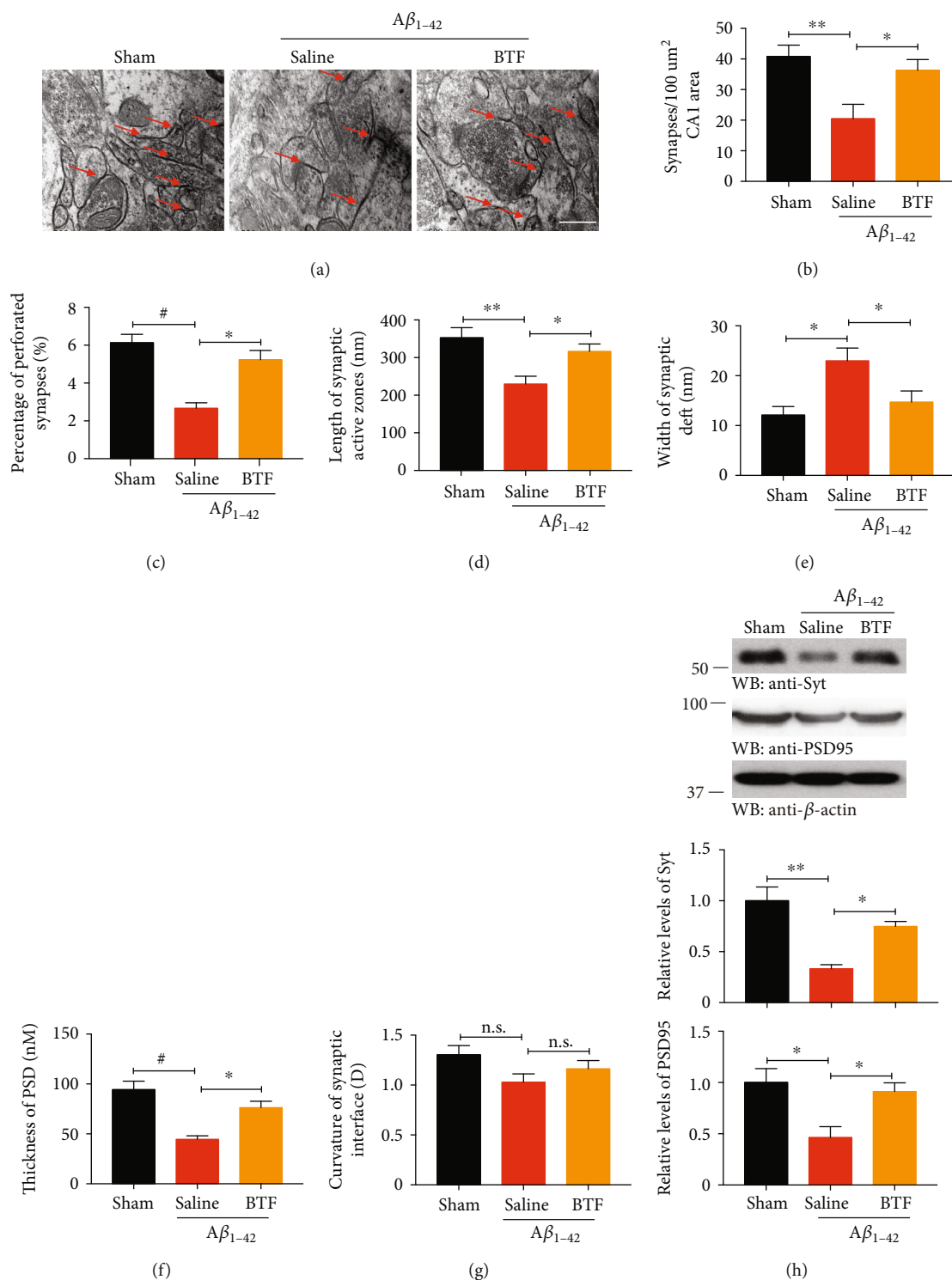
FIGURE 3: Oral administration of BTF prevents synaptic loss in $A\beta_{1-42}$ fibril-infused rats. (a) Representative electron micrographs of synapses. Red arrows indicate the synapses. Scale bar, 1 μm. (b–g) Quantitative analysis of the synaptic density (b) ($F(2, 12) = 7.1$, $p = 0.0092$) and the parameters of synaptic structure in the AC1 region. Data are presented as means ± SEM for the percentage of perforated synapses (c) ($F(2, 12) = 18.27$, $p = 0.0002$), synaptic active zone length (d) ($F(2, 12) = 7.689$, $p = 0.0071$), synaptic cleft width (e) ($F(2, 12) = 6.732$, $p = 0.0110$), PSD thickness (f) ($F(2, 12) = 15.24$, $p = 0.0005$), and synaptic interface curvature (g). $n = 5$ in each group. (h) Immunoblotting analysis of synaptic markers in brain homogenates from rats treated with saline or BTF. BTF treatment increased the expression of synaptic markers in $A\beta_{1-42}$ fibril-infused rats. $^*p < 0.05$, $^{**}p < 0.01$ and $^{\#}p < 0.001$ by one-way ANOVA with Tukey's multicomparison test compared with saline-treated $A\beta_{1-42}$ fibril-infused rats. Western blot data are representative of three independent experiments.

(a)

(b)

(c)
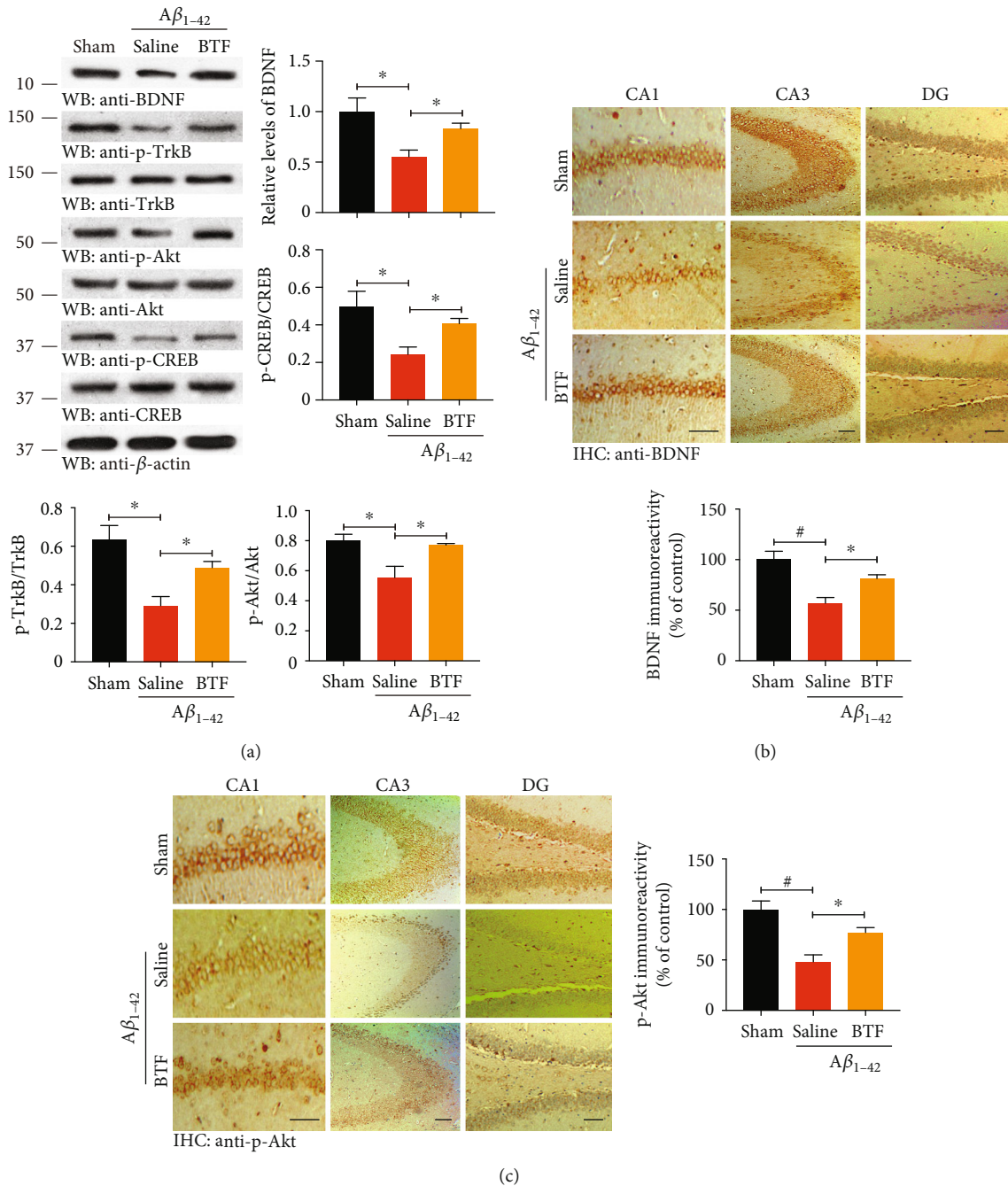
FIGURE 4: BTF promotes BDNF expression and activates downstream signaling pathways in the rat brain. (a) BDNF-TrkB signaling pathways were analyzed by immunoblotting with the indicated antibodies. The expression of BDNF induced by BTF triggered the phosphorylation of TrkB, Akt, and CREB. (b, c) IHC staining for BDNF (b) and p-Akt (c) in different hippocampal regions. BTF treatment significantly escalated their expression in $A\beta_{1-42}$ fibril-infused rats, which were consistent with Western blot results. Quantification of BDNF intensity ($F(2, 12) = 12.21$, $p = 0.0013$) and p-Akt intensity ($F(2, 12) = 14.27$, $p = 0.0007$) are shown. Data are represented as of 12-18 sections prepared from three rats in each group. Scale bar, 150 μm. $^*p < 0.05$, $^\#p < 0.001$ by one-way ANOVA with Tukey's multicomparison test. Western blot data are representative of three independent experiments.

UPLC-MS, those compounds belong to polyphenols (PPs). PP metabolites could indirectly regulate the cerebrovascular system or directly act as neurotransmitters crossing the blood-brain barrier, while the gut microbiota plays a crucial role in metabolizing dietary polyphenols into lipid-soluble metabolites that are absorbed by cells [31, 32]. In our

experiment, we administrated BTF by oral gavage and believed that the metabolites of PPs that were transformed from the gut microbiota or live metabolism could pass through the blood-brain barrier (BBB) and accumulated in the brain.

A pathological hallmark of AD is the presence of amyloid plaques within the brain, an observation that led to the β-
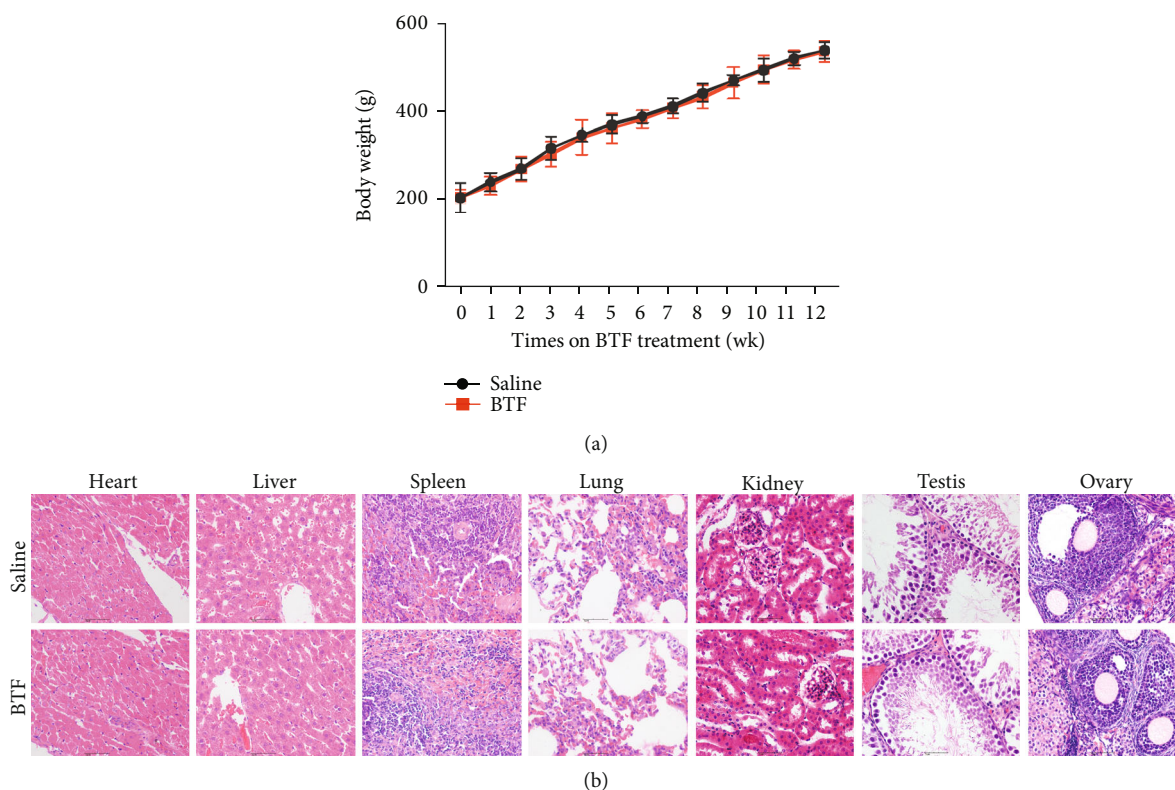
FIGURE 5: Oral administration of BTF presents no toxicity for rats. (a) The monitoring curve of body weight demonstrated no significant difference between saline and BTF treatment groups. (b) Representative images of H&E staining of tissue sections from multiple organs. SD rats (200–220 g) were treated with a daily dose of 54 g/kg of BTF for 12 consecutive weeks ($n = 6$). Continuous weekly weight records were kept, and the heart, liver, spleen, lung, kidney, testis, and ovary were collected for pathological analysis at the end of the study.

amyloid (Aβ) cascade hypothesis of AD [33, 34]. Attention has since focused on the isoforms and their physiological function, specially Aβ_{1-42}. Recent studies have shown that AD may be caused by Aβ aggregates that adopt alternative conformations, resulting in prion-like self-propagation [35–37]. Intracerebroventricular injection of Aβ_{1-42} fibrils has been shown to induce hyperphosphorylation of tau, tangle formation, and leading eventually to neuronal death and dementia and has also been reported as seeds to induce endogenous Aβ aggregation then trigger neurotoxicity [33, 38]. These findings resulted in the development of models using endogenous Aβ and other plaque-associated factors without the need to overexpression of potentially confounding amyloid precursor protein (APP) domains, which naturally became a classic and popular AD animal model. Even so, further investigation on transgenic models of AD will be scheduled to fully assess the potential benefit of BTF and to exclude any side effect caused by impairment due to mechanical injury in the Aβ_{1-42} fibril-infused rats used in our studies.

BDNF exerts its biological functions on neurons through two transmembrane receptors: TrkB and p75 neurotrophin receptor (p75NTR) [39]. TrkB is a high-affinity catalytic receptor for several neurotrophins and is highly enriched in the hippocampus [40]. Phosphorylation of TrkB following stimulation by BDNF triggers the downstream activation of the PI3K/Akt/CREB signaling cascades, driving synaptotagmin and PSD95 synthesizing in endoplasmic reticulum (ER) and trafficking to synapses throughout the neurons, which results in rapid and dendrite-wide sensitization for synaptic potentiation [41, 42]. Intriguingly, BDNF gene transcription is controlled by the CREB family of transcription factors, and PSD95 interacts with TrkB receptor for BDNF [43, 44]. These two circulation pathways promote the high expression of BDNF and PSD95, as well as stable TrkB receptors for responding to BDNF stimulation effect. As a result, the activation of these pathways results in a positive feedback loop in which synapses become more responsive to BDNF, which leads to increased transport of PSD95 to synapses. Together, we noted that BTF significantly stimulated the expression of BDNF and subsequently induced the activation of the TrkB-Akt/CREB cascaded signaling pathways, which resulted in increased synthesis of downstream synaptotagmin and PSD95 in synapses. These results identified a potential mechanism of BTF-induced significant stabilization of synaptic plasticity in Aβ_{1-42} fibril-infused rats.

5. Conclusion

In conclusion, our study generated a chromatographic fingerprint for the Bushen-Tiansui Formula (BTF) that has been utilizing in our clinic department for several years and further confirmed that BTF improved cognitive function through the prevention of synaptic loss, as demonstrated in the classical AD model of Aβ_{1-42} fibril-infused rats. Furthermore, the mechanism investigation revealed that BTF

stimulated the expression of BDNF and triggered the activation of the TrkB/Akt and TrkB/CREB pathways, which resulted in the upregulation of synaptotagmin and PSD95 expression in synapses. In short, this study provides a compelling scientific basis for expanding the application of BTF in the clinic, and the ongoing randomized clinical trial of BTF, in turn, will confirm the reliability of our reporting, which provides a reliable pathway for the treatment of AD.

Data Availability

The data used to support the findings of this study are included within the article.

Conflicts of Interest

The authors declare that they have no conflict of interest.

Authors' Contributions

S.L. conceived the project, designed the experiments, analyzed the data, and wrote the manuscript. C.S designed and performed most of the experiments. P.X. and X.L performed the chromatographic fingerprint analysis. W.J and D.X. assisted with data analysis and critically read the manuscript.

Acknowledgments

References

[1] R. H. Takahashi, E. Capetillo-Zarate, M. T. Lin, T. A. Milner, and G. K. Gouras, "Co-occurrence of Alzheimer's disease β-amyloid and tau pathologies at synapses," *Neurobiology of Aging*, vol. 31, no. 7, pp. 1145–1152, 2010.

[2] E. Karran, M. Mercken, and B. De Strooper, "The amyloid cascade hypothesis for Alzheimer's disease: an appraisal for the development of therapeutics," *Nature Reviews. Drug Discovery*, vol. 10, no. 9, pp. 698–712, 2011.

[3] S. Scheff, D. Price, F. Schmitt, S. DeKosky, and E. Mufson, "Synaptic alterations in CA1 in mild Alzheimer disease and mild cognitive impairment," *Neurology*, vol. 68, no. 18, pp. 1501–1508, 2007.

[4] Y. F. Liu, H. I. Chen, C. L. Wu et al., "Differential effects of treadmill running and wheel running on spatial or aversive learning and memory: roles of amygdalar brain-derived neurotrophic factor and synaptotagmin I," *Journal of Physiology (London)*, vol. 587, no. 13, pp. 3221–3231, 2009.

[5] T. Nakai, T. Nagai, M. Tanaka et al., "Girdin phosphorylation is crucial for synaptic plasticity and memory: a potential role in the interaction of BDNF/TrkB/Akt signaling with NMDA receptor," *The Journal of Neuroscience*, vol. 34, no. 45, pp. 14995–15008, 2014.

[6] S. Wang, L. Yu, H. Yang et al., "Oridonin attenuates synaptic loss and cognitive deficits in an $A\beta_{1-42}$-induced mouse model of Alzheimer's disease," *PLoS One*, vol. 11, no. 3, article e0151397, 2016.

[7] C. Zuccato and E. Cattaneo, "Brain-derived neurotrophic factor in neurodegenerative diseases," *Nature Reviews Neurology*, vol. 5, no. 6, pp. 311–322, 2009.

[8] M. Beck, P. Flachenecker, T. Magnus et al., "Autonomic dysfunction in ALS: a preliminary study on the effects of intrathecal BDNF," *Amyotrophic Lateral Sclerosis*, vol. 6, no. 2, pp. 100–103, 2005.

[9] G. Ochs, R. D. Penn, M. York et al., "A phase I/II trial of recombinant methionyl human brain derived neurotrophic factor administered by intrathecal infusion to patients with amyotrophic lateral sclerosis," *Amyotrophic Lateral Sclerosis and Other Motor Neuron Disorders*, vol. 1, no. 3, pp. 201–206, 2000.

[10] Z. Lin, J. Gu, J. Xiu, T. Mi, J. Dong, and J. K. Tiwari, "Traditional Chinese medicine for senile dementia," *Evidence-based Complementary and Alternative Medicine*, vol. 2012, Article ID 692621, 13 pages, 2012.

[11] Q. Tang, H. Ke, C. Wu et al., "Aqueous extract from You-Gui-Yin ameliorates cognitive impairment of chronic renal failure mice through targeting hippocampal CaMKIIα/CREB/BDNF and EPO/EPOR pathways," *Journal of Ethnopharmacology*, vol. 239, pp. 111925–111935, 2019.

[12] Y. Zhang, C. Lin, L. Zhang et al., "Cognitive improvement during treatment for mild Alzheimer's disease with a Chinese herbal formula: a randomized controlled trial," *PLoS One*, vol. 10, no. 6, article e0130353, 2015.

[13] L. Li, H. Wei, L. Zhang, J. Chu, and L. Zhao, "Modern biological basis of Chinese medical theory that "kidney nourishes marrow and brain is sea of marrow"," *China Journal of Chinese Materia Medica*, vol. 31, pp. 1397–1400, 2006.

[14] C. Sheng, P. Xu, K. Zhou, D. Deng, C. Zhang, and Z. Wang, "Icariin attenuates synaptic and cognitive deficits in an $A\beta_{1-42}$-induced rat model of Alzheimer's disease," *BioMed Research International*, vol. 2017, Article ID 7468872, 12 pages, 2017.

[15] C. S. Goldsbury, S. Wirtz, S. A. Müller et al., "Studies on the in vitro assembly of Aβ 1–40: implications for the search for Aβ fibril formation inhibitors," *Journal of Structural Biology*, vol. 130, no. 2-3, pp. 217–231, 2000.

[16] H. B. Luo, Y. Li, Z. J. Liu et al., "Protective effect of tetrahydroxy stilbene glucoside on learning and memory by regulating synaptic plasticity," *Neural Regeneration Research*, vol. 11, no. 9, pp. 1480–1486, 2016.

[17] A. H. Fischer, K. A. Jacobson, J. Rose, and R. Zeller, "Hematoxylin and eosin staining of tissue and cell sections," *Cold Spring Harbor Protocols*, vol. 2008, no. 6, article pdb.prot4986, 2008.

[18] J. Yu, J. Xie, X. J. Mao et al., "Comparison of laxative and antioxidant activities of raw, processed and fermented Polygoni Multiflori Radix," *Chinese Journal of Natural Medicines*, vol. 10, no. 1, pp. 63–67, 2012.

[19] D. A. Zhou, Y. N. Deng, L. Liu, and J. J. Li, "Effect of kidney-reinforcing and marrow-beneficial traditional Chinese medicine-intervened serum on the proliferation and osteogenic differentiation of bone marrow stromal cells," *Experimental and Therapeutic Medicine*, vol. 9, no. 1, pp. 191–196, 2015.

[20] G. M. Shankar and D. M. Walsh, "Alzheimer's disease: synaptic dysfunction and Aβ," *Molecular Neurodegeneration*, vol. 4, no. 1, p. 48, 2009.

[21] M. Kurella, D. L. Mapes, F. K. Port, and G. M. Chertow, "Correlates and outcomes of dementia among dialysis patients: the

Dialysis Outcomes and Practice Patterns Study," *Nephrology Dialysis Transplantation*, vol. 21, no. 9, pp. 2543–2548, 2006.

[22] J.-M. Bugnicourt, O. Godefroy, J.-M. Chillon, G. Choukroun, and Z. A. Massy, "Cognitive disorders and dementia in CKD: the neglected kidney-brain axis," *Journal of the American Society of Nephrology*, vol. 24, no. 3, pp. 353–363, 2013.

[23] K. Miwa, M. Tanaka, S. Okazaki et al., "Chronic kidney disease is associated with dementia independent of cerebral small-vessel disease," *Neurology*, vol. 82, no. 12, pp. 1051–1057, 2014.

[24] A. M. Murray, "Cognitive impairment in the aging dialysis and chronic kidney disease populations: an occult burden," *Advances in Chronic Kidney Disease*, vol. 15, no. 2, pp. 123–132, 2008.

[25] Z. Wang, *The Essence of Qin-Jin Formulas*, Tianjin science and technology press, 2010.

[26] M. Yang, J. Sun, Z. Lu et al., "Phytochemical analysis of traditional Chinese medicine using liquid chromatography coupled with mass spectrometry," *Journal of Chromatography A*, vol. 1216, no. 11, pp. 2045–2062, 2009.

[27] C. Wang, H. Zeng, and W. Chen, "GC-MS fingerprint of effective components extracted from plastrum testudinis and its application," *Central South Pharmacy*, vol. 2, pp. 74–78, 2007.

[28] H. Zhang, L. Zhang, and Y. Liu, "Studies on chemical components and pharmacological activities of Os Draconis (Longgu) and Ostreae Concha," *China Journal of Chinese Materia Medica*, vol. 36, pp. 1839-1840, 2011.

[29] J. Liu, X. Yang, J. He, M. Xia, L. Xu, and S. Yang, "Structure analysis of triterpene saponins in *Polygala tenuifolia* by electrospray ionization ion trap multiple-stage mass spectrometry," *Journal of Mass Spectrometry*, vol. 42, no. 7, pp. 861–873, 2007.

[30] H.-X. Shi, J. Yang, T. Yang et al., "Alpha-asarone protects endothelial cells from injury by angiotensin II," *Evidence-based Complementary and Alternative Medicine*, vol. 2014, Article ID 682041, 7 pages, 2014.

[31] S. Filosa, F. di Meo, and S. Crispi, "Polyphenols-gut microbiota interplay and brain neuromodulation," *Neural Regeneration Research*, vol. 13, no. 12, pp. 2055–2059, 2018.

[32] S. Schaffer and B. Halliwell, "Do polyphenols enter the brain and does it matter? Some theoretical and practical considerations," *Genes & Nutrition*, vol. 7, no. 2, pp. 99–109, 2012.

[33] J. Hardy and D. Allsop, "Amyloid deposition as the central event in the aetiology of Alzheimer's disease," *Trends in Pharmacological Sciences*, vol. 12, no. 10, pp. 383–388, 1991.

[34] J. A. Hardy and G. A. Higgins, "Alzheimer's disease: the amyloid cascade hypothesis," *Science*, vol. 256, no. 5054, pp. 184-185, 1992.

[35] M. Goedert, "Alzheimer's and Parkinson's diseases: the prion concept in relation to assembled Aβ, tau, and α-synuclein," *Science*, vol. 349, no. 6248, 2015.

[36] M. Jucker and L. C. Walker, "Self-propagation of pathogenic protein aggregates in neurodegenerative diseases," *Nature*, vol. 501, no. 7465, pp. 45–51, 2013.

[37] J. C. Watts, C. Condello, J. Stöhr et al., "Serial propagation of distinct strains of Aβ prions from Alzheimer's disease patients," *Proceedings of the National Academy of Sciences of the United States of America*, vol. 111, no. 28, pp. 10323–10328, 2014.

[38] R. F. Sowade and T. R. Jahn, "Seed-induced acceleration of amyloid-β mediated neurotoxicity in vivo," *Nature Communications*, vol. 8, no. 1, pp. 512–524, 2017.

[39] D. R. Kaplan and F. D. Miller, "Neurotrophin signal transduction in the nervous system," *Current Opinion in Neurobiology*, vol. 10, no. 3, pp. 381–391, 2000.

[40] D. L. Shelton, J. Sutherland, J. Gripp et al., "Human trks: molecular cloning, tissue distribution, and expression of extracellular domain immunoadhesins," *The Journal of Neuroscience*, vol. 15, no. 1, pp. 477–491, 1995.

[41] J. F. McGinty, A. J. Bache, N. T. Coleman, and W.-L. Sun, "The role of BDNF/TrkB signaling in acute amphetamine-induced locomotor activity and opioid peptide gene expression in the rat dorsal striatum," *Frontiers in Systems Neuroscience*, vol. 5, pp. 1–8, 2011.

[42] A. Yoshii and M. Constantine-Paton, "BDNF induces transport of PSD-95 to dendrites through PI3K-AKT signaling after NMDA receptor activation," *Nature Neuroscience*, vol. 10, no. 6, pp. 702–711, 2007.

[43] C. Cao, M. S. Rioult-Pedotti, P. Migani et al., "Impairment of TrkB-PSD-95 signaling in Angelman syndrome," *PLoS Biology*, vol. 11, no. 2, article e1001478, 2013.

[44] X. Tao, S. Finkbeiner, D. B. Arnold, A. J. Shaywitz, and M. E. Greenberg, "Ca^{2+} influx regulates *BDNF* transcription by a CREB family transcription factor-dependent mechanism," *Neuron*, vol. 20, no. 4, pp. 709–726, 1998.

Research Article

The Retinal Inner Plexiform Synaptic Layer Mirrors Grey Matter Thickness of Primary Visual Cortex with Increased Amyloid β Load in Early Alzheimer's Disease

Lília Jorge [1,2] **Nádia Canário,** [1,2] **Ricardo Martins** [1,2] **Beatriz Santiago,** [3,4,5] **Isabel Santana,** [3,4,5] **Hugo Quental,** [1,2,4] **Francisco Ambrósio,** [3,4,5,6] **Rui Bernardes** [1,2,3] **and Miguel Castelo-Branco** [1,2,3]

[1]*Coimbra Institute for Biomedical Imaging and Translational Research (CIBIT), University of Coimbra, Coimbra, Portugal*
[2]*Institute for Nuclear Sciences Applied to Health (ICNAS), University of Coimbra, Coimbra, Portugal*
[3]*Faculty of Medicine, University of Coimbra, Coimbra, Portugal*
[4]*CNC.IBILI Consortium, University of Coimbra, Coimbra, Portugal*
[5]*Department of Neurology, Centro Hospitalar e Universitário de Coimbra (CHUC), Coimbra, Portugal*
[6]*Coimbra Institute for Clinical and Biomedical Research (iCBR), Retinal Dysfunction & Neuroinflammation Lab, Coimbra, Portugal*

Correspondence should be addressed to Miguel Castelo-Branco; mcbranco@fmed.uc.pt

The retina may serve as putative window into neuropathology of synaptic loss in Alzheimer's disease (AD). Here, we investigated synapse-rich layers versus layers composed by nuclei/cell bodies in an early stage of AD. In addition, we examined the associations between retinal changes and molecular and structural markers of cortical damage. We recruited 20 AD patients and 17 healthy controls (HC). Combining optical coherence tomography (OCT), magnetic resonance (MR), and positron emission tomography (PET) imaging, we measured retinal and primary visual cortex (V1) thicknesses, along with V1 amyloid β (Aβ) retention ([11C]-PiB PET tracer) and neuroinflammation ([11C]-PK11195 PET tracer). We found that V1 showed increased amyloid-binding potential, in the absence of neuroinflammation. Although thickness changes were still absent, we identified a positive association between the synapse-rich inner plexiform layer (IPL) and V1 in AD. This retinocortical interplay might reflect changes in synaptic function resulting from Aβ deposition, contributing to early visual loss.

1. Introduction

Alzheimer's disease is characterized by the presence of abnormal extracellular Aβ toxic deposits causing synaptic dysfunction, putative neuroinflammation due to microglia activation, and neuronal loss [1–6], which typically lead to progressive brain atrophy.

The impact of this pathology in the retina as well as other parts of the visual system in AD remains to be understood [7]. In fact, along with the numerous cognitive and neuropsychiatric manifestations, visual complains have often been reported in this condition [7–12] which include loss of contrast and color sensitivity [13–17], visual field loss [18, 19] and deficits in the perception of shape from motion [20–23].

Such visual impairments have been previously attributed to visual cortical damage, including V1 and visual associative areas [24–27]. However, more recently, it has been suggested that neural populations in the retina are also affected by similar pathophysiological mechanisms [28–30], even in the absence of visual cortical atrophy [12, 31].

As a part of the central nervous system (CNS), the retina shares multiple features with the brain, in terms of embryological development, anatomy, and function [32–35]. These similarities along with the visual changes observed in patients

suffering from neurodegenerative diseases have justified the proposal that the retina may serve as a mirror to assess brain changes [10, 36–38]. In fact, the pathological hallmarks of AD, i.e., neuronal loss, Aβ plaques, and neurofibrillary tangles from the hyperphosphorylation of tau protein (pTau), have also been found in the retina [28, 39–43].

Nevertheless, despite all similarities between brain and retina, important biological differences also exist, which concerns the discovery of early disease biomarkers; some features of the retina are particularly prone to such investigation, in particular, the presence of synapse-rich layers. In the retina, neuron cell bodies are organized in specific layers, while the plexiform layers are exclusively dedicated to make the synaptic connection between the different kinds of neurons (for a review, see Hoon et al. [44]), and thus, synapse-rich and nuclei/cell body layers can be easily and independently assessed. For example, the GCL (ganglion cell layer) comprises ganglion cell bodies and displaced amacrine cells [45], while the IPL is densely packed with synapses connecting retinal ganglion cells, amacrine cells, and bipolar cells [44]. This allows testing the dominance of synaptic mechanism vs. cell loss and hence might let to detect subtle initial changes in dendritic integrity given the tenet that the loss of synapses may precede cell loss [46], being more prone to occur in patients with early AD.

In fact, evidence about neurotransmitter changes, structural alterations, and other biochemical markers favours the hypothesis that AD represents, at least in the early stages, a synaptopathy [47, 48]. Considerable evidence suggests that before massive neuronal cell death occurs, there is synaptic dysfunction originated by oligomeric assemblies of the Aβ protein in the hippocampus, one of the first brain structures affected by the pathological mechanisms of the disease [46]. Remarkably, this early loss of synaptic integrity was already demonstrated in the retina of an AD mouse model [49], as well as in ocular neurodegenerative diseases [50]. Therefore, retina might represent an excellent target to detect early neuropathological mechanisms in a faster, direct, and cost-effective way, using *in vivo* eye imaging techniques, than methods to assess the same mechanisms in the brain.

Existing work addressing structural changes in AD, using OCT, has focused primarily on both RNFL (retinal fiber layer) and GCL, and the controversy remains [8, 31, 51–57], whereby differences could appear only in the late stages of the disease [58].

In the present study, we aimed to take advantage of the existence of synaptic versus cell body-rich layers in the retina to investigate whether AD affects differently such layers, as compared to healthy controls, in relation to integrity of V1—the visual area that primarily receives inputs from the retina. To that end, we measured in V1 Aβ levels through [11C]-Pittsburgh Compound B (PiB), neuroinflammation using [11C]-PK11195 radiotracer, and neuronal loss by means of cortical thickness analysis. Regarding the retina, we studied the structural integrity of 4 layers, 2 composed by synapses—IPL and OPL (outer plexiform layer)—and 2 composed by cell bodies—GCL (ganglion cell layer) and INL (inner nuclear layer), the layers of the inner retina closer to the brain.

Taking into account the substantial evidence suggesting that synaptic loss is one of the earliest pathological changes in AD, we hypothesize that synapse-rich layers would better reflect cortical status, considering the early stage of our AD sample.

To the best of our knowledge, the present work is the first to investigate an explicit disease-related morphometric and molecular association between V1 and retinal integrity in AD. Considering the uncertainty of the relative role of visual cortex or retina in the visual deficits observed in this population, it is crucial to study both structures and their potential relationships to common disease mechanisms.

2. Methods

2.1. Participants. A total of 41 subjects were recruited in the present study. We included 20 AD patients with a probable diagnosis supported by biological biomarkers (CSF and PET-PiB) and in mild stages of the disease, according to the Clinical Dementia Rating (CDR = 1). Patients were recruited at the Neurology Department of Coimbra University Hospital. The diagnosis criteria of AD were based on the Diagnostic and Statistical Manual of Mental Disorders–fourth edition (DSM-IVTR) [59] and the National Institute of Neurological and Communicative Disorders and Stroke-Alzheimer's Disease and Related Disorders (NINCDS-ADRDA) [60]. A comprehensive neuropsychological evaluation battery was administered, including (1) cognitive instruments as the Mini-Mental State Examination (MMSE) with Portuguese normative data [61, 62], the Montreal Cognitive Assessment (MoCA) [63, 64], and a comprehensive neuropsychological battery with normative data for the Portuguese population (BLAD) [65] exploring memory and other cognitive domains.

We considered that patients had to be in a stable condition, without acute significant events or recent/undergoing changes in medication; we defined this as exclusion criteria ophthalmological comorbidities or neurological/psychiatric conditions other than AD or CT or MRI demonstration of significant vascular burden (large cortico-subcortical infarct; extensive subcortical white matter lesions superior to 25%; uni- or bilateral thalamic lacune; lacune in head of caudate nucleus; more than 2 lacunes) (8) [60].

For the present study, we selected AD patients with a probable diagnosis supported by biological biomarkers (cerebrospinal fluid (CSF) or PiB-PET). The cut-off values used in our laboratory and applied in the present study were 580 pg/mL for Aβ_{1-42}, 0.068 for Aβ_{42}/Aβ_{40}, 250 pg/mL for tau, and 37 pg/mL for pTau181 (Table 1).

The control group was composed of 21 individuals matched for age, education, and sex, from the community, with no history of CNS, neurodevelopmental, or mental disorders. This group was also submitted to cognitive assessment and showed no significant memory complaints (Subjective Memory Complaints Questionnaire-SMC ≤ 3) [66, 67], had a normal general cognitive status tested by the MoCA (mean ± standard deviation (SD), 24.88 ± 4.24), had preserved daily living activities (Lawton and Brody scale—for female = 8; for male = 5) [68, 69], and no evidence of

TABLE 1: AD patients' CSF biomarker levels.

Variable	$A\beta_{1-42}$ ($n = 17$)	$A\beta_{42}/A\beta_{40}$ ($n = 14$)	Tau ($n = 17$)	pTau ($n = 17$)	Tau/$A\beta_{42}$ ($n = 17$)	$A\beta_{42}$/pTau ($n = 17$)
Mean	510.94	0.057	445.64	63.15	0.98	9.23
SD	215	0.021	246.80	24.36	0.52	6.28

Aβ: amyloid beta; pTau: phosphorylated tau; SD: standard deviation.

moderate or severe depressive symptoms (30-item Geriatric Depressive Scale – GDS-30, mean ± SD6.41 ± 6.20) [70, 71].

All subjects underwent PET imaging with [11C]-PiB and [11C]-PK11195 radiotracers in two different visits with a maximum interval of 1 month. PiB positivity was determined by an experienced nuclear medicine physician, who considered simultaneously a visual regional SUVR (standard uptake value ratio) analysis and the output of a homemade support vector machine classifier. The visual analysis of these images was regional based with emphasis to frontal cortex, parietal/precuneus cortex, temporal cortex, anterior and posterior cingulate cortex, basal ganglia, and occipital cortex.

Four subjects of the control group we found with PiB positive, an increasingly frequent finding, which led to their exclusion, although the cognitive tests performed were within normal ranges.

None of the participants had history of ocular diseases, and all were submitted to a comprehensive ophthalmological examination to guarantee the absence of visual complications, which comprised visual acuity assessment with Snellen chart, ocular tension, slit lamp biomicroscopy, and OCT imaging. We involved only subjects with normal or corrected to normal vision (visual acuity ≥ 8/10), with a refractive error between ±5 diopters, and without significant alterations of the optic disc or macula. Additionally, we considered exclusion criteria family history of glaucoma, or any other hereditary eye disease and diabetes or other systemic diseases that could affect the eye.

The study was approved by the Ethics Committee of the Faculty of Medicine, University of Coimbra. All subjects participated voluntarily and gave their informed written consent for the study, following the tenets of the Declaration of Helsinki, after clarification of the nature and possible implications of the study.

2.2. Retinal Imaging. Imaging data from the retina of both eyes were obtained by optical coherence tomography through the Cirrus HD-OCT system (Carl Zeiss Meditec, Inc., Dublin, CA, USA) with the macular cube 512×128 protocol, by one experienced technician (HQ). This protocol acquires data through a 6 mm square grid centered on the fovea by acquiring a series of 128 horizontal B-scan lines, each composed of 512 A-scans, with an axial resolution of 5 μm.

2.3. MR Imaging. Brain structural data were acquired using a whole-brain approach, with a phased array 12-channel birdcage head coil, in a Siemens Magnetom TIM Trio 3 Tesla scanner (Siemens, Munich, Germany). For each participant, one high-resolution T1-weighted three-dimensional Magnetization Prepared Rapid Acquisition Gradient Echo (MPRAGE) was acquired, with the following acquisition

parameters: $1.0 \times 1.0 \times 1.0$ mm^3 voxel resolution, repetition time (TR) 2530 ms, echo time (TE) 3.42 ms, and field of view (FOV) 256×256 mm. The anatomical sequence comprised 176 slices, a flip angle of 7°, and an inversion time of 1100 ms.

2.4. PET Imaging. The [11C]-PiB PET and [11C]-PK11195 PET acquisitions were performed using a Philips Gemini GXL PET/CT scanner (Philips Medical Systems, Best, the Netherlands). Both acquisitions consisted of dynamic 3-dimensional PET scan of the entire brain (90 slices, 2 mm slice sampling) and a low-dose brain computed tomography (CT) scan, for attenuation correction. The dynamic [11C]-PiB PET image comprised 24 frames (total duration of 90 minutes: 37 frames: 4×15 s + 8×30 s + 9×60 s + 2×180 s + 14×300 s) and the dynamic [11C]-PK11195 image of 22 frames (total duration of 60 minutes: 4×30 s + 4×60 s + 4×120 s + 4×240 s + 6×300 s). The [11C]-PiB PET or [11C]-PK11195 PET image acquisition sessions started immediately after the intravenous bolus injection of approximately 555 MBq of [11C]-PiB or 370 MBq of [11C]-PK11195. To minimize head movement, the patients' head was restrained with a soft elastic tape. The PET images were reconstructed to a $128 \times 128 \times 90$ matrix, with 2 mm isotropic voxel dimension, using the LOR RAMLA algorithm (Philips PET/CT Gemini GXL) with attenuation and scatter correction.

2.5. Cortical Thickness Assessment. Brain imaging processing was conducted in SPM12 software (Wellcome Trust Centre for Neuroimaging, Institute of Neurology, UCL, London, UK) throughout its computational anatomy toolbox (CAT12) (http://dbm.neuro.uni-jena.de/cat/), which allows fully automatic cortex segmentation and cortical thickness measurements.

The anatomic images were firstly reoriented into the AC-PC plane and then automatically corrected in order to diminish the intensity variations caused by the magnetic field and RF-field inhomogeneities. Thereon, automatic cortex segmentation in volume space of white matter-grey matter (WM-GM) and grey matter-cerebrospinal fluid (GM-CSF) boundaries was performed relying on prior probability tissue maps, assigning to each voxel a value representing the proportion of the corresponding tissue type [72].

To the spatial normalization, the subject's brains were aligned to a standard MNI template, resorting to the high-dimensional registration DARTEL algorithm in SPM [73]. At the end of the automatic segmentation procedure, a smoothing on the normalized GM maps was applied by a 15 mm isotropic Gaussian kernel; the datasets were then submitted to well-suited fully automated thickness measurements based on the projection-based thickness method, as

(a)   (b)
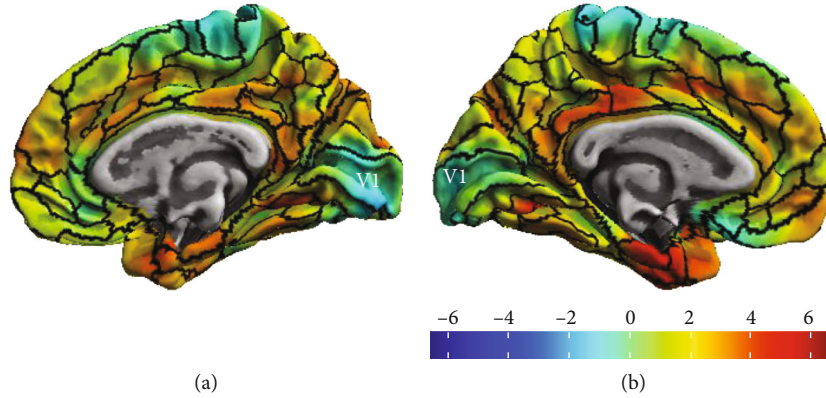
FIGURE 1: Resulting cortical thickness map between HC and AD groups, with the representation of the V1 area: (a) right hemisphere, (b) left hemisphere.

described by [74]. This method creates both a correct cortical thickness map and the central cortical surface in one step. The subsequent analyses were performed in surface space, which allows to reparametrize the surface mesh into a common coordinate system throughout a spherical mapping, improving the correspondence between individual subject's areas.

Moreover, the CAT12 toolbox allows the estimation of ROI-based mean thickness values relying on internal surface maps [75]. We used the ROI-based values provided by the Human Connectome Project (HCP's) multimodal parcellation [76] surface map, which comprises anatomically delineated V1 (see Figure 1). ROI-based thickness measures were extracted for each subject and then imported by SPSS for further statistical analysis.

2.6. Retinal Thickness Assessment. The OCT datasets underwent an automatic segmentation routine using the Iowa Reference Algorithms software (version 4.0.0, Retinal Image Analysis Lab, Iowa Institute for Biomedical Imaging, Iowa City, IA, USA) [77–79], providing the segmentation of retinal nerve fiber layer (RNFL), ganglion cell layer (GCL), inner plexiform layer (IPL), inner nuclear layer (INL), outer plexiform layer (OPL), outer nuclear layer (ONL), inner segment/outer segment junction (IS/OS), outer segment (OS), outer segment photoreceptor/RPE complex (OPR), and retinal pigment epithelium (RPE). In this study, we focused on the individual layers from CGL to OPL (see Figure 2).

Each of the 128 B-scans and all the 5 surface layers were visually inspected in order to check the quality of the segmentation. Manual corrections were performed just in case of an evident algorithm failure. Subsequently, the distance (in voxels) between the respective delimiting surfaces was taken as the thickness of each layer, multiplied by the voxel size in that direction. These measurements were provided by the software based on the number of voxels and imaging depth.

We focused in central vision due to the central magnification present in V1, and given the evidence of a higher involvement of the central vision in the disease [13, 80, 81]. The thickness of each macular layer was computed as the average from a whole area of a 3 mm diameter circular map
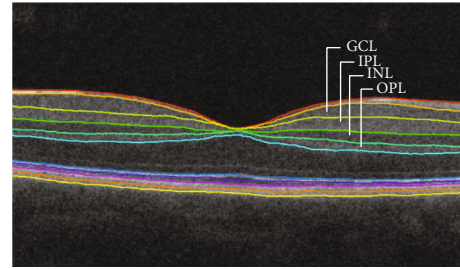
FIGURE 2: Macular image resulting from the segmentation, identifying the layers analyzed in this study. GCL: ganglion cell layer; IPL: inner plexiform layer; INL: inner nuclear layer; OPL: outer plexiform layer.

centered on the foveal pit, corresponding to inner macular ring of the standard EDTRS chart and to an eccentricity of 9.4°.

2.7. PET Imaging Preprocessing and Quantitative Analysis. A sum image obtained using all the frames of the dynamic PET was used to estimate a rigid transformation between the [11C]-PiB PET image space or [11C]-PK11195 PET image space and the T1 anatomical MRI space of each participant, using the 3D-Slicer software (version 4.8.1, BRAINS registration tool, http://www.slicer.org).

The individual MRI scans were spatially normalized to an MNI template using the DARTEL algorithm in SPM12.

The voxel-level quantitative analysis of [11C]-PiB PET images and [11C]-PK11195 PET images was implemented in the MNI space using in-house made software. The individual [11C]-PiB standard uptake value ratio (SUVR) map was computed by summing voxel-level signal from 40 to 70 min postinjection, and dividing by the mean signal from the individual's reference region, the cerebellar grey matter (essentially the cerebellum without the cerebellar peduncles) [82–84]. The individual [11C]-PK11195 binding potential (BP_{ND}) maps were generated using the MRTM2 (Multilinear Reference Tissue Model 2) [85]. The reference region was determined by the algorithm SVCA4 (Supervised Cluster Analysis with 4 classes: grey matter without specific binding, white matter, blood, grey matter with specific binding) [86],

TABLE 2: Demographic features of all participants. Age and education show no significant differences between groups, but a significant difference was found in MoCA.

Variable	AD group ($n = 20$) (mean ± SD)	HC group ($n = 17$) (mean ± SD)	Excluded HC ($n = 4$) (mean ± SD)	p value[*]
Age (years)	65.294 (6.459)	66.250 (6.866)	68.5 (6.191)	0.667
Education (years)	11.412 (5.063)	9.300 (5.930)	9 (3.830)	0.239
Female/male ratio	10/10	7/10	2/2	—
MMSE	23.1 (2.97)	—	—	—
MoCA	14.35 (4.021)	24.88 (4.208)	23 (4.397)	<0.001
CDR	1	—	—	—

MMSE: Mini-Mental State Examination; MoCA: Montreal Cognitive Assessment; CDR: Clinical Dementia Rating; SD: standard deviation; [*]statistical tests performed between AD an HC groups.

TABLE 3: Mean V1 thickness (mean ± SD), V1 [11C]-PiB SUVR (mean ± SD), V1 [11C]-PK11195 BP_{ND} (mean ± SD), and retinal layers thicknesses (mean ± SD) per group. V1 [11C]-PiB uptake showed stark differences in Aβ load.

Variable	AD group ($N = 20$)	HC group ($N = 17$)	p value
V1 (mm)	1.974 (0.114)	1.957 (0.133)	0.719
V1 [11C]-PiB SUVR	1.4350 (0.290)	1.033 (0.156)	<0.0001[*]
V1 [11C]- PK11195 BP_{ND}	0.196 (0.060)	0.205 (0.058)	0.603
GCL (μm)	41.19 (3.59)	42.067 (3.99)	0.488
IPL (μm)	36.70 (3.16)	36.15 (2.80)	0.579
INL (μm)	36.82 (1.99)	36.50 (2.10)	0.646
OPL (μm)	30.42 (3.97)	28.41 (2.17)	0.104

V1: primary visual cortex; [11C]-PiB SUVR: Aβ PET radiotracer; [11C]-PK11195 BP_{ND}: neuroinflammation PET radiotracer binding potential; GCL: ganglion cell layer; IPL: inner plexiform layer; INL: inner nuclear layer; OPL: outer plexiform layer; [*]Bonferroni corrected for multiple comparisons.

which selected a group of grey matter voxels showing a time-activity curve representing the kinetic activity of normal grey matter without [11C]-PK11195 specific binding.

To extract [11C]-PiB uptake and [11C]-PK11195 BP_{ND} in V1, we resorted also to the CAT12 toolbox, following a similar procedure to that one used to measure the V1 thickness values. For each participant, we first mapped each PET volume dataset in native space to the respective individual surfaces, created during the cortical thickness measurement procedure, and then, we extracted the ROI-based values using HCP's multimodal parcellation [76] surface map, which comprises anatomically delineated V1 (Figure 1), the same used for the cortical thickness measurements. Average values of [11C]-PiB uptake and [11C]-PK1119 BP_{ND} in V1 were extracted from both hemispheres to each subject.

3. Statistical Analysis

Twenty mild-stage AD amyloid-positive patients and 17 amyloid-negative HC were considered for both retinal and cortical analyses. After the data normality was assessed using the Shapiro-Wilk test, T-test for unpaired samples or its nonparametric version and Mann-Whitney U test were used for between-group comparisons of the demographic data.

Average values of [11C]-PiB uptake, [11C]-PK11195 BP_{ND}, and thickness in V1 were estimated for each participant across both hemispheres. Concerning the retina, a mean thickness value of both eyes was calculated for each analyzed macular layer. Independent-samples t-tests were computed

for between-group comparisons of retinal layers thickness and V1-measured biomarkers, with exception of OPL thickness for which the Mann-Whitney U test was used, given the nonnormality of the data. Thereon, partial correlation analyses between the retina thickness and V1-driven measures (thickness, Aβ load and microglia activation) were computed for each group to identify possible associations between cortex AD-related biomarkers and retina integrity, controlling for age.

Data analysis was performed with IBM SPSS Statistics (version 22.0), and GraphPad Prism (version 6.0) was used for graphs and for slope analysis. The tests were performed two-tailed, and a threshold of $p < 0.05$ was used for statistical significance.

4. Results

Concerning the demographic data, no difference in age, sex, or education was found between groups, whereas results from cognitive assessment (MoCA) were significantly different between groups, as expected (Table 2). The BLAD battery confirmed that mnestic deficits were beyond cut-off in virtually all patients (95%), as compared to executive function (70%), language (40%), constructive (25%), and calculation deficits (20%).

Mean ± SD values of all variables included in the analysis are depicted in Table 3. Independent-samples t-tests did reveal significant differences between groups regarding the V1 [11C]-PiB uptake (see Figure 3). This shows that amyloid

(a)   (b)   (c)
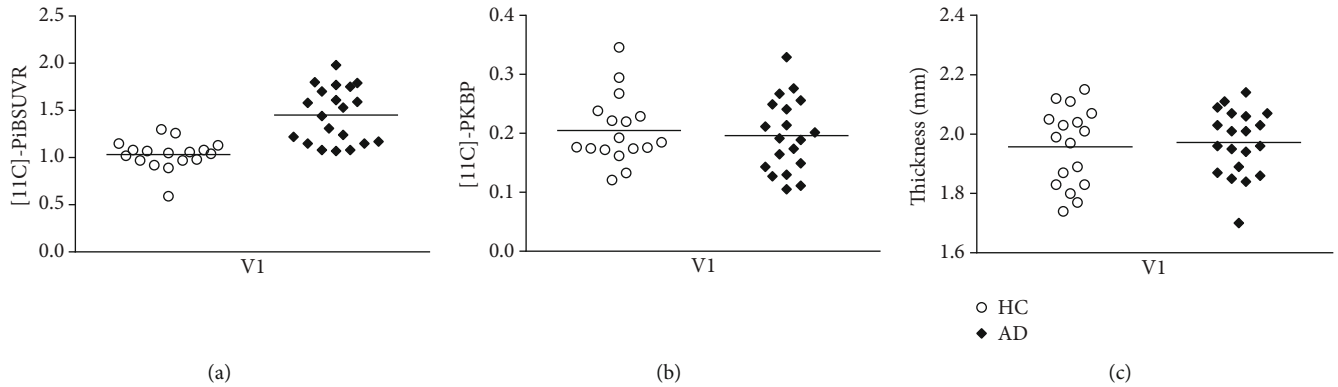
FIGURE 3: V1 measurements in 20 AD patients compared to 17 HC. (a) [11C]-PiB SUVR; (b) [11C]-PK1195 BP_{ND}; (c) V1 thickness. There is a significant difference in the mean of [11C]-PiB SUVR (a) between groups, but not in [11C]-PK1195 BP_{ND} (b) or in V1 thickness (c).

load is already affecting V1, in spite of overall preserved thickness. No evidence for significant neuroinflammation was found as assessed by [11C]-PK11195 BP_{ND}.

The evidence for significant Aβ load in the absence of significant differences in visual pathways thickness assessment is consistent with the notion that our AD patients are at an early stage.

We then asked whether partial (corrected) correlation analysis, performed to study the relationship between the retina and V1, could identify distinct patterns in patients and controls. Results showed a positive correlation between the IPL and V1 thicknesses in AD group (IPL: $r = 0.604$, $p < 0.006$, Bonferroni corrected for multiple comparisons) (Figure 4), whereas no significant associations were found with the other layers (GCL: $r = 0.130$, $p < 0.595$; INL: $r = 0.450$, $p < 0.053$; OPL: $r = -0.295$, $p < 0.221$). Considering the HC group, no significant correlation could be found between the V1 and the thickness of retinal layers. In spite of the significant structural-structural correlations, no significant structural-molecular correlations were found between the retina and V1.

Since we found evidence that V1 is already accumulating Aβ, which also target synapses early on, this positive correlation might suggest initial synaptic AD-related changes in the IPL, which is a specifically synapse-rich region in the retina accumulating amyloid both in animals [87] and humans [40]. Such association makes us suggest that this layer might serve as a biomarker for AD since the assessment of AD-related synaptic changes in the retina is faster, direct, and cost-effective way, using in vivo eye imaging techniques, than methods to assess the same mechanisms in the brain.

5. Discussion

In the present study, we were able to test whether in an early stage of the AD, the neuropathological mechanisms of the disease differently affects the integrity of retinal layers with distinct dominance of either synapses or cell bodies/nuclei between patients and healthy controls, matched for age, education, and sex. We sought for structure-structure associations (by computing partial correlations) at the level of the retina and cortex, while assessing putative biomarkers of
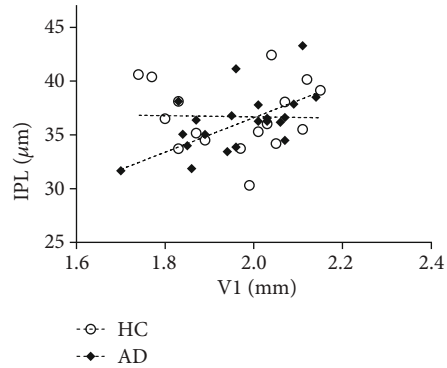
FIGURE 4: Scatterplot graph for the V1 thickness and IPL thickness to HC and AD.

the disease in V1—cortical thickness, neuroinflammation, and Aβ load.

Interestingly, AD patients presented higher levels of Aβ in V1 compared to controls, but no evidence of neuroinflammation. Together with the relatively preserved structural integrity, our results further suggest a relatively early disease stage. Importantly, a positive correlation between V1 thickness and the central IPL was specifically found in the AD group, suggesting a relationship between the eye and brain in the presence of Aβ load even when neuronal loss is not evident.

This striking association between a layer composed by synapses (IPL), closer to the cortex, and V1, suggests initial synaptic changes in the disease. This is an interesting finding considering previous animal studies referring IPL as a potential biomarker for the disease [49].

Taking into account current findings in AD research, namely, the evidence revealing that abnormal deposition of Aβ leads initially to synaptic dysfunction, evolving posteriorly to neuroinflammation and neuronal loss [46, 47], we suggested that in an early stage of the disease, V1 starts suffering from abnormal accumulation of Aβ, prior to detectable neuroinflammation or neuronal loss, which explains a structural association between this region and a macular layer rich in synapses. This pattern of early loss is consistent

with cumulative reports suggesting that primary visual cortex is one of the later regions affected by the pathophysiological mechanisms of the disease, namely, in terms of neurofibrillary tangles (NFT), neuritic plaques (NP), and lesion load [88–90].

Furthermore, since we studied two synapse layers (IPL and OPL), the fact that an association was limited to IPL could be attributed to the fact that this layer is the one close to the brain, possibly suffering at first, at least partially, effects from the retrograde V1 deterioration.

Although visual deficits are one of the earliest manifestations of AD [11], there are few studies addressing specifically V1. Nevertheless, one functional study found changes in the visual field map organization and population receptive field measurements of V1 in two AD patients. In addition, one of the subjects had no changes in V1 surface area, while the other showed a reduced surface area in the most central visual field of V1, whereas the peripheral area showed the opposite pattern, when compared to controls [81].

Regarding the retina, a wide variety of studies has been conducted to assess its microstructural changes but results are still contradictory [8, 30, 53, 58, 91–93]. In particular, a study suggested that both RNFL and GCL were reduced in the AD sample, whereas the external layers did not show significant differences [94]. Moreover, a GC-IPL shrinkage was found across all macular quadrants in an AD as well as in a mild cognitive impairment (MCI) group [95]. In turn, another study found no difference in GC-IPL thickness in AD compared to the control group [96], similarly to our results. Likewise, a recent study in an early-onset AD patient sample showed no significant differences in the thickness of none of the 7 layers segmented, including GCL, IPL, INL, and OPL in this group when comparing to controls [54].

Accordingly, and in contrast with our work, the majority of the studies have assessed patients in mild-to-moderate or moderate-to-severe stage of the disease and with no information of $A\beta$ deposition in AD and control groups. Thus, since AD is defined by progressive neurodegeneration, it would be expected a higher decay of structural integrity in the later stages, mainly in layers composed by neuron cell bodies, resulting from the neuronal loss, in contrast with synapse loss predominant in the initial stages.

Recently, some studies have investigated whether neuronal changes in the retina are associated with other forms of structural changes, such as connectivity assessed with MRI. Particularly, in a work of our group was found a significant relationship between INL and white matter integrity (axial diffusivity) of some cortical regions, including tracts associated with the visual system (optic radiation, splenium of the corpus callosum) [97], providing independent evidence for retinocortical associations. Other study searched for associations between CG-IPL and cortical integrity in three different groups. Results demonstrated that GC-IPL shrinkage was related with smaller GM volumes and WM microstructure in healthy participants in some regions, namely, in occipital cortex and cerebellum. In turn, no association was found in the MCI or AD groups [96]. A recent study from our group also found retinocortical associations in healthy aging [98].

Finally, by means of MRI visual rating scores for cortical atrophy, a correlation in both AD and control groups between total macular thickness and parietal atrophy was reported [54]. This issue was also addressed in a sample largely composed of nondemented participants with cognitive decline, where the association of peripapillary RNFL and macular GCL-IPL thickness with cerebral GM volume was examined. An association between the reduction of occipital and temporal lobes GM volumes with GC-IPL and peripapillary RNFL thickness was found. Moreover, because dendritic atrophy might take place before retinal ganglion cell loss, it was suggested that GC-IPL could be more sensitive to the neurodegenerative process [99].

Based on the notion that synapses are an initial target of the pathological mechanism of the disease [46], an animal study has tested whether the GCL dendritic integrity might provide a marker for cerebral damage in a mouse model of amyloid pathology. By evaluating animals carrying significant cognitive deficits resulting from the cortical deposition of $A\beta$ plaques, the authors verified that although GCL significant loss was absent, there was already significant GCL dendritic atrophy in Tg2576 mice compared to controls. They proposed that dendritic changes precede cell loss and are, therefore, likely to occur in patients with early AD. Furthermore, they raised the hypothesis that in case of a resembling GCL degenerative pattern occurs in the human retinas, the IPL would be a useful biomarker for the early detection of AD-related neurodegeneration [49].

This question was directly addressed in the present work. We report here a striking positive correlation between IPL—the layer comprising synaptic connections between dendrites of ganglion cells and other retinal neurons—and V1 in the AD group that was not present in the control group. Hence, our finding might suggest a possible subtle synaptic/dendritic failure of the retinal CG cells that might be associated with primary visual cortex integrity. In fact, considerable evidence suggests that before a massive neuronal cell death, there is synaptic dysfunction originated by oligomeric assemblies of the $A\beta$ protein in some cortical regions [46, 48]. Thus, in case of the mechanisms underlying the AD can be transposed to the retina, the IPL would be one of the layers more prone to suffer changes in the initial stages of the disease.

Consequently, we propose that prior to tissue loss in the retina, changes in synaptic function and dendritic morphology might occur resulting from $A\beta$ deposition, which could contribute to the earlier decline of the visual abilities involved so remarkably in the disease. Nevertheless, along with further studies better suited to directly examine the retinal synaptic function, it is still important to define the nature of the biological mechanisms underlying visual deficits in AD.

In the present study, we were able to study in detail the visual system in Alzheimer's disease by comparing V1 measurements of AD key features and by investigating differences in the retina thickness of layers with distinct dominance of synapses/neurons cell bodies.

Our results aid in the understanding of visual processing pathway changes in AD patients and might open the door to future work addressing the IPL, using more sensitive

techniques to detect synaptic changes in the early stages or prior to manifestation of AD symptoms, so that it could potentially be used as a potential biomarker for diagnosis and monitoring of the disease.

Data Availability

We will be very glad to share the data of the present manuscript upon request to the corresponding author.

Conflicts of Interest

The authors have no conflict of interest to report.

Acknowledgments

References

[1] J. Avila, N. Pallas, M. Bolós, C. L. Sayas, and F. Hernandez, "Intracellular and extracellular microtubule associated protein tau as a therapeutic target in Alzheimer disease and other tauopathies," *Expert Opinion on Therapeutic Targets*, vol. 20, no. 6, pp. 653–661, 2015.

[2] G. S. Bloom, "Amyloid-β and tau the trigger and bullet in Alzheimer disease pathogenesis," *JAMA Neurology*, vol. 71, no. 4, pp. 505–508, 2014.

[3] J. Hardy and D. Selkoe, "The amyloid hypothesis of Alzheimer's disease: progress and problems on the road to therapeutics," *Science*, vol. 297, no. 5580, pp. 353–356, 2002.

[4] L. T. Oliveira, P. R. Louzada, F. G. de Mello, and S. T. Ferreira, "Amyloid-β decreases nitric oxide production in cultured retinal neurons: a possible mechanism for synaptic dysfunction in Alzheimer's disease?," *Neurochemical Research*, vol. 36, no. 1, pp. 163–169, 2011.

[5] G. Pasqualetti, D. J. Brooks, and P. Edison, "The role of neuroinflammation in dementias," *Current Neurology and Neuroscience Reports*, vol. 15, no. 4, p. 17, 2015.

[6] D. J. Selkoe, "Cell biology of protein misfolding: the examples of Alzheimer's and Parkinson's diseases," *Nature Cell Biology*, vol. 6, no. 11, pp. 1054–1061, 2004.

[7] K. Krasodomska, W. Lubiński, A. Potemkowski, and K. Honczarenko, "Pattern electroretinogram (PERG) and pattern visual evoked potential (PVEP) in the early stages of Alzheimer's disease," *Documenta Ophthalmologica*, vol. 121, no. 2, pp. 111–121, 2010.

[8] F. Berisha, G. T. Feke, C. L. Trempe, J. W. McMeel, and C. L. Schepens, "Retinal abnormalities in early Alzheimer's disease," *Investigative Opthalmology & Visual Science*, vol. 48, no. 5, pp. 2285–2289, 2007.

[9] L. Y. L. Chang, J. Lowe, A. Ardiles et al., "Alzheimer's disease in the human eye. Clinical tests that identify ocular and visual information processing deficit as biomarkers," *Alzheimer's & Dementia*, vol. 10, no. 2, pp. 251–261, 2014.

[10] F. Z. Javaid, J. Brenton, L. Guo, and M. F. Cordeiro, "Visual and ocular manifestations of Alzheimer's disease and their use as biomarkers for diagnosis and progression," *Frontiers in Neurology*, vol. 7, 2016.

[11] B. Katz and S. Rimmer, "Ophthalmologic manifestations of Alzheimer's disease," *Survey of Ophthalmology*, vol. 34, no. 1, pp. 31–43, 1989.

[12] A. A. Sadun and C. J. Bassi, "Optic nerve damage in Alzheimer's disease," *Ophthalmology*, vol. 97, no. 1, pp. 9–17, 1990.

[13] A. Cronin-Golomb, R. Sugiura, S. Corkin, and J. H. Growdon, "Incomplete achromatopsia in Alzheimer's disease," *Neurobiology of Aging*, vol. 14, no. 5, pp. 471–477, 1993.

[14] G. C. Gilmore, K. E. Groth, and C. W. Thomas, "Stimulus contrast and word reading speed in Alzheimer's disease," *Experimental Aging Research*, vol. 31, no. 1, pp. 15–33, 2005.

[15] S. Park, T. F. Brady, M. R. Greene, and A. Oliva, "Disentangling scene content from spatial boundary: complementary roles for the parahippocampal place area and lateral occipital complex in representing real-world scenes," *The Journal of Neuroscience*, vol. 31, no. 4, pp. 1333–1340, 2011.

[16] S. L. Risacher, D. Wudunn, S. M. Pepin et al., "Visual contrast sensitivity in Alzheimer's disease, mild cognitive impairment, and older adults with cognitive complaints," *Neurobiology of Aging*, vol. 34, no. 4, pp. 1133–1144, 2013.

[17] G. Salamone, C. Di Lorenzo, S. Mosti et al., "Color discrimination performance in patients with Alzheimer's disease," *Dementia and Geriatric Cognitive Disorders*, vol. 27, no. 6, pp. 501–507, 2009.

[18] G. L. Trick, L. R. Trick, P. Morris, and M. Wolf, "Visual field loss in senile dementia of the Alzheimer's type," *Neurology*, vol. 45, no. 1, pp. 68–74, 1995.

[19] D. A. Valenti, "Alzheimer's disease: screening biomarkers using frequency doubling technology visual field," *ISRN Neurology*, vol. 2013, Article ID 989583, 9 pages, 2013.

[20] G. C. Gilmore, H. E. Wenk, L. A. Naylor, and E. Koss, "Motion perception and Alzheimer's disease," *Journal of Gerontology*, vol. 49, no. 2, pp. P52–P57, 1994.

[21] B. Graewe, R. Lemos, C. Ferreira et al., "Impaired processing of 3D motion-defined faces in mild cognitive impairment and healthy aging: an fMRI study," *Cerebral Cortex*, vol. 23, no. 10, pp. 2489–2499, 2013.

[22] V. Kavcic, W. Vaughn, and C. J. Duffy, "Distinct visual motion processing impairments in aging and Alzheimer's disease," *Vision Research*, vol. 51, no. 3, pp. 386–395, 2011.

[23] R. Lemos, P. Figueiredo, I. Santana, M. R. Simões, and M. Castelo-Branco, "Temporal integration of 3D coherent motion cues defining visual objects of unknown orientation is impaired in amnestic mild cognitive impairment and Alzheimer's disease," *Journal of Alzheimer's Disease*, vol. 28, no. 4, pp. 885–896, 2012.

[24] R. A. Armstrong, "Visual field defects in Alzheimer's disease patients may reflect differential pathology in the primary visual cortex," *Optometry and Vision Science*, vol. 73, no. 11, pp. 677–682, 1996.

[25] D. G. Cogan, "Visual disturbances with focal progressive dementing disease," *American Journal of Ophthalmology*, vol. 100, no. 1, pp. 68–72, 1985.

[26] G. Leuba and R. Kraftsik, "Visual cortex in Alzheimer's disease: occurence of neuronal death and glial proliferation,

and correlation with pathological hallmarks," *Neurobiology of Aging*, vol. 15, no. 1, pp. 29–43, 1994.

[27] J. H. Morrison, P. R. Hof, and C. Bouras, "An anatomic substrate for visual disconnection in Alzheimer's disease," *Annals of the New York Academy of Sciences*, vol. 640, no. 1, pp. 36–43, 1991.

[28] K. U. Löffler, D. P. Edward, and M. O. Tso, "Immunoreactivity against tau, amyloid precursor protein, and beta-amyloid in the human retina," *Investigative Ophthalmology & Visual Science*, vol. 36, no. 1, pp. 24–31, 1995.

[29] V. Parisi, "Correlation between morphological and functional retinal impairment in patients affected by ocular hypertension, glaucoma, demyelinating optic neuritis and Alzheimer's disease," *Seminars in Ophthalmology*, vol. 18, no. 2, pp. 50–57, 2003.

[30] V. Parisi, R. Restuccia, F. Fattapposta, C. Mina, M. G. Bucci, and F. Pierelli, "Morphological and functional retinal impairment in Alzheimer's disease patients," *Clinical Neurophysiology*, vol. 112, no. 10, pp. 1860–1867, 2001.

[31] P. K. Iseri, Ö. Altinaş, T. Tokay, and N. Yüksel, "Relationship between cognitive impairment and retinal morphological and visual functional abnormalities in Alzheimer disease," *Journal of Neuro-Ophthalmology*, vol. 26, no. 1, pp. 18–24, 2006.

[32] M. S. Byerly and S. Blackshaw, "Vertebrate retina and hypothalamus development," *Wiley Interdisciplinary Reviews. Systems Biology and Medicine*, vol. 1, no. 3, pp. 380–389, 2009.

[33] R. L. Chow and R. A. Lang, "Early eye development in vertebrates," *Annual Review of Cell and Developmental Biology*, vol. 17, no. 1, pp. 255–296, 2001.

[34] R. J. Maude, A. M. Dondorp, A. A. Sayeed, N. P. J. Day, N. J. White, and N. A. V. Beare, "The eye in cerebral malaria: what can it teach us?," *Transactions of the Royal Society of Tropical Medicine and Hygiene*, vol. 103, no. 7, pp. 661–664, 2009.

[35] A. Trost, S. Lange, F. Schroedl et al., "Brain and retinal pericytes: origin, function and role," *Frontiers in Cellular Neuroscience*, vol. 10, 2016.

[36] N. K. Archibald, M. P. Clarke, U. P. Mosimann, and D. J. Burn, "The retina in Parkinson's disease," *Brain*, vol. 132, no. 5, pp. 1128–1145, 2009.

[37] P. A. Calabresi, L. J. Balcer, and E. M. Frohman, "Retinal pathology in multiple sclerosis: insight into the mechanisms of neuronal pathology," *Brain*, vol. 133, no. 6, pp. 1575–1577, 2010.

[38] A. London, I. Benhar, and M. Schwartz, "The retina as a window to the brain —from eye research to CNS disorders," *Nature Reviews Neurology*, vol. 9, no. 1, pp. 44–53, 2013.

[39] L. E. Goldstein, J. A. Muffat, R. A. Cherny et al., "Cytosolic β-amyloid deposition and supranuclear cataracts in lenses from people with Alzheimer's disease," *Lancet*, vol. 361, no. 9365, pp. 1258–1265, 2003.

[40] M. Koronyo-Hamaoui, Y. Koronyo, A. V. Ljubimov et al., "Identification of amyloid plaques in retinas from Alzheimer's patients and noninvasive in vivo optical imaging of retinal plaques in a mouse model," *NeuroImage*, vol. 54, pp. S204–S217, 2011.

[41] C. La Morgia, F. N. Ross-Cisneros, Y. Koronyo et al., "Melanopsin retinal ganglion cell loss in Alzheimer disease," *Annals of Neurology*, vol. 79, no. 1, pp. 90–109, 2016.

[42] C. Schön, N. A. Hoffmann, S. M. Ochs et al., "Long-term in vivo imaging of fibrillar tau in the retina of P301S transgenic mice," *PLoS One*, vol. 7, no. 12, article e53547, 2012.

[43] J. M. Sivak, "The aging eye: common degenerative mechanisms between the Alzheimer's brain and retinal disease," *Investigative Ophthalmology & Visual Science*, vol. 54, no. 1, pp. 871–880, 2013.

[44] M. Hoon, H. Okawa, L. Della Santina, and R. O. L. Wong, "Functional architecture of the retina: development and disease," *Progress in Retinal and Eye Research*, vol. 42, pp. 44–84, 2014.

[45] T. C. Nag and S. Wadhwa, "Ultrastructure of the human retina in aging and various pathological states," *Micron*, vol. 43, no. 7, pp. 759–781, 2012.

[46] D. J. Selkoe, "Alzheimer's disease is a synaptic failure," *Science*, vol. 298, no. 5594, pp. 789–791, 2002.

[47] C. Bastin, M. A. Bahri, F. Meyer et al., "In vivo imaging of synaptic loss in Alzheimer's disease with [18F]UCB-H positron emission tomography," *European Journal of Nuclear Medicine and Molecular Imaging*, vol. 47, no. 2, pp. 390–402, 2020.

[48] D. H. Small, S. S. Mok, and J. C. Bornstein, "Alzheimer's disease and Aβ toxicity: from top to bottom," *Nature Reviews. Neuroscience*, vol. 2, no. 8, pp. 595–598, 2001.

[49] P. A. Williams, R. A. Thirgood, H. Oliphant et al., "Retinal ganglion cell dendritic degeneration in a mouse model of Alzheimer's disease," *Neurobiology of Aging*, vol. 34, no. 7, pp. 1799–1806, 2013.

[50] M. Liu, J. Duggan, T. E. Salt, and M. F. Cordeiro, "Dendritic changes in visual pathways in glaucoma and other neurodegenerative conditions," *Experimental Eye Research*, vol. 92, no. 4, pp. 244–250, 2011.

[51] F. J. Ascaso, N. Cruz, P. J. Modrego et al., "Retinal alterations in mild cognitive impairment and Alzheimer's disease: an optical coherence tomography study," *Journal of Neurology*, vol. 261, no. 8, pp. 1522–1530, 2014.

[52] G. Coppola, A. Di Renzo, L. Ziccardi et al., "Optical coherence tomography in Alzheimer's disease: a meta-analysis," *PLoS One*, vol. 10, no. 8, article e0134750, 2015.

[53] L. Gao, Y. Liu, X. Li, Q. Bai, and P. Liu, "Abnormal retinal nerve fiber layer thickness and macula lutea in patients with mild cognitive impairment and Alzheimer's disease," *Archives of Gerontology and Geriatrics*, vol. 60, no. 1, pp. 162–167, 2015.

[54] J. Haan, S. F. Janssen, J. A. Kreeke, P. Scheltens, F. D. Verbraak, and F. H. Bouwman, "Retinal thickness correlates with parietal cortical atrophy in early-onset Alzheimer's disease and controls," *Alzheimer's & Dementia: Diagnosis, Assessment & Disease Monitoring*, vol. 10, no. 1, pp. 49–55, 2018.

[55] S. Jentsch, D. Schweitzer, K.-U. Schmidtke et al., "Retinal fluorescence lifetime imaging ophthalmoscopy measures depend on the severity of Alzheimer's disease," *Acta Ophthalmologica*, vol. 93, no. 4, pp. e241–e247, 2015.

[56] H. Kergoat, M. J. Kergoat, L. Justino, H. Chertkow, A. Robillard, and H. Bergman, "An evaluation of the retinal nerve fiber layer thickness by scanning laser polarimetry in individuals with dementia of the Alzheimer type," *Acta Ophthalmologica Scandinavica*, vol. 79, no. 2, pp. 187–191, 2001.

[57] S. A. Kurna, G. Akar, A. Altun, Y. Agirman, E. Gozke, and T. Sengor, "Confocal scanning laser tomography of the optic nerve head on the patients with Alzheimer's disease compared to glaucoma and control," *International Ophthalmology*, vol. 34, no. 6, pp. 1203–1211, 2014.

[58] Y. Lu, Z. Li, X. Zhang et al., "Retinal nerve fiber layer structure abnormalities in early Alzheimer's disease: evidence in optical

coherence tomography," *Neuroscience Letters*, vol. 480, no. 1, pp. 69–72, 2010.

[59] American Psychiatric Association, *Diagnostic and Statistical Manual of Mental Disorders (DSM-IV-TR)*, American Psychiatric Association Publishing, Washington, DC, 4th edition, 2000.

[60] G. M. McKhann, D. S. Knopman, H. Chertkow et al., "The diagnosis of dementia due to Alzheimer's disease: recommendations from the National Institute on Aging-Alzheimer's Association workgroups on diagnostic guidelines for Alzheimer's disease," *Alzheimer's & Dementia*, vol. 7, no. 3, pp. 263–269, 2011.

[61] M. F. Folstein, S. E. Folstein, and P. R. McHugh, ""Mini-mental state". A practical method for grading the cognitive state of patients for the clinician," *Journal of Psychiatric Research*, vol. 12, no. 3, pp. 189–198, 1975.

[62] S. Freitas, M. R. Simões, L. Alves, and I. Santana, "The relevance of sociodemographic and health variables on MMSE normative data," *Applied Neuropsychology*, vol. 22, no. 4, pp. 311–319, 2014.

[63] S. Freitas, M. R. Simões, L. Alves, and I. Santana, "Montreal cognitive assessment: validation study for mild cognitive impairment and Alzheimer disease," *Alzheimer Disease and Associated Disorders*, vol. 27, no. 1, pp. 37–43, 2013.

[64] Z. S. Nasreddine, N. A. Phillips, V. Ã.©. BÃ©dirian et al., "The Montreal Cognitive Assessment, MoCA: a brief screening tool for mild cognitive impairment," *Journal of the American Geriatrics Society*, vol. 53, no. 4, pp. 695–699, 2005.

[65] M. Guerreiro, *Contributo da neuropsicologia para o estudo das demências [Contribution of Neuropsychology to the Study of Dementia]*, University of Lisbon, 1998.

[66] S. Ginó, T. Mendes, F. Ribeiro, A. Mendonça, M. Guerreiro, and C. Garcia, "Escala de Queixas de Memória [Subjective memory complaints]," in *Grupo de Estudos de Envelhecimento Cerebral e Demências [Study Group on Brain Aging and Dementia]. Escalas e Testes Na Demência [Scales and Tests in Dementia]*, C. Mendonça, C. Garcia, and M. Guerreiro, Eds., pp. 116–120, GEECD, Lisbon, 2008.

[67] B. Schmand, C. Jonker, C. Hooijer, and J. Lindeboom, "Subjective memory complaints may announce dementia," *Neurology*, vol. 46, no. 1, pp. 121–125, 1996.

[68] M. P. Lawton and E. M. Brody, "Assessment of older people: self-maintaining and instrumental activities of daily living," *The Gerontologist*, vol. 9, 3 Part 1, pp. 179–186, 1969.

[69] S. Madureira and A. Verdelho, "Escala de Actividades Instrumentais de Vida Diária [Instrumental activities of daily living]," in *Grupo de Estudos de Envelhecimento Cerebral e Demências [Study Group on Brain Aging and Dementia]. Escalas e Testes Na Demência [Scales and Tests in Dementia]*, C. Mendonça, C. Garcia, and M. Guerreiro, Eds., pp. 121–124, GEECD, Lisbon, 2008.

[70] J. Barreto, A. Leuschner, F. Santos, and M. Sobral, "Escala de Depressão Geriátrica [Geriatric depressive scale]," in *Grupo de Estudos de Envelhecimento Cerebral e Demências [Study Group on Brain Aging and Dementia]. Escalas e Testes Na Demência [Scales and Tests in Dementia]*, C. Mendonça, C. Garcia, and M. Guerreiro, Eds., pp. 69–72, GEECD, Lisbon, 2008.

[71] J. A. Yesavage, T. L. Brink, T. L. Rose et al., "Development and validation of a geriatric depression screening scale: a preliminary report," *Journal of Psychiatric Research*, vol. 17, pp. 37–49, 1983.

[72] J. Ashburner and K. J. Friston, "Unified segmentation," *Neuro-Image*, vol. 26, no. 3, pp. 839–851, 2005.

[73] J. Ashburner, "A fast diffeomorphic image registration algorithm," *NeuroImage*, vol. 38, no. 1, pp. 95–113, 2007.

[74] R. Dahnke, R. A. Yotter, and C. Gaser, "Cortical thickness and central surface estimation," *NeuroImage*, vol. 65, pp. 336–348, 2013.

[75] C. Gaser and R. Dahnke, *CAT-A Computational Anatomy Toolbox for the Analysis of Structural MRI Data*, Organization for Human Brain Mapping, 2016.

[76] M. F. Glasser, T. S. Coalson, E. C. Robinson et al., "A multimodal parcellation of human cerebral cortex," *Nature*, vol. 536, no. 7615, pp. 171–178, 2016.

[77] M. D. Abràmoff, M. K. Garvin, and M. Sonka, "Retinal imaging and image analysis," *IEEE Reviews in Biomedical Engineering*, vol. 3, pp. 169–208, 2010.

[78] M. K. Garvin, M. D. Abramoff, Xiaodong Wu, S. R. Russell, T. L. Burns, and M. Sonka, "Automated 3-D intraretinal layer segmentation of macular spectral-domain optical coherence tomography images," *IEEE Transactions on Medical Imaging*, vol. 28, no. 9, pp. 1436–1447, 2009.

[79] K. Li, X. Wu, D. Z. Chen, and M. Sonka, "Optimal surface segmentation in volumetric images—a graph-theoretic approach," *IEEE Transactions on Pattern Analysis and Machine Intelligence*, vol. 28, no. 1, pp. 119–134, 2006.

[80] J. C. Blanks, Y. Torigoe, D. R. Hinton, and R. H. I. Blanks, "Retinal pathology in Alzheimer's disease. I. Ganglion cell loss in foveal/parafoveal retina," *Neurobiology of Aging*, vol. 17, no. 3, pp. 377–384, 1996.

[81] A. A. Brewer and B. Barton, "Visual cortex in aging and Alzheimer's disease: changes in visual field maps and population receptive fields," *Frontiers in Psychology*, vol. 5, p. 74, 2014.

[82] J. F. J. Bonilla and J. M. C. Carril, "Molecular neuroimaging in degenerative dementias," *Revista Española de Medicina Nuclear e Imagen Molecular (English Edition)*, vol. 32, no. 5, pp. 301–309, 2013.

[83] R. L. McNamee, S.-H. Yee, J. C. Price et al., "Consideration of optimal time window for Pittsburgh compound B PET summed uptake measurements," *Journal of Nuclear Medicine*, vol. 50, no. 3, pp. 348–355, 2009.

[84] F. Oliveira, A. Leuzy, J. Castelhano et al., "Data driven diagnostic classification in Alzheimer's disease based on different reference regions for normalization of PiB-PET images and correlation with CSF concentrations of Aβ species," *Neuro-Image: Clinical*, vol. 20, pp. 603–610, 2018.

[85] M. Ichise, J.-S. Liow, J.-Q. Lu et al., "Linearized reference tissue parametric imaging methods: application to [11C] DASB positron emission tomography studies of the serotonin transporter in human brain," *Journal of Cerebral Blood Flow and Metabolism*, vol. 23, no. 9, pp. 1096–1112, 2016.

[86] M. Yaqub, B. N. van Berckel, A. Schuitemaker et al., "Optimization of supervised cluster analysis for extracting reference tissue input curves in (R)-[11C]PK11195 brain PET studies," *Journal of Cerebral Blood Flow and Metabolism*, vol. 32, no. 8, pp. 1600–1608, 2012.

[87] S. E. Perez, S. Lumayag, B. Kovacs, E. J. Mufson, and S. Xu, "β-amyloid deposition and functional impairment in the retina of the APPswe/PS1DeltaE9 transgenic mouse model of Alzheimer's disease," *Investigative Ophthalmology and Visual Science*, vol. 50, no. 2, pp. 793–800, 2009.

[88] P. Giannakopoulos, G. Gold, M. Duc, J. P. Michel, P. R. Hof, and C. Bouras, "Neuroanatomic correlates of visual agnosia in Alzheimer's disease: a clinicopathologic study," *Neurology*, vol. 52, no. 1, pp. 71–77, 1999.

[89] G. R. Jackson and C. Owsley, "Visual dysfunction, neurodegenerative diseases, and aging," *Neurologic Clinics*, vol. 21, no. 3, pp. 709–728, 2003.

[90] D. A. Lewis, M. J. Campbell, R. D. Terry, and J. H. Morrison, "Laminar and regional distributions of neurofibrillary tangles and neuritic plaques in Alzheimer's disease: a quantitative study of visual and auditory cortices," *The Journal of Neuroscience*, vol. 7, no. 6, pp. 1799–1808, 1987.

[91] A. Kesler, V. Vakhapova, A. D. Korczyn, E. Naftaliev, and M. Neudorfer, "Retinal thickness in patients with mild cognitive impairment and Alzheimer's disease," *Clinical Neurology and Neurosurgery*, vol. 113, no. 7, pp. 523–526, 2011.

[92] T. Moreno-Ramos, J. Benito-León, A. Villarejo, and F. Bermejo-Pareja, "Retinal nerve fiber layer thinning in dementia associated with Parkinson's disease, dementia with Lewy bodies, and Alzheimer's disease," *Journal of Alzheimer's Disease*, vol. 34, no. 3, pp. 659–664, 2013.

[93] C. Paquet, M. Boissonnot, F. Roger, P. Dighiero, R. Gil, and J. Hugon, "Abnormal retinal thickness in patients with mild cognitive impairment and Alzheimer's disease," *Neuroscience Letters*, vol. 420, no. 2, pp. 97–99, 2007.

[94] E. Marziani, S. Pomati, P. Ramolfo et al., "Evaluation of retinal nerve fiber layer and ganglion cell layer thickness in Alzheimer's disease using spectral-domain optical coherence tomography," *Investigative Ophthalmology & Visual Science*, vol. 54, no. 9, article 5953, 2013.

[95] C. Y. Cheung, Y. T. Ong, S. Hilal et al., "Retinal ganglion cell analysis using high-definition optical coherence tomography in patients with mild cognitive impairment and Alzheimer's disease," *Journal of Alzheimer's Disease*, vol. 45, no. 1, pp. 45–56, 2015.

[96] S. Liu, Y. T. Ong, S. Hilal et al., "The association between retinal neuronal layer and brain structure is disrupted in patients with cognitive impairment and Alzheimer's disease," *Journal of Alzheimer's Disease*, vol. 54, no. 2, pp. 585–595, 2016.

[97] C. Alves, L. Jorge, N. Canário et al., "Interplay between macular retinal changes and white matter integrity in early Alzheimer's disease," *Journal of Alzheimer's Disease*, vol. 70, no. 3, pp. 723–732, 2019.

[98] L. Jorge, N. Canário, H. Quental, R. Bernardes, and M. Castelo-Branco, "Is the retina a mirror of the aging brain? Aging of neural retina layers and primary visual cortex across the lifespan," *Frontiers in Aging Neuroscience*, vol. 11, p. 360, 2020.

[99] Y.-T. Ong, S. Hilal, C. Y. Cheung et al., "Retinal neurodegeneration on optical coherence tomography and cerebral atrophy," *Neuroscience Letters*, vol. 584, pp. 12–16, 2015.

Review Article

Circuitry and Synaptic Dysfunction in Alzheimer's Disease: A New Tau Hypothesis

Siddhartha Mondragón-Rodríguez [iD], [1,2] **Humberto Salgado-Burgos,** [3] **and Fernando Peña-Ortega** [2]

[1] *CONACYT National Council for Science and Technology, México, Mexico*
[2] *UNAM Developmental Neurobiology and Neurophysiology, Institute of Neurobiology, National Autonomous University of México, Querétaro, Mexico*
[3] *UADY Neurosciences Department, Autonomous University of Yucatán, 97000 Mérida, Yucatán, Mexico*

Correspondence should be addressed to Siddhartha Mondragón-Rodríguez; sidmonrod@gmail.com

For more than five decades, the field of Alzheimer's disease (AD) has focused on two main hypotheses positing amyloid-beta (Aβ) and Tau phosphorylation (pTau) as key pathogenic mediators. In line with these canonical hypotheses, several groups around the world have shown that the synaptotoxicity in AD depends mainly on the increase in pTau levels. Confronting this leading hypothesis, a few years ago, we reported that the increase in phosphorylation levels of dendritic Tau, at its microtubule domain (MD), acts as a neuroprotective mechanism that prevents N-methyl-D-aspartate receptor (NMDAr) overexcitation, which allowed us to propose that Tau protein phosphorylated near MD sites is involved in neuroprotection, rather than in neurodegeneration. Further supporting this alternative role of pTau, we have recently shown that early increases in pTau close to MD sites prevent hippocampal circuit overexcitation in a transgenic AD mouse model. Here, we will synthesize this new evidence that confronts the leading Tau-based AD hypothesis and discuss the role of pTau modulating neural circuits and network connectivity. Additionally, we will briefly address the role of brain circuit alterations as a potential biomarker for detecting the prodromal AD stage.

1. Introduction

Alzheimer's disease (AD) is a public health problem for our aging societies and is histopathologically defined by extracellular amyloid-beta (Aβ) deposits and intracellular hyperphosphorylated Tau (pTau) deposits [1–7]. Although many areas of the brain are affected during AD development, the hippocampus, a circuit related to spatial orientation and cognitive functions, is a major focus of AD research attention [1, 2, 5–7]. Current AD hypotheses postulate that (a) due to Aβ increase, Tau becomes abnormally phosphorylated, and (b) pTau dissociates from microtubules and (c) aggregates into neurofibrillary tangles (NFTs) [3], causing neuronal dysfunction and, eventually, cell death [4]. In support of its pathological role, pTau has been directly linked to several neurodegenerative disorders (tauopathies), such as AD,

frontotemporal dementia, Parkinson's disease, Down syndrome, and Pick's disease [5–7].

As mentioned, abnormally phosphorylated Tau is a key mediator of Aβ-induced dendrite dysregulation and synaptic dysfunction [8, 9]. In this regard, a study performed with AD patients who had relatively low levels of Aβ and high levels of Tau showed dysfunction in synaptic plasticity and a faster cognitive decline [10]. Thus, considering that pTau aggregates correlate better with cognitive impairment in AD than Aβ aggregates [11], pTau has emerged as the new therapeutic target against AD and related neurodegenerative disorders [12]. Intensive research focusing on the pathological role of pTau has strongly nurtured the use of pTau as a therapeutic target [12, 13]. These therapeutic approaches have been restricted to a reduction of Tau levels and lowering activity of kinases that phosphorylate Tau [12, 13]. However, as for

the numerous AD therapies that have aimed towards Aβ, we predict that the Tau-based strategy will render mild outcomes. To justify this hypothesis, it is critically important to discuss not only the pathological but also the physiological functions of pTau [13, 14], namely, its recently described synaptic functions [13–15]. By doing so, we will confront and update the current Tau-based AD hypotheses. Additionally, this review will highlight the novel pTau function of regulating neural activity and preventing Aβ-induced synaptic overexcitation [13, 14, 16]. This review also appraises the available evidence on neural network dysfunction in preclinical and confirmed AD, identifies research gaps on current AD hypotheses, and points towards new research directions to understand and treat this disease.

2. Tau Phosphorylation and Synaptic Plasticity

Tau is a microtubule-associated protein that promotes microtubule stability and function [17]. Tau is encoded by the microtubule-associated Tau gene, which comprises 16 exons on chromosome 17q21 [17]. Tau has more than 45 phosphorylation sites located in its proline-rich domain (Figure 1, residues 172-251) and C-terminal domain (Figure 1, residues 368-441) [2, 5, 6, 13–15]. Additionally, Tau has a microtubule domain (MD) segment that functions as a protein-protein binding domain (Figure 1, microtubule binding), therefore promoting microtubule stabilization and regulating the structure and proper function of neurons [17]. It is well documented that Tau protein is principally located in the soma and axons of neurons [3, 17]. However, recent evidence showed that Tau is also a dendritic protein [13–15]. Specifically, it was confirmed that endogenous Tau localizes at the postsynapses in neurons under physiological conditions [14]. This raised an important question: what is the role of Tau protein at the postsynapsis? According to recent data, it appears that dendritic Tau modulates plastic mechanisms involved in memory storage [8, 9, 14–16]. At the physiological and molecular levels, long-lasting synaptic plasticity changes are considered the cellular correlates of memory storage [18–22]. Among those synaptic plasticity phenomena related to memory, synaptic strength can be long-lasting enhanced (long-term potentiation (LTP)) or long-lasting depressed (long-term depression (LTD)), and these changes can persist from hours to days [18–22]. The cellular mechanisms underlying LTD, depicted in Figure 2, are triggered by N-methyl-D-aspartate receptor (NMDAr) activation at the synapse [18–22]. Broadly, this process involves the following steps: (1) calmodulin (CaM) binds Ca^{2+}, increased via NMDAr, which leads to CaM/Ca^{2+}-dependent protein phosphatase 2B (PP2B) activation [21], which in turn leads to protein phosphatase 1 (PP1) activation through the dephosphorylation of its inhibitor-1 [21]. Then, (2) activated PP1 dephosphorylates key targets required for LTD, such as Ser845 at the AMPAr subunit GluA1 [21, 22], Ser295 at the postsynaptic density protein 95 (PSD95), and activates glycogen synthase kinase-3β (GSK3β) [23, 24] (Figure 2). (3) Activated GSK3β phosphorylates Tau protein at flanking MD [25] (Figures 1 and 2), (4) leading to the dissociation of Tau/Fyn (a member of the Src-tyrosine kinase family)/PSD95 complex [13, 14]. Interestingly, we have observed that changes in the Tau phosphorylation levels, in sites near the Tau's MD, modulate its interaction with PSD95 and Fyn kinase [13, 14] (Figures 1 and 2). Specifically, we found that increasing pTau at sites such as Ser396, Ser404, Thr205, Thr231, and Ser235 (Figure 1 and 2) promoted dissociation of the Tau/Fyn/PSD95 complex, which is a determinant for LTD induction [13, 14]. In the same regard, it was reported that Tau phosphorylated at Ser396, followed by activation of NMDAr, is necessary for the expression of hippocampal LTD (i.e., pTau shifts synaptic plasticity from LTP to LTD) [15]. Altogether, we proposed that phosphorylation of Tau's MD is a crucial part of a regulatory mechanism that controls NMDAr activity [13, 14]. In other words, non-phosphorylated Tau contributes to LTP, while pTau contributes to LTD [9, 13–16]. Additionally, (5) dissociation of the Tau/Fyn/PSD95 complex promotes the loss of its interactions with GluA2 and with N-ethylmaleimide-sensitive factor (NSF) that cause clathrin-mediated endocytosis of receptors during NMDAr-LTD [18, 22, 26]. (6) In opposition, phosphoinositide 3-kinase (PI3K), in an AKT-dependent pathway, can modulate GSK3β activity [27], allowing PP1 and PP2B to dephosphorylate Tau protein at the following sites: Ser199, Ser202, Thr205, Thr212, Ser214, Ser235, Ser262, Ser396, Ser404, and Ser409 [28]. (7) Dephosphorylated Tau recruits Fyn to target the PSD-95/NMDAr complex, leading to LTP induction [13, 14, 22, 29] (Figure 2).

Summarizing, we proposed that phosphorylation of Tau's MD is a crucial part of a physiological regulatory mechanism that controls NMDAr activity and synaptic coupling [13, 14, 29].

3. Amyloid-Beta as an Effector of Phosphorylated Tau

The proteolysis of amyloid precursor protein (APP) into aggregation-prone Aβ peptides (mainly of 40 or 42 amino acids) has long been implicated in the etiopathogenesis of AD [1, 8–14, 30–36]. In the vast body of evidences that supports the synaptotoxic role of Aβ42 oligomers and its consequences, there are key observations: Aβ42 oligomers extracted from the late-onset AD brains (1) inhibit LTP [30], (2) enhance LTD [13, 14, 29, 31], (3) impair memory [30], (4) decrease synapse density [32], (5) reduce the number of NMDAr on the cell surface at synapses [33], and (6) interfere with the reuptake of extracellular glutamate [34]. Additionally, (7) Aβ42 oligomers induce Tau hyperphosphorylation at AD-relevant sites (near Tau's MD) [14, 35] that (8) cause excitotoxicity and neuritic dystrophy [35, 36]. In our hands, the application of monomeric Aβ42 to rat slice cultures leads to the formation of Aβ42 oligomers over the incubation time of 5 days [14], which correlates with increased pTau at Ser396, Ser404, Thr231, and Ser235 sites [14]. Our data showed that Aβ42 oligomers initially induce the phosphorylation of a few specific sites on Tau, rather than increase global Tau phosphorylation at all sites, as seen in advanced AD [37]. Importantly, the early phosphorylated sites are close to the Tau's MD (Figure 1). This is consistent with other reports where phosphorylation of Tau protein at
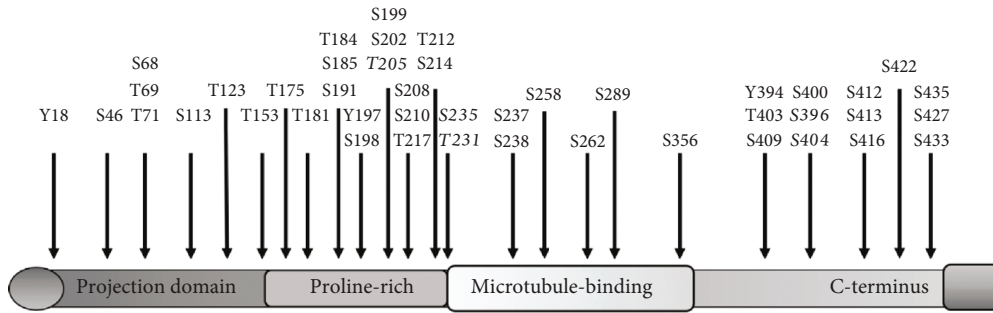
FIGURE 1: Tau sequence can be subdivided into two active domains that are phosphorylated throughout. Tau protein contains an assembly domain (carboxy-terminus section that contains the microtubule-binding and flanking regions; right). It also contains a middle region (comprising the proline-rich domain that contains multiple Thr-Pro of Ser-Pro motifs). Finally, Tau contains the amino-terminal section (left).
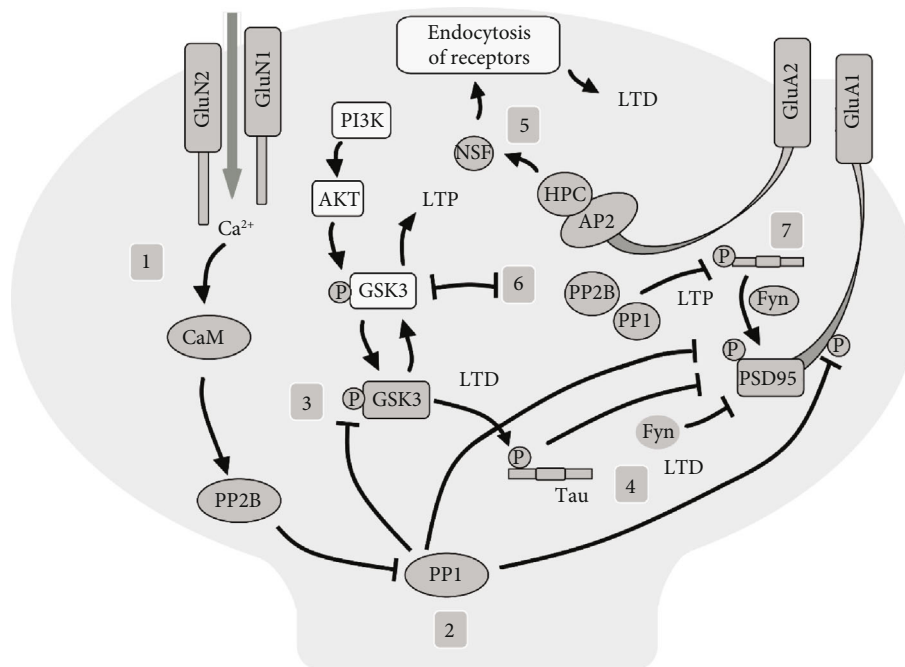

FIGURE 2: Tau phosphorylation and its involvement in long-term depression (LTD). (1) Calmodulin (CaM) detects a Ca^{2+} increment due to NMDAr activation, leading to protein phosphatase-2B (PP2B) activation and the subsequent activation of the PP1. (2) PP1 dephosphorylates Ser845 at the AMPAr subunit GluA1, Ser295 at PSD95, and GSK3β. (3) Active GSK3β leads to pTau near MD (microtubule domain). (4) pTau induced LTD by the dissociation of Tau/Fyn/PSD95 complex. (5) Dissociation of Tau/Fyn/PSD95 leads to disruption of interaction between GluA2 and with N-ethylmaleimide-sensitive factor (NSF) that cause clathrin-mediated endocytosis of receptors during NMDAr-LTD. (6) Inactive GSK3β (through the PI3K/AKT pathway) and dephosphorylated Tau (that recruits Fyn kinase to target the PSD95/NMDAr complex) promote long-term potentiation (LTP) (arrow = activation, flat line = inhibition).

Ser396/Ser404 sites was found as one of the earliest phosphorylation events during AD and related tauopathies [2, 5–7]. Further supporting the above findings, significant increases of Tau protein at the Thr231 site was reported in human patients during the early stages of AD development [38]. Indeed, it was reported that abnormal Tau processing is characterized by a sequential phosphorylation as follows: (1) Thr231, (2) Ser 202/Thr205, and (3) Thr212/Ser214 [38]. Of relevance, it is well established that Tau phosphorylation promotes the formation of tangle-like filament morphology [39, 40] and proaggregant Tau actively contributes to impaired memory and loss of LTP [8, 9, 41]. These results

explain the weakening of synapses that morphologically would result in a loss of dendritic spines and functionally in a loss of memory [41–43]. Thus, indicating that the ability of Tau to aggregate is a crucial factor in disease development [2–6, 39–44]. However, a recent study showed that intracerebroventricular injection of Tau soluble aggregates, but not monomers or fibrils, increased the threshold for LTD induction in a prion protein-dependent manner [45]. Interestingly, Tau soluble aggregates blocked Aβ-induced LTD facilitation, whereas a subthreshold dose of Tau soluble aggregates promotes Aβ-induced LTP inhibition [45]. The data suggest that Tau soluble aggregates reduce the dynamic

range of synaptic plasticity and that the prion protein acts as a common mediator of the synaptotoxicity induced by soluble Aβ and Tau [45].

Further supporting the mechanistic link between Aβ and Tau, injection of synthetic Aβ into the brain of transgenic mice that accumulate NFTs, owing to the overexpression of human Tau with a P301L mutation, induced a five-fold increase in the number of NFTs in regions near the injection sites [44]. Although the molecular mechanism functionally linking Aβ42 to Tau, as well as its contribution to the pathophysiological mechanism behind AD progression, remains under extensive study, it was reported that Aβ42 increased pTau and that GSK3β inhibition blocked the increased pTau and prevented Aβ42-induced impairment of LTP in mice [9]. It is known that GSK3β directly phosphorylates Tau on Thr181, Ser202, Thr205, Thr231, Ser396, Ser400, and Ser404 [25, 40, 46]. Thus, there is evidence for increased activation of GSK3β in human patients during early stages of AD [3, 37, 47, 48]. Based on that, deregulation of GSK3β has been proposed as a center-stage event linking extracellular Aβ and intracellular Tau protein [3, 48]. In this regard, it was reported that transgenic mice expressing a phosphorylation defective mutant GSK3β show impaired memory, impaired hippocampal LTP, and facilitated LTD [48]. Mechanistically, it has been proposed that during AD and related dementias, GSK3β activity may become deregulated due to its increased expression or as a result of alterations in upstream regulators of GSK3β, leading to enhancement of NMDAr-LTD and neurodegeneration [18].

Although it is not entirely clear how Aβ42 initiates the toxic cascade that causes all the synaptic alterations and the accumulation of proaggregant pTau, the activation of GSK3β seems to be the crucial executor of Aβ42 toxicity.

4. Tau and Synaptic Dysfunction

A recent study demonstrated that Aβ42 oligomers induce *de novo* synthesis of Tau protein, and its hyperphosphorylation at multiple residues, in the somatodendritic compartment, which is mediated by the Fyn/ERK/S6 signaling pathway [49]. This observation further supports an alternative mechanism for AD synaptic dysfunction, mediated by the aberrant translation and cellular redistribution of Tau protein in the somatodendritic region, which is due to the overstimulation of AMPA and NMDA receptors, as reported [50]. Indeed, the presence of Tau-mRNA in a dendritic ribonucleoprotein (RNP) complex allows for its local translation upon glutamatergic stimulation [50]. The interaction of Tau-mRNA containing RNP with Myosin Va, a postsynaptic motor protein, suggests that Tau-mRNA is transported into dendritic spines [50].

In addition to the alternative mechanism just described, a widely accepted theory for AD synaptic dysfunction proposes that Aβ42 oligomers induce Tau translocation from the axon to the dendritic spines causing early synaptotoxic effects (excitotoxicity) and progressive dendritic spine loss [8, 51, 52]. Supporting this theory, it was reported that oligomeric Aβ42 increases the redistribution of Tau to the somatodendritic compartment in AD mouse models [51,

52]. Thus, overexpression of Tau in cultured neurons and AD mice increases Tau in the somatodendritic compartment [51]. Importantly, the increased postsynaptic Tau was linked to spine loss in a Tau transgenic mouse model [51, 52]. Additional results showed that Aβ42 oligomers, through NMDAr, increased intracellular Ca^{2+} and triggered activation of AMP-activated kinase (AMPK), which leads to increased pTau (sites Ser262, Ser356, and Thr231) and dendritic spine loss [52–54]. In related studies, soluble Aβ oligomers, at picomolar concentrations, disrupt hippocampal LTP in slices and *in vivo* and impair the memory of complex learned behaviors in rodents [55]. Aβ oligomers also decrease dendritic spine density in organotypic slice cultures and contribute to excitotoxicity [55].

It is well known that a major component of the excitotoxicity process is the overactivation of NMDAr [56, 57]. NMDArs are heteromeric complexes formed by subunits NR1, NR2A, and NR2B [18, 56, 57]. Fyn kinase phosphorylates the NR2B subunit, which facilitates its interaction with PSD95 [58, 59]. It has been proposed that this interaction increases NMDAr stability and activity [18, 58, 59]. Furthermore, excess Fyn upregulates NMDAr activity, therefore affecting the levels of Ca^{2+} and causing calcium-driven excitotoxicity [8, 16, 52]. Additionally, it has been reported that there is a disturbance in intracellular Ca^{2+} homeostasis via changes in the calbindin D$_{28K}$ protein, causing a reduction in the number of cells and a shrinking of its dendritic trees [60]. Furthermore, it has been reported that increased Fyn correctly targeted to the postsynaptic compartment causes memory deficits, excitotoxicity, and seizures and induces premature mortality in APP transgenic mice [8, 52]. Mechanistically, this can be explained by Tau protein directly binding to Fyn kinase; therefore, a Tau-dependent increase of Fyn, in dendritic spines, enhances excitotoxic signaling [8, 52].

Acute excitotoxicity is not the only Tau-dependent effect of Aβ42 oligomers. Aβ42 oligomers also have been found to cause Tau microtubule disassembly and ectopic cell-cycle reentry, which leads to neuronal death [61]. Because microtubules are essential for the efficient delivery of synaptic components to axon terminals and postsynaptic components to dendritic terminals [61], the Aβ-induced Tau-dependent effects on microtubules constitute important threats to synaptic function.

Based on these findings, several groups have proposed the elimination of Tau protein as a potential therapeutic approach that could aid in mitigating AD disease progression [8, 9, 12]. In line with this hypothesis, it was reported that the absence of Tau disrupts postsynaptic targeting of Fyn kinase, which correlates with reduced NMDAr-mediated excitotoxicity and hence mitigation of Aβ-induced toxicity [8]. Additionally, knocking out the endogenous Tau gene relieved the APP mice from memory deficits, seizures, and premature mortality [8]. In addition, it was reported that the absence of Tau protein prevented Aβ-induced impairment of LTP [9].

Although all these interactions remain under extensive study, the exact mechanism of coupling between these two proteins is still unknown. One proposed pathological interaction between Aβ42 and pTau comprises the following cascades: (1) Aβ42 causes abnormal activation of Tau kinases

[3, 9, 14, 35, 40, 47, 52, 55], (2) activated Tau kinases cause abnormal phosphorylation of Tau protein at several sites [3, 14, 25, 35–37], and finally, (3) the abnormally phosphorylated Tau contributes to excitotoxicity [8, 62]. Therefore, scientists have proposed the blockade of Tau kinases as a potential therapeutic target against AD [9, 12, 13]. The rationale is simple: blocking Tau kinases will lead to non-phosphorylated Tau and, consequently, to less cytotoxicity [9, 12, 13].

5. Tau and Neuronal Network Activity

Cognitive capacities rely on a variety of brain network activity patterns, which represent distinct operating brain modes that are closely linked to fine changes in neuronal synchrony and are adjustable to behavioral demands [63, 64]. Therefore, alterations in synchronized network activities could help to explain cognitive deficits observed during AD development and tauopathies [65]. In this regard, recent studies support the early network dysfunction (neuronal hyperactivity, altered oscillatory activity, and loss of neuronal synchrony) as a crucial event that may lead to neurodegeneration and AD development [63–69]. In line with this hypothesis, it has been reported that hippocampal and cortex hyperactivity, which increases the risk of seizures, is presented in the early stages of AD [70, 71]. Indeed, convulsive seizures occur in over 80% of patients with an early stage of AD [71]. Thus, studies reported spontaneous epileptic activity with reduced gamma oscillations in AD [71, 72]. Notably, this activity depends on the inhibitory synaptic activity provided by the GABAergic parvalbumin-positive (PV+) interneurons [70, 73]. Increasing repetitive firing of PV+ cells favors gamma oscillations of neural networks [73–77]. In consequence, if the neural network synchronization is primarily controlled by the PV+ cells, then the disinhibition of principal cells (PCs) may produce less organized network activity leading to impaired information processing and cognitive function.

It has been hypothesized that the modifications in synaptic neuronal circuitries and the cognitive alterations in AD are produced by damage to PV+ interneurons that control the fine-tuning of neuronal network oscillations [76–81]. According to this hypothesis, the brain network alterations, rather than protein deposition, could account for the early pathogenesis of the disease development [67, 68]. Although the exact causes and mechanisms of network alterations have not been defined, interneuron dysfunction has emerged as a strong candidate [79–82]. Additional evidence suggests that GABAergic transmission of the PV+ cells is altered in AD, especially due to modifications in the function and number of cells; i.e., bodies and axons suffer size reduction, whereas the number of PV+ cells suffered the loss of over 70% in AD postmortem patients [82]. The cellular and molecular basis of this interneuron dysfunction has been studied in AD mouse models [67, 68, 70, 79]. For example, since gamma oscillations are mainly generated by PV+ cells, through their direct control of PCs firing [83], and since alterations in PV+ cell activity affect gamma oscillations and memory in AD mouse models [68, 69, 84], the rescue of PV+ cell activity promises the restoration of oscillatory activity, network synchrony, and memory [80, 84]. Notably, mouse models and

humans with AD had reduced levels of voltage-gated sodium channels subunit Nav1.1 in interneurons [84]. Thus, restoring PV+ cell activity through the overexpression of these channels increased inhibitory activity and restored oscillatory activity in AD mouse models [80]. Additionally, the restoration of PV+ cells contributed to the reduction of hypersynchrony, memory deficits, and premature mortality of AD mouse models [80]. In our hands, we found that oscillatory activity was significantly less rhythmic in a young (post-natal day 30) AD mouse model [68]. Additionally, AD mice displayed significantly less coupling between slow (2-10 Hz) and fast (25-250 Hz) oscillatory frequencies. Mechanistically, we found that the intrinsic excitability of PV+ cells was significantly reduced in the p30 AD mouse model [68]. Because PV+ cells play a vital role in coordinating hippocampal synchrony between slow and fast oscillations [85], restoring PV+ cell activity could also help to restore the brain synchrony and cognitive functions in early stages of AD.

Following the same line of thought, recent data showed that enhancing G-protein-coupled inwardly rectifying potassium (GirK) channels, which would contribute to neuronal inhibition, can control the excess of neuronal excitability [86, 87]. Indeed, intracerebroventricular injection of Aβ42 or the GirK channel blocker tertiapin impaired GABAA-mediated field potentials and GirK-mediated field potentials, as well as its LTP [86], which is prevented by the application of the GirK channel activator ML297 [86]. The GirK channel activator ML297 also rescues glutamatergic LTP and habituation memory from its inhibition induced by Aβ42 [87].

So far, the described data have established the potential role of changes in inhibitory function affecting brain network activity during the early stages of AD development; however, the role of Tau protein in this process and in neural network dysfunction overall remains to be discussed. In this regard, it has been shown that abnormal Tau disrupts the ongoing network activity of neocortical pyramidal cells before cell death [88]. Interestingly, abnormal Tau decreased the activity of subpopulations of neurons, which, in turn, reduced the activity of the neocortical networks [89]. In line with these findings, aggregation of abnormally phosphorylated Tau protein in the entorhinal cortex (EC) was enough to disrupt the coordination of local field potentials between its efferent regions [89]. At the cellular level, it is known that the application of Tau soluble oligomers in the CA1 region of the hippocampus and layer VI of the neocortex increases the input resistance, reduces the amplitude of the action potential, and slows the rise and decay times of the action potential, without modifying synaptic transmission, but impairing the induction of LTP [90]. Furthermore, Tau oligomers isolated from human AD patients produced an inhibition of the hippocampal LTP and induced memory dysfunction in rodents [91]. In our hands, we found that PCs and PV+ cells in p30 triple-transgenic AD mice accumulate pTau at MD sites and that this accumulation correlated with changes in hippocampal oscillatory activity [92, 93]. Taken together, the latest evidence supports pTau accumulation in PCs and interneurons as an essential event that contributes to firing instability and, therefore, to brain network alterations, especially during very early stages of disease progression.
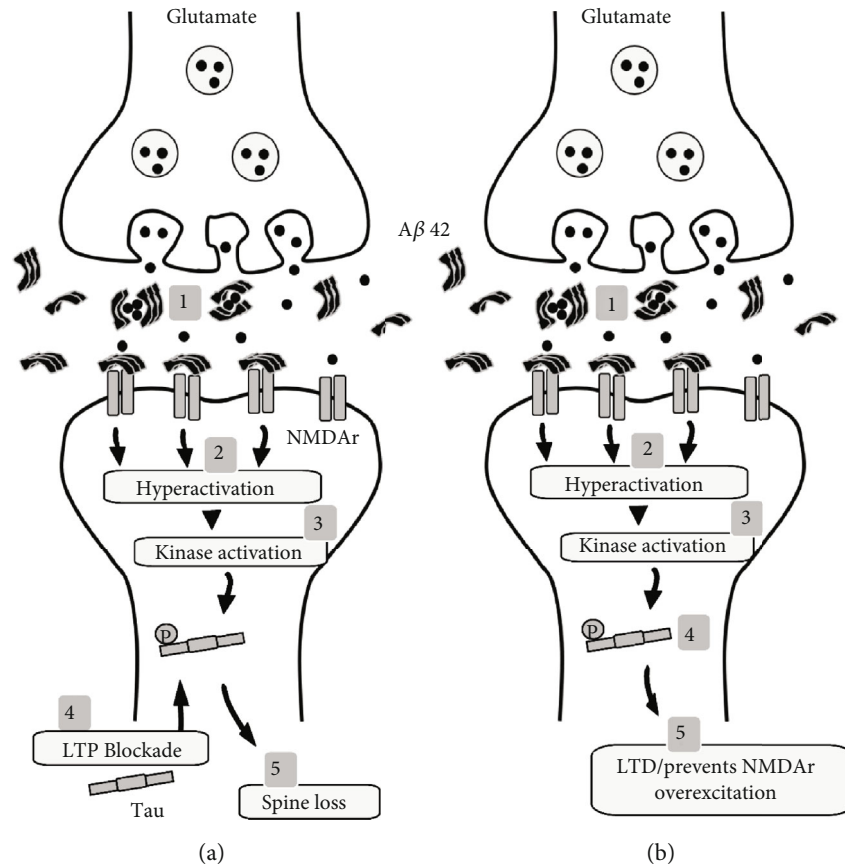
Figure 3: pTau protein at MD (microtubule domain) prevents NMDAr overexcitation, which accounts for protection rather than damage. (a) Aβ42 oligomers repeatedly affect neurons by blocking glutamate reuptake (1), which leads to hyperactivation (2), kinase activation (3), Tau hyperphosphorylation, and Tau translocation from the axon to the dendritic spines (4) causing LTP blockade and progressive spine loss (5). (b) Alternatively, Aβ42 oligomers block glutamate reuptake (1), which leads to hyperactivation (2), kinase activation (3), and Tau phosphorylation at MD sites (4), which alternatively promote LTD, preventing further NMDAr-mediated overexcitation and producing neuroprotection (5).

In summary, the Aβ42 oligomers and pTau induce changes in synaptic functions of PCs and interneurons and compromise the function of neuronal networks (i.e., long-term synaptic plasticity and synchronized networks).

6. Classical Tau Hypothesis versus New Hypothesis

As previously discussed, a current model of AD synaptic dysfunction proposes that (1) Aβ42 oligomers induce abnormal kinase activation, (2) leading to Tau hyperphosphorylation and (3) translocation from the axon to the dendritic spines causing (4) LTP blockade, (5) progressive synaptic dysfunction, (6) progressive dendritic spine loss, and (7) early network dysfunction. Adding to the synaptic/network dysfunction, it was recently reported that Aβ42 oligomers block glutamate reuptake and overactivate NMDAr, leading to hyperactivation and neurodegeneration during early stages of disease progression [34, 94] (Figure 3(a)). Thus, from the classical point of view, all the data argued so far could favor the existence of a toxic cascade of Aβ42-pTau/synaptic damage/network dysfunction. However, we firmly believe that our data, along with recently published data, will help

to unveil a new hypothesis in which Tau phosphorylated near the MD could have a protective role during the early stages of AD development [13–16, 29, 92, 93]. One molecular basis for this alternative hypothesis is that pTau protein at MD sites is physiologically located at the synaptic terminals [13, 14, 29]. Furthermore, pTau protein at MD sites is not exclusively translocated from axons to dendrites, as suggested by the classical hypothesis [3, 8, 49, 50, 52]. Second, pTau protein at MD sites prevents NMDAr overexcitation [13, 14, 29], which accounts for protection rather than damage, at the very least, during the early stages of disease progression. If our alternative hypothesis is true, it would be expected that the induction of epileptic activity, partially mediated by NMDAr hyperexcitation, could be prevented by elevating levels of pTau at MD sites. It has to be remembered, the prevalence rates of seizures are significantly increased in patients with AD [95–97]. In fact, we confirmed this by challenging p30 triple transgenic AD mice with the potassium channel blocker 4-aminopyridine, a potent proepileptic drug [92, 93]. We found that the p30 triple-transgenic AD mice exhibited a dramatic reduction in seizure-like activity after the 4-aminopyridine application [92, 93]. We also found that this reduction in the induction of epileptic activity correlated

with pTau's MD accumulation in PCs [92]. Collectively, our results provide support for the alternative role of pTau protein during normal physiological conditions and early stages of AD development [7, 13, 14, 92, 93]. Importantly, it was reported that during the early stage of AD development, phosphorylation of Tau protein at its site Thr205 alleviated Aβ-induced neuronal death and provided protection from excitotoxicity [16]. Thus, an AD model with elevated pTau is more resistant to seizure activity induced by the proepileptic drug pentylenetetrazole [16]. Further supporting our hypothesis, and in agreement with our previously published data [14], this reduction in hyperexcitability is related to an increase in pTau-dependent disruption of PSD95/Tau/Fyn interactions and to the inhibition of Aβ-induced toxicity [16]. Altogether, these new pieces of evidence support a novel protective role of pTau (mainly by preventing NMDAr overexcitation) during early stages of AD development.

7. Conclusions and Perspectives

For the past decade, we have accumulated evidence that supports an alternative pTau hypothesis during the early stages of disease progression. The following is a summary of this evidence: (1) Tau phosphorylation at specific sites (near MD) appears during early stages of disease progression in the brain tissue from AD, Parkinson's disease, Down syndrome, and frontotemporal dementia cases [2, 5–7, 98, 99]. (2) These phosphorylation events precede early truncation events in Tau protein (i.e., truncation at site Asp421) and early conformational changes (i.e., folding from the amino terminus to the MD) [2, 5, 6, 98, 99]. (3) The phosphorylation events occur prior to the apparition of the classical fibrillar structures (NFTs and Aβ plaques) [2, 5, 6, 98, 99]. (4) Endogenous pTau near MD sites is physiologically located at postsynaptic sites where it interacts with the PSD95-NMDAr complex [13, 14, 29]. We showed that Tau binds directly to PSD95 protein [13, 14, 29]. (5) Increases in pTau at MD sites serve as a regulatory mechanism that prevent NMDAr overexcitation [13, 14, 29, 92]. (6) Increased pTau at MD sites confers protection from epileptic activity by reducing hippocampal excitability [13, 14, 92]. Finally, (7) we showed that increases in pTau at MD sites confer protection by disrupting PSD95/Tau/Fyn interaction and promoting LTD [13, 14, 29].

Collectively, our data, along with current published data, nurture the alternative pTau hypothesis [13, 14, 29, 92]. However, many scientific efforts are needed to further support the nonpathological role of pTau during early stages of disease progression, or even under physiological conditions. Despite this, if Tau phosphorylation at MD sites is involved in neuroprotection rather than neurodegeneration, the therapeutic strategies aimed at reducing Tau and pTau could phase nothing but a mild outcome [7, 13, 14, 29, 92]. In order to appropriately design therapeutic AD strategies, the link between Aβ and Tau/pTau at the synapse needs to be fully unveiled. For example, what are the molecular mechanism leading to synapse loss? Which forms of Aβ and Tau are toxic at the synapse? Additionally, we need to better understand the exact role of soluble versus aggregated species of Aβ

and Tau/pTau in physiology and pathology [100]. Alternatively, unveiling the role of Tau/pTau in modulating PCs and interneuron activity (i.e., PV+ cells) could potentially prevent cognitive decline in the latter stages of AD [101, 102]. As previously discussed, it is becoming clear that early brain network changes are announcing that the complex homeostatic network that maintains brain function has been challenged. Therefore, very early brain circuit alterations could serve as a potential biomarker for detecting the prodromal neurodegeneration stage [7, 29, 67, 68, 92]. Aiming to restore brain network function may help to prevent the latter neurodegenerative stages of AD. The rationale is not straightforward if we seek to restore brain network function during AD. Thus, understanding the basic principles of firing homeostasis in neuronal circuits is required. Perhaps a broad outlook on brain network circuit damaging processes could offer new therapeutic targets and strategies for restoring brain functions.

Abbreviations

AD:	Alzheimer's disease
APP:	Amyloid precursor protein
Aβ:	Amyloid-beta
pTau:	Hyperphosphorylated Tau
MD:	Microtubule domain
LTP:	Long-term potentiation
LTD:	Long-term depression
NMDAr:	N-Methyl-D-aspartate receptor
AKT:	Protein kinase B
GSK-3β:	Glycogen synthase kinase-3β
PI3K:	Phosphatidylinositol 3-kinase
CaM:	Calmodulin
PP2B:	Protein phosphatase 2B
PP1:	Protein phosphatase 1
PSD95:	Postsynaptic density protein 95
AMPK:	AMP-activated kinase
PV+:	Parvalbumin positive
GirK:	G-protein-coupled inwardly rectifying potassium channels
RNP:	Ribonucleoprotein
PC:	Principal cells
NFTs:	Neurofibrillary tangles.

Conflicts of Interest

The authors declare no competing financial interests.

Authors' Contributions

Acknowledgments

References

[1] M. Goedert and R. A. Crowther, "Amyloid plaques, neurofibrillary tangles and their relevance for the study of Alzheimer's disease," *Neurobiology of Aging*, vol. 10, no. 5, pp. 405-406, 1989.

[2] S. Mondragón-Rodríguez, G. Basurto-Islas, I. Santa-Maria et al., "Cleavage and conformational changes of tau protein follow phosphorylation during Alzheimer's disease," *International Journal of Experimental Pathology*, vol. 89, no. 2, pp. 81–90, 2008.

[3] E. Mandelkow, "The tangled tale of tau," *Nature*, vol. 402, no. 6762, pp. 588-589, 1999.

[4] Y. E. Cho, M. H. Lee, and B. J. Song, "Neuronal cell death and degeneration through increased nitroxidative stress and tau phosphorylation in HIV-1 transgenic rats," *PLoS One*, vol. 12, no. 1, article e0169945, 2017.

[5] S. Mondragón-Rodríguez, R. Mena, L. I. Binder, M. A. Smith, G. Perry, and F. García-Sierra, "Conformational changes and cleavage of tau in Pick bodies parallel the early processing of tau found in Alzheimer pathology," *Neuropathology and Applied Neurobiology*, vol. 34, no. 1, pp. 62–75, 2008.

[6] S. Mondragón-Rodríguez, G. Perry, J. Luna-Muñoz, M. C. Acevedo-Aquino, and S. Williams, "Phosphorylation of tau protein at sites $Ser^{396-404}$ is one of the earliest events in Alzheimer's disease and Down syndrome," *Neuropathology and Applied Neurobiology*, vol. 40, no. 2, pp. 121–135, 2014.

[7] S. Mondragón-Rodríguez, G. Perry, F. Pena-Ortega, and S. Williams, "Tau, amyloid beta and deep brain stimulation: aiming to restore cognitive deficit in Alzheimer's disease," *Current Alzheimer Research*, vol. 14, no. 1, pp. 40–46, 2017.

[8] L. M. Ittner, Y. D. Ke, F. Delerue et al., "Dendritic function of tau mediates amyloid-β toxicity in Alzheimer's disease mouse models," *Cell*, vol. 142, no. 3, pp. 387–397, 2010.

[9] O. A. Shipton, J. R. Leitz, J. Dworzak et al., "Tau protein is required for amyloid -induced impairment of hippocampal long-term potentiation," *The Journal of Neuroscience*, vol. 31, no. 5, pp. 1688–1692, 2011.

[10] G. Koch, F. di Lorenzo, M. F. del Olmo et al., "Reversal of LTP-like cortical plasticity in Alzheimer's disease patients with tau-related faster clinical progression," *Journal of Alzheimer's Disease*, vol. 50, no. 2, pp. 605–616, 2016.

[11] D. A. Lewis, G. A. Higgins, W. G. Young et al., "Distribution of precursor amyloid-beta-protein messenger RNA in human cerebral cortex: relationship to neurofibrillary tangles and neuritic plaques," *Proceedings of the National Academy of Sciences of the United States of America*, vol. 85, no. 5, pp. 1691–1695, 1988.

[12] E. E. Congdon and E. M. Sigurdsson, "Tau-targeting therapies for Alzheimer disease," *Nature Reviews. Neurology*, vol. 14, no. 7, pp. 399–415, 2018.

[13] S. Mondragón-Rodríguez, G. Perry, X. Zhu, and J. Boehm, "Amyloid beta and tau proteins as therapeutic targets for Alzheimer's disease treatment: Rethinking the current strategy," *International Journal of Alzheimer's Disease*, vol. 2012, Article ID 630182, 7 pages, 2012.

[14] S. Mondragón-Rodríguez, E. Trillaud-Doppia, A. Dudilot et al., "Interaction of endogenous tau protein with synaptic proteins is regulated by N-methyl-d-aspartate receptor-dependent tau phosphorylation," *The Journal of Biological Chemistry*, vol. 287, no. 38, pp. 32040–32053, 2012.

[15] P. Regan, T. Piers, J. H. Yi et al., "Tau phosphorylation at serine 396 residue is required for hippocampal LTD," *The Journal of Neuroscience*, vol. 35, no. 12, pp. 4804–4812, 2015.

[16] A. Ittner, S. W. Chua, J. Bertz et al., "Site-specific phosphorylation of tau inhibits amyloid-β toxicity in Alzheimer's mice," *Science*, vol. 354, no. 6314, pp. 904–908, 2016.

[17] Y. Wang and E. Mandelkow, "Tau in physiology and pathology," *Nature Reviews Neuroscience.*, vol. 17, no. 1, pp. 5–21, 2016.

[18] G. L. Collingridge, S. Peineau, J. G. Howland, and Y. T. Wang, "Long-term depression in the CNS," *Nature Reviews. Neuroscience*, vol. 11, no. 7, pp. 459–473, 2010.

[19] C. Lüscher and R. C. Malenka, "NMDA receptor-dependent long-term potentiation and long-term depression (LTP/LTD)," *Cold Spring Harbor Perspectives in Biology*, vol. 4, no. 6, 2012.

[20] S. A. Connor and Y. T. Wang, "A place at the table: LTD as a mediator of memory genesis," *The Neuroscientist*, vol. 22, no. 4, pp. 359–371, 2016.

[21] R. Mulkey, C. Herron, and R. Malenka, "An essential role for protein phosphatases in hippocampal long-term depression," *Science*, vol. 261, no. 5124, pp. 1051–1055, 1993.

[22] G. L. Collingridge, J. T. R. Isaac, and Y. T. Wang, "Receptor trafficking and synaptic plasticity," *Nature Reviews Neuroscience*, vol. 5, no. 12, pp. 952–962, 2004.

[23] M. J. Kim, K. Futai, J. Jo, Y. Hayashi, K. Cho, and M. Sheng, "Synaptic accumulation of PSD-95 and synaptic function regulated by phosphorylation of serine-295 of PSD-95," *Neuron*, vol. 56, no. 3, pp. 488–502, 2007.

[24] S. Peineau, C. S. Nicolas, Z. A. Bortolotto et al., "A systematic investigation of the protein kinases involved in NMDA receptor-dependent LTD: evidence for a role of GSK-3 but not other serine/threonine kinases," *Molecular Brain*, vol. 2, no. 1, p. 22, 2009.

[25] B. R. Sperbera, S. Leight, M. Goedert, and V. M.-Y. Lee, "Glycogen synthase kinase-3β phosphorylates tau protein at multiple sites in intact cells," *Neuroscience Letters*, vol. 197, no. 2, pp. 149–153, 1995.

[26] C. L. Palmer, W. Lim, P. G. R. Hastie et al., "Hippocalcin functions as a calcium sensor in hippocampal LTD," *Neuron*, vol. 47, no. 4, pp. 487–494, 2005.

[27] H.-Y. Man, Q. Wang, W.-Y. Lu et al., "Activation of PI3-kinase is required for AMPA receptor insertion during LTP of mEPSCs in cultured hippocampal neurons," *Neuron*, vol. 38, no. 4, pp. 611–624, 2003.

[28] F. Liu, I. Grundke-Iqbal, K. Iqbal, and C.-X. Gong, "Contributions of protein phosphatases PP1, PP2A, PP2B and PP5 to the regulation of tau phosphorylation," *European Journal of Neuroscience*, vol. 22, no. 8, pp. 1942–1950, 2005.

[29] S. Mondragón-Rodríguez, G. Perry, X. Zhu, P. I. Moreira, M. C. Acevedo-Aquino, and S. Williams, "Phosphorylation of tau protein as the link between oxidative stress, mitochondrial dysfunction, and connectivity failure: implications for Alzheimer's disease," *Oxidative Medicine and Cellular Longevity*, vol. 2013, 6 pages, 2013.

[30] G. M. Shankar, S. Li, T. H. Mehta et al., "Amyloid-beta protein dimers isolated directly from Alzheimer's brains impair synaptic plasticity and memory," *Nature Medicine*, vol. 14, no. 8, pp. 837–842, 2008.

[31] N.-W. Hu, A. J. Nicoll, D. Zhang et al., "mGlu5 receptors and cellular prion protein mediate amyloid-β-facilitated synaptic long-term depression in vivo," *Nature Communications*, vol. 5, no. 1, 2014.

[32] P. N. Lacor, M. C. Buniel, P. W. Furlow et al., "Abeta oligomer-induced aberrations in synapse composition, shape, and density provide a molecular basis for loss of connectivity in Alzheimer's disease," *The Journal of Neuroscience*, vol. 27, no. 4, pp. 796–807, 2007.

[33] E. M. Snyder, Y. Nong, C. G. Almeida et al., "Regulation of NMDA receptor trafficking by amyloid-β," *Nature Neurosci.*, vol. 8, no. 8, pp. 1051–1058, 2005.

[34] B. Zott, M. M. Simon, W. Hong et al., "A vicious cycle of β amyloid-dependent neuronal hyperactivation," *Science*, vol. 365, no. 6453, pp. 559–565, 2019.

[35] E. Lain, B. Penke, A. Delacourte, D. Gündisch, H. Schröder, and B. Witter, "Effects of A$\beta_{1\text{-}42}$ fibrils and of the tetrapeptide Pr-IIGL on the phosphorylation state of the τ-protein and on the α7 nicotinic acetylcholine receptor in vitro," *European Journal of Neuroscience*, vol. 21, no. 4, pp. 879–888, 2005.

[36] D. J. Selkoe and J. Hardy, "The amyloid hypothesis of Alzheimer's disease at 25 years," *EMBO Molecular Medicine*, vol. 8, no. 6, pp. 595–608, 2016.

[37] G. V. W. Johnson, "Tau phosphorylation in neuronal cell function and dysfunction," *Journal of Cell Science*, vol. 117, no. 24, pp. 5721–5729, 2004.

[38] J. Luna-Muñoz, L. Chávez-Macías, F. García-Sierra, and R. Mena, "Earliest stages of tau conformational changes are related to the appearance of a sequence of specific phospho-dependent tau epitopes in Alzheimer's disease," *Journal of Alzheimer's Disease*, vol. 12, no. 4, pp. 365–375, 2007.

[39] C. A. Rankin and T. C. Gamblin, "Assessing the toxicity of tau aggregation," *Journal of Alzheimer's Disease*, vol. 14, no. 4, pp. 411–416, 2008.

[40] C. A. Rankin, Q. Sun, and T. C. Gamblin, "Tau phosphorylation by GSK-3β promotes tangle-like filament morphology," *Molecular Neurodegeneration*, vol. 2, no. 1, p. 12, 2007.

[41] A. Sydow, A. van der Jeugd, F. Zheng et al., "Tau-induced defects in synaptic plasticity, learning, and memory are reversible in transgenic mice after switching off the toxic tau mutant," *Journal of Neuroscience*, vol. 31, no. 7, pp. 2511–2525, 2011.

[42] M. Higuchi, T. Ishihara, B. Zhang et al., "Transgenic mouse model of tauopathies with glial pathology and nervous system degeneration," *Neuron*, vol. 35, no. 3, pp. 433–446, 2002.

[43] T. A. Fulga, I. Elson-Schwab, V. Khurana et al., "Abnormal bundling and accumulation of F-actin mediates tau-induced neuronal degeneration in vivo," *Nature Cell Biology*, vol. 9, no. 2, pp. 139–148, 2007.

[44] J. Gotz, "Formation of Neurofibrillary Tangles in P301L Tau Transgenic Mice Induced by Abeta 42 Fibrils," *Science*, vol. 293, no. 5534, pp. 1491–1495, 2001.

[45] T. Ondrejcak, N.-W. Hu, Y. Qi et al., "Soluble tau aggregates inhibit synaptic long-term depression and amyloid β-facilitated LTD in vivo," *Neurobiology of Disease*, vol. 127, pp. 582–590, 2019.

[46] T. Li and H. K. Paudel, "Glycogen synthase kinase 3beta phosphorylates Alzheimer's disease-specific Ser396 of microtubule-associated protein tau by a sequential mechanism," *Biochemistry*, vol. 45, no. 10, pp. 3125–3133, 2006.

[47] J.-H. Cho and G. V. W. Johnson, "Glycogen synthase kinase 3 beta induces caspase-cleaved tau aggregation in situ," *Journal*

[48] *of Biological Chemistry*, vol. 279, no. 52, pp. 54716–54723, 2004.

I. Dewachter, L. Ris, T. Jaworski et al., "GSK3beta, a centre-staged kinase in neuropsychiatric disorders, modulates long term memory by inhibitory phosphorylation at serine-9," *Neurobiology of Disease*, vol. 35, no. 2, pp. 193–200, 2009.

[49] C. Li and J. Gotz, "Somatodendritic accumulation of tau in Alzheimer's disease is promoted by Fyn-mediated local protein translation," *The EMBO Journal*, vol. 36, no. 21, pp. 3120–3138, 2017.

[50] S. Kobayashi, T. Tanaka, Y. Soeda, O. F. X. Almeida, and A. Takashima, "Local somatodendritic translation and hyperphosphorylation of tau protein triggered by AMPA and NMDA receptor stimulation," *eBioMedicine*, vol. 20, pp. 120–126, 2017.

[51] H. Zempel, F. J. A. Dennissen, Y. Kumar et al., "Axodendritic sorting and pathological missorting of tau are isoform-specific and determined by axon initial segment architecture," *The Journal of Biological Chemistry*, vol. 292, no. 29, pp. 12192–12207, 2017.

[52] A. Ittner and L. M. Ittner, "Dendritic tau in Alzheimer's disease," *Neuron*, vol. 99, no. 1, pp. 13–27, 2018.

[53] M. Domise, S. Didier, C. Marinangeli et al., "AMP-activated protein kinase modulates tau phosphorylation and tau pathology in vivo," *Scientific Reports*, vol. 6, no. 1, 2016.

[54] G. Amadoro, M. T. Ciotti, M. Costanzi, V. Cestari, P. Calissano, and N. Canu, "NMDA receptor mediates tau-induced neurotoxicity by calpain and ERK/MAPK activation," *Proceedings of the National Academy of Sciences of the United States of America*, vol. 103, no. 8, pp. 2892–2897, 2006.

[55] D. J. Selkoe, "Soluble oligomers of the amyloid β-protein impair synaptic plasticity and behavior," *Behavioural Brain Research*, vol. 192, no. 1, pp. 106–113, 2008.

[56] V. Vyklicky, M. Korinek, T. Smejkalova et al., "Structure, Ffunction, and pharmacology of NMDA receptor channels," *Physiological Research*, vol. 63, Suppl 1, pp. S191–S203, 2014.

[57] Y. Zhong and R. B. Shultz, "Minocycline targets multiple secondary injury mechanisms in traumatic spinal cord injury," *Neural Regeneration Research*, vol. 12, no. 5, pp. 702–713, 2017.

[58] G. Lee, S. T. Newman, D. L. Gard, H. Band, and G. Panchamoorthy, "Tau interacts with Src-family non-receptor tyrosine kinases," *Journal of Cell Science*, vol. 111, Part 21, 1998.

[59] T. Nakazawa, S. Komai, T. Tezuka et al., "Characterization of Fyn-mediated tyrosine phosphorylation sites on GluRε2 (NR2B) subunit of the N-methyl-d-aspartate receptor," *Biological Chemistry*, vol. 276, no. 1, pp. 693–699, 2001.

[60] G. Lally, R. L. M. Faull, H. J. Waldvogel, S. Ferrari, and P. C. Emson, "Calcium homeostasis in ageing: studies on the calcium binding protein calbindin D$_{28K}$," *Journal of Neural Transmission*, vol. 104, no. 10, pp. 1107–1112, 1997.

[61] R. B. Vallee and G. S. Bloom, "Mechanisms of fast and slow axonal transport," *Annual Review of Neuroscience*, vol. 14, no. 1, pp. 59–92, 1991.

[62] K. Ando, A. Maruko-Otake, Y. Ohtake, M. Hayashishita, M. Sekiya, and K. M. Iijima, "Stabilization of microtubule-unbound tau via tau phosphorylation at Ser262/356 by Par-1/MARK contributes to augmentation of AD-Related phosphorylation and Aβ42-induced tau toxicity," *PLOS Genetics*, vol. 12, no. 3, p. e1005917, 2016.

[63] H. H. Jasper, "Cortical excitatory state and variability in human brain rhythms," *Science*, vol. 83, no. 2150, pp. 259-260, 1936.

[64] G. Buzsáki and A. Draguhn, "Neuronal oscillations in cortical networks," *Science*, vol. 304, no. 5679, pp. 1926–1929, 2004.

[65] S. Frere and I. Slutsky, "Alzheimer's disease: from firing instability to homeostasis network collapse," *Neuron*, vol. 97, no. 1, pp. 32–58, 2018.

[66] R. G. Canter, J. Penney, and L.-H. Tsai, "The road to restoring neural circuits for the treatment of Alzheimer's disease," *Nature*, vol. 539, no. 7628, pp. 187–196, 2016.

[67] S. Mondragón-Rodríguez, N. Gu, C. Fasano, F. Peña-Ortega, and S. Williams, "Functional connectivity between hippocampus and lateral septum is affected in very young Alzheimer's transgenic mouse model," *Neuroscience*, vol. 401, pp. 96–105, 2019.

[68] S. Mondragón-Rodríguez, N. Gu, F. Manseau, and S. Williams, "Alzheimer's transgenic model is characterized by very early brain network alterations and β-CTF fragment accumulation: reversal by β-secretase inhibition," *Frontiers in Cellular Neuroscience*, vol. 12, 2018.

[69] R. A. Sperling, P. S. LaViolette, K. O'Keefe et al., "Amyloid deposition is associated with impaired default network function in older persons without dementia," *Neuron*, vol. 63, no. 2, pp. 178–188, 2009.

[70] J. J. Palop and L. Mucke, "Amyloid-β–induced neuronal dysfunction in Alzheimer's disease: from synapses toward neural networks," *Nature Neuroscience*, vol. 13, no. 7, pp. 812–818, 2010.

[71] J. C. Amatniek, W. A. Hauser, C. DelCastillo-Castaneda et al., "Incidence and predictors of seizures in patients with Alzheimer's disease," *Epilepsia*, vol. 47, no. 5, pp. 867–872, 2006.

[72] B. J. Snider, J. Norton, M. A. Coats et al., "Novel presenilin 1 mutation (S170F) causing Alzheimer disease with Lewy bodies in the third decade of life," *Archives of Neurology*, vol. 62, no. 12, pp. 1821–1830, 2005.

[73] V. S. Sohal, F. Zhang, O. Yizhar, and K. Deisseroth, "Parvalbumin neurons and gamma rhythms enhance cortical circuit performance," *Nature*, vol. 459, no. 7247, pp. 698–702, 2009.

[74] J. A. Cardin, M. Carlén, K. Meletis et al., "Driving fast-spiking cells induces gamma rhythm and controls sensory responses," *Nature*, vol. 459, no. 7247, pp. 663–667, 2009.

[75] T. Klausberger and P. Somogyi, "Neuronal diversity and temporal dynamics: the unity of hippocampal circuit operations," *Science*, vol. 321, no. 5885, pp. 53–57, 2008.

[76] E. O. Mann and O. Paulsen, "Role of GABAergic inhibition in hippocampal network oscillations," *Trends in Neurosciences*, vol. 30, no. 7, pp. 343–349, 2007.

[77] T. F. Freund and I. Katona, "Perisomatic inhibition," *Neuron*, vol. 56, no. 1, pp. 33–42, 2007.

[78] Y. Wang, C. A. Dye, V. Sohal et al., "Dlx5 and Dlx6 regulate the development of parvalbumin-expressing cortical interneurons," *The Journal of Neuroscience*, vol. 30, no. 15, pp. 5334–5345, 2010.

[79] J. J. Palop and L. Mucke, "Network abnormalities and interneuron dysfunction in Alzheimer disease," *Nature Reviews. Neuroscience*, vol. 17, no. 12, pp. 777–792, 2016.

[80] M. Martinez-Losa, T. E. Tracy, K. Ma et al., "Nav1.1-overexpressing interneuron transplants restore brain rhythms and cognition in a mouse model of Alzheimer's disease," *Neuron*, vol. 98, no. 1, pp. 75–89.e5, 2018.

[81] E. V. Varela, G. Etter, and S. Williams, "Excitatory-inhibitory imbalance in Alzheimer's disease and therapeutic significance," *Neurobiology of Disease*, vol. 127, pp. 605–615, 2019.

[82] E. Sanchez-Mejias, C. Nuñez-Diaz, R. Sanchez-Varo et al., "Distinct disease-sensitive GABAergic neurons in the perirhinal cortex of Alzheimer's mice and patients," *Brain Pathology*, vol. 30, no. 2, pp. 345–363, 2019.

[83] B. Amilhon, C. Y. L. Huh, F. Manseau et al., "Parvalbumin interneurons of hippocampus tune population activity at theta frequency," *Neuron*, vol. 86, no. 5, pp. 1277–1289, 2015.

[84] L. Verret, E. O. Mann, G. B. Hang et al., "Inhibitory interneuron deficit links altered network activity and cognitive dysfunction in Alzheimer model," *Cell*, vol. 149, no. 3, pp. 708–721, 2012.

[85] E. Stark, L. Roux, R. Eichler, Y. Senzai, S. Royer, and G. Buzsáki, "Pyramidal cell-interneuron interactions underlie hippocampal ripple oscillations," *Neuron*, vol. 83, no. 2, pp. 467–480, 2014.

[86] I. Sánchez-Rodríguez, A. Gruart, J. Delgado-García, L. Jiménez-Díaz, and J. Navarro-López, "Role of GirK channels in long-term potentiation of synaptic inhibition in an in vivo mouse model of early amyloid- β pathology," *International Journal of Molecular Sciences*, vol. 20, no. 5, p. 1168, 2019.

[87] I. Sánchez-Rodríguez, S. Djebari, S. Temprano-Carazo et al., "Hippocampal long-term synaptic depression and memory deficits induced in early amyloidopathy are prevented by enhancing G-protein-gated inwardly rectifying potassium channel activity," *Journal of Neurochemistry*, vol. 153, no. 3, pp. 362–376, 2020.

[88] N. Menkes-Caspi, H. G. Yamin, V. Kellner, T. L. Spires-Jones, D. Cohen, and E. A. Stern, "Pathological tau disrupts ongoing network activity," *Neuron*, vol. 85, no. 5, pp. 959–966, 2015.

[89] S. E. Tanninen, B. Nouriziabari, M. D. Morrissey et al., "Entorhinal tau pathology disrupts hippocampal-prefrontal oscillatory coupling during associative learning," *Neurobiology of Aging*, vol. 58, pp. 151–162, 2017.

[90] E. Hill, T. K. Karikari, K. G. Moffat, M. J. E. Richardson, and M. J. Wall, "Introduction of tau oligomers into cortical neurons alters action potential dynamics and disrupts synaptic transmission and plasticity," *eNeuro*, vol. 6, no. 5, pp. ENEURO.0166–ENEU19.2019, 2019.

[91] T. Ondrejcak, I. Klyubin, G. T. Corbett et al., "Cellular prion protein mediates the disruption of hippocampal synaptic plasticity by soluble tau in vivo," *The Journal of Neuroscience*, vol. 38, no. 50, pp. 10595–10606, 2018.

[92] S. Mondragón-Rodríguez, A. Salas-Gallardo, P. González-Pereyra et al., "Phosphorylation of tau protein correlates with changes in hippocampal theta oscillations and reduces hippocampal excitability in Alzheimer's model," *The Journal of Biological Chemistry*, vol. 293, no. 22, pp. 8462–8472, 2018.

[93] S. Mondragón-Rodríguez, B. Ordaz, E. Orta-Salazar, S. Díaz-Cintra, F. Peña-Ortega, and G. Perry, "Hippocampal unicellular recordings and hippocampal-dependent innate behaviors in an adolescent mouse model of Alzheimer's disease," *Bio-Protocol*, vol. 10, no. 4, 2020.

[94] B. Zott, M. A. Busche, R. A. Sperling, and A. Konnerth, "What happens with the circuit in Alzheimer's disease in mice and humans?," *Annual Review of Neuroscience*, vol. 41, no. 1, pp. 277–297, 2018.

[95] N. Nicastro, F. Assal, and M. Seeck, "From here to epilepsy: the risk of seizure in patients with Alzheimer's disease," *Epileptic Disorders*, vol. 18, no. 1, pp. 1–12, 2016.

[96] N. Garg, R. Joshi, and B. Medhi, "Cracking novel shared targets between epilepsy and Alzheimer's disease: need of the hour," *Reviews in the Neurosciences*, vol. 29, no. 4, pp. 425–442, 2018.

[97] B. Cretin, N. Philippi, O. Bousiges et al., "Do we know how to diagnose epilepsy early in Alzheimer's disease?," *Revue Neurologique (Paris)*, vol. 173, no. 6, pp. 374–380, 2017.

[98] S. Mondragón-Rodríguez, G. Basurto-Islas, L. I. Binder, and F. García-Sierra, "Conformational changes and cleavage; are these responsible for the tau aggregation in Alzheimer's disease?," *Future Neurology*, vol. 4, no. 1, pp. 39–53, 2009.

[99] S. Mondragón-Rodríguez, G. Basurto-Islas, H.-g. Lee et al., "Causes versus effects: the increasing complexities of Alzheimer's disease pathogenesis," *Expert Review of Neurotherapeutics*, vol. 10, no. 5, pp. 683–691, 2014.

[100] G. S. Bloom, "Amyloid-β and tau: the trigger and bullet in Alzheimer disease pathogenesis," *JAMA Neurology*, vol. 71, no. 4, pp. 505–508, 2014.

[101] H. Zhang, L. Zhang, D. Zhou et al., "Ablating ErbB4 in PV neurons attenuates synaptic and cognitive deficits in an animal model of Alzheimer's disease," *Neurobiology of Disease*, vol. 106, pp. 171–180, 2017.

[102] V. Cattaud, C. Bezzina, C. C. Rey, C. Lejards, L. Dahan, and L. Verret, "Early disruption of parvalbumin expression and perineuronal nets in the hippocampus of the Tg2576 mouse model of Alzheimer's disease can be rescued by enriched environment," *Neurobiology of Aging*, vol. 72, pp. 147–158, 2018.

Research Article

A Customized Next-Generation Sequencing-Based Panel to Identify Novel Genetic Variants in Dementing Disorders: A Pilot Study

Giuseppe Lanza [iD],[1,2] **Francesco Calì,**[2] **Mirella Vinci,**[2] **Filomena Irene Ilaria Cosentino,**[2] **Mariangela Tripodi,**[2] **Rosario Sebastiano Spada,**[2] **Mariagiovanna Cantone** [iD],[3] **Rita Bella,**[4] **Teresa Mattina,**[5] **and Raffaele Ferri**[2]

[1]*Department of Surgery and Medical-Surgical Specialties, University of Catania, Catania, Italy*
[2]*Oasi Research Institute–IRCCS, Troina, Italy*
[3]*Department of Neurology, Sant'Elia Hospital, ASP Caltanissetta, Caltanissetta, Italy*
[4]*Department of Medical and Surgical Sciences and Advanced Technologies, University of Catania, Catania, Italy*
[5]*Department of Biomedical and Biotechnological Sciences, University of Catania, Catania, Italy*

Correspondence should be addressed to Mariagiovanna Cantone; m.cantone@asp.cl.it

Purpose. The advancements in the next-generation sequencing (NGS) techniques have allowed for rapid, efficient, and cost-time-effective genetic variant detection. However, in both clinical practice and research setting, sequencing is still often limited to the use of gene panels clinically targeted on the genes underlying the disease of interest. *Methods.* We performed a neurogenetic study through an *ad hoc* NGS-based custom sequencing gene panel in order to screen 16 genes in 8 patients with different types of degenerative cognitive disorders (Alzheimer's disease, mild cognitive impairment, frontotemporal dementia, and dementia associated with Parkinson's disease). The study protocol was based on previous evidence showing a high sensitivity and specificity of the technique even when the panel is limited to some hotspot exons. *Results.* We found variants of the *TREM2* and *APP* genes in three patients; these have been previously identified as pathogenic or likely pathogenic and, therefore, considered "disease causing." In the remaining subjects, the pathogenicity was evaluated according to the guidelines of the American College of Medical Genetics (ACMG). In one patient, the p.R205W variant in the *CHMP2B* gene was found to be likely pathogenic of the disease. A variant in the *CSF1R* and *SERPINI1* genes found in two patients was classified as benign, whereas the other two (in the *GRN* and *APP* genes) were classified as likely pathogenic according to the ACMG. *Conclusions.* Notwithstanding the preliminary value of this study, some rare genetic variants with a probable disease association were detected. Although future application of NGS-based sensors and further replication of these experimental data are needed, this approach seems to offer promising translational perspectives in the diagnosis and management of a wide range of neurodegenerative disorders.

1. Introduction

Dementia comprises a group of degenerative disorders leading to a progressive decline in cognitive function and, in some cases, to changes in behavior and motor impairment, ranging from a slowness in some motor activities to an overt parkinsonism. Dementia affects approximately 47.5 million cases worldwide, with 7.7 million new cases reported annually [1]. Similar to other degenerative disorders, no disease-modifying treatment is available for primary dementia and

an early diagnosis is one of the best predictors of the disease outcome [2, 3]. In this context, an in-depth understanding of the molecular basis for dementia can provide a path for an early diagnosis and the development of new targeted treatment modalities.

As in any other degenerative disease, genetics is a critical risk factor for dementia, with 5-10% of the cases being familial, often attributed to different genes [4, 5]. However, it is likely that evaluating the incidence of familial cases based only on clinical observation leads to an underestimation of the real number of cases, since other medical conditions may be the cause of death for presymptomatic individuals before the onset of neurodegeneration. Furthermore, genetic testing is still not a universally recommended diagnostic tool for dementia [6–8]. Thus, clinicians who choose to use genetic testing often engage in the screening of a small subset of genes, with a focus on the genotype of patients with known variants with high penetrance, rather than on the sequencing of all genes of the disease. These clinical considerations and the high cost of the testing lead to a significant bias in the estimation of the incidence rates, which cannot be considered epidemiologically accurate.

As a general rule, degenerative cognitive and movement disorders may be caused, at least in part, by single, pathogenic variants (monogenic) or by multiple, small effect, variants (oligogenic) that synergistically act to mediate disease expression [9]. In this context, the application of new methods, such as the next-generation sequencing (NGS) techniques, has led to rapid and efficient genetic variant detection along with a reduction of the cost.

Three types of NGS applications are currently available in the clinical setting: the whole-genome sequencing (WGS), the whole-exome sequencing (WES), and the targeted gene panels [10]. While WGS is a nonspecific approach evaluating the entire genome information of an individual, WES targets only the protein-coding regions of the genome, based on the evidence that disease-associated variants are significantly overrepresented in their coding regions. However, although WES is the most frequently used approach, it has some limitations [10]. For instance, its cost still remains high when employing adequate coverage, which makes the cumulative cost for studies using large sample sizes expensive. A second challenge is that this approach often provides an excessive amount of genetic variations from the exome that often overwhelms researchers, especially if a genetic diagnosis is required for genotype-specific treatments. Another issue is that it generates secondary findings that are sometimes unrelated to the disease of interest [11]. Conversely, the use of targeted gene panels focuses on the specific genes potentially underlying the disease under investigation [9].

The recent improvement of technology employed in the genetic testing of neurodegenerative disorders has seen the introduction of powerful parallel DNA sequencing methods that allow researchers to systematically screen individual genomes for the sequencing of DNA variations at base-pair resolution [12]. The technological improvement has also helped to address the question on missing hereditability and to uncover novel potentially pathogenic genetic variants. Therefore, the targeted sequencing of a clinically significant gene panel may lead to an efficient technique that is also cost-time effective when compared to the use of Sanger sequencing [13].

In this pilot study, we used an *ad hoc* NGS-based custom-designed sequencing gene panel to identify genetic variants in patients with degenerative cognitive disorders, namely, Alzheimer's disease (AD), mild cognitive impairment (MCI), frontotemporal dementia (FTD), and dementia associated with Parkinson's disease (PD). In clinical practice, their identification and differential diagnosis are often challenging, and despite the improvements in diagnosis due to biomarker testing, dementias can have overlapping symptoms and may share common genetic background [14]. In this scenario, genetic testing can help the diagnosis, uncover the specific etiology of the disease, provide information for the family, and indicate eligibility for clinical trials.

The tool used in this study allowed to screen for variants in 16 genes implicated in neurodegenerative disease pathways. The study protocol was based on previous evidence by Beck and colleagues [13], who showed a high sensitivity and specificity of the technique even when the panel is limited to some hotspot exons. More work is needed to improve information available in the literature and databases about the pathogenicity and penetrance of variants. For this reason, the further molecular characterization of patients helps to provide additional evidence for the clinical and mutational heterogeneity of dementia and to better define the genotype-phenotype correlation. This is relevant not only for a deeper understanding of dementing processes but also for the genetic counseling and therapeutic approach of patients and relatives.

2. Materials and Methods

2.1. Participants. The genetic panel was tested in 8 patients (4 females) with one of the following clinical diagnosis: AD ($n = 2$), MCI ($n = 2$), FTD ($n = 2$), and PD-associated dementia ($n = 2$). The age at the time of examination ranged from 34 to 87 years, whereas the age range at onset was between 32 and 84 years. Table 1 summarizes the relevant clinical and demographic data and the main laboratory and instrumental findings. All participants were Caucasian and of Sicilian ancestry.

Family history was collected through a detailed interview with a first-degree relative or the proband spouse. The clinical and past medical history of each patient was collected, and all of the available documents related to the affected members (e.g., medical records, certificates, and drug prescriptions) were acquired. In four subjects (patients 2, 4, 5, and 6), a family history of neurodegenerative disease was reported, whereas the other four cases were considered sporadic, as determined by the patient recall and confirmed by the caregivers. All clinical diagnoses were supplied by a trained neurologist, in accordance with the current diagnostic criteria for AD [15], MCI [16], FTD [17], and PD-dementia [18]. Recruitment occurred between July 2017 and October 2018.

All subjects (or their legal guardians) gave their informed consent for inclusion before they participated in the study.

TABLE 1: Patients' clinical-demographic data and main laboratory-instrumental findings.

Patient's number	1	2	3	4	5	6	7	8
Sex	M	M	F	F	F	M	F	M
Age	35	34	69	59	71	66	87	85
Parents' consanguinity	—	+	+	—	—	—	—	—
Family history	—	+ (brother)	+	+ (mother, brother)	+ (father, sister)	+ (not specified)	—	—
Age at onset	34	32	66	54	66	65	82	84
Past medical history	Unremarkable	Traumatic brain injury at 1-year old; smoking and cannabis abuse	Hypothyroidism dyslipidemia; lumbar disc protrusions and spondylosis	Mild hypothyroidism	Hypertension; dyslipidemia	Peripheral L facial nerve palsy; R-side sphenoidal meningioma	Diabetes; chronic ischemic heart disease	Duodenal ulcer; benign prostatic hyperplasia
Clinical presentation	Urge incontinence; behavioral changes (irritability, apathy); gait and speech slowness	Behavioral changes (verbal aggressivity, personal carelessness); speech and memory deficit; disorientation; postural instability with some falls	Motor slowness; L hand tremor; progressive memory deficit; depressed mood; episodes of falls; insomnia with excessive daytime sleepiness	Behavioral changes; obsessive thoughts; delirium and complex visual hallucinations (> mysticism); dysphagia; episodes of loss of consciousness; incontinence	Progressive memory deficit and disorientation; slight behavioral changes (apathy, irritability); lack of insight	Progressive speech disorder, with anomia and deficit of object naming; irritability	Progressive memory deficit; loss of personal independence	Progressive memory deficit and disorientation; loss of personal independence; episodes of falls without loss of consciousness; mild bilateral kinetic tremor of the hands
Clinical signs	Hypomimic face; gait and speech slowness; R>L hand postural tremor; L>R upper limb bradykinesia and plastic hypertonus; diffuse brisk tendon reflexes; bilateral Babinski sign; frontal release signs	Gait disorder; mild cerebellar signs; L-beating nystagmus; bilateral palmomental reflex	Hypomimic face; bradykinesia; parkinsonian gait; head and voice tremor; postural instability; L>R upper limb postural and kinetic tremor; L Hoffman sign; bilateral palmomental reflex	Hypomimic face, drooling; akathisia; dysarthria; dysphagia; mandibular contracture; diffuse plastic hypertonus and bradykinesia; bilateral palmomental reflex	Diffuse brisk tendon reflexes; L Hoffman sign; bilateral palmomental reflex	L facial nerve palsy; bilateral sensory-neural hearing loss, anomia, semantic paraphasia	Frontal release signs; diffuse hypoexcitable tendon reflexes	Limping gait; inconstant R hand tremor; diffuse brisk tendon reflexes; positive frontal release signs
ADL	6/6	4/6	5/6	2/6	6/6	6/6	4/6	3/6
IADL	8/8	5/8	3/8	0/8	8/8	8/8	0/8	0/8
Neuropsychologic evaluation	Moderate major neurocognitive disorder	Severe major neurocognitive disorder with behavioral changes	Mild neurocognitive disorder	Severe major neurocognitive disorder with behavioral changes	Mild neurocognitive disorder	Mild neurocognitive disorder	Severe major neurocognitive disorder	Severe major neurocognitive disorder

Normal

TABLE 1: Continued.

Patient's number	1	2	3	4	5	6	7	8
Extensive laboratory exams		Folate: 7.0 nmol/l (n.v. 10.4-42.4); homocysteine: 37.6 μmol/l (n.v. 3.6-15.0)	Thyroid stimulating hormone: 6.8 mcrUI/ml (n.v. 0.3-4.2)	Erythrocyte sedimentation rate: 50 mm/h (n.v. 2-12)	Low-density lipoprotein: 165 mg/dl (n.v. 0-100)	Prostate specific antigen: 9.2 ng/ml (n.v. 1.0-5.4)	Glycated hemoglobin: 6.1% (n.v. <6.0)	Hemoglobin 10.7 g/dll (n.v. 13.0-17.5); free thyroxine 28.1 pg/ml (n.v. 9.3-17.0)
EEG	Normal	Low-amplitude alpha rhythm; sporadic muscular activations, not correlated with EEG changes	Normal	Normal	Normal	Sporadic slow activity over the frontal and temporal regions	Diffuse slow activity	Diffuse slow activity
Brain MRI	Diffuse cortical and subcortical atrophy (>midbrain, and corpus callosum); ischemic WMLs (> periventricular and frontal regions)	Diffuse cortical and subcortical atrophy (>frontal and temporal lobes, corpus callosum); multiple ischemic WMLs (> periventricular)	Diffuse cortical atrophy; chronic vascular lesion of periventricular frontal regions; mild ischemic WMLs	Diffuse cortical and subcortical atrophy (>frontal and perisylvian regions); mild ischemic WMLs	Moderate cortical atrophy (>frontal and temporal regions); mild ischemic WMLs	R-side parasellar meningioma; moderate diffuse cortical atrophy; mild ischemic WMLs	Diffuse cortical and subcortical atrophy	Diffuse cortical and subcortical atrophy
Other exams	EMG: normal. Multimodal EPs: normal. CSF: total tau: 266 pg/ml (n.v. 136 ± 89). Perfusional SPECT: bilateral frontal, parietal, and temporal hypoperfusion. DAT-scan SPECT: L>R nigrostriatal denervation	EMG: normal. Multimodal EPs: normal. CSF analysis: normal	Unremarkable	EMG: diffuse neurogenic changes (>bilateral deltoid and right biceps brachii muscles); no cranial muscle denervation. Spine MRI: disc protrusion C5-C6, L4-L5, and L5-S1; spondylosis	Transthoracic echocardiogram: L ventricle enlargement	Supra-aortic vessels ultrasound: bilateral carotid artery thickening	Chest X-ray: signs of chronic obstructive pulmonary disease. Transthoracic echocardiogram: L ventricle hypertrophy and moderate mitral valve insufficiency	Chest X-ray: signs of chronic obstructive pulmonary disease. Transthoracic echocardiogram: L ventricle enlargement
Diagnosis at discharge	PD-dementia	FTD	PD-dementia	FTD	MCI	MCI	AD	AD

Legend (in alphabetic order): -=absent/negative; +=present/positive; AD=Alzheimer's disease; ADL=activity of daily living; CSF=cerebrospinal fluid; DAT=dopamine transporter; EEG=electroencephalogram; EPs=evoked potentials; FTD=frontotemporal dementia; F=female; IADL=instrumental activity of daily living; L=left; M=male; MCI=mild cognitive impairment; MRI=magnetic resonance imaging; n.v.=normal values; PD=Parkinson's disease; R=right; SPECT=single-photon emission computed tomography; WMLs=white matter lesions.

The study was conducted in accordance with the Declaration of Helsinki of 1964 and its later amendments, and the protocol was approved by the Ethics Committee of the Oasi Research Institute–IRCCS in Troina, Italy (approval code: 2018/07/18/CE-IRCCS-OASI/14).

2.2. NGS Sequencing. Blood samples were collected from all patients. DNA and plasma were obtained according to standard procedures. Genomic DNA was isolated from lymphocytes using the salt chloroform extraction method, checked for degradation on agarose gel, and quantified by the Qubit 2.0 Fluorometer. The Ion AmpliSeq™ Dementia Research Gene Panel [13] was used to identify genetic variations associated with dementia. This panel contains 214 amplicons in 2 pools.

A polymerase chain reaction amplicon-based library preparation (AmpliSeq Designer software, Life Technologies, CA, USA) was used to screen the following dementia disease genes: *PRNP* (prion protein; Ex2), *APP* (amyloid precursor protein; Ex1, 3, 4, 9, 10, 12, 13, 15-18), *PSEN1* (presenilin 1; Ex2-12), *PSEN2* (presenilin 2; Ex5-8, 13), *GRN* (granulin; Ex1-13), *MAPT* (microtubule-associated protein tau; Ex2, 6-14, coverage 98%), *TREM2* (triggering receptor expressed on myeloid cells 2; Ex1-5), *CHMP2B* (charged multivesicular body protein 2b; Ex5-6), *CSF1R* (colony stimulating factor 1 receptor; Ex12-22), *FUS* (fused in sarcoma; Ex3, 5, 6, 12-15), *ITM2B* (integral membrane protein 2B; Ex6, *coverage* = 98%), *NOTCH3* (notch receptor 3; Ex3-4), *SERPINI1* (serpin family I member 1; Ex2-9), *TARDBP* (TAR DNA binding protein; Ex2-6), *TYROBP* (TYRO protein tyrosine kinase binding protein; Ex1-5), *VCP* (valosin-containing protein; Ex1-17), and *SQSTM1* (sequestosome 1; Ex1, 2-8, *coverage* = 98%), according to Beck and colleagues [13].

Template preparation, clonal amplification, recovery, and enrichment of template-positive Ion Sphere™ Particles and loading of sequencing-ready Ion Torrent semiconductor chips (Ion 314) were performed with the Ion Chef™ System. Sequencing runs were performed using the Ion S5 Sequencing kit (Thermo Fisher Scientific). Data of runs were processed using the Ion Torrent Suite 5.10, Variant Caller 5.10, Coverage Analysis 5.10 (Thermo Fisher Scientific), Ion Reporter (Thermo Fisher Scientific), and/or wANNOVAR tools [19]. DNA sequences were displayed by using Integrated Genomics Viewer [20]. Sanger sequencing was performed to confirm all mutations.

Variants were assessed using the PolyPhen-2, SIFT, MutationTaster, FATHMM, and PROVEAN software tools. Additionally, the CADD database was used to classify variants as harmful or not based on a numerical cut-off value ($>20 = harmful$). We removed all the common variants (*minor allele frequency* > 1%) reported in the public databases 1000 Genome Project and Exome Sequencing. According to these databases, variants can be classified as tolerated, deleterious, benign, neutral, harmful note, and harmful. Finally, based on the American College of Medical Genetics (ACMG) guidelines [21], an evidence of pathogenicity was assigned to each variant identified as follows: 1 (benign), 2 (likely benign), 3 (uncertain significance), 4 (likely pathogenic), and 5 (pathogenic).

3. Results

NGS analysis by using the 16 abovementioned genes panel (*PRNP*, *PSEN1*, *PSEN2*, *APP*, *GRN*, *MAPT*, *TREM2*, *CHMP2B*, *CSF1R*, *FUS*, *ITM2B*, *NOTCH3*, *SERPINI1*, *TARDBP*, *TYROBP*, and *VCP*) was successfully completed in all patients. By using the Ion AmpliSeq™ Dementia Research Gene Panel [13], we saw an average of 98% of bases at >20x coverage. The average read depth per sample was 420x. The number of variants/patient was ~180.

Table 2 illustrates the patients in whom the variants were revealed, as well as the position, gene inheritance pattern, type (splicing, missense, and others), genotype, and which ones were already known. In particular, the variants c.482 +2T>C in the *TREM2* gene [22], the c.C613T in the *CHMP2B* gene [23, 24], and the c.G2137A in the *APP* gene [25] were already known. Conversely, the variants c.G2239A in the *CSF1R* gene, the c.G289A in the *SERPIN1* gene, the c.C110G in the *GRN* gene, and the c.G1604A in the *APP* gene were not previously described.

Table 3 shows the results of the *in silico* analysis of the variants that resulted pathogenic according to the established classification criteria and provided data on the allelic frequency in the general population. All Sanger-sequenced variants were in accordance with the NGS results.

4. Discussion

4.1. Main Findings. The development of NGS sequencing technology has allowed for a rapid and efficient analysis of several genes simultaneously, thus providing significant clinical advantages, especially for the diagnosis of complex diseases with high genetic heterogeneity (i.e., different genes responsible for the same clinical phenotype), such as cognitive impairment and movement disorders.

In this study, we support previous evidence by Beck and colleagues [13] by showing that, although limited to some hotspot exons, the panel has a high sensitivity and specificity. The possibility to screen the main genes involved in dementia, including the early-onset forms, with a good probability of success and at a relatively reduced cost, is the main advantage. On the other hand, the fact that only a few exons in a limited number of genes can be examined is a limitation. The exoma-trios approach, although more expensive, would probably disclose additional results. Nevertheless, prior to ordering genetic testing, clinicians must determine the appropriate genes to test and the best type of genetic test to use. Without this analysis, interpretation of genetic results is difficult. Patients and relatives should be counseled about the benefits and limitations of the different types of genetic tests, so they can make an informed decision about testing.

In our study, the application of a customized panel of 16 dementia-associated genes in 8 patients allowed to identify one or more variants and related pathogenetic role. Some of these variants were not reported before, whereas others were already known. Namely, mutations of the *TREM2* (patients 1 and 2), *CHMP2B* (patient 3), and *APP* (patient 5) genes have already been found to be pathogenic or likely pathogenic in the literature and, therefore, they can be considered "disease

Table 2: Patients' genetic features.

Patient's number	Chromosome	Gene	Inheritance pattern	Mutation type	Variant	Protein	Genotype	Reference	dbSNP number
1	6	TREM2	Autosomal recessive	Splicing	c.482 +2T>C	—	Homozygous	Paloneva et al. [22]	rs386834144
2	6	TREM2	Autosomal recessive	Splicing	c.482 +2T>C	—	Homozygous	Paloneva et al. [22]	rs386834144
3	3	CHMP2B	Autosomal dominant	Missense	c.C613T	p.R205W	Heterozygous	Kim et al. [23] Zhang et al. [24]	rs373536428
4	5	CSF1R	Autosomal dominant	Missense	c.G2239A	p.G747R	Heterozygous	This study	rs41355444
5	21	APP	Autosomal dominant	Missense	c.G2137A	p.A713T	Heterozygous	Carter et al. [25]	rs63750066
6	3	SERPINI1	Autosomal dominant	Missense	c.G289A	p.V97I	Heterozygous	This study	rs61750375
7	17	GRN	Autosomal dominant	Missense	c.C110G	p.A37G	Heterozygous	This study	No data
8	6	APP	Autosomal dominant	Missense	c.G1604A	p.R535H	Heterozygous	This study	No data

causing" [26]. In patient 3, a segregation within the family was not reported, and the same variant has been described also in patients with different phenotypes [23, 24] and not in the general population; therefore, further functional studies are needed.

In the remaining patients, given that the variants were not present in the databases (HGMD, ClinVar), the pathogenicity was evaluated according to the ACMG guidelines [21]. The variants found in patients 4 and 6 (CSF1R and SERPINI1 genes) should be classified as classes 2 and 1, respectively, whereas the other two variants (GRN gene in patient 7 and APP gene in patient 8) should be both classified as class 4. Of note, the missense p.R535H mutation in patient 8 was located in a relevant functional "collagen-binding" domain of the APP protein. In particular, the specific binding of the APP to extracellular matrix molecules suggests that APP regulates cell interactions and has a function as a cell adhesion molecule and/or substrate adhesion molecule [27].

To summarize, four new variants have been identified in our study. While in patients 4 and 6 the variant has been classified as benign or likely benign, thus not playing a significant pathogenic role, in patients 7 and 8, the in silico analysis, the data from CADD_phred, and the absence of the variant in the general population allow to hypothesize a pathogenic role. However, additional functional studies and further data supporting a potential pathogenicity (e.g., allelic frequency in the ethnic population, segregation within the family, effects at the protein level, and protein domain) are needed.

To date, the role for novel variants of unknown significance in both common and rare dementia-associated genes has not been exhaustively elucidated, although some novel, likely pathogenic variants have been recently reported in Italian patients with dementia [28]. In our study, the splicing variant c.482+2T>C was found on the TREM2 gene in patients 1 and 2, who were not relatives, not even distant. Given the prevalence of this variant in Italy and particularly

in the Sicilian population (6/20 alleles, 30%) [22, 29], the occurrence of a "founder effect" might be hypothesized. Further studies with larger samples are necessary, although these data may help in disentangling the role of the genetic variant observed [30].

The present results also support the hypothesis that early-onset dementia may be the result of interconnected mechanisms that lead to neurodegeneration where the implication of the same genes can be seen in one or more systems [31, 32]. Most of the genes tested here play a pivotal role in multiple cellular pathways rather than being involved in a single form of dementia. Some of these pathways include the energy metabolism, the phospholipid and cholesterol efflux, the intracellular and vesicle trafficking, and the neuronal-viability and survival that are usually compromised in every neurodegenerative process and involve several other molecular actors [32].

This implicates a potential additive/synergic effect in early-onset forms of dementia associated with the inter- and intrafamilial expressivity, as recently demonstrated by using a NGS-based analysis in patients with early-onset dementia [12]. For instance, the TREM2 gene, coding for a microglial lipid sensor that interacts with several factors involved in the metabolism of lipids, could decrease the occurrence threshold of dementia [33]. This means that TREM2 mutation can cause an aberrant innate immune cell signaling that contributes to several neurodegenerative pathway initiations and propagations [12], including those involved in FTD and PD-dementia [32].

It also appears that early-onset cases are associated with rare variants or risk alleles, which can help in correlating genotype and phenotype. Overall, these findings strengthen the use of an exome/whole NGS approach and stimulate studies on larger samples and with expanded panels of candidate genes. In the specific case of the AD patient carrying the GRN mutation, since missense mutations do not affect the

TABLE 3: Results of the *in silico* analysis, along with evidence of pathogenicity.

Patient's number	Gene	Variant	SIFT	PolyPhen-2 HDIV	MutationTaster	FATHMM	PROVEAN	CADD_phred	1000 Genomes (allele frequency)	Pathogenicity (ACMG guidelines) [21]	ClinVar
1	TREM2	c.482 +2T>C							No data	5	Likely pathogenic
2	TREM2	c.482 +2T>C							No data	5	Likely pathogenic
3	CHMP2B	c.C613T							No data	4	No data
4	CSF1R	c.G2239A	T	B	N	D	N	8.944	0.001	2	Likely benign
5	APP	c.G2137A							No data	5	Likely pathogenic
6	SERPINI1	c.G289A	T	B	N	D	N	0.024	0.002	1	Benign/likely benign
7	GRN	c.C110G	T	D	N	T	N	20.4	No data	4	No data
8	APP	c.G1604A	T	D	D	T	N	28.5	No data	4	No data

Legend: A=harmful note; B=benign; D=deleterious; N=neutral; T=tolerated; ACMG=American College of Medical Genetics; 1=benign; 2=likely benign; 3=uncertain significance; 4=likely pathogenic; 5=pathogenic.

progranulin levels, a pathogenic role seems unlikely. However, as no functional study has been performed, we cannot exclude a pathogenic role other than "loss of function", being this gene implicated in the pathophysiological mechanisms leading to AD [12].

The NGS-based custom-designed resequencing panel used in our study has proven to be a rapid and accurate diagnostic sensor for the in-parallel screening of several neurodegenerative genes, thus allowing to identify disease-specific risk markers and potentially overlapping pathways across the most common dementing diseases. Moreover, after the library preparation, we could analyze the genetic data for 24 samples in less than 30 h.

Finally, data from targeted NGS panels may provide further insights on the genes implicated in neuronal plasticity and microglial neurogenesis. In particular, an intriguing relationship between some causative gene expressions and changes in synaptic morphology and neuronal plasticity has recently been identified. For instance, the *APP* gene family and its products are able to modulate phenomena of hippocampal long-term plasticity [34], as well as the microglial *TREM2* gene might have a role in the synaptic loss depending on the AD stage [35], whereas the *CHMP2* gene regulates synaptic plasticity in dendritic spines [36]. Accordingly, genetic studies could pave the way for the *in vivo* and "real-time" functional evaluation of cortical circuits by using non-invasive brain stimulation techniques (NIBS) [37–39] and even for the NIBS-related neurobiological after-effects (gene activation/regulation, *de novo* protein expression, morphological changes, changes in intrinsic firing properties and modified network activities resulting from changed inhibition, homeostatic processes, and glial function) [40–42]. In patients with causative mutations, genetic findings, coupled with clinical, psychocognitive, neuroradiological, and electrophysiological data, will allow to adopt preventive strategies in the presymptomatic stage, to start treatment since the very early stages of the disease [43–46] and to multidimensionally monitor the disease progression [47, 48].

4.2. Limitations. The main limitation of this study is its small sample size that precludes data generalization and further conclusions and, therefore, it should be considered preliminary.

Despite its efficiency and rapidity, NGS approaches have some limitations. One of these is that the sensor cannot discover novel disease loci, since it only captures variants within the selected genes and related exons. Another limitation is that it cannot capture multinucleotide repeat expansions in genes, which is, however, a limitation that characterizes all NGS platforms [49]. Indeed, the current NGS methods cannot help in the detection of some neurological conditions, such as Huntington's disease, Friedreich's ataxia, Fragile X syndrome, myotonic dystrophy, and a subset of spinocerebellar ataxias (diagnoses not included in the present study), that are caused by multinucleotide repeat expansions [50, 51]. Further studies that aim at the identification of new mutations in genes apart from the ones that the exons describe or those located in the conventional splicing sites are needed.

A third limitation lies in the fact that genetic penetrance and expressivity differ because of the modifier genes, allelic variations, environmental factors, and complex environmental and genetic interactions, thus explaining, at least in part, the phenotype differences observed in these patients. Another caveat is that *in silico* analyses require cautious handling and further evidence within the clinical and diagnostic setting to predict the effects produced by each variant needed to refuse or support the pathogenetic role of new variants in the daily clinical practice [30].

Finally, as commonly observed in this type of study, the pathogenicity of genetic variants in late-onset diseases through mechanisms of segregation of the variant within the family is complex and often challenging for different reasons (e.g., the unavailability of DNA from the parents of the patient or a late onset of the clinical phenotype in other family members, such as siblings or cousins). In the present study, the sequencing was not performed in the family members of the four patients with family history of dementia and, therefore, we could not verify whether the affected relatives were carriers of the same variants. The verification of the role played by polygenic risk variants in dementia requires the implementation of a systematic screening of both rare and common variants in several dementia-associated genes and in prospective cohorts.

Notwithstanding the abovementioned limitations and the complex nature of neurodegenerative process and progression, we were able to detect some rare variants with a probable, but not absolutely certain, disease association, based on allele frequency in the general population and the predictive score of multiple *in silico* software. As the etiology of degenerative diseases is often heterogeneous and multiple factors (e.g., dietary intake, traumatic brain injury, vascular disease, infections, or toxin exposure) can confer a variable risk to the disease onset and course, these genetic variants (especially the novel variants) need future validations to determine their effect size and the contribution to disease. Of particular interest are variants in genes with multiple disease associations, as they may provide clues on the development of innovative therapies. This further confirms the evidence that dementia-associated genes do have pleiotropic effects on different neurodegenerative disorders.

5. Conclusions

Notwithstanding the preliminary value and the limitations of the study, the "targeted gene" panel used here might allow to increase the number of potentially dementia-related variants and to extend the clinical features associated with genetic variants described in the *TREM2, CHMP2B, APP*, and *GRN* genes. The development and continuous advances of NGS technologies have opened an exciting window on the molecular diagnostics of several diseases caused by mutations of a large number of genes. Translationally, this technique has demonstrated reliability and accuracy, along with a significant reduction in DNA sequencing costs compared to tests based on the Sanger method. The future application of NGS-based sensors and the further replication of these experimental data will replace the so-called "gene-by-gene"

approach with a "panel of genes" strategy that offers promising perspectives in the diagnosis and management of dementia and other neurodegenerative disorders.

Data Availability

The authors declare that all the data regarding this submission are fully available within the manuscript.

Conflicts of Interest

The authors declare that they have no known competing financial interests or personal relationships that could have appeared to influence the work reported in this paper.

Authors' Contributions

GL, FC, and MV designed the study; MV, FIIC, MT, and TM collected the data; FIIC, MT, RSS, and MC interpreted the data; GL, FC, RB, TM, and RF prepared and revised the manuscript; MC, RB, and RF conducted literature search; and RSS and RF collected funds. All authors approved the submitted version and agreed to be personally accountable for the author's own contributions and ensuring questions related to the accuracy or integrity of any part of the work. Giuseppe Lanza and Francesco Calì equally contributed to this work.

Acknowledgments

References

[1] The Lancet Neurology, "WHO takes up the baton on dementia," *The Lancet Neurology*, vol. 14, no. 5, p. 455, 2015.

[2] L. E. Hebert, J. Weuve, P. A. Scherr, and D. A. Evans, "Alzheimer disease in the United States (2010-2050) estimated using the 2010 census," *Neurology*, vol. 80, no. 19, pp. 1778–1783, 2013.

[3] L. Robinson, E. Tang, and J. P. Taylor, "Dementia: timely diagnosis and early intervention," *BMJ*, vol. 350, no. jun15 14, 2015.

[4] R. Guerreiro, J. Bras, J. Hardy, and A. Singleton, "Next generation sequencing techniques in neurological diseases: redefining clinical and molecular associations," *Human Molecular Genetics*, vol. 23, no. R1, pp. R47–R53, 2014.

[5] J. D. Rohrer, A. M. Isaacs, S. Mizielinska et al., "_C9orf72_ expansions in frontotemporal dementia and amyotrophic lateral sclerosis," *Lancet Neurology*, vol. 14, no. 3, pp. 291–301, 2015.

[6] J. S. Goldman, S. E. Hahn, J. W. Catania et al., "Genetic counseling and testing for Alzheimer disease: Joint practice guidelines of the American College of Medical Genetics and the National Society of Genetic Counselors," *Genetics in Medicine*, vol. 13, no. 6, pp. 597–605, 2011.

[7] D. Grimes, J. Gordon, B. Snelgrove et al., "Supplement 4: Canadian Guidelines on Parkinson's Disease," *Canadian Journal of Neurological Sciences / Journal Canadien des Sciences Neurologiques*, vol. 39, no. S4, pp. S1–S30, 2012.

[8] M. J. Strong, G. M. Grace, M. Freedman et al., "Consensus criteria for the diagnosis of frontotemporal cognitive and behavioural syndromes in amyotrophic lateral sclerosis," *Amyotrophic Lateral Sclerosis*, vol. 10, no. 3, pp. 131–146, 2009.

[9] S. M. K. Farhan, O. N. D. R. I. Investigators, A. A. Dilliott et al., "The ONDRISeq panel: custom-designed next-generation sequencing of genes related to neurodegeneration," *NPJ Genomic Medicine*, vol. 1, no. 1, 2016.

[10] S. M. K. Farhan and R. A. Hegele, "Exome sequencing: new insights into lipoprotein disorders," *Current Cardiology Reports*, vol. 16, no. 7, p. 507, 2014.

[11] R. C. Green, J. S. Berg, W. W. Grody et al., "ACMG recommendations for reporting of incidental findings in clinical exome and genome sequencing," *Genetics in Medicine*, vol. 15, no. 7, pp. 565–574, 2013.

[12] C. Bonvicini, C. Scassellati, L. Benussi et al., "Next Generation Sequencing Analysis in Early Onset Dementia Patients," *Journal of Alzheimer's Disease*, vol. 67, no. 1, pp. 243–256, 2019.

[13] J. Beck, A. Pittman, G. Adamson et al., "Validation of next-generation sequencing technologies in genetic diagnosis of dementia," *Neurobiology of Aging*, vol. 35, no. 1, pp. 261–265, 2014.

[14] J. S. Goldman and V. M. Van Deerlin, "Alzheimer's disease and frontotemporal dementia: the current state of genetics and genetic testing since the advent of next-generation sequencing," *Molecular Diagnosis & Therapy*, vol. 22, no. 5, pp. 505–513, 2018.

[15] G. M. McKhann, D. S. Knopman, H. Chertkow et al., "The diagnosis of dementia due to Alzheimer's disease: Recommendations from the National Institute on Aging-Alzheimer's Association workgroups on diagnostic guidelines for Alzheimer's disease," *Alzheimer's & Dementia*, vol. 7, no. 3, pp. 263–269, 2011.

[16] M. S. Albert, S. T. DeKosky, D. Dickson et al., "The diagnosis of mild cognitive impairment due to Alzheimer's disease: Recommendations from the National Institute on Aging-Alzheimer's Association workgroups on diagnostic guidelines for Alzheimer's disease," *Alzheimer's & Dementia*, vol. 7, no. 3, pp. 270–279, 2011.

[17] L. Chare, J. R. Hodges, C. E. Leyton et al., "New criteria for frontotemporal dementia syndromes: clinical and pathological diagnostic implications," *Journal of Neurology, Neurosurguery and Psychiatry*, vol. 85, no. 8, pp. 865–870, 2014.

[18] L. F. R. Vasconcellos and J. S. Pereira, "Parkinson's disease dementia: diagnostic criteria and risk factor review," *Journal of Clinical and Experimental Neuropsychology*, vol. 37, no. 9, pp. 988–993, 2015.

[19] X. Chang and K. Wang, "WANNOVAR: annotating genetic variants for personal genomes via the web," *Journal of Medical Genetics*, vol. 49, no. 7, pp. 433–436, 2012.

[20] H. Thorvaldsdottir, J. T. Robinson, and J. P. Mesirov, "Integrative genomics viewer (IGV): high-performance genomics data visualization and exploration," *Briefings in Bioinformatics*, vol. 14, no. 2, pp. 178–192, 2013.

[21] S. Richards, on behalf of the ACMG Laboratory Quality Assurance Committee, N. Aziz et al., "Standards and guidelines for

the interpretation of sequence variants: a joint consensus recommendation of the American College of Medical Genetics and Genomics and the Association for Molecular Pathology," *Genetics in Medicine*, vol. 17, no. 5, pp. 405–423, 2015.

[22] J. Paloneva, T. Manninen, G. Christman et al., "Mutations in two genes encoding different subunits of a receptor signaling complex result in an identical disease phenotype," *The American Journal of Human Genetics*, vol. 71, no. 3, pp. 656–662, 2002.

[23] E.-J. Kim, Y.-E. Kim, J.-H. Jang et al., "Analysis of frontotemporal dementia, amyotrophic lateral sclerosis, and other dementia-related genes in 107 Korean patients with frontotemporal dementia," *Neurobiology of Aging*, vol. 72, pp. 186.e1–186.e7, 2018.

[24] H. Zhang, W. Cai, S. Chen et al., "Screening for possible oligogenic pathogenesis in Chinese sporadic ALS patients," *Amyotrophic Lateral Sclerosis & Frontotemporal Degeneration*, vol. 19, no. 5-6, pp. 419–425, 2018.

[25] D. A. Carter, E. Desmarais, M. Bellis et al., "More missense in amyloid gene," *Nature Genetics*, vol. 2, no. 4, pp. 255-256, 1992.

[26] D. W. Sirkis, L. W. Bonham, R. E. Aparicio et al., "Rare TREM2 variants associated with Alzheimer's disease display reduced cell surface expression," *Acta Neuropathologica Communications*, vol. 4, no. 1, p. 98, 2016.

[27] D. Beher, L. Hesse, C. L. Masters, and G. Multhaup, "Regulation of amyloid protein precursor (APP) binding to collagen and mapping of the binding sites on APP and collagen type I," *The Journal of Biological Chemistry*, vol. 271, no. 3, pp. 1613–1620, 1996.

[28] A. Bartoletti-Stella, S. Baiardi, M. Stanzani-Maserati et al., "Identification of rare genetic variants in Italian patients with dementia by targeted gene sequencing," *Neurobiology of Aging*, vol. 66, no. 180, pp. 180.e23–180.e31, 2018.

[29] A. Salmaggi, E. Maccagnano, A. Musso, L. Di Lena, J. Paloneva, and A. Boiardi, "An Italian family with Nasu-Hakola disease," *Journal of Neurology*, vol. 250, no. 7, pp. 878–880, 2003.

[30] F. Cali, M. Cantone, F. I. I. Cosentino et al., "Interpreting genetic variants: hints from a family cluster of Parkinson's disease," *Journal of Parkinson's Disease*, vol. 9, no. 1, pp. 203–206, 2019.

[31] G. Lanza, M. Cantone, S. Musso, E. Borgione, C. Scuderi, and R. Ferri, "Early-onset subcortical ischemic vascular dementia in an adult with mtDNA mutation 3316G>A," *Journal of Neurology*, vol. 265, no. 4, pp. 968-969, 2018.

[32] M. Ciani, C. Bonvicini, C. Scassellati et al., "The missing heritability of sporadic frontotemporal dementia: new insights from rare variants in neurodegenerative candidate genes," *International Journal of Molecular Sciences*, vol. 20, no. 16, p. 3903, 2019.

[33] M. Colonna and Y. Wang, "TREM2 variants: new keys to decipher Alzheimer disease pathogenesis," *Nature Reviews Neuroscience*, vol. 17, no. 4, pp. 201–207, 2016.

[34] S. Ludewig and M. Korte, "Novel insights into the physiological function of the APP (gene) family and its proteolytic fragments in synaptic plasticity," *Frontiers in Molecular Neuroscience*, vol. 9, 2017.

[35] L. Sheng, M. Chen, K. Cai et al., "Microglial Trem2 induces synaptic impairment at early stage and prevents amyloidosis at late stage in APP/PS1 mice," *The FASEB Journal*, vol. 33, no. 9, pp. 10425–10442, 2019.

[36] R. Chassefeyre, J. Martinez-Hernandez, F. Bertaso et al., "Regulation of postsynaptic function by the dementia-related ESCRT-III subunit CHMP2B," *Journal of Neuroscience*, vol. 35, no. 7, pp. 3155–3173, 2015.

[37] R. Bella, M. Cantone, G. Lanza et al., "Cholinergic circuitry functioning in patients with vascular cognitive impairment - no dementia," *Brain Stimulation*, vol. 9, no. 2, pp. 225–233, 2016.

[38] G. Lanza, R. Bella, S. Giuffrida et al., "Preserved transcallosal inhibition to transcranial magnetic stimulation in nondemented elderly patients with leukoaraiosis," *BioMed Research International*, vol. 2013, Article ID 351680, 5 pages, 2013.

[39] M. Pennisi, G. Lanza, M. Cantone et al., "Cortical involvement in celiac disease before and after long-term gluten-free diet: A Transcranial Magnetic Stimulation study," *PloS One*, vol. 12, no. 5, p. e0177560, 2017.

[40] G. Cirillo, G. Di Pino, F. Capone et al., "Neurobiological aftereffects of non-invasive brain stimulation," *Brain Stimulation*, vol. 10, no. 1, pp. 1–18, 2017.

[41] R. Bordet, R. Ihl, A. D. Korczyn et al., "Towards the concept of disease-modifier in post-stroke or vascular cognitive impairment: a consensus report," *BMC Medicine*, vol. 15, no. 1, p. 107, 2017.

[42] F. Fisicaro, G. Lanza, A. A. Grasso et al., "Repetitive transcranial magnetic stimulation in stroke rehabilitation: review of the current evidence and pitfalls," *Therapeutic Advances in Neurological Disorders*, vol. 12, article 175628641987831, 2019.

[43] A. Benussi, M. Cosseddu, I. Filareto et al., "Impaired long-term potentiation–like cortical plasticity in presymptomatic genetic frontotemporal dementia," *Annals of Neurology*, vol. 80, no. 3, pp. 472–476, 2016.

[44] M. Cantone, G. Di Pino, F. Capone et al., "The contribution of transcranial magnetic stimulation in the diagnosis and in the management of dementia," *Clinical Neurophysiology*, vol. 125, no. 8, pp. 1509–1532, 2014.

[45] G. Lanza, B. Lanuzza, D. Aricò et al., "Impaired short-term plasticity in restless legs syndrome: a pilot rTMS study," *Sleep Medicine*, vol. 46, pp. 1–4, 2018.

[46] R. Bella, R. Ferri, G. Lanza et al., "TMS follow-up study in patients with vascular cognitive impairment-no dementia," *Neuroscience Letters*, vol. 534, pp. 155–159, 2013.

[47] L. Vinciguerra, G. Lanza, V. Puglisi et al., "Update on the neurobiology of vascular cognitive impairment: from lab to clinic," *International Journal of Molecular Sciences*, vol. 21, no. 8, p. 2977, 2020.

[48] M. Pennisi, A. Bramanti, M. Cantone, G. Pennisi, R. Bella, and G. Lanza, "Neurophysiology of the "Celiac Brain": disentangling gut-brain connections," *Frontiers in Neuroscience*, vol. 11, no. 11, 2017.

[49] A. B. Singleton, "Exome sequencing: a transformative technology," *The Lancet Neurology*, vol. 10, no. 10, pp. 942–946, 2011.

[50] A. R. La Spada, H. L. Paulson, and K. H. Fischbeck, "Trinucleotide repeat expansion in neurological disease," *Annals of Neurology*, vol. 36, no. 6, pp. 814–822, 1994.

[51] J. R. Stevens, E. E. Lahue, G.-M. Li, and R. S. Lahue, "Trinucleotide repeat expansions catalyzed by human cell-free extracts," *Cell Research*, vol. 23, no. 4, pp. 565–572, 2013.

Research Article

A Brain Network Constructed on an L1-Norm Regression Model Is More Sensitive in Detecting Small World Network Changes in Early AD

Hao Liu,[1] Haimeng Hu,[2] Huiying Wang,[3] Jiahui Han,[4] Yunfei Li,[5] Huihui Qi,[6] Meimei Wang,[6] Sisi Zhang,[6] Huijin He,[2] and Xiaohu Zhao [5,6]

[1]*Department of Radiology, Shanghai Jiao Tong University Affiliated Sixth People's Hospital, Shanghai, China*
[2]*Department of Imaging, Huashan Hospital, Fudan University, Shanghai, China*
[3]*Ophthalmology Department, Huashan Hospital, Fudan University, Shanghai, China*
[4]*College of Optical and Electronic Technology, China Jiliang University, Hangzhou, China*
[5]*Department of Imaging, The Fifth People's Hospital of Shanghai, Fudan University, Shanghai, China*
[6]*Department of Imaging, Shanghai Tongji Hospital, Tongji University School of Medicine, Tongji University, Shanghai, China*

Correspondence should be addressed to Xiaohu Zhao; xhzhao999@263.net

Most previous imaging studies have used traditional Pearson correlation analysis to construct brain networks. This approach fails to adequately and completely account for the interaction between adjacent brain regions. In this study, we used the L1-norm linear regression model to test the small-world attributes of the brain networks of three groups of patients, namely, those with mild cognitive impairment (MCI), Alzheimer's disease (AD), and healthy controls (HCs); we attempted to identify the method that may detect minor differences in MCI and AD patients. Twenty-four AD patients, 33 MCI patients, and 27 HC elderly subjects were subjected to functional MRI (fMRI). We applied traditional Pearson correlation and the L1-norm to construct the brain networks and then tested the small-world attributes by calculating the following parameters: clustering coefficient (Cp), path length (Lp), global efficiency (Eg), and local efficiency (Eloc). As expected, L1 could detect slight changes, mainly in MCI patients expressing higher Cp and Eloc; however, no statistical differences were found between MCI patients and HCs in terms of Cp, Lp, Eg, and Eloc, using Pearson correlation. Compared with HCs, AD patients expressed a lower Cp, Eloc, and Lp and an increased Eg using both connectivity metrics. The statistical differences between the groups indicated the brain networks constructed by the L1-norm were more sensitive to detect slight small-world network changes in early stages of AD.

1. Introduction

The human brain network has been proven to possess small-world properties that confer several advantages [1, 2] including high local and global efficiency (Eloc and Eg, respectively) in information communication [3], optimal synchronization of neural activity among different brain regions via central hubs, and most importantly, protection of the brain from random failure through redundant densely neighbored connections and from targeted attacks under disease conditions, due to high resilience conferred by high centrality and clustering [4]. These brain neuronal networks are well balanced and highly efficient, with local specialization and global integration [5].

Alzheimer's disease (AD) is the most common type of dementia; it is a neurodegenerative disease characterized by memory loss in its early stages, followed by a progressive decline in other behavioral and cognitive functions [6]. Mild cognitive impairment (MCI) may be a transitional state between healthy aging and AD, according to neuropathological studies [7, 8], and an estimated 10–15% of MCI patients convert to AD each year [9].

AD has been considered a disconnection syndrome according to research by Delbeuck et al., implying that a

functional disconnection between distant brain areas could plausibly explain the cognitive dysfunction in AD patients [10], and changes in small-world properties may reflect this disconnection. The clustering coefficient (Cp) reflects the connection status of the entire network, and the Eloc of the network is described from the perspective of local information transmission. The shortest path length (Lp) represents the efficiency of the overall information transmission of the network, and the Eg is a more intuitive measure of the rate of information transmission across the network. Alterations in small-world properties, particularly abnormal regions or global changes, may serve as potential biomarkers for early detection, diagnosis, and treatment evaluation [11]. Characterizing the underlying architecture of brain networks may contribute comprehensive insights into the pathogenesis of network dysfunctional mechanisms in AD [12].

Many researchers have explored small-world brain network properties in patients with AD and found inconsistent results. Liu [13] and others found that patients with AD demonstrated the largest clustering coefficients compared to MCI patients and healthy controls. However, YaPeng and colleagues [14] found that there was a decline in clustering coefficients in AD patients compared with healthy controls. According to a study by Lo et al. [15], AD patients have an increased Lp and decreased Eg in the white matter network. It is worth noting that studies on the altered brain network pattern in AD patients have not produced consistent results till date; this may be attributed to differences in the disease stages in patients, analytical approaches, and imaging modalities [16]. In this study, we speculated that the analytical method may explain the differences in the results to a certain extent.

The majority of previous brain network studies have been based on threshold correlation, to localize the focal regions of high connectivity [17–19]. A typical method is Pearson correlation analysis, which constructs a time-series correlation matrix for each study participant, and then calculates the Pearson correlation coefficient for the brain regions of each participant. A correlation coefficient value closer to 1 indicates high synchronicity between the two brain regions. The correlation is used as a measure of network connectivity similarity between two regions; however, the main limitation of correlation-based connectivity analyses is that it fails to consider the interaction between adjacent regions [20]. In addition to Pearson correlation, diverse methods are available for analyzing the similarity in fMRI data (between pairs of time series and in a multivariate fashion); these include partial correlation and mutual information. However, both methods have certain limitations. First, although partial correlation is a useful measure for removing confounding effects in highly corrected networks after factoring out indirect edges [21], it is obviously subject to the number of regions, which must be smaller than the length of the time series owing to the inverse covariance matrix [22]; therefore, it is not used as extensively as the Pearson correlation. More importantly, it has been demonstrated that the Pearson correlation is more valid and reliable than the partial correlation [23]. Second, mutual information is also a powerful method, since it is sensitive in disclosing frequency-specific couplings;

therefore, it is usually applied in the exploration of different characteristics among different frequency bands of magneto-encephalography or electroencephalography [23]. Additionally, mutual information can reflect both, linear and nonlinear dependencies [24]. In the present study, we used an L1-norm regression model to construct a brain network, which is also called sparse representation-based brain network construction [20, 21, 25]. The L1-norm regression model fully considers the interaction between brain regions when calculating the brain functional network. By using this regression model, a sparse representation of brain connectivity can be obtained with only a few significant connections. The contributions from insignificant or spurious connections are nullified, making it relatively easier to interpret the constructed sparse connectivity. The linear regression model enables a brain region to be represented (in terms of a time series) by the linear combination of other brain regions, with the contribution of every region reflected by the magnitude of the regression coefficient (or connection strength). This provides insight into the correlation between the specified brain region and the rest of the regions, by filtering out the insignificant or spurious connections; this has been exploited in some previous studies. For instance, Wee et al. [20] and Li et al. [25] proved that the L1-norm regression networks have greater sensitivity and higher classification accuracy in identifying patients, and Lee et al. [21] utilized the L1-norm penalty to explore the differences in other network characteristics (number of edges and clusters) within a lobe and between lobes for comparing children with autism spectrum disorders with pediatric control subjects. However, in the first two cases, they concentrated on the classification accuracy via the support vector machine, instead of studying the characteristics of small-world networks and the meaning of the changed parameters of networks in patients. In this study, we focused on studying the differences in parameters of small-world networks constructed by both Pearson correlation and L1-norm regression; the differences were evaluated between the normal subjects and patients with AD and MCI, with the purpose of providing some clues to the understanding of these conditions.

Most previous research used the network methods to construct the network, and some of which focused on classification to patients and normal controls. In the present study, we applied two network construction methods in graph theoretical analysis with statistical comparisons on the brain network attributes. The statistical comparison of brain network properties is just as important as the classification papers as it can provide empirical evidence of disease-related changes and help to reveal which regions are more likely to be altered in the future (by using region-wise graph theoretical metrics).

2. Materials and Methods

2.1. Subjects and Image Acquisition. Our study was approved by the Ethics committee of Shanghai Huashan Hospital. A total of 82 subjects were enrolled from this hospital; all participants were categorized into three groups: healthy controls (HCs) ($n = 27$), patients with MCI ($n = 37$), and patients with

TABLE 1: Demographics and clinical information.

Characteristics	HC ($n = 27$)	MCI ($n = 33$)	AD ($n = 24$)	P
Age	63.74 ± 7.80	68.00 ± 9.89	67.54 ± 10.48	0.166[a]
Female/male	11/16	22/11	13/11	0.133[b]
MMSE	28.84 ± 1.19	26.61 ± 1.66	21.46 ± 1.67	<0.001[a]

Data are presented as the means ± standard deviations (SD). [a]The P value was obtained using one-way ANOVA. [b]The P value was obtained using the Pearson chi-squared test.

AD ($n = 28$). AD patients were diagnosed by a qualified neurologist using criteria for amnestic AD, which include a culturally adapted Chinese version of the Mini-Mental State Examination (CM-MMSE) scores of between 12 and 27 (inclusive) and clinical dementia rating (CDR) scores of 1 or 2. MCI patients had MMSE scores of between 23 and 30 (inclusive) and CDR scores of 0.5 or 1, and the HCs had MMSE scores of between 26 and 30 (inclusive) and CDR scores of 0. The data for 8 subjects (4 patients each, with AD and MCI) were excluded owing to excessive motion. Details regarding the clinical and demographic data of the remaining 74 subjects are shown in Table 1; there were no significant differences among the three groups in terms of gender or age.

All subjects underwent whole-brain resting-state functional magnetic resonance imaging (fMRI) with a 3.0 T Siemens Verio scanner. Resting-state BOLD functional fMRI data were collected using an echo-planar imaging (EPI) sequence with the following scanning parameters: TR = 2000 ms, TE = 35 ms, FOV = 25.6 cm × 25.6 cm, flip angle = 90°, matrix size = 64 × 64, slices = 33, and slice thickness = 4 mm, with no slice gap. Subjects were instructed to stay awake, keep their eyes open, and minimize head movement; no other instructions were provided.

2.2. Image Analysis

2.2.1. Data Preprocessing. Unless specifically stated otherwise, all preprocessing was performed using statistical parametric mapping (SPM8, http://www.fil.ion.ucl.ac.uk/spm). The first 5 images were discarded considering the magnetization equilibrium, and the remaining 155 images were corrected for the acquisition time delay among different slices. The images were then realigned to the first volume for head-motion correction. The fMRI images were further spatially normalized to the Montreal Neurological Institute (MNI) EPI template and were resampled to a 2 mm cubic voxel. Several sources of spurious variance including the estimated motion parameters, linear drift, and average time series in the cerebrospinal fluid, and white matter regions were removed from the data through linear regression. Finally, temporal band-pass filtering (0.03-0.06 HZ) was performed to reduce the effects of low-frequency drift and high-frequency noise [26, 27].

The time course of head motion was obtained by estimating the translations in each direction and the angular rotations around each axis for each of the 155 consecutive volumes. All the subjects included in this study exhibited a maximum displacement of less than 3 mm (smaller than the size of a voxel in plane) at each axis and an angular motion of less than 3 degrees for each axis.

2.3. Brain Network Construction

2.3.1. Anatomical Parcellation. The registered fMRI data were segmented into 90 regions (45 for each hemisphere) using an automated anatomical labeling template [28, 29], which has been used in several previous studies [26]. For each subject, a representative time series of each individual region was then obtained by simply averaging the fMRI time series over all voxels in this region.

2.3.2. Brain Networks Constructed through Pearson Correlation Analysis. The Pearson correlation coefficients of each area were calculated for each pair of 90 functionally connected regions. Considering the brain regions as a set of nodes and the correlation coefficients as signed weights on the set of edges, the functional connectivity examines interregional correlations in neuronal variability [25]. The sparse brain functional connectivity of the ith and jth ROI can be solved using the following formula:

$$ r\left(x_i, x_j\right) = \frac{\sum_{t=1}^{T}\left[x_i(t) - <x_i>\right]\left[x_j(t) - <x_j>\right]}{\sqrt{\sum_{t=1}^{T}\left[x_i(t) - <x_i>\right]^2 \sum_{t=1}^{T}\left[x_j(t) - <x_j>\right]^2}}, \quad (1) $$

where T is the total number of time points, x_i is the time series of the ith ROI, $x_i(t)$ is the tth time point of the ith ROI, x_i is the average of the time series of the ith subject, $<x_i>$ is the mean time series of the ith ROI, and $r(x_i, x_j)$ is the weight vector that quantifies the degree of influence of the ith ROI to the jth ROI given that $i \neq j$.

The absolute r values were then converted into a binary connection matrix to construct a graphic model of a brain network.

All other considered topological properties were calculated using Gretna software. They included the small-worldliness, Cp, Lp, Eg, and Eloc; each of which has previously been described and used in several studies. Table 2 provides an overview of the parameters and their meanings in brain functional networks.

2.3.3. Brain Networks Constructed through L1-Norm Linear Regression Model [22]. In order to provide an adequately complete interaction between many brain regions, we forced the inferred connectivity networks via L1-norm regularization. Using a total of M ROIs, the regional mean time series of the pth ROI for the nth subject, γ_p^n, is a response vector that

TABLE 2: Statistical difference in small-world parameters through the Pearson correlation analysis and the sparse L1-norm regularization method.

Small-world parameter	Cp	Lp	Eg	Eloc	Sigma	Lambda	Gamma
HCs & MCI Pearson	×	×	×	×	×	×	√
HCs & MCI L1-norm	√	×	×	√	√	√	√
HCs & AD Pearson	√	√	√	√	×	√	√
HCs & AD L1-norm	√	√	√	√	√	√	√

"×" implies no statistical difference between two groups at any threshold. "√" implies a statistical difference ($P < 0.05$) between two groups at certain thresholds.

can be estimated as a linear combination of time series of other ROIs, as follows:

$$\gamma_p^n = A_p^n \alpha_p^n + e_p^n, \qquad (2)$$

where e_p^n is the error; $\gamma_p^n = [\gamma_p^n(1); \gamma_p^n(2; \cdots; \gamma_p^n(T)]$ with T being the number of time points in the time series; $A_p^n = \gamma_1^n, \cdots, \gamma_{p-1}^n, \gamma_{p+1}^n, \cdots, \gamma_M^n$ is a data matrix of the pth ROI (all time series except for the pth ROI), and $\alpha_p^n = \alpha_1^n; \cdots; \alpha_{p-1}^n; \alpha_{p+1}^n; \cdots; \alpha_M^n$ is the weight vector that quantifies the degree of influence of other ROIs to the pth ROI. The sparse brain functional connectivity modeling of the nth subject and pth ROI can be considered a standard L1-norm-regularized optimization problem, with the following objective function:

$$f\left(\alpha_p^n\right) = \frac{1}{2}\left\|\gamma_p^n - A_p^n \alpha_p^n\right\|_2^2 + \lambda\left\|\alpha_p^n\right\|_1, \qquad (3)$$

where $\lambda > 0$ is the regularization parameter controlling the "sparsity" of the model, with a higher value corresponding to a sparser model; i.e., more elements in α_p^n are zero. λ was preselected.

2.4. Small-World Properties of the Brain Functional Networks Based on Two Methods. All the considered small-world properties including the Cp, Lp, Eg, and Eloc were calculated using Gretna software. Statistical comparisons of small-world properties between AD and HCs and MCI and HCs were performed through a two-sample two-tailed t-test for each value in the same sparsity degrees of 0.10 to 0.50, with an interval of 0.01 ($P < 0.05$, Bonferroni correction).

3. Results

3.1. Judgment of Small-World Attributes. Figure 1 shows the brain function connectivity matrix of a normal subject and an AD patient obtained by the Pearson correlation and L1-norm regularization method, and Supplementary Figure 2 represents the mean FC matrices of NC, MCI, and AD patients obtained through the two methods. As it can be seen from the figures, the networks constructed by L1-norm regularization are more sparse.

The gamma indicates the ratio of the clustering coefficients between the real and random networks, the lambda implies the ratio of the path length between real and random networks, and the sigma is a scalar quantitative measurement

of the small-worldliness of a network. If gamma > 1 and lambda ≈ 1, and/or sigma = gamma/lambda > 1 in a network fit, it implies the network has small-worldliness.

The sigma, lambda, and gamma of the brain networks of AD and MCI patients and HCs generated through the Pearson correlation and L1-norm modeling are shown in Supplementary Figure 1. The fit $\gamma > 1$ and $\lambda \approx 1$ in both groups (Supplementary Figure 1); therefore, the functional networks of AD and MCI patients and HCs fit the definition of small-worldliness [30].

3.2. Altered Small-World Properties of Functional Networks in AD Patients. Using the L1-norm regularization method, AD patients showed a lower Cp and Eloc compared to the HCs (Figures 2(a) and 2(c)) and a lower Lp and higher Eg (Figures 2(b) and 2(d)). Pearson correlation analysis yielded similar results (Figures 2(e) and 2(h)).

3.3. Changes in Small-World Properties in MCI Patients through the L1-Norm Linear Regression Modeling Method. Using the L1-norm regularization method, we found a higher Cp and Eloc in MCI patients (Figures 3(e) and 3(g)); however, there was no statistical difference between the MCI and HC groups in terms of Lp and Eg (Figures 3(f) and 3(h)). However, MCI patients exhibited no statistical differences from HCs in Cp, Lp, Eg, and Eloc through Pearson correlation analysis (Figures 3(a)-3(d)). The statistical differences in small-world parameters between AD patients and HCs and MCI patients and HCs according to the two methods are presented in Table 2, and the P values are shown in Tables 3 and 4.

4. Discussion

In the present study, we have applied two kinds of network construction methods in graph theoretical analysis with statistical comparisons on the brain network attributes among healthy controls and patients with MCI and AD. The statistical comparison of brain network properties can provide empirical evidence of disease-related brain network changes and may help to identify which brain regions are more vulnerable to the disease.

4.1. Two Network Constructing Metrics on Small-World Networks in AD Patients. In the present study, we used the L1-norm regularization and Pearson correlation to construct brain functional networks, and our results revealed that the small-world properties of the networks in MCI and AD patients were disrupted compared to HCs. Both methods
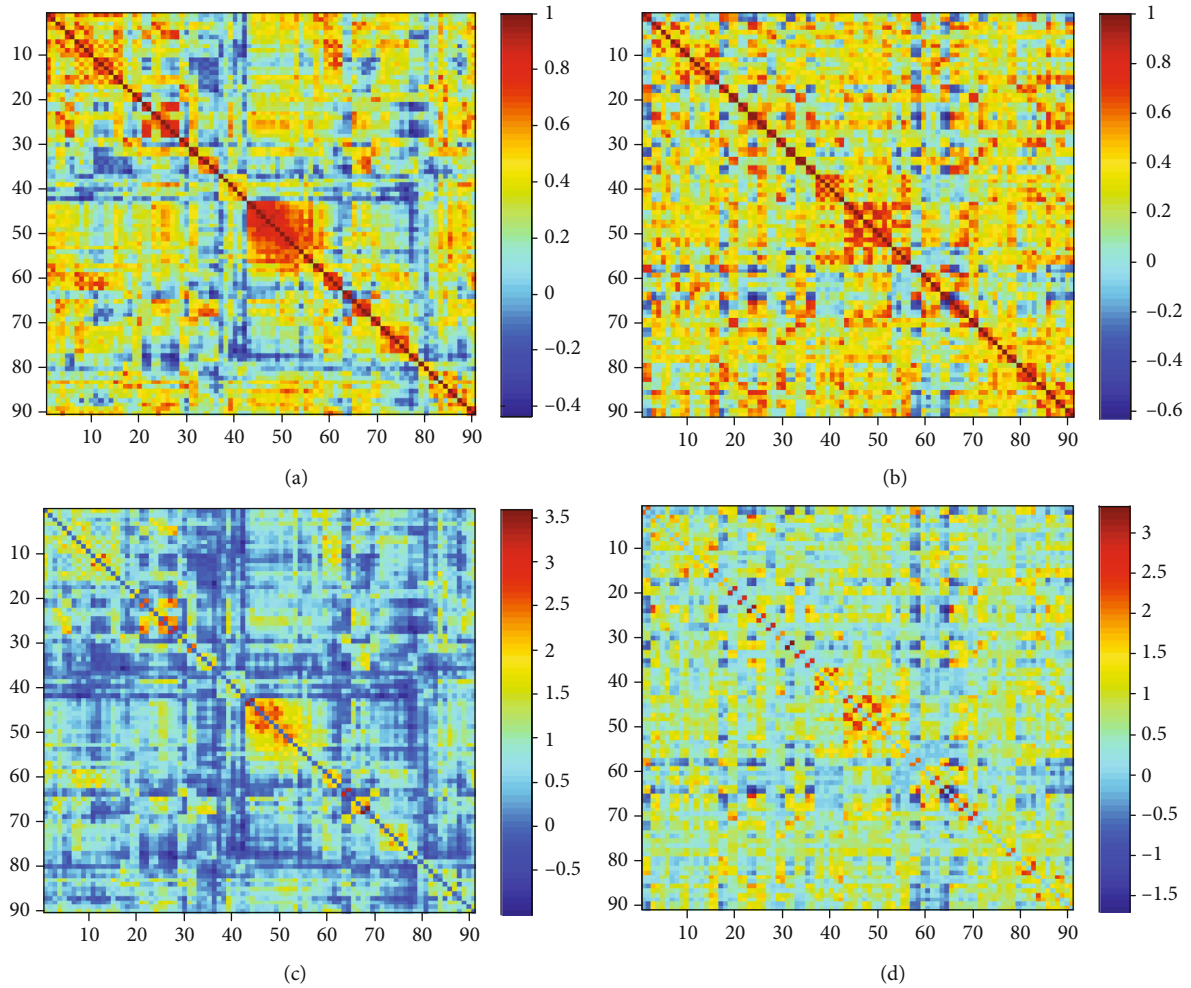
FIGURE 1: (a, b) Images representing the brain function connectivity matrix of a normal subject and an AD patient obtained by the Pearson method. (c, d) Images showing the brain function connectivity matrix of a normal subject and an AD patient is obtained by constrained sparse method. It can be clearly seen from the figure that the constraint sparse method calculates that the number of connections is sparser.

used in the present study manifested similar results in AD patients. Furthermore, the sparse L1-norm regularization method detected differences between MCI patients and HCs in terms of Cp and Eloc that were not revealed by the Pearson correlation method. The network constructed via L1-norm is relatively more sensitive to detecting changes in brain networks at early stages of AD.

The sparse L1-norm regularization and Pearson correlation results revealed that Cp and Eloc increased in MCI patients compared to HCs; however, the Pearson correlation results showed no significant differences in small-world properties between MCI patients and HCs. Here, we considered the L1-norm regularization to be more sensitive in detecting changes in brain networks during disease progression.

Different AD small-world characteristics in previous studies may have several possible explanations. Firstly, AD subjects may have been at different stages of the disease [16], or researchers may have applied different research approaches to construct the brain networks, which obviously cannot overlap among studies. The third explanation is diverse brain network connectivity metrics among different

studies. The main connectivity metrics are wavelet correlation [31, 32], Pearson correlation [16, 33], and synchronization likelihood [34] among others. Different methods have distinct emphases, resulting in various areas of application. For instance, wavelet correlation, mutual information, and synchronization likelihood are relatively sensitive to reveal frequency-specific couplings; therefore, they are often expected to focus on different characteristics among different frequency bands [25, 35]. The rationale for comparing only the Pearson correlation and L1-norm regression in this study has been described in the Introduction. In this study, we used two methods to study brain network topology connections; our results indicate that the network constructed through L1-norm is more sensitive in detecting brain network changes at early stages of AD than traditional the Pearson correlation analysis. Lastly, the temporal band-pass filtering frequency intervals of fMRI data have been shown to influence small-world characteristics [35]. The small-world topology exhibited variations in different frequency intervals, and the small-world topology connections were most prominent from 0.03 to 0.06 Hz [35]. Therefore, different studies using different frequency bands may affect the research results.
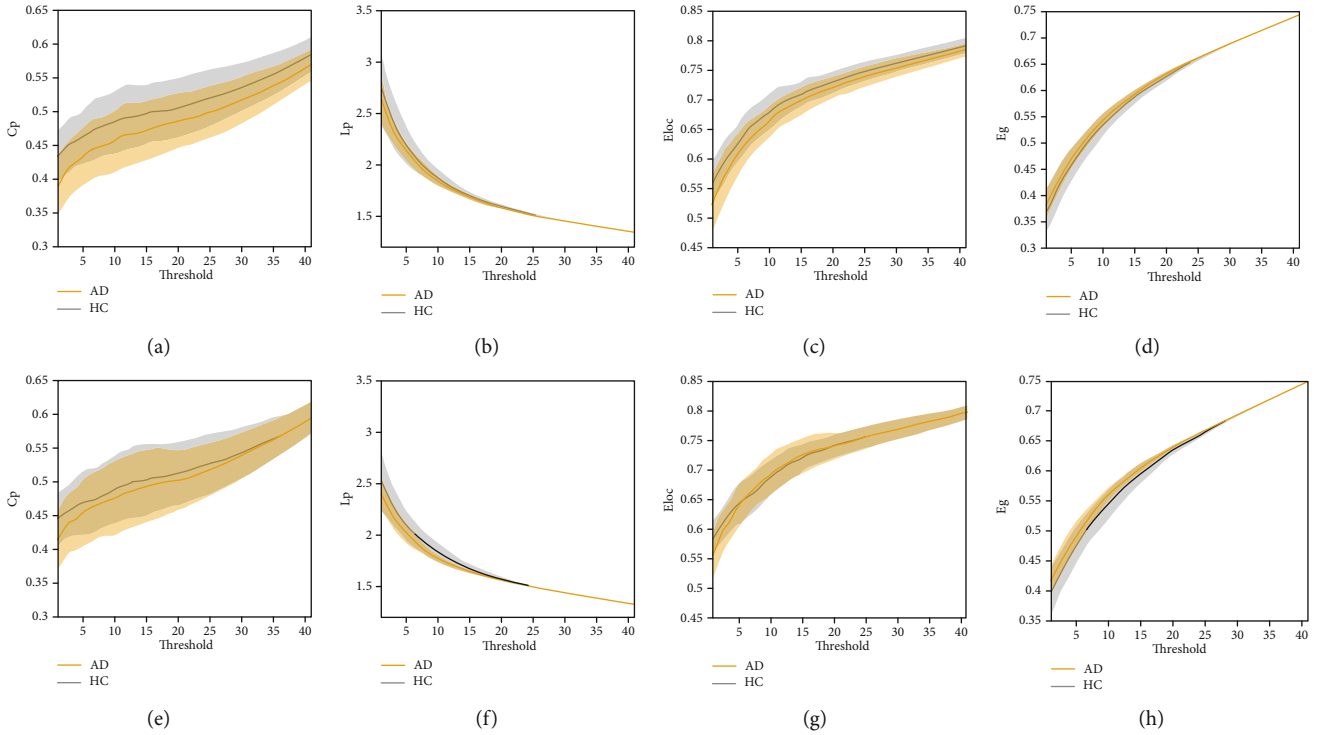
FIGURE 2: Small-world network parameters of the HCs (grey line) and AD patients (red line) using Pearson correlation (a-d) and sparse L1-norm regularization (e-f). Shaded areas indicate the standard error.
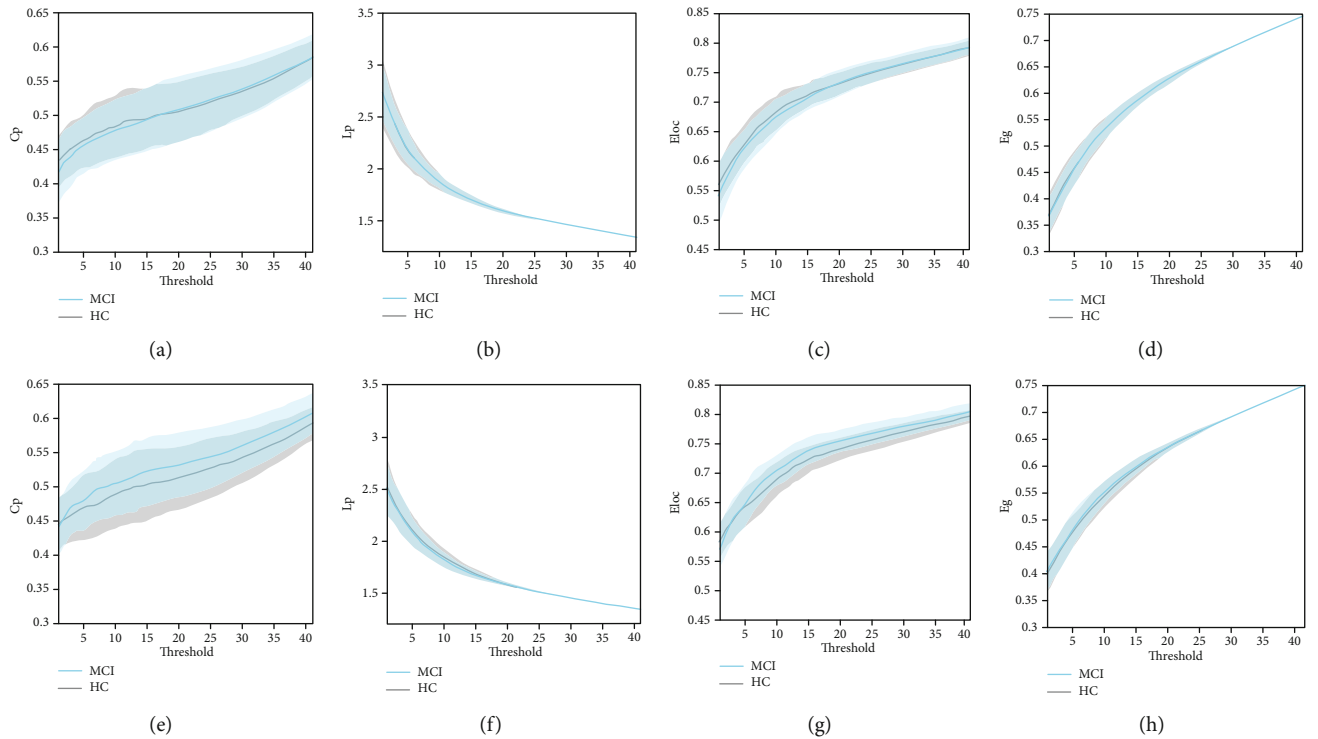
FIGURE 3: Small-world network parameters of the HCs (grey line) and MCI patients (blue line) using Pearson correlation (a-d) and sparse L1-norm regularization (e-f). Shaded areas indicate the standard error.

4.2. Changes of Small-World Parameters in AD and MCI Patients. AD is associated with regional brain damage, and the first degenerative changes in the progression of the dis-

ease occur in the medial temporal lobe, including the hippocampus and entorhinal cortex [36]. The change in structure may be related to changes in functional connectivity; AD is

TABLE 3: P values of statistical tests on the small-world parameters using the Pearson correlation.

	Pearson							
	HCs-MCI				HCs-AD			
Density	Cp	Lp	Eloc	Eg	Cp	Lp	Eloc	Eg
0.10	0.1268	0.9187	0.1155	0.9525	0.0003	0.2392	0.0037	0.2360
0.11	0.3087	0.9684	0.2561	0.8327	0.0015	0.0015	0.0015	0.1167
0.12	0.2659	0.9690	0.2193	0.8313	0.0056	0.1149	0.0447	0.1338
0.13	0.4545	0.7472	0.4051	0.6461	0.0053	0.1526	0.0309	0.1665
0.14	0.5202	0.7936	0.4554	0.7249	0.0142	0.1386	0.0679	0.1429
0.15	0.5859	0.9621	0.3493	0.8537	0.0294	0.1636	0.0811	0.1651
0.16	0.4722	0.9518	0.1644	0.9834	0.0274	0.1316	0.0453	0.1332
0.17	0.5262	0.8694	0.2357	0.9360	0.0243	0.1051	0.0554	0.1043
0.18	0.5761	0.9350	0.2965	0.9977	0.0227	0.1123	0.0379	0.1089
0.19	0.6939	0.9829	0.4784	0.9780	0.0405	0.0755	0.0529	0.0751
0.20	0.5394	0.9560	0.2543	0.9457	0.0602	0.0692	0.0809	0.0702
0.21	0.4987	0.9668	0.2059	0.9706	0.0621	0.0606	0.0613	0.0610
0.22	0.6309	0.9575	0.3123	0.0948	0.0514	0.0460	0.0540	0.0453
0.23	0.8353	0.9446	0.4697	0.9571	0.0530	0.0509	0.0779	0.0517
0.24	0.9606	0.9696	0.7109	0.9354	0.0581	0.0419	0.1052	0.0421
0.25	0.8044	0.9403	0.4114	0.9264	0.0513	0.0431	0.0597	0.0428
0.26	0.9847	0.8136	0.7172	0.8084	0.0757	0.0492	0.0788	0.0489
0.27	0.8434	0.8457	0.9301	0.8383	0.0986	0.0475	0.1162	0.0469
0.28	0.8173	0.7518	0.8996	0.7447	0.1258	0.0457	0.1949	0.0449
0.29	0.7488	0.7970	0.7585	0.7904	0.1113	0.0547	0.1781	0.0536
0.30	0.7482	0.8693	0.8552	0.8633	0.1158	0.0586	0.1667	0.0564
0.31	0.7721	0.9482	0.8242	0.9617	0.0840	0.0452	0.0961	0.0443
0.32	0.8327	0.9876	0.9435	0.9967	0.0709	0.0376	0.0614	0.0367
0.33	0.8401	0.9403	0.9304	0.9254	0.0835	0.0291	0.1004	0.0282
0.34	0.7937	0.9522	0.9274	0.9656	0.0812	0.0289	0.0763	0.0282
0.35	0.7832	0.8418	0.8605	0.8518	0.0788	0.0388	0.1017	0.0382
0.36	0.8013	0.9321	0.8800	0.9439	0.0692	0.0321	0.0895	0.0315
0.37	0.8055	0.8433	0.7944	0.8546	0.0632	0.0288	0.0927	0.0282
0.38	0.7331	0.7647	0.7207	0.7751	0.0577	0.0344	0.0749	0.0337
0.39	0.7362	0.7284	0.6966	0.7359	0.0635	0.0688	0.0919	0.0678
0.40	0.7569	0.6168	0.7407	0.6229	0.0705	0.0652	0.0762	0.0644
0.41	0.7640	0.6147	0.7313	0.6198	0.0668	0.0986	0.0762	0.0979
0.42	0.7556	0.5889	0.6980	0.5930	0.0658	0.1195	0.0784	0.1189
0.43	0.7405	0.6004	0.6796	0.6044	0.0692	0.1613	0.07980	0.1608
0.44	0.7279	0.4710	0.6795	0.4731	0.0623	0.2047	0.0678	0.2043
0.45	0.7556	0.4533	0.7202	0.4549	0.0495	0.1766	0.0517	0.1763
0.46	0.7977	0.4604	0.7725	0.4620	0.0461	0.1350	0.0426	0.1348
0.47	0.8088	0.9559	0.7894	0.9562	0.0438	0.1573	0.0402	0.1571
0.48	0.8237	0.6741	0.8026	0.6743	0.0422	0.2881	0.0434	0.2880
0.49	0.8359	0.9303	0.7923	0.9307	0.0411	0.2309	0.0417	0.2309
0.50	0.8142	0.8711	0.8203	0.8713	0.0442	0.2390	0.0434	0.2390

characterized by a significantly lower Cp, which is indicative of disrupted local connectivity, according to fMRI research by Supekar and his colleagues [31]. Similar results have been observed in previous MEG studies [37]; however, structural MRI has shown opposite results in that AD patients revealed higher Cp [6, 33]. Additionally, some researchers have found no difference between AD and HCs in terms of Cp using EEG [9] and fMRI [38] data.

In addition to regional damage, AD is associated with the abnormal functional integration of different brain regions through disconnection mechanisms [39]; at present, it is well-recognized that supporting daily cognitive activities

TABLE 4: *P* values of statistical tests on the small-world parameters using L1-norm regularization.

| | L1 | | | | | | | |
| | HCs-MCI | | | | HCs-AD | | | |
Density	Cp	Lp	Eloc	Eg	Cp	Lp	Eloc	Eg
0.10	0.6404	0.6401	0.2053	0.6698	0.0094	0.0609	0.0087	0.0650
0.11	0.8735	0.6150	0.4472	0.6107	0.0571	0.0276	0.0464	0.0289
0.12	0.2529	0.8256	0.6400	0.8083	0.1530	0.0240	0.02705	0.0221
0.13	0.3362	0.7639	0.7519	0.7210	0.1158	0.0309	0.2327	0.0249
0.14	0.5208	0.6125	0.7867	0.5841	0.2948	0.0321	0.7430	0.0250
0.15	0.1987	0.5490	0.2687	0.5339	0.4026	0.0240	0.9364	0.0188
0.16	0.0615	0.5434	0.0315	0.5273	0.5959	0.0164	0.5482	0.0128
0.17	0.1097	0.3825	0.0414	0.3702	0.4658	0.0106	0.5719	0.0077
0.18	0.1713	0.3504	0.0392	0.3455	0.4488	0.0086	0.5532	0.0056
0.19	0.1935	0.3035	0.0329	0.3001	0.3856	0.0088	0.7197	0.0058
0.20	0.2930	0.3442	0.0780	0.3360	0.4392	0.0052	0.6151	0.0031
0.21	0.2393	0.3440	0.0634	0.3292	0.4695	0.0090	0.5605	0.0061
0.22	0.2863	0.3161	0.0749	0.3060	0.3866	0.0162	0.8317	0.0117
0.23	0.1949	0.3589	0.0224	0.3522	0.4969	0.0205	0.5873	0.0176
0.24	0.1506	0.3247	0.0116	0.3107	0.5647	0.0151	0.6287	0.0132
0.25	0.1500	0.2947	0.0203	0.2876	0.5015	0.0155	0.8236	0.0131
0.26	0.1252	0.3362	0.0079	0.3272	0.5859	0.0226	0.6054	0.0204
0.27	0.1268	0.3625	0.0055	0.3528	0.5271	0.0157	0.5921	0.0146
0.28	0.1231	0.5806	0.0073	0.5630	0.4757	0.0063	0.6751	0.0058
0.29	0.1084	0.4627	0.0083	0.4503	0.4424	0.0020	0.8784	0.0019
0.30	0.1204	0.4288	0.0073	0.4158	0.3962	0.0028	0.9967	0.0026
0.31	0.1390	0.5207	0.0168	0.5065	0.4080	0.0045	0.8910	0.0043
0.32	0.1529	0.4481	0.0241	0.4324	0.4109	0.0050	0.8349	0.0048
0.33	0.1489	0.4787	0.0297	0.4626	0.4345	0.0072	0.8090	0.0070
0.34	0.1563	0.5108	0.0366	0.5022	0.4657	0.0067	0.8855	0.0065
0.35	0.1744	0.6842	0.0422	0.6702	0.4738	0.0038	0.9402	0.0037
0.36	0.1311	0.6812	0.0357	0.6682	0.5861	0.0042	0.9568	0.0041
0.37	0.1139	0.9121	0.0365	0.9262	0.5866	0.0017	0.9777	0.0017
0.38	0.1082	0.9140	0.0371	0.9014	0.6304	0.0018	0.9563	0.0017
0.39	0.1125	0.1125	0.9457	0.0470	0.6672	0.0024	0.9689	0.0024
0.40	0.9689	0.9824	0.0502	0.9936	0.7539	0.0041	0.9337	0.0041
0.41	0.0883	0.8723	0.0513	0.8820	0.7815	0.0096	0.9568	0.0096
0.42	0.0963	0.7882	0.0510	0.7959	0.8187	0.0253	0.9438	0.0253
0.43	0.0869	0.2272	0.0435	0.2263	0.8455	0.0293	0.9137	0.0293
0.44	0.0900	0.2301	0.0533	0.2293	0.8602	0.0400	0.9498	0.0400
0.45	0.0550	0.3039	0.0282	0.3031	0.9713	0.0641	0.7727	0.0641
0.46	0.0496	0.7239	0.0267	0.7225	0.9647	0.1426	0.7920	0.1426
0.47	0.0419	0.8847	0.0256	0.8838	0.9285	0.2016	0.7830	0.2016
0.48	0.0428	0.5887	0.0291	0.5882	0.9356	0.1712	0.8272	0.1712
0.49	0.0397	0.6768	0.0297	0.6765	0.8201	0.1953	0.7302	0.1953
0.50	0.0403	0.6358	0.0346	0.6355	0.7253	0.2424	0.6726	0.2424

requires a high level of functional interaction between different brain regions [13]. Both methods used in our study revealed that the global efficiency and Lp decreased in AD patients; this may reflect the impairment of functional connections between different brain regions, implying abnormal topological organization. This result is consistent with those

of numerous previous studies [16]. The present results showed that the network topological properties were disrupted in AD patients, and combined with the evidence for decreased long-distance and local efficiency, our data further support the notion of AD as a disconnection syndrome. AD patients have been shown to have disrupted system integrity

in the brain neuronal networks that could possibly be responsible for cognitive and memory decline, thus potentially providing insight into the basic mechanisms underlying this disease [40].

Unlike in AD patients, Cp and Eloc increased in MCI patients compared to that of HCs. MCI is considered a transitional stage between healthy aging and early AD; it is therefore a state of progressive global cognitive decline that includes the loss of memory, reasoning, and language. Abnormalities in functional integrity and functional compensation coexist in patients with MCI, and the increased Cp and Eloc may primarily result from a compensatory mechanism. Increased activity or functional connectivity within the right hemisphere has been observed in patients with MCI in a resting state or during various cognitive tasks [41–44]. In attention-demanding tasks, patients with MCI exhibit greater activation in the bilateral posterior parietal and dorsolateral prefrontal cortices than healthy elderly subjects. In a word-memory task, patients with MCI exhibit a significant increase in the activation of many compensatory regions compared to HCs [41–43]. According to a study by Liang et al. [45], patients with MCI may use additional neural resources in the right prefrontal regions to compensate for losses in cognitive function. It is worth mentioning that Lp and Eg did not differ significantly between MCI patients and HCs using both methods. We suggest that several local areas of the brain are affected, and the global connection is disrupted in AD patients.

5. Limitations

This study has certain limitations. First, the sample size in our study was small. We intend to further expand the sample size in the future to perform more in-depth and comprehensive research. Second, we only compared the differences between small-world networks that were constructed using the L1-norm regularization and Pearson correlation. Other approaches to construct brain networks will be included in further research.

6. Conclusions

In this study, we used the sparse L1-norm regularization and Pearson correlation to construct the brain network of AD and MCI patients and HCs and demonstrated that the functional networks of all the groups exhibited small-world topology. More importantly, we showed that AD patients had significantly decreased characteristic Cp and local efficiency in functional networks, implying a disconnectivity and topological disruption in the AD brain networks; we also found that instead of Lp and Eg, Cp and Eloc were impaired first during AD progression. In particular, constructing the brain network through the sparse L1-norm regularization is relatively more sensitive in detecting brain network changes in early stages of AD. The present study provided further important implications for understanding the basic mechanisms of AD.

Data Availability

Previously reported imaging data were used to support this study and are available at doi: 10.3389/fnagi.2018.00344.

Conflicts of Interest

The authors declare that the research was conducted in the absence of any commercial or financial relationships that could be construed as potential conflicts of interest.

Authors' Contributions

Xiaohu Zhao designed the experiments; Haimeng Hu, Huijin He, and Huiying Wang collected the data; Jiahui Han, Huihui Qi, Yunfei Li, Meimei Wang, and Sisi Zhang analyzed the data, and Hao Liu and Yunfei Li prepared the manuscript. Hao Liu, Haimeng Hu, and Huiying Wang contributed equally to this work.

Supplementary Materials

Supplementary 1. Supplementary Figure 1: the figures a, b, and c represent the mean FC matrices of NC, MCI, and AD patients obtained by the Pearson method. The figures d, e, and f show the mean FC matrices of NC, MCI, and AD patients obtained by the constrained sparse method.

Supplementary 2. Supplementary Figure 2: the sigma (red line), lambda (green line), and gamma (purple line) of the brain networks of patients with AD (c, f), MCI (b, e), and HCs (a, d) are shown using Pearson correlation (a, b, and c) and L1-norm (d, e, and f). Both groups fit $\gamma > 1$ and $\lambda \approx 1$. The functional networks of AD and MCI patients and HCs fit the definition of small-worldliness [26]. The γ means the ratio of the clustering coefficients between real and random network. The λ means the ratio of the path length between real and random network, and the σ means scalar quantitative measurement of the small-worldliness of a network.

References

[1] D. S. Bassett and E. Bullmore, "Small-world brain networks," *The Neuroscientist*, vol. 12, pp. 512–523, 2016.

[2] M. P. van den Heuvel and H. E. Hulshoff Pol, "Exploring the brain network: a review on resting-state fMRI functional connectivity," *European Neuropsychopharmacology*, vol. 20, no. 8, pp. 519–534, 2010.

[3] V. Latora and M. Marchiori, "Efficient behavior of small-world networks," *Physical Review Letters*, vol. 87, no. 19, p. 198701, 2001.

[4] Y. Zhou and Y. W. Lui, "Small-World Properties in Mild Cognitive Impairment and Early Alzheimer's Disease: A Cortical Thickness MRI Study," *ISRN Geriatrics*, vol. 2013, 11 pages, 2013.

[5] L. Tian, J. Wang, C. Yan, and Y. He, "Hemisphere- and gender-related differences in small-world brain networks: a resting-state functional MRI study," *NeuroImage*, vol. 54, no. 1, pp. 191–202, 2011.

[6] T. Nir, N. Jahanshad, C. R. Jack, M. W. Weiner, A. W. Toga, and P. M. Thompson, "Small world network measures predict white matter degeneration in patients with early-stage mild cognitive impairment," *2012 9th IEEE International Symposium on Biomedical Imaging (ISBI)*, vol. 88, pp. 1405–1408, 2012.

[7] W. R. Markesbery, F. A. Schmitt, R. J. Kryscio, D. G. Davis, C. D. Smith, and D. R. Wekstein, "Neuropathologic substrate of mild cognitive impairment," *Archives of Neurology*, vol. 63, no. 1, pp. 38–46, 2006.

[8] J. C. Morris, M. Storandt, J. P. Miller et al., "Mild cognitive impairment represents early-stage Alzheimer disease," *Archives of Neurology*, vol. 58, no. 3, pp. 397–405, 2001.

[9] B. Winblad, K. Palmer, M. Kivipelto et al., "Mild cognitive impairment–beyond controversies, towards a consensus: report of the international working group on mild cognitive impairment," *Journal of Internal Medicine*, vol. 256, no. 3, pp. 240–246, 2004.

[10] X. Delbeuck, M. Van der Linden, and F. Collette, "Alzheimer's disease as a disconnection syndrome?," *Neuropsychology Review*, vol. 13, no. 2, pp. 79–92, 2003.

[11] Y. Worbe, "Neuroimaging signature of neuropsychiatric disorders," *Current Opinion in Neurology*, vol. 28, no. 4, pp. 358–364, 2015.

[12] C. J. Stam, "Modern network science of neurological disorders," *Nature Reviews Neuroscience*, vol. 15, no. 10, pp. 683–695, 2014.

[13] Z. Liu, Y. Zhang, H. Yan et al., "Altered topological patterns of brain networks in mild cognitive impairment and Alzheimer's disease: a resting-state fMRI study," *Psychiatry Research*, vol. 202, no. 2, pp. 118–125, 2012.

[14] L. YaPeng, Q. Yuanyuan, C. Xi, and L. Wei, "Exploring the functional brain network of Alzheimer's disease: based on the computational experiment," *PLoS One*, vol. 8, article e73186, 2013.

[15] C. Y. Lo, P. N. Wang, K. H. Chou, J. Wang, Y. He, and C. P. Lin, "Diffusion tensor tractography reveals abnormal topological organization in structural cortical networks in Alzheimer's disease," *The Journal of Neuroscience*, vol. 30, no. 50, pp. 16876–16885, 2010.

[16] X. Zhao, Y. Liu, X. Wang et al., "Disrupted small-world brain networks in moderate Alzheimer's disease: a resting-state FMRI study," *PLoS One*, vol. 7, no. 3, article e33540, 2012.

[17] V. M. Eguiluz, D. R. Chialvo, G. A. Cecchi, M. Baliki, and A. V. Apkarian, "Scale-free brain functional networks," *Physical Review Letters*, vol. 94, no. 1, article 018102, 2005.

[18] J. Cao and K. Worsley, "The geometry of correlation fields with an application to functional connectivity of the brain," *The Annals of Applied Probability*, vol. 9, pp. 1021–1057, 1999.

[19] M. A. Koch, D. G. Norris, and M. Hund-Georgiadis, "An investigation of functional and anatomical connectivity using magnetic resonance imaging," *NeuroImage*, vol. 16, no. 1, pp. 241–250, 2002.

[20] C. Y. Wee, P. T. Yap, D. Zhang, L. Wang, and D. Shen, "Group-constrained sparse fMRI connectivity modeling for mild cognitive impairment identification," *Brain Structure & Function*, vol. 219, no. 2, pp. 641–656, 2014.

[21] H. Lee, D. S. Lee, H. Kang, B. N. Kim, and M. K. Chung, "Sparse brain network recovery under compressed sensing," *IEEE Transactions on Medical Imaging*, vol. 30, no. 5, pp. 1154–1165, 2011.

[22] X. Liang, J. H. Wang, C. G. Yan et al., "Effects of different correlation metrics and preprocessing factors on small-world brain functional networks: a resting-state functional MRI study," *PLoS One*, vol. 7, no. 3, article e32766, 2012.

[23] O. David, D. Cosmelli, and K. J. Friston, "Evaluation of different measures of functional connectivity using a neural mass model," *NeuroImage*, vol. 24, pp. 659–673, 2004.

[24] S. M. Smith, K. L. Miller, G. Salimi-Khorshidi et al., "Network modelling methods for fMRI," *NeuroImage*, vol. 54, no. 2, pp. 875–891, 2011.

[25] W. K. Li, Z. X. Wang, L. M. Zhang, L. S. Qiao, and D. G. Shen, "Remodeling Pearson's correlation for functional brain network estimation and autism spectrum disorder identification," *Frontiers in Neuroinformatics*, vol. 11, p. 55, 2017.

[26] B. Wang, Y. Niu, L. Miao et al., "Decreased complexity in Alzheimer's disease: resting-state fMRI evidence of brain entropy mapping," *Frontiers in Aging Neuroscience*, vol. 9, p. 378, 2017.

[27] Z. Zhang, Y. Liu, T. Jiang et al., "Altered spontaneous activity in Alzheimer's disease and mild cognitive impairment revealed by regional homogeneity," *NeuroImage*, vol. 59, no. 2, pp. 1429–1440, 2012.

[28] N. Tzourio-Mazoyer, B. Landeau, D. Papathanassiou et al., "Automated anatomical labeling of activations in SPM using a macroscopic anatomical parcellation of the MNI MRI single-subject brain," *NeuroImage*, vol. 15, no. 1, pp. 273–289, 2002.

[29] H. Liu, L. Zhang, Q. Xi et al., "Changes in brain lateralization in patients with mild cognitive impairment and Alzheimer's disease: a resting-state functional magnetic resonance study from Alzheimer's disease Neuroimaging Initiative," *Frontiers in Neurology*, vol. 9, p. 3, 2018.

[30] D. J. Watts and S. H. Strogatz, "Collective dynamics of 'small-world' networks," *Nature*, vol. 393, no. 6684, pp. 440–442, 1998.

[31] K. Supekar, V. Menon, D. Rubin, M. Musen, and M. D. Greicius, "Network analysis of intrinsic functional brain connectivity in Alzheimer's disease," *PLoS Computational Biology*, vol. 4, no. 6, article e1000100, 2008.

[32] Z. Wang, X. Jia, P. Liang et al., "Changes in thalamus connectivity in mild cognitive impairment: evidence from resting state fMRI," *European Journal of Radiology*, vol. 81, no. 2, pp. 277–285, 2012.

[33] Z. Yao, Y. Zhang, L. Lin, Y. Zhou, C. Xu, and T. Jiang, "Abnormal cortical networks in mild cognitive impairment and Alzheimer's disease," *PLoS Computational Biology*, vol. 6, no. 11, article e1001006, 2010.

[34] J. M. Buldú, R. Bajo, F. Maestú et al., "Reorganization of functional networks in mild cognitive impairment," *PLoS One*, vol. 6, no. 5, article e19584, 2011.

[35] S. Achard, R. Salvador, B. Whitcher, J. Suckling, and E. Bullmore, "A resilient, low-frequency, small-world human brain functional network with highly connected association cortical hubs," *The Journal of Neuroscience*, vol. 26, no. 1, pp. 63–72, 2006.

[36] E. Braak, K. Griffing, K. Arai, J. Bohl, H. Bratzke, and H. Braak, "Neuropathology of Alzheimer's disease: what is new since a. Alzheimer?," *European Archives of Psychiatry and Clinical Neuroscience*, vol. 249, pp. 14–22, 1999.

[37] C. J. Stam, W. de Haan, A. Daffertshofer et al., "Graph theoretical analysis of magnetoencephalographic functional connectivity in Alzheimer's disease," *Brain*, vol. 132, no. 1, pp. 213–224, 2009.

[38] E. J. Sanz-Arigita, M. M. Schoonheim, J. S. Damoiseaux et al., "Loss of 'small-world' networks in Alzheimer's disease: graph analysis of FMRI resting-state functional connectivity," *PLoS One*, vol. 5, no. 11, article e13788, 2010.

[39] M. Bozzali, G. J. Parker, L. Serra et al., "Anatomical connectivity mapping: a new tool to assess brain disconnection in Alzheimer's disease," *NeuroImage*, vol. 54, no. 3, pp. 2045–2051, 2011.

[40] Y. He, Z. Chen, G. Gong, and A. Evans, "Neuronal networks in Alzheimer's disease," *The Neuroscientist*, vol. 15, no. 4, pp. 333–350, 2009.

[41] F. Clement and S. Belleville, "Compensation and disease severity on the memory-related activations in mild cognitive impairment," *Biological Psychiatry*, vol. 68, no. 10, pp. 894–902, 2010.

[42] C. Rosano, H. J. Aizenstein, J. L. Cochran et al., "Event-related functional magnetic resonance imaging investigation of executive control in very old individuals with mild cognitive impairment," *Biological Psychiatry*, vol. 57, no. 7, pp. 761–767, 2005.

[43] Y. Yang, P. Liang, S. Lu, K. Li, and N. Zhong, "The role of the DLPFC in inductive reasoning of MCI patients and normal agings: an fMRI study," *Science in China Series C, Life Sciences*, vol. 52, no. 8, pp. 789–795, 2009.

[44] F. Bai, D. R. Watson, H. Yu, Y. Shi, Y. Yuan, and Z. Zhang, "Abnormal resting-state functional connectivity of posterior cingulate cortex in amnestic type mild cognitive impairment," *Brain Research*, vol. 1302, pp. 167–174, 2009.

[45] P. Liang, Z. Wang, Y. Yang, X. Jia, and K. Li, "Functional disconnection and compensation in mild cognitive impairment: evidence from DLPFC connectivity using resting-state fMRI," *PLoS One*, vol. 6, no. 7, article e22153, 2011.

Research Article

Relationship between Urinary Alzheimer-Associated Neuronal Thread Protein and Apolipoprotein Epsilon 4 Allele in the Cognitively Normal Population

Yuxia Li [iD],[1,2] **Meimei Kang** [iD],[2] **Can Sheng** [iD],[1] **Guanqun Chen** [iD],[1] **Taoran Li** [iD],[1] **Jun Wang** [iD],[1] **Yanning Cai** [iD],[3] **Rong Wang** [iD],[2,4,5] **and Ying Han** [iD][1,5,6]

[1]*Department of Neurology, Xuanwu Hospital of Capital Medical University, Beijing, China*
[2]*Central Laboratory, Xuanwu Hospital, Capital Medical University, Beijing, China*
[3]*Department of Neurobiology, Xuanwu Hospital, Capital Medical University, Beijing, China*
[4]*Beijing Geriatric Medical Research Center, Beijing, China*
[5]*Center of Alzheimer's Disease, Beijing Institute for Brain Disorders, Beijing, China*
[6]*National Clinical Research Center for Geriatric Disorders, Beijing, China*

Correspondence should be addressed to Rong Wang; wangrong@xwh.ccmu.edu.cn and Ying Han; sophiehanying@gmail.com

We investigated the relationship between urinary Alzheimer-associated neuronal thread protein (AD7c-NTP) levels and apolipoprotein epsilon 4 (*ApoE ε4*) alleles, as well as other factors that cause cognitive decline, in the cognitively normal population. We recruited 329 cognitively normal right-handed Han Chinese subjects who completed *ApoE* gene testing and urinary AD7c-NTP testing. There was no significant difference in urinary AD7c-NTP levels between the normal control and subjective cognitive decline groups. Urinary AD7c-NTP levels were significantly higher in subjects with *ApoE ε3/4* and *4/4* [0.6074 (0.6541) ng/mL] than in subjects without *ApoE ε4* [0.4368 (0.3392) ng/mL and 0.5287 (0.3656) ng/mL], and urinary AD7c-NTP levels positively correlated with *ApoE* genotype grade ($r = 0.165$, $p = 0.003$). There were significant differences in urinary AD7c-NTP levels between subjects with and without a history of coronary heart disease or diabetes. Urinary AD7c-NTP levels were not related to years of education, nature of work, family history of dementia, a history of hypertension, stroke, anemia, or thyroid dysfunction. Urinary AD7c-NTP levels were positively correlated with *ApoE* grade in the cognitively normal population. The relationship between risk factors of cognitive decline and urinary AD7c-NTP levels provides a new way for us to understand AD and urinary AD7c-NTP.

1. Introduction

Alzheimer's disease (AD) is the most common form of dementia, accounting for 60%–80% of all dementia, and imposes a substantial socioeconomic burden on society and families [1–4]. Furthermore, AD is an irreversible, disabling degenerative disease of the central nervous system. In the absence of curative treatments once the disease has progressed to AD dementia, primary prevention and early diagnosis in the preclinical stage of AD have been the main research focuses in recent years [5]. It is therefore crucial to explore early biomarkers of AD to enable the early diagnosis of this disease, with the ultimate aim of treating and preventing dementia in preclinical AD.

Urinary AD7c-NTP, a peripheral biomarker for AD, is increased in mild cognitive impairment (MCI) and AD [6–9]. Previous studies have reported that AD7c-NTP immunoreactivity colocalizes with neurofibrillary tangles and dystrophic neurites, and increased AD7c-NTP levels are associated with tau-immunoreactive neurofibrillary tangles [10]. Furthermore, overexpression of AD7c-NTP is associated with neurite sprouting and cell death, which is reflected in AD neurodegeneration [11]. Recent research suggests that urinary AD7c-NTP is increased in hypertensive patients with

cognitive impairment [12]. In addition, a previous study reported that urinary AD7c-NTP is elevated in late-life depression with cognitive impairment [13]. Furthermore, existing research recognizes that urinary AD7c-NTP has a critical role in cognitive decline, but not in depression or other diseases [12–15]. Urinary AD7c-NTP testing is noninvasive, radiation-free, repeatable, and easy to carry out. Therefore, urinary AD7c-NTP may be a promising peripheral biomarker for detecting cognitive decline and disease progression [16]. Although previous studies have reported that cognitive decline is associated with elevated urinary AD7c-NTP, it is not clear which factors, aside from decreased cognitive function, are associated with elevated urinary AD7c-NTP [13, 15, 17, 18]. It has not been reported whether other medical history factors that may lead to a decline in cognitive function, such as carbon monoxide poisoning (COP), general anesthesia, or thyroid dysfunction, are associated with urinary AD7c-NTP levels in the normal cognitive population.

Subjective cognitive decline (SCD) refers to self-experienced persistent cognitive decline compared with a previously normal status, while standardized cognitive tests give objectively normal results [19, 20]. SCD is considered to be a preclinical phase of AD in patients who are objectively cognitively normal [21, 22]. Approximately 14.1% of SCD patients convert to AD within 4 years [21]. SCD-plus, proposed by the Subjective Cognitive Decline Initiative, is considered closer to the early stage of AD [20, 23]. The conversion rate for SCD-plus to MCI is 18.9% [22]. Therefore, both early diagnosis of AD and monitoring of progression in the SCD stage are essential for the early prevention and treatment of AD.

The apolipoprotein E epsilon 4 (*ApoE ε4*) allele is considered to be a risk factor for AD, and *ApoE ε4* may influence the rate of cognitive decline in early AD [24]. Clinical studies and autopsies have demonstrated that people with heterozygous *ApoE ε4* are three times more likely to develop AD than noncarriers (odds ratio (OR) = 3.2), and people with a homozygous genotype of *ApoE ε4/4* are 14 times more likely to develop AD (OR = 14.9) [25]. *ApoE ε4* carriers have lower concentrations of Aβ1–42, higher total tau and phosphorylated-tau, and a higher degree of brain atrophy than individuals without *ApoE ε4* allele [26]. ApoE is thought to be involved in plaque formation, and this idea is supported by the finding that ApoE is involved in the deposition or clearance of Aβ by direct protein-to-protein interaction [27, 28]. We know that increased urinary AD7c-NTP levels are associated with tau-immunoreactive neurofibrillary tangles and amyloid-β (Aβ) deposition; similarly, the *ApoE* allele is also associated with hyperphosphorylated tau and Aβ deposition, which are the pathological hallmarks of AD [10, 27, 29, 30]. However, the relationship between the two biomarkers remains unclear. Assuming that these two biomarkers are highly consistent and can reflect the risk of disease development, it may be beneficial to monitor the progression of AD using urinary AD7c-NTP as a noninvasive biomarker. Therefore, this study investigated the correlation between urinary AD7c-NTP and *ApoE* genotype and explored whether urinary AD7c-NTP is affected by other factors that

may lead to cognitive decline, further demonstrating the feasibility of urinary AD7c-NTP as a biomarker of AD.

2. Materials and Methods

2.1. Participants. This study is part of the Sino Longitudinal Study on Cognitive Decline (SILCODE) [31]. The study was approved by the Xuanwu Hospital Research Ethics Review Committee (ClinicalTrials.gov identifier: NCT03370744), and all participants signed their informed consent. A total of 329 cognitively normal right-handed Han Chinese subjects participated in the study, of which 151 were diagnosed with SCD and 178 were used as the cognitively normal controls (NC). All subjects were recruited through standardized public advertisements or memory clinics. SCD diagnosis was carried out by two experienced neurologists in the Department of Neurology, Xuanwu Hospital, Capital Medical University, based on the SCD-plus diagnostic framework of the Subjective Cognitive Decline Initiative [20, 23]. The inclusion criteria for SCD included Han Chinese nationality; right-handedness; older than 60 years; decline in memory as the primary symptom, rather than in any other cognitive domain; sustained cognitive decline in self-perception, independent of acute events, as compared with the previous healthy state; continuous concerns or worries associated with memory loss; cognitive function reported to be worse than that of others in the same age group; memory loss certified by an informed person; subject failed to meet the criteria for MCI or AD [32, 33].

The NCs were recruited from local communities through broadcast and online media advertising. The inclusion criteria for NC included Han Chinese nationality; right-handedness; older than 60 years; no memory or other cognitive decline complaints, with no concerns or worries about their cognition; normal scores in standardized neuropsychological tests, scale-adjusted for sex, age, and education; negative result for nervous system physical examinations; without any relevant medical histories or family histories; and accessory examinations revealed no diseases that could cause cognitive decline [31]. The exclusion criteria for all participants included congenital and acquired severe cognitive decline, MCI, AD, vascular cognitive dysfunction, or other dementia; a history of stroke, severe psychiatric disease, Parkinson's disease, multiple sclerosis, or brain tumor; alcohol or drug abuse; syphilis or acquired immune deficiency syndrome; severe liver and kidney dysfunction; severe hearing or visual impairment; and failure to cooperate with the study protocol.

2.2. Neuropsychological Assessment and Laboratory Measurements. All subjects underwent detailed medical history inquiries, neurological examinations, and medical system examinations and completed a neuropsychological assessment for diagnosis and differential diagnosis. Medical history collection included detailed inquiries about previous hypertension, diabetes, coronary heart disease, stroke, anemia, abnormal thyroid function, history of surgery under general anesthesia, history of COP, history of head trauma, and family history of dementia. Neuropsychological assessment scales included the Mini-Mental State Examination (MMSE), Montreal Cognitive Assessment-Basic (MoCA-B),

Animal Verbal Fluency Test, Boston Naming Test (30 items), Auditory Verbal Learning Test-HuaShan (AVLT-H), Shape Trails (test A and test B), 17-item Hamilton Depression Rating Scale (HAMD), Hamilton Anxiety Scale (HAMA), and Functional Activities Questionnaire (FAQ). MMSE scores > 24 were considered normal for subjects with more than 6 years of education, while MMSE scores > 20 were considered normal for subjects with 1–6 years of education. When the subject was illiterate, an MMSE score > 17 was considered normal [34]. MoCA-B scores were considered normal when they were MoCA − B > 19 for the subjects with 0–6 years of education, >22 for those with 7–12 years of education, and>24 for those with 13 or more years of education [35].

All participants had blood samples collected in the morning after 8 hours with no food or water. Laboratory tests included a routine blood test, routine urine test, blood biochemistry, homocysteine, activated partial thromboplastin time, antibody tests for syphilis and human immunodeficiency virus, thyroid series, serum folic acid test, and serum vitamin B_{12} test, which were used to exclude other diseases that may lead to memory loss. *ApoE* gene testing was performed on all the subjects by Professor Yanning Cai. *ApoE* genotyping was performed by sequencing codons 112 and 158 of exon 4 of the *ApoE* gene [36].

2.3. Urinary AD7c-NTP Laboratory Detection. The levels of AD7c-NTP in urine samples were measured using the enzyme-linked immunosorbent assay AD7c-NTP kit (Anqun Biological Technology Co. Ltd., Shenzhen, China). All subjects collected clean midstream urine samples in the morning and placed them in Eppendorf tubes containing boric acid (2 g/L) as a preservative. Samples were centrifuged immediately and stored in a refrigerator at 4°C. The urine samples were observed visually. If the urine was cloudy or dark, it was discarded, and urine samples were collected the next morning. According to the manufacturer's instructions, the concentrated washing solution was diluted with distilled water at a ratio of 1 : 25. First, approximately $100\,\mu L$ of the sample was added, and the solution was incubated at 37°C for 60 min. The sample was then removed, the liquid on the plate was shaken off, and five consecutive wash steps were performed using phosphate-buffered saline (PBS) before the sample was patted dry. Next, $100\,\mu L$ of biotinylated rabbit anti-AD7c-NTP antibody was added and incubated at 37°C for 30 min. The reaction plate was removed, washed thoroughly with PBS, and patted dry. Next, $100\,\mu L$ of horseradish peroxidase-labeled avidin was added to the reaction plate, which was then sealed and incubated at 37°C for 30 min. After washing five times with PBS, $50\,\mu L$ of chromogenic reagents A and B were added in turn, mixed well, and incubated at 37°C for 15 min. Finally, the reaction was stopped by adding $50\,\mu L$ of sulfuric acid as the stop buffer and mixing well. A microplate reader was used to measure the absorbance (A value) at 450 nm wavelength, and the AD7c-NTP concentration was calculated according to the formula.

2.4. Classification of Demographic Characteristics and Blood ApoE Genotype. Education levels were grouped by high school level and divided into less than 12 years, 12 years, and more than 12 years of education. The nature of each subject's employment was classified into manual labor, mental labor, or mixed labor.

Previous clinical- or autopsy-based studies reported that AD risk is increased in people with genotypes *ApoE ε2/4*, *ApoE ε3/4*, and *ApoE ε4/4*; in contrast, AD risk is decreased in people with genotypes *ApoE ε2/2* and *ApoE ε2/3* [25]. Based on this information, all subjects were divided into four groups according to their genotype. Grade 1 included genotypes *ApoE ε2/2* and *ApoE ε2/3* (the risk of AD is reduced with these two genotypes, OR = 0.6 for each), grade 2 was made up of the genotype *ApoE ε3/3* (this genotype neither increases nor decreases the risk of AD), grade 3 included the *ApoE ε2/4* genotype (this genotype confers a mildly elevated risk of AD; OR = 2.6), and grade 4 was made up of the genotypes *ApoE ε3/4* and *ApoE ε4/4* (these genotypes confer a significantly increased risk of AD; OR = 3.2 and OR = 14.9; Table 1).

History of coronary heart disease (CHD) verified by medical documents and the diagnosis was based on the 2013 ESC guidelines for the diagnosis and management of stable coronary artery disease [37]. A diagnosis of diabetes was based on the American Diabetes Association criteria for elevated fasting blood glucose (≥ 7.0 mmol/L or ≥ 126 mg/dL) for patients with a history of diabetes [38]. Hypertension was defined as a clinical history of hypertension for more than 1 year, excluded secondary hypertension [39]. A history of stroke was defined as a history of cerebral infarction, cerebral hemorrhage, or subarachnoid hemorrhage and was certified by medical documents. Anemia was defined as hemoglobin below 120 g/L in men and 110 g/L in women. A history of hyperthyroidism and hypothyroidism, COP, general anesthesia, and head trauma, and a family history of dementia (FHD), were all self-reported and verified using medical or hospital records. Subjects with these histories were assigned to the positive group (+), while subjects without these histories were assigned to the negative group (−).

2.5. Statistical Analysis. All data were analyzed using the Statistical Package for Social Sciences (SPSS) v22.0 software. Data with continuous variables were expressed as the mean ± standard deviation (SD). Data for discontinuous variables were expressed as the median (interquartile range). Counting data were analyzed using the chi-square test. The two-independent-sample t-test was adopted to compare data between two groups, and the analysis of variance (ANOVA) was used to compare data among three or four groups. The Mann–Whitney U test was used to compare data for discontinuous variables, while the Kruskal–Wallis test for multiple comparisons was used for discontinuous variables. Further, Spearman correlation analysis was used to analyze the correlation between *ApoE* allele and urinary AD7c-NTP levels. A threshold of $p < 0.05$ was considered statistically significant.

3. Results

3.1. Participant Demographic Data. We recruited 329 right-handed Han Chinese subjects with an average age of 64.16

TABLE 1: Demographics and clinical features of the study participants.

Variables	Subject group	Age (y)	Male: female	No. cases	Percent (%)
Education level	<12	64.62 ± 5.24	23 : 82	105	31.92
	=12	64.28 ± 6.22	24 : 50	74	22.49
	>12	63.78 ± 7.25	54 : 96	150	45.59
ApoE allele	Grade 1 (2/2 + 2/3)	64.23 ± 4.99	13 : 27	40	12.16
	Grade 2 (3/3)	64.21 ± 6.53	67 : 141	208	63.22
	Grade 3 (2/4)	64.55 ± 5.82	4 : 7	11	3.34
	Grade 4 (3/4 + 4/4)	63.91 ± 7.04	17 : 53	70	21.28
Nature of work	Mental labor	64.67 ± 6.51	70 : 150	220	66.87
	Manual labor	62.54 ± 5.43	10 : 27	37	11.25
	Mixed labor	63.43 ± 6.52	21 : 51	72	21.88
CHD	+	66.23 ± 5.91	11 : 11	22	6.69
	—	64.01 ± 6.45	90 : 217	307	93.31
Diabetes	+	65.38 ± 6.06	16 : 21	37	11.25
	—	64.01 ± 6.47	85 : 207	292	88.75
Hypertension	+	65.04 ± 6.18	46 : 64	110	33.43
	—	63.72 ± 6.52	55 : 164	219	66.57
Stroke	+	65.04 ± 7.11	8 : 16	24	7.29
	—	64.09 ± 6.38	93 : 212	305	92.71
Anemia	+	62.69 ± 7.56	1 : 15	16	4.86
	—	64.24 ± 6.37	100 : 213	313	95.14
Thyroid dysfunction	+	63.29 ± 8.22	7 : 14	21	6.38
	—	64.22 ± 6.30	94 : 214	308	93.62
COP	+	65.94 ± 6.25	16 : 34	50	15.20
	—	63.84 ± 6.42	85 : 194	279	84.80
General anesthesia	+	64.51 ± 6.03	20 : 56	76	23.10
	—	64.06 ± 6.56	81 : 172	253	76.90
Head trauma	+	67.27 ± 4.80	4 : 7	11	3.34
	—	64.05 ± 6.46	97 : 221	318	96.66
FHD	+	63.24 ± 5.87	17 : 65	82	24.92
	—	64.47 ± 6.59	84 : 163	247	75.08
Diagnosis	SCD	63.77 ± 6.25	43 : 108	151	45.90
	NC	64.49 ± 6.58	58 : 120	178	54.10

Key: CHD: history of coronary heart disease; COP: carbon monoxide poisoning; FHD: family history of dementia; SCD: subjective cognitive decline; NC: normal controls.

± 6.43 years; 30.7% ($n = 101$) of the subjects were male (Table 1). Disease prevalence, including the prevalence of CHD, diabetes, hypertension, stroke, anemia, and thyroid dysfunction, is recorded in Table 1. Past medical history, such as COP, general anesthesia, head trauma, and family history of dementia, is also shown in Table 1. Personal history data, including years in education and nature of work, are shown in Table 1, and subjects were grouped according to their personal history or past medical history. ApoE genotype was detected and consisted of ApoE ε2/2 (2 subjects), ApoE ε2/3 (38 subjects), ApoE ε3/3 (208 subjects), ApoE ε2/4 (11 subjects), ApoE ε3/4 (68 subjects), and ApoE ε4/4

(2 subjects). The subjects were divided into four groups based on ApoE genotype (Table 1).

3.2. Urinary AD7c-NTP Levels by Years of Education and Nature of Work. According to the Kruskal–Wallis test, there were no significant differences in urinary AD7c-NTP levels among subjects with different years of education or nature of work ($p > 0.05$, Table 2).

3.3. Urinary AD7c-NTP Levels by Past Medical History and Family History of Dementia. In Table 2, there was a significant difference in urinary AD7c-NTP levels between subjects

TABLE 2: Comparison of urinary AD7c-NTP levels in different demographic characteristics groups, nonneurological disease groups, and different *ApoE* allele grade groups.

Variables	Subject group	AD7c-NTP (ng/mL)	H/Z	p
Education level	<12	0.5562 (0.5261)		
	=12	0.5165 (0.3971)	0.233	0.890
	>12	0.5368 (0.3310)		
Nature of work	Mental labor	0.5184 (0.3681)		
	Manual labor	0.6311 (0.6305)	2.902	0.234
	Mixed labor	0.5711 (0.3899)		
CHD	+	0.7921 (0.7347)	-2.854	0.004*
	—	0.5246 (0.3823)		
Diabetes	+	0.6355 (0.5824)	-2.725	0.006*
	—	0.5211 (0.3889)		
Hypertension	+	0.5232 (0.4389)	-0.014	0.989
	—	0.5381 (0.3925)		
Stroke	+	0.6267 (0.6099)	-1.738	0.082
	—	0.5315 (0.3880)		
Anemia	+	0.5784 (0.4786)	-0.079	0.937
	—	0.5322 (0.4091)		
Thyroid dysfunction	+	0.6241 (0.8910)	-0.245	0.806
	—	0.5322 (0.3897)		
COP	+	0.5964 (0.5298)	-0.392	0.695
	—	0.5265 (0.3918)		
General anesthesia	+	0.5665 (0.4077)	-0.776	0.438
	—	0.5265 (0.4035)		
Head trauma	+	0.4969 (0.2551)	-0.274	0.784
	—	0.5342 (0.4212)		
FHD	+	0.5417 (0.3776)	-0.442	0.658
	—	0.5322 (0.4428)		
Diagnosis	SCD	0.5483 (0.4838)	-1.359	0.174
	NC	0.5164 (0.3667)		
ApoE allele	Grade 1 (2/2 + 2/3)	0.4368 (0.3392)		
	Grade 2 (3/3)	0.5287 (0.3656)	9.080	0.028*
	Grade 3 (2/4)	0.5580 (0.9201)		
	Grade 4 (3/4 + 4/4)	0.6074 (0.6541)		

Key: AD7c-NTP: Alzheimer-associated neuronal thread protein; CHD: history of coronary heart disease; COP: carbon monoxide poisoning; FHD: family history of dementia; SCD: subjective cognitive decline; NC: normal controls; Data in AD7c-NTP were shown in median (interquartile range).

with a history of CHD and subjects without a history of this disease ($Z = -2.854$, $p = 0.004$). There was also a significant difference in urinary AD7c-NTP levels between subjects with and without a history of diabetes ($Z = -2.725$, $p = 0.006$). According to the Mann–Whitney U test, there were no significant differences in urinary AD7c-NTP levels in subjects with a family history of dementia or other medical histories such as hypertension, stroke, anemia, thyroid dysfunction, COP, general anesthesia, or head trauma ($p > 0.05$, Table 2).

3.4. Urinary AD7c-NTP Levels by SCD Diagnosis and ApoE Genotype. There was no significant difference in urinary AD7c-NTP levels between the NC [0.5164 (0.3667) ng/mL] and SCD [0.5483 (0.4838) ng/mL] groups ($p > 0.05$, Table 2). The Kruskal–Wallis test revealed that there were significant differences in urinary AD7c-NTP levels among subjects

with different ApoE genotypes ($H = 9.080$, $p < 0.05$, Table 2). Furthermore, urinary AD7c-NTP levels in subjects with *ApoE ε3/4* and *ApoE ε4/4* were significantly higher [0.6074 (0.6541) ng/mL] than in subjects without *ApoE ε4* [0.4368 (0.3392) ng/mL and 0.5287 (0.3656) ng/mL].

Moreover, Spearman correlation analysis revealed that urinary AD7c-NTP levels were positively correlated with *ApoE* grade; that is, urinary AD7c-NTP levels increased with increased *ApoE* grade ($r = 0.165$, $p = 0.003$, Figure 1).

4. Discussion

The present study was designed to investigate the relationship between urinary AD7c-NTP levels and *ApoE ε4* alleles, as well as with other factors associated with cognitive decline in the cognitively normal population. Our study revealed that
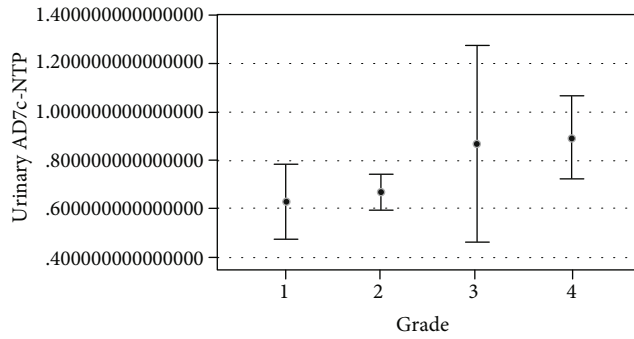
Figure 1: Correlation analysis between urinary Alzheimer-associated neuronal thread protein and *ApoE* allele grade. The line segment shows the 95% confidence interval.

(i) urinary AD7c-NTP levels were not significantly different among subjects with different years of education and nature of work; (ii) there were significant differences in urinary AD7c-NTP between subjects with and without a history of CHD or diabetes; (iii) urinary AD7c-NTP levels were not significantly different in people with a family history of dementia or a history of hypertension, stroke, anemia, or thyroid dysfunction; and (iv) urinary AD7c-NTP levels in subjects with *ApoE ε4* were significantly higher than in subjects without *ApoE ε4*, and urinary AD7c-NTP levels increased with an increase in *ApoE* grade.

4.1. The Relationship between Urinary AD7c-NTP Levels, Personal History, and SCD Diagnosis.

In the present study, urinary AD7c-NTP levels were not significantly different among subjects with different years of education or nature of work. These findings are in line with other reports that urinary AD7c-NTP is not affected by demographic factors or common chronic diseases [14]. Previous evidence suggests that being married and living in an urban environment can decrease the risk of cognitive impairment [40]. In the current study, although urinary AD7c-NTP levels were not increased in subjects with fewer years of education or who had worked in manual labor, the speed of cognitive decline affected by cognitive reserve remains a focus for neurologists.

In the present study, it was revealed that the levels of urinary AD7c-NTP were not higher in SCD patients compared with the NC group. This result is consistent with previous results from our research group [15]. The reason for these results may be that SCD is still a very early stage of the disease when neuropsychological test scores are normal; thus, tau protein may not be increased or detected at this stage [41]. Findings from the DELCODE study included a decline in memory and language in SCD, and SCD-plus features were associated with lower Aβ42 and a lower Aβ42/tau ratio but were not associated with total tau or p-tau-181 levels [42]. Furthermore, the DELCODE study reported lower CSF-Aβ42 levels and lower CSF-Aβ42/tau ratios in SCD patients than in healthy controls, while total tau and p-tau-181 levels were not elevated in the SCD group [42]. Urinary AD7c-NTP levels are a good indicator of tau protein levels; there is no increase in tau in SCD, and this evidence further supports our result of normal urinary AD7c-NTP levels in SCD

patients. Urinary AD7c-NTP is a promising biomarker for AD, and its level is proportional to the degree of dementia [43]. SCD is still in the preclinical AD stage, without objective evidence of cognitive impairment, and this may be one of the reasons why urinary AD7c-NTP was not elevated in subjects with SCD.

4.2. The Relationship between Urinary AD7c-NTP Levels and Family History of Dementia or Past Medical History.

Previous studies have reported that a family history of dementia increases the risk of developing dementia [44, 45]. In the current study, urinary AD7c-NTP levels were not different in people with or without a family history of dementia. This result suggests that a family history of dementia does not increase urinary AD7c-NTP levels. This may be because urinary AD7c-NTP is an indicator of tau, and there may not be any abnormal increase in tau in these subjects with a family history of dementia.

Another important finding was that urinary AD7c-NTP levels were elevated in people with a history of CHD and diabetes. CHD and diabetes are both risk factors for AD and dementia [40, 46]. Previous research has demonstrated that cholesterol metabolic disorder is a common cause and risk factor of CHD and AD [47]. There is evidence that *ApoE ε4* alleles and hyperlipidemia play a crucial role in the relationship between AD and CHD. Hyperlipidemia could aggravate coronary atherosclerosis and damage the blood–brain barrier, as well as promote Aβ protein production and tau deposition in the brain [47]. Diabetes increases the risk of AD by affecting glucose transmission to the brain and reducing glucose metabolism. It has been reported that glucose/lipid metabolism, oxidative stress, mitochondrial dysfunction, and protein changes in metabolic disorders caused by diabetes can all increase the prevalence of AD by promoting pathological changes in Aβ in diabetic patients [48]. Our results from the present study suggest that urinary AD7c-NTP is elevated in subjects with AD risk factors, and that urinary AD7c-NTP may therefore be a peripheral biomarker to predict AD risk factors.

Urinary AD7c-NTP levels were not elevated in people with a medical history of hypertension, stroke, anemia, or thyroid dysfunction in the current study. This result is also in accordance with earlier observations by our team, which revealed that urinary AD7c-NTP levels were not affected by common chronic diseases such as hypertension, stroke, dyslipidemia, renal insufficiency, cancer, chronic lung disease, chronic liver disease, or symptoms of depression [14]. The present study differs from the previous one in that we chose different diseases, but they are all chronic diseases that may cause cognitive decline. Hypertension and stroke are known risk factors for AD and dementia [40, 46]. A recent study reported that urinary AD7c-NTP is increased in hypertensive patients with cognitive decline; in contrast, the subjects in our study were from a population with a high risk of AD, but with normal cognition [12]. In our study, subjects with hypertension and normal cognition did not show elevated urinary AD7c-NTP. Anemia and high levels of hemoglobin are associated with an increased risk of AD [49]. Recent evidence suggests that hypothyroidism and hyperthyroidism are

associated with AD, and hypothyroidism or hyperthyroidism may be one cause of cognitive impairment, including AD [50]. Although these diseases may increase the risk of cognitive decline, there is little evidence that these diseases are associated with increased tau protein. This may help to explain why there was no increase in urinary AD7c-NTP levels in subjects with a history of these diseases in the current study. COP, general anesthesia, and head trauma may also contribute to cognitive decline [51–53]. Cognitive impairment after COP is thought to be related to delayed encephalopathy caused by carbon monoxide, which is a symptom of frontal lobe dysfunction [51, 54]. A recent study reported that major surgery is associated with a small amount of long-term cognitive decline: cognitive decline after surgery was approximately double the level that it was before surgery [55]. Some studies have also demonstrated that about half of all patients with mild traumatic brain injury had long-term cognitive impairment and cognitive decline, including in learning and memory, attention, executive function, and processing speed [53]. Nevertheless, none of these causes of cognitive impairment involve neurodegeneration. Thus, in our study, we did not find elevated urinary AD7c-NTP levels in subjects with a history of COP, general anesthesia, or head trauma.

4.3. The Relationship between Urinary AD7c-NTP Levels and ApoE Genotype. The most important finding to emerge from the present analysis was that urinary AD7c-NTP levels were significantly higher in subjects with *ApoE ε4* genotypes than in subjects without *ApoE ε4* genotypes and that urinary AD7c-NTP levels increased with increased *ApoE* grade. This finding is consistent with that of previous studies [56], which have shown that urinary AD7c-NTP levels are elevated in MCI patients with *ApoE ε4* alleles [56].

Carrying the *ApoE ε4* allele is considered to be the primary genetic risk factor for sporadic AD [57]. Previous studies have confirmed that *ApoE ε4* prevalence is 51% in the cognitively normal population, 64% in patients with mild cognitive impairment, and 66% in patients with AD [58]. In particular, *ApoE ε4* carriers are more likely to develop AD at an earlier age than those without an *ApoE ε4* allele [59]. Previous studies have reported that heterozygous *ApoE ε4* carriers shift the risk curve to develop the disease 5 years earlier, while homozygous *ApoE ε4/4* carriers shift it to develop the disease 10 years earlier, and *ApoE ε2* carriers shift it to develop the disease 5 years later [59, 60]. Furthermore, evidence has revealed that *ApoE* influences $A\beta$ deposition in a dose- and isoform-specific fashion ($\varepsilon4 > \varepsilon3 > \varepsilon2$) [61]. Therefore, in this study, we ranked the *ApoE* alleles according to their AD risk.

Urinary AD7c-NTP levels were higher in subjects with *ApoE ε4* than in subjects without *ApoE ε4* in the present study. This result may be because both *ApoE* and urinary AD7c-NTP are related to tau and $A\beta$ deposition. Substantial evidence suggests that the *ApoE ε4* allele is related to increased $A\beta$ deposition, rapid thinning of the cortex, and accelerated cognitive decline, while the *ApoE ε2* allele is related to a decrease in $A\beta$ deposits, slower thinning of the cortex, and slower cognitive decline [62–65]. Reports from experiments on animals show that the *ApoE ε4* allele disrupts memory function in rodents, and further studies have indi-

cated that fragments of the *ApoE ε4* allele may contribute to both plaque and tangle formation [66]. It has been demonstrated that the *ApoE* genotype can affect tau neuropathological changes in AD patients [47]. In the current study, there was a positive correlation between urinary AD7c-NTP levels and *ApoE* grades. There is evidence that *ApoE ε4* is associated with a higher density of paired helical filament tau tangles, while *ApoE ε2* is associated with fewer paired helical filament tau tangles in AD patients with $A\beta$ [61]. In addition, experiments on animals have shown that the *ApoE* allele affects tau pathogenesis and tau-mediated neurodegeneration [67].

ApoE allele and urinary AD7c-NTP levels are both promising biomarkers of AD. Previous studies have shown that the combined detection of *ApoE ε4* and urinary AD7c-NTP is a reliable biomarker for the early diagnosis of AD and that the predictive value is significantly increased compared with the detection of either one individually [56, 68]. The high consistency of these two biomarkers also provides a new way for us to understand and think about AD. The combination of two biomarkers may help the early diagnosis of AD and improve the diagnostic accuracy of AD and be better than one biomarker alone.

There are, however, some limitations to this study. First, subjects with normal cognition were recruited, and the correlation between urinary AD7c-NTP levels and *ApoE* allele in patients with abnormal cognition, such as with MCI or AD, should be further analyzed. Second, because of the low incidence of *ApoE ε2/4* in the population, this study included only 11 subjects with *ApoE ε2/4* out of 329 cognitively normal subjects; this genotype was relatively rare compared with other genotypes. Third, a longitudinal, multicenter, large study is needed to observe dynamic changes in AD7c-NTP levels in urine.

5. Conclusions

There were significant differences in urinary AD7c-NTP levels between subjects with and without a history of CHD or diabetes. Urinary AD7c-NTP levels were positively correlated with *ApoE* grade in the cognitively normal population. The relationship between AD risk factors and urinary AD7c-NTP levels may provide a new way for us to understand AD and urinary AD7c-NTP.

Data Availability

The data used to support the findings of the present research are available from the corresponding authors once requested.

Conflicts of Interest

There is no conflict of interest.

Acknowledgments

References

[1] L. Jia, M. Quan, Y. Fu et al., "Dementia in China: epidemiology, clinical management, and research advances," *The Lancet Neurology*, vol. 19, no. 1, pp. 81–92, 2020.

[2] J. Jia, C. Wei, S. Chen et al., "The cost of Alzheimer's disease in China and re-estimation of costs worldwide," *Alzheimers Dement*, vol. 14, no. 4, pp. 483–491, 2018.

[3] J. Garre-Olmo, "Epidemiology of Alzheimer's disease and other dementias," *Revista de Neurologia*, vol. 66, no. 11, pp. 377–386, 2018.

[4] B. Sabayan and F. Sorond, "Reducing Risk of Dementia in Older Age," *JAMA*, vol. 317, no. 19, p. 2028, 2017.

[5] R. A. Armstrong, "Risk factors for Alzheimer's disease," *Folia Neuropathologica*, vol. 57, no. 2, pp. 87–105, 2019.

[6] R. Wang, J. I. Zhijuan, S. Sheng et al., "Detection of urine neural thread protein for diagnosis of Alzheimer disease and its clinical significance," *Chinese Journal of Laboratory Medicine*, vol. 33, no. 1, pp. 46–50, 2010.

[7] L. Ma, R. Wang, Y. Han et al., "Development of a novel urine Alzheimer-associated neuronal thread protein ELISA kit and its potential use in the diagnosis of Alzheimer's disease," *Journal of Clinical Laboratory Analysis*, vol. 30, no. 4, pp. 308–314, 2016.

[8] L. Ma, J. Chen, R. Wang et al., "The level of Alzheimer-associated neuronal thread protein in urine may be an important biomarker of mild cognitive impairment," *Journal of Clinical Neuroscience*, vol. 22, no. 4, pp. 649–652, 2015.

[9] B. D. Ku, H. Kim, Y. K. Kim, and H. U. Ryu, "Comparison of urinary Alzheimer-associated neural thread protein (AD7c-NTP) levels between patients with amnestic and nonamnestic mild cognitive impairment," *American Journal of Alzheimer's Disease & Other Dementias®*, vol. 35, 2020.

[10] S. M. de la Monte, R. I. Carlson, N. V. Brown, and J. R. Wands, "Profiles of neuronal thread protein expression in Alzheimer's disease," *Journal of Neuropathology and Experimental Neurology*, vol. 55, no. 10, pp. 1038–1050, 1996.

[11] S. M. Monte, K. Ghanbari, W. H. Frey et al., "Characterization of the AD7C-NTP cDNA expression in Alzheimer's disease and measurement of a 41-kD protein in cerebrospinal fluid," *The Journal of Clinical Investigation*, vol. 100, no. 12, pp. 3093–3104, 1997.

[12] Y. Zhang, Y. Li, R. Wang, G. Sha, H. Jin, and L. Ma, "Elevated urinary AD7c-NTP levels in older adults with hypertension and cognitive impairment," *Journal of Alzheimer's Disease*, vol. 74, no. 1, pp. 237–244, 2020.

[13] Q. E. Zhang, S. Ling, P. Li et al., "The association between urinary Alzheimer-associated neuronal thread protein and cognitive impairment in late-life depression: a controlled pilot study," *International Journal of Biological Sciences*, vol. 14, no. 11, pp. 1497–1502, 2018.

[14] H. Jin, S. Guan, R. Wang et al., "The distribution of urinary Alzheimer-associated neuronal thread protein and its association with common chronic diseases in the general population," *Journal of Alzheimer's Disease*, vol. 65, no. 2, pp. 433–442, 2018.

[15] Y. Li, M. Kang, H. Wang et al., "Urinary Alzheimer-associated neuronal thread protein is not elevated in patients with subjective cognitive decline and patients with depressive state," *Journal of Alzheimer's Disease*, vol. 71, no. 4, pp. 1115–1123, 2019.

[16] Y. C. Youn, K.-W. Park, S.-H. Han, and S. Y. Kim, "Urine neural thread protein measurements in Alzheimer disease," *Journal of the American Medical Directors Association*, vol. 12, no. 5, pp. 372–376, 2011.

[17] Z. Rui, Y. Xin Rui, and P. Dan Tao, "Vallie of Alzheimer-associated neuronaI thread protein level in urine for diagnosing Ahheimer's disease," *Chinese Journal of Geriatrics*, vol. 31, no. 7, pp. 575–577, 2012.

[18] P. J. Kahle, M. Jakowec, S. J. Teipel et al., "Combined assessment of tau and neuronal thread protein in Alzheimer's disease CSF," *Neurology*, vol. 54, no. 7, pp. 1498–1504, 2000.

[19] F. Jessen, R. E. Amariglio, R. F. Buckley et al., "The characterisation of subjective cognitive decline," *The Lancet Neurology*, vol. 19, no. 3, pp. 271–278, 2020.

[20] F. Jessen, R. E. Amariglio, M. van Boxtel et al., "A conceptual framework for research on subjective cognitive decline in preclinical Alzheimer's disease," *Alzheimer's & Dementia*, vol. 10, no. 6, pp. 844–852, 2014.

[21] A. J. Mitchell, H. Beaumont, D. Ferguson, M. Yadegarfar, and B. Stubbs, "Risk of dementia and mild cognitive impairment in older people with subjective memory complaints: meta-analysis," *Acta Psychiatrica Scandinavica*, vol. 130, no. 6, pp. 439–451, 2014.

[22] M. A. Fernández-Blázquez, M. Ávila-Villanueva, F. Maestú, and M. Medina, "Specific features of subjective cognitive decline predict faster conversion to mild cognitive impairment," *Journal of Alzheimer's Disease*, vol. 52, no. 1, pp. 271–281, 2016.

[23] J. L. Molinuevo, L. A. Rabin, R. Amariglio et al., "Implementation of subjective cognitive decline criteria in research studies," *Alzheimer's & Dementia*, vol. 13, no. 3, pp. 296–311, 2017.

[24] S. Cosentino, N. Scarmeas, E. Helzner et al., "APOE epsilon 4 allele predicts faster cognitive decline in mild Alzheimer disease," *Neurology*, vol. 70, Issue 19, Part 2, pp. 1842–1849, 2008.

[25] L. A. Farrer, L. A. Cupples, J. L. Haines et al., "Effects of age, sex, and ethnicity on the association between apolipoprotein E genotype and Alzheimer disease," *JAMA*, vol. 278, no. 16, pp. 1349–1356, 1997.

[26] V. Leoni, "The effect of apolipoprotein E (ApoE) genotype on biomarkers of amyloidogenesis, tau pathology and neurodegeneration in Alzheimer's disease," *Clinical Chemistry and Laboratory Medicine*, vol. 49, no. 3, pp. 375–383, 2011.

[27] D. B. Carter, "The interaction of amyloid-β with ApoE," *Sub-Cellular Biochemistry*, vol. 38, pp. 255–272, 2005.

[28] J. M. Riphagen, I. H. G. M. Ramakers, W. M. Freeze et al., "Linking APOE-ε4, blood-brain barrier dysfunction, and inflammation to Alzheimer's pathology," *Neurobiology of Aging*, vol. 85, pp. 96–103, 2020.

[29] N. Zhang, L. Zhang, Y. Li et al., "Urine AD7c-NTP predicts amyloid deposition and symptom of agitation in patients with Alzheimer's disease and mild cognitive impairment," *Journal of Alzheimer's Disease*, vol. 60, no. 1, pp. 87–95, 2017.

[30] P. Scheltens, K. Blennow, M. M. B. Breteler et al., "Alzheimer's disease," *The Lancet*, vol. 388, no. 10043, pp. 505–517, 2016.

[31] X. Li, X. Wang, L. Su, X. Hu, and Y. Han, "Sino Longitudinal Study on Cognitive Decline (SILCODE): protocol for a Chinese longitudinal observational study to develop risk prediction models of conversion to mild cognitive impairment in individuals with subjective cognitive decline," *BMJ Open*, vol. 9, no. 7, article e028188, 2019.

[32] A. J. Jak, M. W. Bondi, L. Delano-Wood et al., "Quantification of five neuropsychological approaches to defining mild cognitive impairment," *The American Journal of Geriatric Psychiatry*, vol. 17, no. 5, pp. 368–375, 2009.

[33] R. A. Sperling, P. S. Aisen, L. A. Beckett et al., "Toward defining the preclinical stages of Alzheimer's disease: recommendations from the National Institute on Aging-Alzheimer's Association workgroups on diagnostic guidelines for Alzheimer's disease," *Alzheimers Dement*, vol. 7, no. 3, pp. 280–292, 2011.

[34] S. Xiao, "Application and value of neuropsychological test and rating scale in Alzheimer's disease," *Chinese Journal of Contemporary Neurology and Neurosurgery*, vol. 5, no. 3, pp. 137–140, 2005.

[35] P. Julayanont, S. Tangwongchai, S. Hemrungrojn et al., "The montreal cognitive assessment-basic: a screening tool for mild cognitive impairment in illiterate and low-educated elderly adults," *Journal of the American Geriatrics Society*, vol. 63, no. 12, pp. 2550–2554, 2015.

[36] P. A. Boyle, A. S. Buchman, R. S. Wilson, J. F. Kelly, and D. A. Bennett, "The APOE ε4 allele is associated with incident mild cognitive impairment among community-dwelling older persons," *Neuroepidemiology*, vol. 34, no. 1, pp. 43–49, 2010.

[37] Task Force Members, G. Montalescot, U. Sechtem et al., "2013 ESC guidelines on the management of stable coronary artery disease: the Task Force on the management of stable coronary artery disease of the European Society of Cardiology," *European Heart Journal*, vol. 34, no. 38, pp. 2949–3003, 2013.

[38] American Diabetes Association, "Standards of medical care in diabetes–2011," *Diabetes Care*, vol. 34, Supplement 1, pp. S11–S61, 2010.

[39] A. V. Chobanian, G. L. Bakris, H. R. Black et al., "The seventh report of the joint national committee on prevention, detection, evaluation, and treatment of high blood pressure the JNC 7 report," *JAMA*, vol. 289, no. 19, pp. 2560–2572, 2003.

[40] S. Xiu, Q. Liao, L. Sun, and P. Chan, "Risk factors for cognitive impairment in older people with diabetes: a community-based study," *Therapeutic Advances in Endocrinology and Metabolism*, vol. 10, 2019.

[41] M. Ávila-Villanueva and M. A. Fernández-Blázquez, "Subjective cognitive decline as a preclinical marker for Alzheimer's disease: the challenge of stability over time," *Frontiers in Aging Neuroscience*, vol. 9, p. 377, 2017.

[42] L. Miebach, S. Wolfsgruber, A. Polcher et al., "Which features of subjective cognitive decline are related to amyloid pathology? Findings from the DELCODE study," *Alzheimer's Research & Therapy*, vol. 11, no. 1, p. 66, 2019.

[43] S. Shi and J. Zhang, "A literature review of AD7c-ntp as a biomarker for Alzheimer's disease," *Annals of Indian Academy of Neurology*, vol. 16, no. 3, pp. 307–309, 2013.

[44] F. J. Wolters, S. J. van der Lee, P. J. Koudstaal et al., "Parental family history of dementia in relation to subclinical brain disease and dementia risk," *Neurology*, vol. 88, no. 17, pp. 1642–1649, 2017.

[45] K. Sleegers, K. Bettens, A. De Roeck et al., "A 22-single nucleotide polymorphism Alzheimer's disease risk score correlates with family history, onset age, and cerebrospinal fluid Aβ42," *Alzheimer's & Dementia*, vol. 11, no. 12, pp. 1452–1460, 2015.

[46] M. V. F. Silva, C. de Mello Gomide Loures, L. C. V. Alves, L. C. de Souza, K. B. G. Borges, and M. das Graças Carvalho, "Alzheimer's disease: risk factors and potentially protective measures," *Journal of Biomedical Science*, vol. 26, no. 1, p. 33, 2019.

[47] W. Chen, F. Jin, G. Cao et al., "ApoE4 may be a promising target for treatment of coronary heart disease and Alzheimer's disease," *Current Drug Targets*, vol. 19, no. 9, pp. 1038–1044, 2018.

[48] Y. Sun, C. Ma, H. Sun et al., "Metabolism: a novel shared link between diabetes mellitus and Alzheimer's disease," *Journal of Diabetes Research*, vol. 2020, Article ID 4981814, 12 pages, 2020.

[49] F. J. Wolters, H. I. Zonneveld, S. Licher et al., "Hemoglobin and anemia in relation to dementia risk and accompanying changes on brain MRI," *Neurology*, vol. 93, no. 9, pp. e917–e926, 2019.

[50] K. Bavarsad, M. Hosseini, M.-. A.-. R. Hadjzadeh, and A. Sahebkar, "The effects of thyroid hormones on memory impairment and Alzheimer's disease," *Journal of Cellular Physiology*, vol. 234, no. 9, pp. 14633–14640, 2019.

[51] K. Yanagiha, K. Ishii, and A. Tamaoka, "Acetylcholinesterase inhibitor treatment alleviated cognitive impairment caused by delayed encephalopathy due to carbon monoxide poisoning," *Medicine*, vol. 96, no. 8, p. e6125, 2017.

[52] I. Urits, V. Orhurhu, M. Jones, D. Hoyt, A. Seats, and O. Viswanath, "Current perspectives on postoperative cognitive dysfunction in the ageing population," *Turkish Journal of Anaesthesiology and Reanimation*, vol. 47, no. 6, pp. 439–447, 2019.

[53] K. McInnes, C. L. Friesen, D. E. MacKenzie, D. A. Westwood, and S. G. Boe, "Correction: Mild Traumatic Brain Injury (mTBI) and chronic cognitive impairment: a scoping review," *PLoS One*, vol. 14, no. 6, article e0218423, 2019.

[54] L. K. Weaver, "Clinical practice. Carbon monoxide poisoning," *The New England Journal of Medicine*, vol. 360, no. 12, pp. 1217–1225, 2009.

[55] B. M. Krause, S. Sabia, H. J. Manning, A. Singh-Manoux, and R. D. Sanders, "Association between major surgical admissions and the cognitive trajectory: 19 year follow-up of Whitehall II cohort study," *BMJ*, vol. 366, article l4466, 2019.

[56] C. Wang, Y. Cui, J. Yang et al., "Combining serum and urine biomarkers in the early diagnosis of mild cognitive impairment that evolves into Alzheimer's disease in patients with the apolipoprotein E ε4 genotype," *Biomarkers*, vol. 20, no. 1, pp. 84–88, 2014.

[57] A. M. Saunders, W. J. Strittmatter, D. Schmechel et al., "Association of apolipoprotein E allele ε4 with late-onset familial and sporadic Alzheimer's disease," *Neurology*, vol. 43, no. 8, pp. 1467–1472, 1993.

[58] N. Mattsson, C. Groot, W. J. Jansen et al., "Prevalence of the apolipoprotein E ε4 allele in amyloid β positive subjects across the spectrum of Alzheimer's disease," *Alzheimer's & Dementia*, vol. 14, no. 7, pp. 913–924, 2018.

[59] P. Pastor, C. M. Roe, A. Villegas et al., "Apolipoprotein E ε4 modifies Alzheimer's disease onset in an E280A PS1 kindred," *Annals of Neurology*, vol. 54, no. 2, pp. 163–169, 2003.

[60] S. Noguchi, K. Murakami, N. Yamada et al., "Apolipoprotein E genotype and Alzheimer's disease," *The Lancet*, vol. 342, no. 8873, pp. 737-738, 1993.

[61] J. M. Farfel, L. Yu, P. L. De Jager, J. A. Schneider, and D. A. Bennett, "Association of APOE with tau-tangle pathology with and without β-amyloid," *Neurobiology of Aging*, vol. 37, pp. 19–25, 2016.

[62] A. Drzezga, T. Grimmer, G. Henriksen et al., "Effect of APOE genotype on amyloid plaque load and gray matter volume in Alzheimer disease," *Neurology*, vol. 72, no. 17, pp. 1487–1494, 2009.

[63] N. M. Wisdom, J. L. Callahan, and K. A. Hawkins, "The effects of apolipoprotein E on non-impaired cognitive functioning: A meta- analysis," *Neurobiology of Aging*, vol. 32, no. 1, pp. 63–74, 2011.

[64] A. Serrano-Pozo, J. Qian, S. E. Monsell, R. A. Betensky, and B. T. Hyman, "APOEε2 is associated with milder clinical and pathological Alzheimer disease," *Annals of Neurology*, vol. 77, no. 6, pp. 917–929, 2015.

[65] M. Fan, B. Liu, Y. Zhou et al., "Cortical thickness is associated with different apolipoprotein E genotypes in healthy elderly adults," *Neuroscience Letters*, vol. 479, no. 3, pp. 332–336, 2010.

[66] J. Raber, Y. Huang, and J. W. Ashford, "ApoE genotype accounts for the vast majority of AD risk and AD pathology," *Neurobiology of Aging*, vol. 25, no. 5, pp. 641–650, 2004.

[67] Y. Shi, Alzheimer's Disease Neuroimaging Initiative, K. Yamada et al., "ApoE4 markedly exacerbates tau-mediated neurodegeneration in a mouse model of tauopathy," *Nature*, vol. 549, no. 7673, pp. 523–527, 2017.

[68] Z. Lei, W. Yan, Z. Feng-chun, Z. Jin-rong, and L. Hongmei, "Combined detection of Apolipoprotein E ε4 allele and urinary AD7c-NTP in the early diagnosis of Alzheimer's disease," *Journal of Apoplexy and Nervous Diseases*, vol. 31, no. 7, pp. 585–589, 2014.